

**DESIGN, SYNTHESIS, AND EVALUATION OF SOME  
NEW COUMARIN DERIVATIVES FOR ANTIDIABETIC  
ACTIVITY**

Thesis Submitted for the Award of the Degree of

**DOCTOR OF PHILOSOPHY**

**in**

**Pharmaceutical Chemistry**

**By**

**Rachana Sameer Bhimanwar**

**Registration Number: 41800862**

**Supervised By**

**Dr. Vikas Sharma (26231)**

**Department of Pharmaceutical Chemistry**

**(Associate Professor)**

**Lovely Professional University**

**Co-Supervised by**

**Dr. Amit Mittal (31641)**

**Department of Pharmaceutical Chemistry**

**(Professor)**

**Lovely Professional University**



**LOVELY PROFESSIONAL UNIVERSITY, PUNJAB**

**2024**

## **DECLARATION**

I, hereby declare that the present work in the thesis entitled “Design, synthesis, and evaluation of some new coumarin derivatives for antidiabetic activity” in fulfilment of degree of **Doctor of Philosophy (Ph. D.)** is outcome of research work carried out by me under the supervision of Dr. Vikas Sharma, working as Associate Professor in the Department of Pharmaceutical Chemistry, School of Pharmaceutical Sciences of Lovely Professional University, Punjab, India. In keeping with general practice of reporting scientific observations, due acknowledgements have been made whenever work described here has been based on findings of other investigator. This work has not been submitted in part or full to any other University or Institute for the award of any degree.

**(Signature of Scholar)**

Rachana Sameer Bhimanwar

Registration No.: 41800862

Department of Pharmaceutical Chemistry, School of Pharmaceutical Sciences

Lovely Professional University,

Punjab, India

## **CERTIFICATE**

This is to certify that the work reported in the Ph. D. thesis entitled “Design, synthesis, and evaluation of some new coumarin derivatives for antidiabetic activity” submitted in fulfillment of the requirement for the award of degree of **Doctor of Philosophy (Ph.D.)** in the Department of Pharmaceutical Chemistry, School of Pharmaceutical Sciences, is a research work carried out by Rachana Sameer Bhimanwar (41800862) is bonafide record of her original work carried out under my supervision and that no part of thesis has been submitted for any other degree, diploma or equivalent course.

**(Signature of Supervisor)**

Dr. Vikas Sharma

Associate Professor

Pharmaceutical Chemistry,

School of Pharmaceutical Sciences

Lovely Professional University

**(Signature of Co-Supervisor)**

Dr. Amit Mittal

Professor

Pharmaceutical Chemistry

School of Pharmaceutical Sciences

Lovely Professional University

## ACKNOWLEDGMENT

Composing this dissertation has been one of the most significant academic challenges I have faced, and the completion of this study would not have been possible without the unwavering support, patience, and guidance of several individuals. I extend my deepest gratitude to those who have played instrumental roles in this journey. First and foremost, I express my gratitude to God Almighty for bestowing me with strength and abilities throughout my life.

I am sincerely thankful to the honourable Chancellor, Mr. Ashok Mittal, and Pro-chancellor **Mrs. Rashmi Mittal** of Lovely Professional University for their support. A special mention goes to **Prof. (Dr.) Monica Gulati**, Dean and Head of the School of Pharmaceutical Sciences at LPU, whose constant encouragement and learning environment facilitated the completion of this research work.

I also want to express special gratitude and indebtedness for my supervisor, **Dr. Vikas Sharma**, Department of Pharmaceutical Chemistry at the School of Pharmaceutical Sciences, Lovely Professional University, and my co-supervisor, **Dr. Amit Mittal**. They have demonstrated exceptional mentorship, providing invaluable guidance throughout my academic path. Their insightful conversations and constructive feedback have motivated me to delve into different facets of the subject, greatly enriching my understanding. I deeply appreciate their support in nurturing my research pursuits and fostering my growth as a scholar. Their commitment to dedicating significant time to my advancement is genuinely commendable and highly valued. Their unwavering support, tireless efforts, and eminent guidance have played a crucial role throughout my research journey.

I would also like to thank **Dr. Sohan Chitlange**, Principal, Dr D Y Patil Institute of Pharmaceutical Sciences and Research, Pimpri, Pune for providing a supportive research environment for carrying out my research. I am also grateful to **Dr. Asha Thomas, Dr. R. P. Bhole and Dr. R. D. Wavhale** for their timely suggestions and encouragement for my research work.

I express my gratitude to **Dr. Snehal Chaudhari**, Assistant Professor at the University of Wisconsin-Madison, for generously sharing time and knowledge in conducting in vitro cell-based assays. I am very much fortunate to have her as my

collaborator. I am also extremely grateful for Biocyte Institute of Research and Development, Sangli for extending IAEC permission for carrying out animal studies.

The thesis has also benefitted from comments and suggestions made by faculty staffs **Dr. Gurvinder Singh, Dr. Pankaj Wadhwa**, Lovely School of Pharmaceutical Sciences, LPU, which have contributed greatly to the improvement of the thesis. Their suggestions helped to understand and rectify my mistakes on time.

I am also thankful to my colleagues Ms. Gauri Paradkar, Mr. Satish Mandave, Ms. Shubhangi Shekade and Ms. Anagha Ghodse for their stimulating discussions and willingness to assist me in my research work.

I am also thankful to my student Ganesh Yeole for his help. I am very much thankful to laboratory staff specially Ms. Kishori Kenjale and other non-teaching staff of chemistry department for their willing assistance and support.

I would like to acknowledge Central Instrumentation Facility, Savitribai Phule Pune University, Pune for their generous help for spectral characterization of research samples. I would also like to acknowledge DST FIST facility at Dr. D Y Patil Institute of Pharmaceutical Sciences and Research, Pune for providing instrumentation facility.

I dedicate this thesis to my family: Mr. Sameer Bhimanwar (Husband), Master Hitarth Bhimanwar (Lovable son), Mr. Rajendra Joshi (Father), Mrs. Rohini Joshi (Mother), Mr. Vinayak Joshi (Brother) and my In-laws. Their unconditional love, wholehearted support, and patience have been my pillar of strength. I appreciate their belief in me, cheering me through both the good and challenging times.

I want to extend my heartfelt thanks to my GOD for bestowing upon me the inner strength needed to traverse the arduous path of pursuing my doctoral degree. This academic journey has been filled with ups and downs, much like a thrilling roller coaster ride, yet it is my unwavering faith in a divine presence that has been my guiding light throughout this challenging endeavour.

**"Success is not the key to happiness. Happiness is the key to success. If you love what you are doing, you will be successful." - Albert Schweitzer**

Thanks

Rachana Sameer Bhimanwar

## **TABLE OF CONTENT**

<b>Sr. No.</b>	<b>Chapter title</b>	<b>Page No.</b>
<b>CHAPTER 1</b>	<b>Introduction</b>	<b>1-15</b>
1.1	Diabetes mellitus (DMs)	1
1.2	Discovery of TGR5	6
1.3	Advantages of TGR5 target	8
1.4	TGR5 interaction with ligand	9
1.5	Drug Discovery	10
1.5.1	Computational Approach	10
1.5.2	Homology Modelling	11
1.6	Coumarin derivatives	12
<b>CHAPTER 2</b>	<b>Literature review</b>	<b>16-35</b>
2.1	Naturally-occurring TGR5 agonists	16
2.2	Semi-synthesized TGR5 agonist	18
2.3	Synthetic TGR5 agonists	22
2.4	Coumarin as antidiabetic	33
<b>CHAPTER 3</b>	<b>Rational and Objectives</b>	<b>36-39</b>
<b>CHAPTER 4</b>	<b>Work plan</b>	<b>40-43</b>
4.1.	Preparation and Validation of Homology model of TGR5	40
4.2.	Molecular Docking Studies	41
4.3.	Synthesis and characterisation of compounds	42
4.4.	<i>In Vitro</i> evaluation of synthesized compound	42
4.5.	<i>In Vivo</i> evaluation of synthesized compound	42
<b>CHAPTER 5</b>	<b>Material, Methods and Experimental</b>	<b>44-66</b>
5.1	Materials	44
5.2	Methods	45
5.2.1	<i>In-Silico</i> studies (Homology modelling and molecular docking studies)	45
5.2.1.1	Homology Modelling	45
5.2.1.2	Molecular docking studies	48

5.2.1.3	Molecular dynamics study	52
5.2.1.4	<i>In Silico</i> Drug-likeness analysis	54
5.2.2	Synthesis of the identified test compounds	54
5.2.2.1	Synthesis of Ethyl 7-hydroxy-2-oxo-2 <i>H</i> -1-benzopyran-3-carboxylate	56
5.2.2.2	Synthesis of ethyl 7-(benzyloxy)-2-oxo-2 <i>H</i> -1-benzopyran-3-carboxylate	56
5.2.2.3	Synthesis of 7-(benzyloxy)-2-oxo-2 <i>H</i> -1-benzopyran-3-carboxylic acid	56
5.2.2.4	Synthesis of Compounds (3-9a)	57
5.2.2.5	Synthesis of 7-(2-bromoethoxy)-3-propanoyl-2 <i>H</i> -1-benzopyran-2-one	57
5.2.2.6	Synthesis of ethyl 7-[2-(2,5-dimethylphenoxy)ethoxy]-2-oxo-2 <i>H</i> -1-benzopyran-3-carboxylate	57
5.2.2.7	Synthesis of ethyl 7-[2-(2,3-dimethylphenoxy)ethoxy]-2-oxo-2 <i>H</i> -1-benzopyran-3-carboxylate	58
5.2.2.8	Synthesis of 7-[2-(2,5-dimethylphenoxy)ethoxy]-2-oxo-2 <i>H</i> -1-benzopyran-3-carboxylic acid	58
5.2.2.9	Synthesis of 7-[2-(2,3-dimethylphenoxy)ethoxy]-2-oxo-2 <i>H</i> -1-benzopyran-3-carboxylic acid	58
5.2.2.10	General procedure for Synthesis of Compounds (13a, 14a, 15a, 16a, 17a)	59
5.2.2.11	General procedure for Synthesis of Compounds (13b, 14b, 15b, 16b)	59
5.2.3	Biological evaluation through <i>In Vitro</i> and <i>In Vivo</i> studies	59
5.2.3.1	<i>In vitro</i> studies	59
5.2.3.1.1	Nature of cell	60
5.2.3.1.2	Cell viability assay	60
5.2.3.1.3	GLP-1 secretion assay	60

5.2.3.1.4	Real-time qPCR assay	61
5.2.3.1.5	Quantification and Statistical analysis	62
5.2.3.2	<i>In vivo</i> Studies	62
5.2.3.2.1	Brine shrimp lethality assay	63
5.2.3.2.2	Acute toxicity studies	63
5.2.3.2.3	Oral glucose tolerance test (OGTT)	65
<b>CHAPTER 6</b>	<b>Result and discussion</b>	<b>67-131</b>
6.1	<i>In-silico</i> studies	<b>67</b>
6.1.1	Homology Modelling	67
6.1.1.1	Protein modelling using Swiss Model	67
6.1.1.2	Protein modelling using I-Tasser	68
6.1.2	Molecular Docking studies	72
6.1.2.1	Validation of docking studies	72
6.1.3	Molecular dynamic studies	85
6.1.3.1	RMSD Plot evaluation	85
6.1.3.2	RMSF Plot evaluation	86
6.1.3.3	Radius of gyration evaluation	87
6.1.3.4	Interaction profiling and per residue energy contribution	89
6.1.3.5	Binding Free Energies	89
6.1.4	<i>In silico</i> ADME of selected lead compounds	93
6.2	Synthesis of most potent compounds	94
6.2.1	Synthesis of compounds from Series A	94
6.2.2	Synthesis of compounds from Series B and C	96
6.2.3	Spectral characterization of compounds (1-9a)	97-106
6.2.4	Spectral characterization of compounds (11-17a)	107-114
6.3	Biological evaluation through In Vitro and In Vivo studies	115
6.3.1	In vitro studies	115
6.3.1.1	Cell viability assay	115
6.3.1.2	GLP 1 assay	118



6.3.1.3	TGR5 gene expression assay	121
6.3.2	<i>In Vivo</i> studies	123
6.3.2.1	Brine shrimp lethality Assay	123
6.3.2.2	Acute toxicity studies	124
6.3.2.3	Oral glucose tolerance test	125
6.4	Structure Activity relationship	128-131
<b>CHAPTER 7</b>	<b>Summary and Conclusions</b>	<b>132-138</b>
7.1	Summary	132
7.2	Conclusion	<b>134</b>
<b>CHAPTER 8</b>	<b>References</b>	<b>139-151</b>
<b>CHAPTER 9</b>	<b>Annexures</b>	<b>152-180</b>

### List of Tables

Table No.	Name	Page No.
1	List of Antidiabetic drugs	3-5
2	List of Templates from Swiss model	47
3	List of Models from I-Tasser	47
4	Designed compounds library	50-51
5	Allocation of groups of animals	66
6	Comparison results for TGR5 Model using Swiss Model and I- Tasser	72
7	The intermolecular interactions and binding affinity of lead compounds for TGR5.	74-79
8	Per residue interaction score contributed to the total docking score of the compound.	90
9	Data for the selected lead compound, INT-777, and bile acid's cumulative binding free energies from 100 nanoseconds within the binding pocket of TGR5	90
10	ADME properties predicted of top lead compounds.	93
11	Results of cell viability assay	115-116
12	Results of GLP 1 Assay	118-119
13	Results of Relative gene expression of TGR5	121
14	Brine shrimp lethality Assay	123
15	Clinical observations in treated animals	125
16	Results of OGTT test	126

## **LIST OF FIGURES**

<b>Figure No.</b>	<b>Name</b>	<b>Page No.</b>
1.	3D structure of TGR5	7
2.	Role of TGR5	8
3.	Structure of TGR5 receptor A) Structure with five heteromeric chains B) Ligplot of interaction of INT777 with TGR5	9
4.	Homology Modelling	11
5.	Pechmann condensation	13
6.	Claisen condensation	13
7.	Perkin reaction	13
8.	Wittig reaction	14
9.	Knoevenagel Condensation	14
10.	Reaction mediated synthesis of coumarin	15
11.	Flavonoids from <i>Chromolaenaodorata</i>	16
12.	Triterpenoid extract from leaves of <i>Oleaeuropaea</i>	17
13.	Quinovic acid from <i>Fagoniacretica</i>	18
14.	LCA derivatives	18
15.	CA derivatives	19
16.	Cholic acid derivatives	20
17.	Derivatives of Chenodeoxycholic acid	20
18.	OA derivative DKS26.	21
19.	Hyodeoxycholic acid	21
20.	2-Phenoxy nicotinamide derivatives	22
21.	Oxadiazole derivatives	23
22.	4-phoxynicotinamide-5-carboxamide derivatives	25
23.	4-Phenyl pyridine derivatives	26
24.	4-Benzofuranyloxynicotinamide derivatives as TGR5 agonists	27
25.	Thiazole derivative as TGR5 agonist	28

26.	Tetrahydrobenzimidazoles derivatives	29
27.	Imidazole derivatives	30
28.	2-mercapto triazole derivatives	31
29.	Tetrahydropyrido[4,3-d]pyrimidine amide derivative	32
30.	3-aryl-4-isoxazolecarboxamides as TGR5 agonist	33
31.	Coumarine-hydrazone derivative	34
32.	Cinnamic acid-coumarin hybrid derivative	34
33.	Coumarin derivative with oxime ester	35
34.	3-(4'-benzoyl amino-phenyl) coumarin derivative	35
35.	LigPlot of interaction of TGR5 with INT777	36
36.	Design strategy of a) Pharmacophore model b) Central core c) Ring A and Ring B	39
37.	Flow diagram for Homology Modelling	46
38.	Active sites in the modelled protein (indicated by red colour)	49
39.	Secondary structural view of TGR5 protein complex with co-crystal ligand INT-777.	49
40.	Flow diagram for Molecular docking study	52
41.	Synthetic scheme	55
42.	Flow diagram for Cell Titer-Glo assay	61
43.	Flow diagram for GLP-1 secretion Assay	61
44.	Albino Wister rats	64
45.	Use of glucometer to determine blood glucose level	66
46.	a) Sequence alignment of Chain A of model and Secondary structure of (b) 5iu7 and model using (c) Swiss model 5iu7	69
47.	Ramachandran Plot of Model (PDB ID: 5iu7) generated by Swiss Model server	69
48.	ERRAT Results of Model generated by Swiss Model	70
49.	a) Sequence alignment of model and template b) Secondary structure of template and (c) model generated using I- Tasser	70
50.	Ramchandran Plot of Model 1 generated by I-Tasser	71
51.	ERRAT Results of Model 1 generated by I-Tasser	71

52.	(a) Superimposition of re-docked INT777 (red) onto co-crystallized form (yellow) in the active site (b) Molecular Interaction of INT777 with TGR5.	73
53.	3D and 2D Intermolecular interactions between top 10 lead compounds with TGR5 (A) 6a, (B) 14a, (C) 14b, (D) 16a, (E) 16b, (F) 15a, (G) 6c, (H) 6b, (I) 8a and (J) 8b	80-83
54.	(a) RMSD plot (b) RMSF plot for TGR5 complex atoms upon binding of lead compounds, INT-777 and Bile Acid, during 100ns MD simulation.	88
55.	(a) Radius of gyration plot reflecting the changes observed in the conformational behaviour of the protein and all protein–ligand complexes (b) The SASA curve depicts the change in the protein–ligand complexes' solvent accessibility	88
56.	Protein-ligand contact plot: showing a timeline representation of the interactions and contacts (H-bonds, Hydrophobic, Ionic, Water bridges). (a) TGR5-INT-777, (b) TGR5-Bile Acid, (c) TGR5-6a, (d) TGR5-16a, (e) TGR5-14b, (f) TGR5-16b, and (g) TGR5-14a complexes.	91
57.	Scatter plot for the per residue interaction contribution to the total docking score.	92
58.	Proposed fragments and probable fragmentation pathway for compound 6a	102
59.	Proposed fragments and probable fragmentation pathway for compound 15a	111
60.	Relative cell viability percentage vs synthesized compounds at three concentrations levels	117
61.	GLP 1 levels (pg/mL) vs synthesized compounds (1-17a) at three concentration levels 0.1µm, 1µm and 10µm.	120
62.	Relative gene expression of TGR5 for compounds. Each reading is the mean of four replicates.	122
63.	Effect of 15a on OGTT: (A) Plasma blood glucose; (B) blood	127

	glucose AUC <sub>0-240 min.</sub>	
64.	General structure of Series A	128
65.	General structure of Series B and C	130
66.	3D and 2D Intermolecular interactions between lead compound 15a with TGR5	131

### **ABBREVIATIONS**

<b>List of Symbol</b>	<b>Abbreviation</b>
%	Percentage
°C	Degree celcius
μM	Micromolar
ADME	Absorption, Distribution, Metabolism, and Excretion
ANOVA	One-way analysis of variance
A <sup>o</sup>	Armstrong
BAT	Brown adipose tissue
BeA	Betulinic acid
CA	Cholic acid
CADD	Computer Aided drug design
CASTp	Computed Atlas of Surface Topography of Proteins
CDCA	Chenodeoxycholic acid
CDCl <sub>3</sub>	Chloroform
CREB	CREB
DCA	Deoxycholic acid
DIPEA	N,N-Diisopropylethylamine
DMF	dimethylformamide
DMs	Diabetes mellitus
DMSO	Dimethylsulfoxide
DPP-IV	Dipeptidyl peptidase 4
EC <sub>50</sub>	Half maximal effective concentration
FTIR	Fourier Transform Infrared Spectroscopy
FXR	Nuclear receptor farnesoid X
g/kg	Gram/kilogram
GLP-1	Glycogen like protein-1
gm	Gram

HATU	Hexa fluorophosphates Azabenzotriazole Tetramethyl Uronium
HCl	Hydrochloric acid
HR-MS	High-resolution mass spectrometry
hrs	Hours
HTS	High-throughput screening
IC <sub>50</sub>	Half-maximal inhibitory concentration
IDF	International diabetes federation
kcal/mol	Kilocalorie/mole
LBDD	Ligand-based drug design
LCA	Lithocholic acid
MD	Molecular dynamics
mg/kg	Milligram/kilogram
min	Minute
ml	Millilitre
mmol	Milimole
mp	Melting point
N	Normal
NaOH	Sodium hydroxide
nM	Nanomolar
NMR	Nuclear magnetic resonance
OA	Oleanolic acid
OFS	Oligofructose
PKA	Protein kinase A
PPAR	Peroxisome proliferator-activated receptor
pM	Picomolar
ProQ	Protein Quality predictor
ProSA	Protein Structure Analysis
PTP1B	Protein tyrosine phosphatase 1B



QSAR	Quantitative Structure-Activity Relationship
RAMPAGE	Ramchandran plot Assessment
RCSB PDB	Research Collaboratory for Structural Bioinformatics Protein Data Bank
ROCS	Rapid Overlay of Chemical Structures
Rf	Retention factor
Rg	Radius of Gyration
RMSD	Root mean square deviation
rpm	Rotation per minute
SAR	structure-activity relationship
SASA	Solvent Accessible Surface Area
SAVES	Structure Analysis and Verification Server
SBDD	Structure-based drug design
SGLT2	Sodium-Glucose Cotransporter Type 2
TGR5	Takeda G protein-coupled
UA	Ursolic acid

# INTRODUCTION



## **CHAPTER 1**

### **1. INTRODUCTION**

#### **1.1. Diabetes mellitus (DMs)**

A medical condition where body become deficit of insulin either by incapability of producing insulin or due to unresponsiveness of the cells towards the produced insulin that results in increase in blood glucose level.

Diabetes is classified into three types those are Type I diabetes (inability of insulin production), Type II diabetes (unresponsive for insulin production) and gestational diabetes (most common in all diabetes types) and Gestational diabetes occurs in women during pregnancy and mostly get resolves after delivery.<sup>1,2</sup>

1. Type 1 Diabetes: During this condition, beta cells in pancreas were destroyed by immune system. Various factors are believed to result to this condition, but exact cause is unknown. The onset of the disorder is usually sudden and dramatic, usually occurring during childhood or adolescence. Insulin therapy is necessity for regulation of sugar levels in people with Type 1 diabetes throughout their lives. Pumps and injections are two ways to administer insulin.<sup>3,4</sup>
2. Type 2 Diabetes: In this condition, cells in the body become irresponsive to insulin effectively as a result of insulin resistance, as well as insufficient production of insulin over time. A number of factors influence it, including genetics and lifestyle factors such as obesity and inactivity. It is typically seen in adults, but is becoming more prevalent among younger individuals. The treatment includes lifestyle changes, oral medications to enhance insulin sensitivity or stimulate insulin release, and sometimes insulin therapy.<sup>5</sup>
3. Gestational Diabetes: When women produce less insulin than necessary to meet the increased insulin demand during pregnancy, they may suffer from gestational diabetes. Insulin resistance is linked to hormonal changes during pregnancy that cause the body to produce less insulin. Generally, it occurs in the mid trimester of a woman's pregnancy. It is important to monitor sugar levels, make dietary changes, and use insulin if necessary, in order to manage gestational diabetes.<sup>6</sup>

The International diabetes federation (IDF) Atlas 2022 predicts increase in number of diabetic patients aged 20-79 years between 2030 and 2045, to 643 million with 6.7 million deaths in 2021.<sup>7</sup> The consequences of diabetes extend beyond individuals' health to their economies. The prevalence of diabetes will increase globally in the years ahead, posing a significant health threat. Therefore it is important to take precautionary measures with lifestyle modifications like regular physical activity, healthy diet, and maintenance of a body weight which will successfully manage Type II diabetes in long-term.<sup>8,9</sup>

**Progression of Diabetes:** Diabetes progresses through five stages, each marked by worsening beta-cell dysfunction. In Stage 1, beta-cells respond to insulin resistance or reduced cell mass by increasing insulin secretion to maintain normal blood glucose. This phase is defined by maintained beta-cell functionality and preserved acute glucose-stimulated insulin secretion (GSIS). In Stage 2, glucose levels start to increase, typically reaching 5.0-6.5 mmol/L, as beta-cell mass and function begin to decline, leading to diminished GSIS and beta-cell dedifferentiation. Stage 3 marks the onset of early decompensation, progressing into Stage 4, where stable decompensation occurs with significant beta-cell dedifferentiation. In Stage 5, beta-cell mass is severely reduced, often resulting in ketosis. This progression is primarily driven by declining beta-cell function and increasing insulin resistance. New therapies aim to address these dysfunctions without promoting weight gain or hypoglycemia.<sup>10</sup>

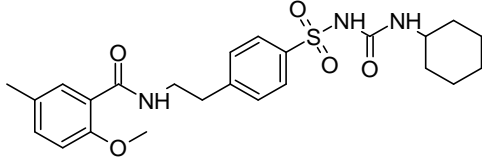
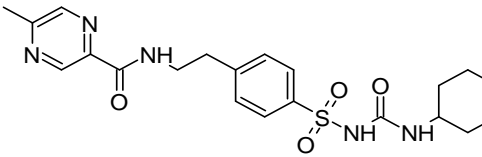
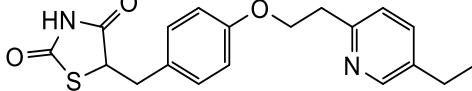
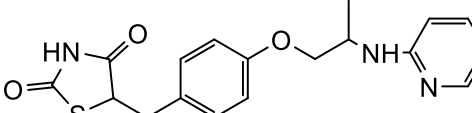
Apart from various precautionary measures drugs are available for treatment of diabetes with various modes of actions targeting different pathways. Present treatment to Type II diabetes includes various mechanisms.<sup>11</sup>

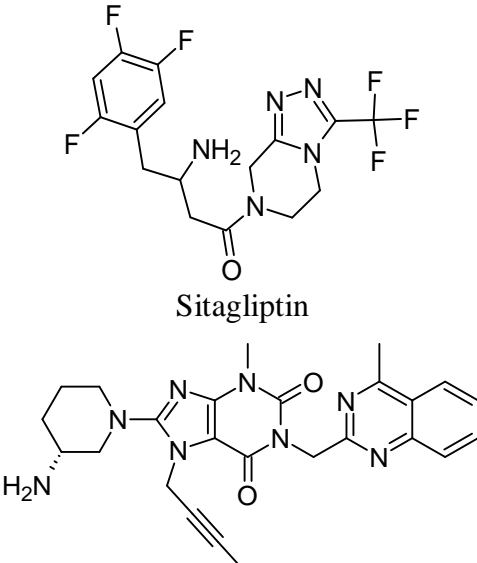
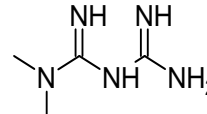
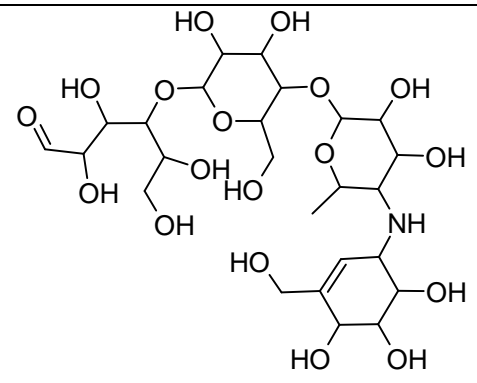
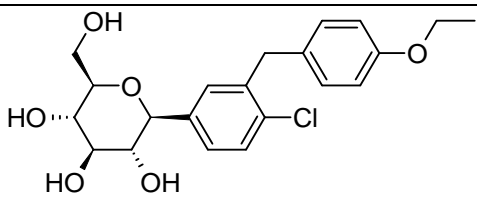
1. Use of biguanides to inhibit gluconeogenesis (Metformin)
2. The increase in insulin secretion by pancreatic beta cells with sulphonylureas (Glipizide, Glimepiride, Gliclazide, Glibenclamide), and with metaglinides (Replaglinide)
3. Increasing the sensitivity of insulin in the muscles, adipose tissue, and liver with thiazolidinediones (Rosiglitazone, Pioglitazone)

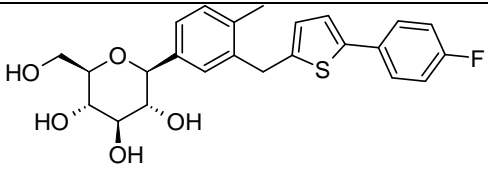
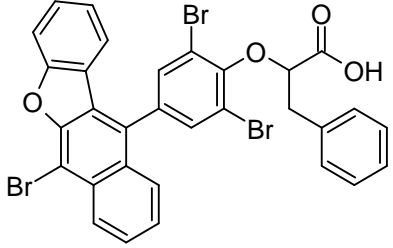
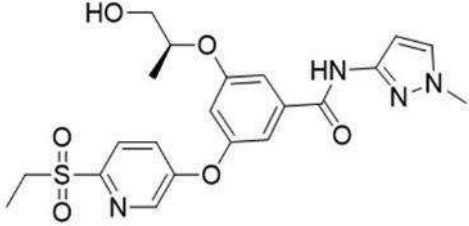
4. The inhibition of the glucosidase enzyme with the use of an alpha-glucosidase inhibitor (Acarbose) reduces carbohydrates absorption from the GIT.
5. Inhibition of glucose reabsorption through the kidneys and removal of excess glucose from the body through urine using SGLT2 inhibitors (Canagliflozin, Dapagliflozin, Empagliflozin).

Many drugs with different mechanism of actions are available for treatment of Diabetes Type II.<sup>12</sup>

**Table 1: List of Anti-diabetic drugs**

Class	Mode of Action	Structures of the drugs
Sulfonylureas <sup>13</sup>	Increase in insulin secretion through stimulation of pancreas	 <p>Glyburide</p>  <p>Glipizide</p>
Peroxisome proliferator-activated receptor (PPAR) agonist <sup>14,15</sup> Ex. Thiazolidinedione	Regulate insulin secretion	 <p>Pioglitazone</p>  <p>Rosiglitazone</p>

<p>Dipeptidyl peptidase 4 (DPP-IV) inhibitors<sup>16, 17</sup></p>	<p>It inhibit the DPP-4 enzyme which avoid the breakdown of GLP and thus regulate insulin secretion</p>	 <p>Sitagliptin</p> <p>Linagliptin</p>
<p>Biguanides<sup>18</sup></p>	<p>Reduction in concentration of glucose level by inhibiting the liver to produce glucose.</p>	 <p>Metformin</p>
<p><math>\alpha</math>-glucosidase inhibitors<sup>19</sup></p>	<p>Slowdown the breakdown of dietary carbohydrate</p>	 <p>Acarbose</p>
<p>SGLT2inhibitors.<sup>20,21</sup></p>	<p>This does not allows the kidneys reabsorb blood glucose thus lower blood levels and the excess glucose in the blood is removed from the</p>	 <p>Dapagliflozin</p>

	body through urine	 <p>Canagliflozin</p>
GLP1 receptor agonists <sup>22</sup>	It lowers the secretion of glucagon and increase nutrient-induced release of insulin.	<p>H-His-Gly-Glu-Gly-Thr-Phe-Thr--Ser-Asp-Leu-Ser-Lys-Gln-Met--Glu-Glu-Glu-Ala-Vla-Arg-Leu--Phe-Ile-Glu-Trp-Leu-Lys-Asn--Gly-Gly-Pro-Ser-Ser-Gly-Ala-Pro-Pro-Ser-NH<sub>2</sub></p> <p>Exenatide</p>
Protein tyrosine phosphate 1B (PTP1B) inhibitors <sup>23</sup>	PTP1B hinders insulin signaling by promoting the dephosphorylation of tyrosine residues on insulin substrate and insulin and leptin receptors.	 <p>Ertiprotafib</p>
Glucokinase activators <sup>24</sup>	GK activators (GKAs) possess the ability to boost pancreatic insulin secretion and facilitate the glycogen synthesis in the liver,	 <p>MK-0941</p>

In recent years, newer antidiabetic drugs have been developed, including DPP-IV inhibitors (Sitagliptin and Linagliptin) that inhibit the DPP-4 enzyme, which in turn avoids the breakdown of GLP and influences insulin secretion. Furthermore, Glycogen like protein-1 (GLP-1) agonists, such as Exenatide are also co-administered

with DDP-IV inhibitors to decrease glucagon release and stimulate glucose metabolism. Glucagon antagonists, glucokinase activators, fructose 1, 6 bisphosphate agonists, and fatty acid receptor agonists are also new approaches for lowering glucose in type II diabetes which may be used to develop new medications.<sup>25-27</sup> There are, however, several side effects associated with current treatments, including weight gain, digestive problems, and edema. Sometime causes episodes of hypoglycemic conditions and over time causes loss of responsiveness.<sup>28</sup> Despite these advances, development of safe and effective therapeutic anti-diabetic agents remain a great challenge.

## **1.2. Discovery of TGR5**

In search of new therapy action, bile acid receptors emerged as a new pharmacological tool in the treatment of various metabolic disorders. In the year 1999, bile acids were found to be signalling molecules, acting as hormones and regulatory ligands of lipid, glucose, and overall energy metabolism.<sup>29</sup> The primary bile acids present in humans are Cholic acid (CA) and Chenodeoxycholic acid (CDCA) as well as the secondary bile acids deoxycholic acid (DCA) and lithocholic acid (LCA).<sup>30</sup> The role that bile acids play in various metabolic disorders owes to its binding with the FXR receptor (nuclear receptor farnesoid X)<sup>31-33</sup> and TGR5 receptor (Takeda G-protein-coupled) present in various organs. TGR5 identified as a cell surface bile acid receptor is also known as GPR131, GPBAR1, GPCR19, BG37; M-BAR (Fig. 1).<sup>34, 35</sup> The TGR5 gene code consists of 993 base pairs, encoding a 330 amino acids protein with the seven transmembrane helices. It is a characteristic feature of GPCRs. The cDNA sequence of hTGR5 has >80% homology with that of bovid, rabbit, and rodent species.<sup>36-38</sup>

TGR5 receptor is expressed in the kidney, liver, heart, lung, muscles, gallbladder, brown adipose tissue, and some selected areas of the CNS.<sup>40, 41</sup> TGR5 receptor gets activated by bile acid-like LCA, DCA, CDCA, and CA. Bile acids promote intracellularly cAMP production in enteroendocrine cell line STC-1 cells that result in GLP-1 secretion via activation of the TGR5 gene expressed in a murine enteroendocrine cell line.<sup>42</sup> Adenylate cyclase inhibitors were used to examine this, and it was discovered that they suppressed bile acid-induced GLP-1 secretion. This



suggested that bile acids regulate insulin secretion in cells by affecting GLP-1 production. The increase in insulin secretion reduces the liver's production of glucose.<sup>43</sup>

In another study, it was proved that TGR5 activation also stimulates insulin secretion via activation of protein kinase A (PKA) and phosphorylation of CREB (CREB) (Hodge et al. 2016). In addition, TGR5 has various other potential roles that include modulation of inflammation, increases in the basal metabolic rate (Fig. 2). Furthermore, published data by Watanabe et.al.<sup>44, 45</sup> suggested that activation of TGR5 might be beneficial for the treatment of diabetes and obesity by increasing the energy expenditure in brown adipose tissue.<sup>46</sup>

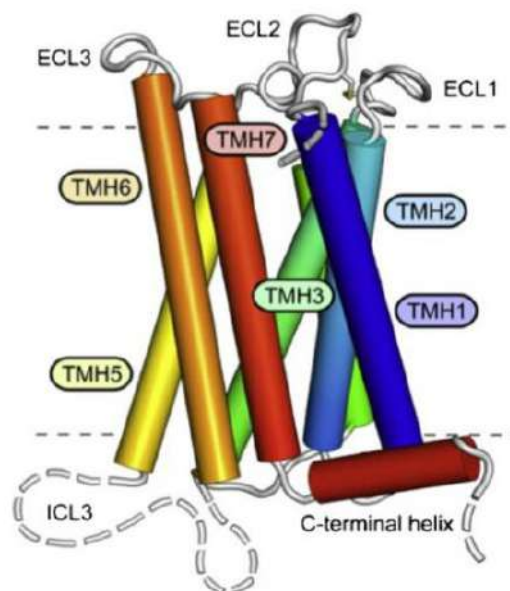


**Figure 1: 3D structure of TGR5**<sup>39</sup>

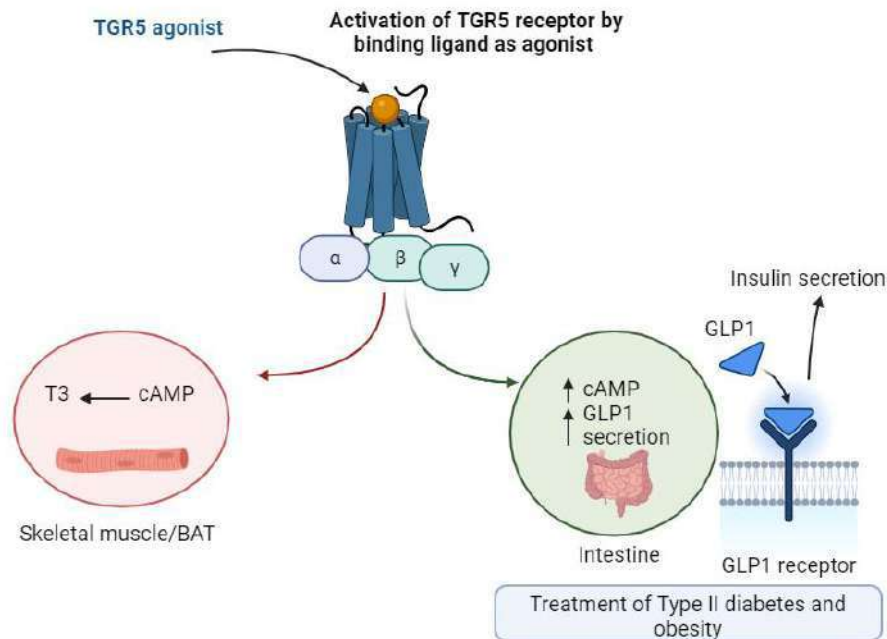


**Figure 2: Role of TGR5**

### 1.3. Advantages of TGR5

- ▶ In search of Type 2 diabetes alternative treatment, there is a recent surge for the therapy which includes increase in secretion of GLP-1 levels for diabetes treatment.
- ▶ The secretion of GLP-I resulted due to activation of TGR5. Thomas et.al. 2009, demonstrated the rise in GLP level in an enteroendocrine cell line. The bile acids role in glucose homeostasis was confirmed.<sup>46</sup>
- ▶ It increases the metabolic rate of muscle and brown adipose tissue that results in an increased metabolic rate. A cAMP-dependent type 2 iodothyronine deiodinase (D2), is induced by administration of bile acids in Brown Adipose Tissue (BAT).
- ▶ It is widely accepted that TGR5 is important target to treat metabolic diseases because of all these positive effects TGR5 has on metabolism. Therefore, TGR5 can be considered as novel target which increases endogenous GLP-1 secretion and simultaneously manage body glucose levels, weight of body and associated complications

#### 1.4. TGR5 interaction with ligand

The TGR5- ligand coupling is believed to be many of the beneficial effects of bile acids, bile acid derivatives such as protecting against obesity, diabetes and reducing inflammation.<sup>47</sup> INT777 is the first semi-synthetic bile acid derivative having high affinity for TGR5 with  $EC_{50}$  0.82  $\mu$ M.<sup>48</sup>

The cryo-EM structure of the TGR5 complex bound to the INT777 molecule (PDB ID: 7CFN) is deposited in RCSB PDB database in 2020 with a 3.0Å resolution using Electron microscopy. There are five heteromeric chains in the TGR5-Chain A, B, G, N and R. Each of which has a sequence length of 394 amino acids, 358 amino acids, 58 amino acids, 128 amino acids and 330 amino acids, respectively.<sup>48</sup> The structure of the INT777-TGR5 complex can be used to study the interactions between other bile acids in TGR5. INT777 reveals the complete binding analysis and showed the presence of interactions such as hydrophobic and Hydrogen bonds. INT777 showed hydrogen bond interactions with active site residues of TGR5 such as Tyr240, Ser247 (bond distance of 2.89Å and 2.69Å respectively). In addition, an active site residue contains Tyr89, Leu244, Leu263, Leu266, Leu166, Leu74, Trp75, Phe96, and Phe161. The binding mode of INT777-TGR5 is depicted in Fig. 3.

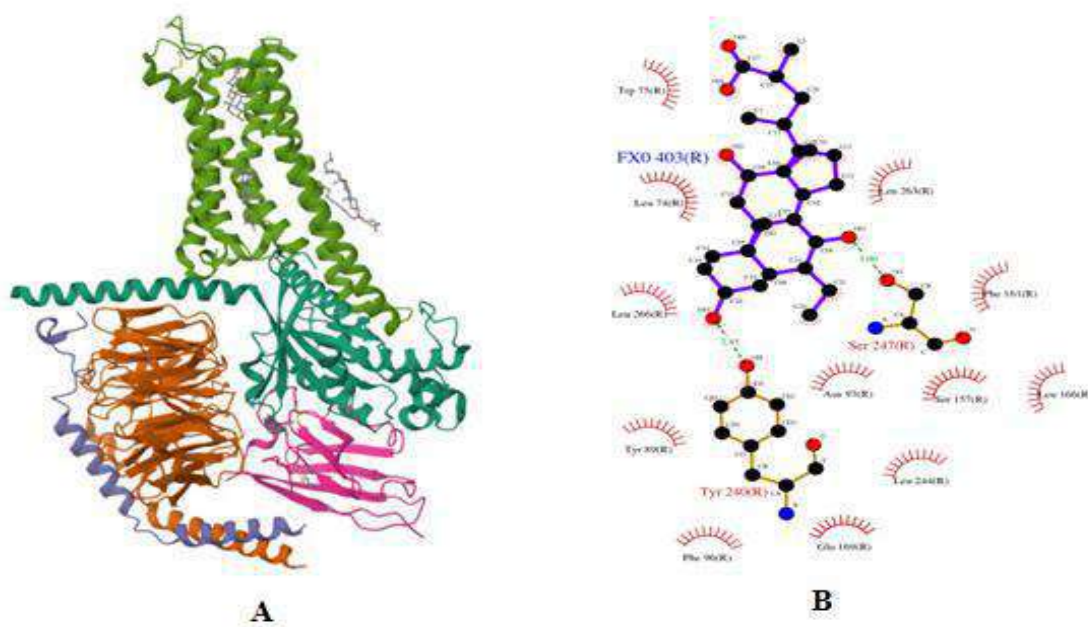


**Figure 3: Structure of TGR5 receptor A) Structure with five heteromeric chains  
B) Ligplot of interaction of INT777 with TGR5**

## 1.5. Drug Discovery

Drug discovery aims at advancing the development of new medicines in order to cure and alleviate many symptoms, as well as treating some untreatable diseases, that still plague humankind to this day. From ideation to development to approval, the discovery process of a new drug involves a number of different phases and processes.<sup>49</sup> Drug discovery uses a variety of ways to find possible new therapeutic entities. To list some, computational techniques are used in conjunction with experimental methods, translational studies, or clinical trials to identify potential new therapeutic entities.<sup>49</sup>

Traditionally, a method of drug discovery would take years, to find effective drugs. As a rough estimate, the cost of drug discovery is estimated to be about US \$2.8 billion, and it takes around 12-15 years for the entire process to be completed.<sup>49</sup>

### 1.5.1. Computational Approach

Computational approaches have become essential part of drug discovery and development process. Also, it improves understanding of chemical systems in different ways, and is considerably less expensive and time-consuming than a laboratory experiment.<sup>49</sup>

Various methods, either individually or in combination, are employed for the design and discovery of drugs. These approaches encompass molecular modelling, ligand and structure based drug designs, screening virtually (VS), molecular dynamics (MD) simulation, as well as considerations of absorption, distribution, metabolism, excretion, and toxicity (ADMET).<sup>50</sup>

Computer Aided drug design (CADD) is largely classified into two methods.<sup>51</sup>

#### ***Ligand-based drug design (LBDD)***

A key aspect of the study involves understanding the impact of a ligand's chemical structure on the biological activity of that ligand. This procedure includes developing Quantitative Structure-Activity Relationship models and employing scaffold or lead hopping strategies. QSAR models seek to establish connections by analysing changes in a ligand's molecular structure and their impact on observed biological activity. Lead hopping is a strategic method in drug discovery, involving

the alteration or substitution of the chemical scaffold of a lead compound to generate new molecules with improved properties.<sup>52</sup>

### ***Structure-based drug design (SBDD)***

It depends on understanding the three-dimensional structures of biological macromolecules, primarily proteins. The goal is to create ligands that can bind selectively and with high affinity to specific protein targets. For this method, receptor structure is needed. NMR and X-ray crystallography are commonly used techniques to determine receptor's structure. Computational methods such as threading and homology modelling can be used if the protein structure is unknown.<sup>53</sup>

#### **1.5.2. Homology Modelling**

During the process of homology modelling, one or more known protein structures are identified that are likely to resemble a query sequence that has been given a homology model. The sequence alignment of target protein and selected templates produced a structural model of target protein. The homology model's quality depends on alignment of sequences and structure of template. From the identification of templates to the alignment and prediction of protein structures, homology modelling incorporates the entire process.<sup>53</sup> The steps involved in Homology Modelling shown in Fig. 4.

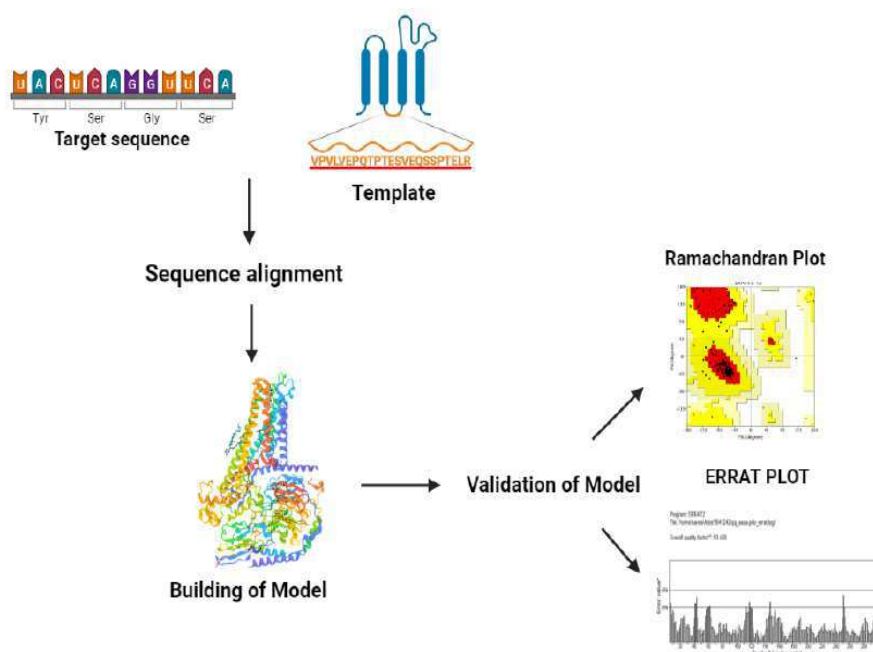


**Figure 4: Homology Modelling**

In our present study, an iterative approach involving virtual screening was utilized to get scaffolds suitable for developing novel TGR5 modulators.<sup>54</sup> Ligand-based drug design, scaffold, and lead hopping are common strategies that researchers use to discover structurally novel compounds. The lead hopping method begins with a known active compound as a query molecule and then leads to a new novel compound that shares properties with the known active compound.<sup>54, 55</sup> The Rapid Overlay of Chemical Structures (ROCS) is a shape comparison program that can be utilized to identify new scaffolds for a given target. The use of ROCS led to the identification of several novel compounds that share structural similarities with known active compounds. Thus, lead hopping is of great interest for lead identification in the drug discovery process.<sup>55</sup>

### 1.6. Coumarin Derivatives

The coumarin (1, 2-benzopyrone class) is versatile molecule that has been assessed for various pharmacological activities like antimicrobial activity, antidiabetic properties, and antioxidant, among others. The coumarin consists of benzene rings fused to the pyrone rings of 2-hydroxy-Z-cinnamic acid. The synthesis of coumarin derivatives involves a variety of methods, each offering unique advantages in terms of effectiveness, specificity, and scalability.

Here's an overview of these methods (Fig. 10).<sup>56, 57</sup>

- *Pechmann condensation*

In the traditional method of coumarin synthesis, known as the Pechmann condensation, phenols undergo reaction with  $\beta$ -ketoesters or  $\beta$ -diketones under acidic conditions (Fig. 5). Numerous catalysts were explored for this reaction, including sulfuric acid, trifluoroacetic acid, phosphorous pentoxide, among others, all aiding in the facilitation of the Pechmann condensation process. This reaction typically proceeds through the generation of an intermediate oxocarbenium ion, followed by intramolecular cyclization to generate coumarin derivatives.

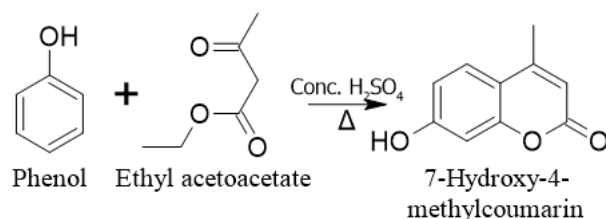


**Figure 5: Pechmann condensation**

- *Claisen condensation:*

The synthesis of coumarin derivative with claisen condensation involves reaction of phenol with allyl alcohol that achieved by employing trifluoroacetic acid (TFA) as a homogeneous promoter (Fig.6).

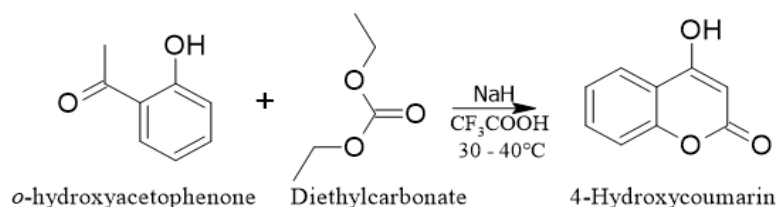


**Figure 6: Claisen condensation**

- *Perkin Reaction:*

The Perkin reaction involved reaction of aromatic aldehyde with acetic anhydride or its equivalent, leading to the cyclization of the resulting  $\alpha$ ,  $\beta$ -unsaturated carboxylic acid intermediate (Fig. 7). Widely used for synthesizing coumarin derivatives with diverse substituents, this method offers versatility.

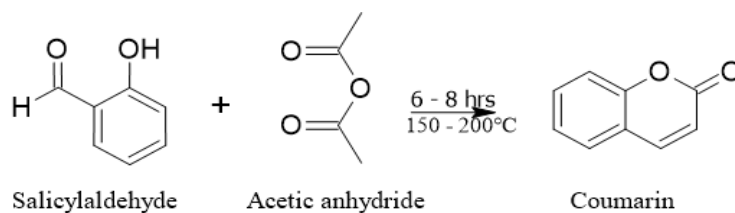


**Figure 7: Perkin reaction**

- *Wittig Reaction:*

Another approach to synthesizing coumarin derivatives is the Wittig reaction, which entails reaction of phosphonium ylide with carbonyl compound, resulting in the

formation of an alkene product (Fig. 8). Subsequent intramolecular cyclization of the alkene intermediate leads to the production of coumarin derivatives.

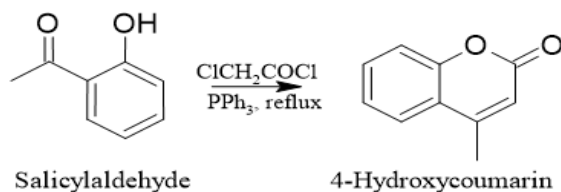


**Figure 8: Wittig reaction**

- *Knoevenagel Condensation:*

The Knoevenagel condensations involve the reaction of an aldehyde or ketone with compound containing a methylene group, such as malononitrile or ethyl cyanoacetate, in presence of base. The reaction requires the inclusion of 2-hydroxy benzaldehydes and a coupling reagent with an active methylene group, conducted under high temperatures. This method is suitable to synthesize coumarin derivatives by utilizing appropriate starting materials.

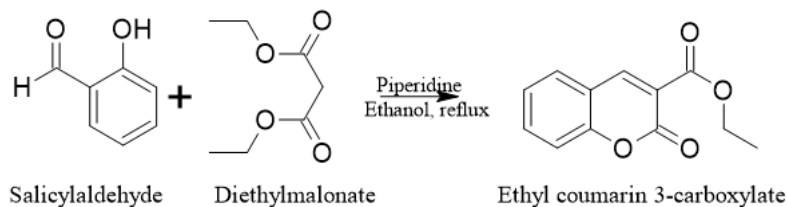


**Figure 9: Knoevenagel Condensation**

- *Microwave-Assisted Synthesis:*

A microwave irradiation method has been used to accelerate coumarin synthesis reactions, resulting in shorter reaction times and greater yields than conventional heating. Microwave-assisted Pechmann and Knoevenagel condensation reactions have been successfully employed for synthesizing coumarin derivatives.



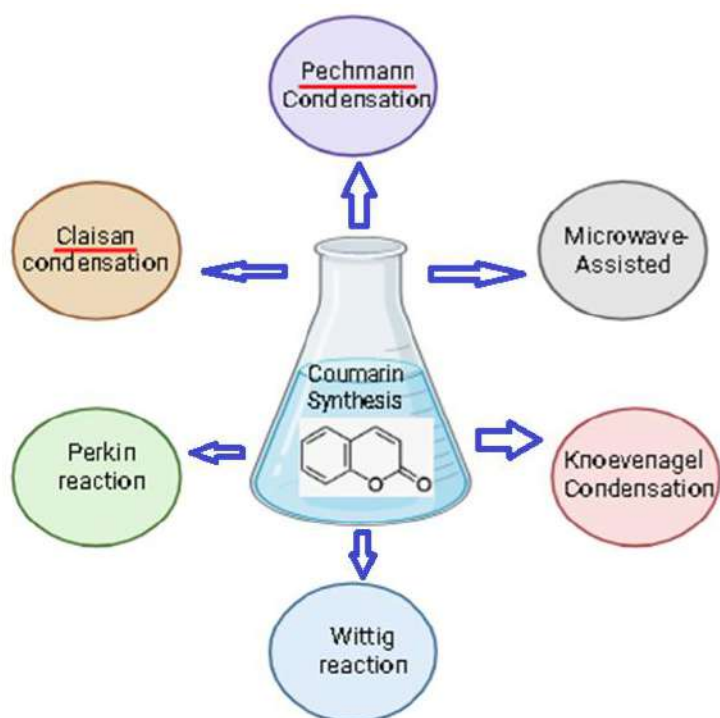


**Figure 10: Reactions mediated synthesis of coumarin**

# LITERATURE REVIEW



## **2. LITERATURE REVIEW**

Literature review is structured into three sections, each delving into TGR5 agonistic effects of natural components sourced from plants<sup>58-60</sup>, semi-synthesized TGR5 agonist, and synthetic alternatives. Steroidal ligands encompass a variety of compounds such as bile salts, bile salt derivatives,<sup>61</sup> 6-hydroxylated bile acids,<sup>63</sup> CA derivative,<sup>64</sup> CDCA acid,<sup>65</sup> oleanolic acid derivatives,<sup>66</sup> etc. Synthetic agonists include nicotinamide,<sup>68</sup> oxadiazole,<sup>69</sup> pyrimidine,<sup>70</sup> Tetrahydrobenzimidazole,<sup>74</sup> thiazole,<sup>75</sup> imidazole<sup>76</sup> etc.

### 2.1. Naturally-occurring TGR5 agonists

This part of the review focuses on plants containing anti-diabetic phytochemicals acting as TGR5 agonists, considering their mechanisms of action.

### 2.1.1. *Chromolaena odorata*

Omotuyi *et al.* investigated TGR5 agonist activity of phytoconstituents derived from *Chromolaena odorata* (*C. odorata*).<sup>58</sup> Docking studies were performed by authors on different phytoconstituents within the homology model of TGR5, yielding 5,7-dihydroxy-6,4-dimethoxyflavanone (1) with dock score of -11.5 kcal/mol and homoesperetin-7-rutinoside (2) with -11.0 kcal/mol dock score. These phytoconstituents demonstrated stronger binding to TGR5 compared to INT-777 (Fig. 11). Animal studies carried out by researchers revealed that the ingestion of phytoconstituents derived from *C. odorata* led to an elevated release of GLP-1 in bloodstream when compared to control. Specifically, there was a 128% increase at 10 mg/kg dose and a 275% increase at 30 mg/kg in GLP-1 levels.

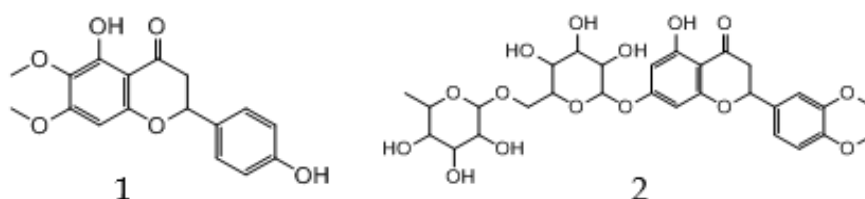


**Figure 11: Flavonoids from *Chromolaena odorata***

### 2.1.2. *Olea europaea*

Genet, C., *et al.*<sup>59</sup> established TGR5 agonist activity of Oleanolic acid (OA), Betulinic acid (BeA) and Ursolic acid (UA) triterpenoids derived from *Olea europaea* leaves. BeA (3) emerged as most potent TGR5 agonist, displaying an efficacy of 83% and an EC<sub>50</sub> of 1.04  $\mu$ M, surpassing other triterpenoids like OA (EC<sub>50</sub> 2.25  $\mu$ M) and UA (EC<sub>50</sub> 2.2  $\mu$ M). The authors investigated the structure-activity relationship (SAR) studies focused on BeA, specifically examining modifications at the 3<sup>rd</sup> position hydroxyl group, the 17-C carboxyl group, and the 20-C alkene group. The study's findings indicated that converting the hydroxyl group to a ketone group resulted in decreased activity (EC<sub>50</sub> 4.71  $\mu$ M) in the formation of compound 4. Genet and colleagues, in their conclusion, underscored the importance of maintaining the hydrogen donor's hydroxyl and carboxylic acid groups. Further alterations to the alkene involved substituting it with an epoxide (5), leading to an EC<sub>50</sub> of 6.91  $\mu$ M (Fig. 12).

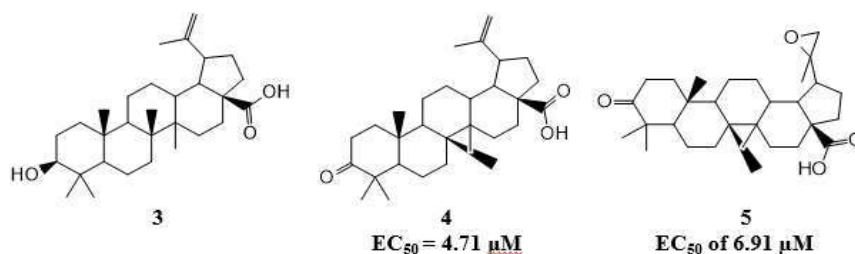


**Figure 12: Triterpenoid extract from leaves of *Olea europaea***

Additionally, Lo *et al.* examined the functional impact of BeA on hTGR5 (CHO) Chinese hamster ovary K1 cells. The study showed that BeA, like LCA, induced a dose-dependent increase uptake of glucose by activating the TGR5 receptor.<sup>60</sup>

### 2.1.3. *Fagonia cretica*

Jafri *et al.*, investigated *Fagonia cretica* extract or it's the GLP-1 secretary activity, and<sup>61</sup> believed to possess anti-diabetic properties. The analysis by authors identified quinovic acid (compound 6) in the extract, as depicted in Fig. 13. Additionally, two glycoside derivatives of quinovic acid were recognized. These displayed notable and specific GLP-1 secretagogue activity in STC-1 cells. The crude extract of *F. cretica*

induced GLP-1 secretion. Importantly, there was a notable increase in TGR5 activity at concentrations of 100  $\mu\text{M}$  of quinovic acid and two derivatives, resulting in increases in cAMP production.<sup>61</sup>

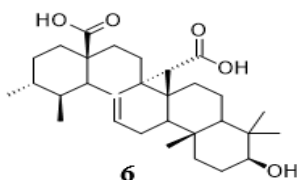


**Figure 13: Quinovic acid from *Fagonia cretica***

## 2.2. Semi-synthesized TGR5 agonist

### 2.2.1. Lithocholic Acid (LCA) derivatives

Sato *et al.*<sup>62</sup> explored the structure activity relationship of TGR5 agonists, comparing them to semi-synthetic bile acids derivatives. They used Luciferase assay in CHO cells expressing hTGR5 to evaluate potency. LCA (7), a derivative of natural bile acids, proved most potent with an  $\text{EC}_{50}$  of 0.58  $\mu\text{M}$ , especially when the steroid nucleus lacked hydroxylation at positions 6, 7, and 12. A semi-synthetic BA derivative was constructed by modification in the main steroidal body and side chain of the molecule. A powerful TGR5 agonist, the body-modified 7-methyl derivative of LCA (8), displayed an  $\text{EC}_{50}$  of 0.076  $\mu\text{M}$ . Authors also tried shortening the acidic side, as in compound 9 ( $\text{EC}_{50}$  10.14  $\mu\text{M}$ ), that further reduced TGR5 activity. LCA derivatives (7, 8) were identified as potent and selective TGR5 agonists, depicted in Fig. 14.

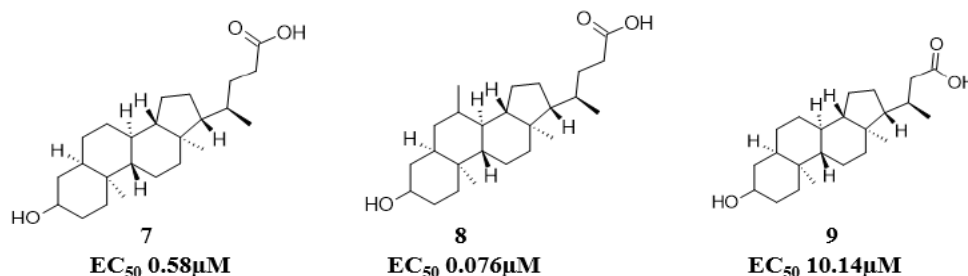


**Figure 14: LCA derivatives**

### 2.2.2. Cholic acid (CA) derivatives

In a different investigation, Pellicciari *et al.*<sup>63</sup> conducted a study involving the integration of 23-methyl and 6R-ethyl groups into the chemical framework of CA (10) for improvisation in its potency, selectivity, and metabolic stability. Within this research, synthesis of 6R-ethyl-23(S)-methylcholic acid (INT-777, 11) was carried out and was subjected to both physicochemical and biological analysis. Further, authors evaluated the impact of compounds on TGR5 activities in hTGR5 transfected CHO cells with measuring their potential to boost luciferase reporter activity; INT-777, with an EC<sub>50</sub> of 0.82  $\mu$ M, emerged as a newly identified potent and selective TGR5 agonist (Fig. 15).

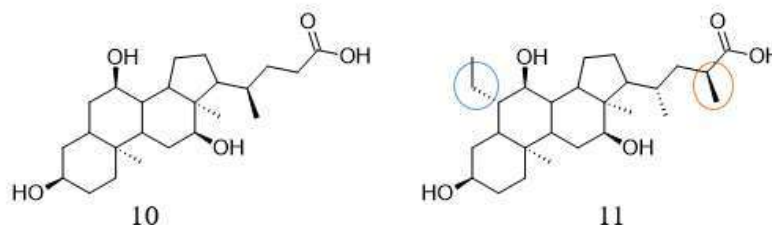


**Figure 15: CA derivatives**

Rosatelli *et al.*<sup>64</sup> conducted Fluorescence Resonance Energy Transfer assays in NCI–H716 cells to further investigate the substitution of C<sub>7</sub> and C<sub>23</sub> in CA on TGR5 ligands. The activation of TGR5 was evaluated by measuring cAMP levels using an FRET assay, with reference compounds INT-777 (11) and CA (10). The TGR5 agonistic activity of C<sub>7</sub> $\beta$ -alkyl and C<sub>23</sub>-modified CA derivatives was scrutinized. The FRET assay identified C<sub>7</sub> $\beta$ butyl-CA (12) and C<sub>23</sub>difluoro-CA (13) as among most selective and potent TGR5 agonists (Fig. 16). The most promising potency was observed with 7 $\beta$ butyl-CA (12), exhibiting EC<sub>50</sub> values of 5  $\mu$ M. additionally, docking studies conducted by authors disclosed presence of hydrophobic pocket at C-7 of BAs within TGR5, in addition to the selective binding pocket.

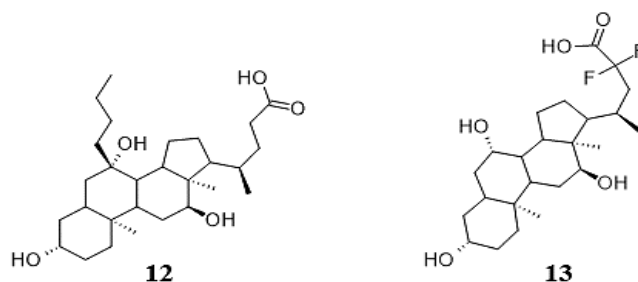


**Figure 16: Cholic acid derivatives**

### 2.2.3. Chenodeoxycholic acid derivatives

A screening of derivatives of chenodeoxycholic acid for their potency as TGR5 agonists was conducted by Nakhi *et al.*<sup>65</sup> The 7<sup>th</sup> position hydroxyl group of CDCA (14) was methylated, resulting in the EC<sub>50</sub> value reduction and increase in potency. In comparison to CDCA, the pyrrolidine analogue (15) showed potency that was ten fold higher, and the 1,3,4-oxadiazole analogue (16) displayed potency that was 70 times greater. Moreover, alterations in the side chain resulted in the creation of analogue 16 containing 1,3,4-oxadiazole, demonstrating significantly enhanced TGR5 agonistic activity in comparison to other derivatives, with an 0.223  $\mu$ M EC<sub>50</sub>. When all modifications were combined, the 7-methylated oxadiazole analogue 17 demonstrated high receptor agonist activity with an EC<sub>50</sub> of 5.6 nM (Fig. 17).

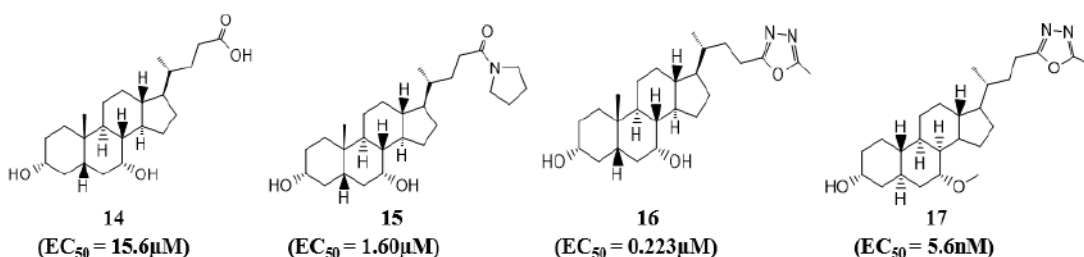


**Figure 17: Derivatives of Chenodeoxycholic acid**

### 2.2.4. Oleanolic acid derivatives

Chen and colleagues<sup>66</sup> extended the research of Genet, C *et al.*, investigating the anti-hyperglycaemic capabilities of the OA derivative DKS26 (18). *In vivo* administration of 100 mg/kg DKS26 resulted in decreased plasma glucose and GSP levels, improved oral glucose tolerance, and elevated levels of plasma insulin. Additionally, DKS26

was examined for its influence on intestinal L cells, specifically NCI-H716 cells undergoing endocrine differentiation. *In vitro* experiments indicated that treatment with 10  $\mu$ M DKS26 elevated cAMP, GLP-1 and levels of phosphorylated PKA. In summary, DKS26 (Fig. 18) was found to elevate GLP-I and also expression *in vivo* by modulating cAMP/PKA pathway, thereby contributing to hypoglycaemic and islet-protective effects.

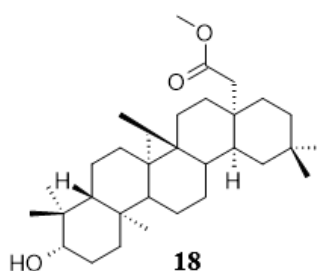


**Figure 18: OA derivative DKS26**

#### 2.2.5. 6 $\alpha$ -hydroxylated bile acid derivatives

Makki *et al.*<sup>67</sup> recently explored the impact of oligofructose (OFS) on gut microbiota and the generation of 6 $\alpha$ -hydroxylated bile acids (hyodeoxycholic acid 19) (Fig. 19), leading to increased TGR5-GLP1 receptor activity. This enhancement is advantageous for weight reduction and improved metabolism in mice. For determining the OFS effect on bile acid production directly, primary bile acids from mouse gallbladders were cultured in a growth medium containing output from a Western Style Diet (WSD) and WSD-OFS diet. Secondary bile acids produced by bacteria from OFS fed mice were more efficient than those from WSD-fed mice. The conclusion drawn from the present study was that oligofructose enriches bacteria responsible to produce 6 $\alpha$ -hydroxylated bile acids.

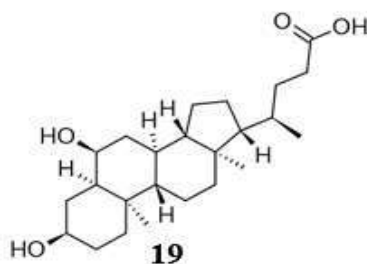


**Figure 19: Hyodeoxycholic acid**



## 2.3. Synthetic TGR5 agonists

### 2.3.1. 2-Phenoxy nicotinamide derivatives

Martin and colleagues conducted a high-throughput screening using collection from Roche's proprietary compound to identify new small molecule agonists for TGR5.<sup>68</sup> In hit-to-lead development, compound 20 displayed 0.396  $\mu\text{M}$   $\text{EC}_{50}$  and 2.02  $\mu\text{M}$  against murine and human receptors, respectively. Authors further explored SAR by investigating pattern of substitution of the phenoxy side chain. Important SAR points are summarised below:

In the study, achievement of TGR5 agonist activity was demonstrated by incorporating a halogen i.e. dichloro at 2, 5 position at phenoxy group, delivered the most potent compound 21 ( $\text{hEC}_{50}$  = 0.010  $\mu\text{M}$ ). Modification in the Tetrahydroquinoline side chain in compound 21. Modifications such as indole and benzoazepine of tetrahydroquinoline moiety resulted in compounds that lack activity with  $\text{hEC}_{50}$  1.71  $\mu\text{M}$  and 3.56  $\mu\text{M}$  respectively. The introduction of fluorine at positions 6 (21a) and 7 (21b), 6,7 difluoro (21c), 6 methyl 8 fluoro (21d) at Tetrahydroquinoline side chain of compound 21 led to a reduction in compound potency. Notably, switching to tetrahydroquinoxalines side chain in compound 22 showed  $\text{hEC}_{50}$  0.062  $\mu\text{M}$ . Further substitution of free NH group from 22 with cyclopropyl (22a,  $\text{hEC}_{50}$  0.010  $\mu\text{M}$ ) displayed the highest reactivity, as depicted in Fig. 20.

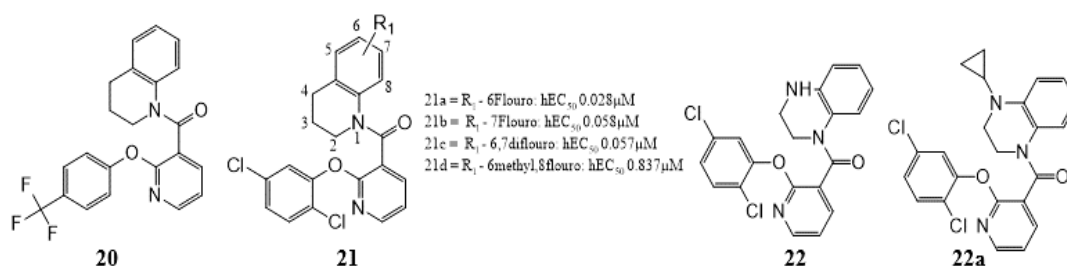


**Figure 20: 2-Phenoxy nicotinamide derivatives**

### 2.3.2. Oxadiazole derivatives

Expanding on the foundation laid by Takeda's compounds (23) and their 3, 4, 5-trisubstituted 4, 5-dihydro-1, 2, 4-oxadiazole core, Zhu, J., *et al.*<sup>69</sup> unveiled a class of potent TGR5 agonists. Zhu *et. al* investigated various heterocyclic cores including

triazole, imidazole and oxadiazole followed by optimisation of the potent TGR5 agonist.<sup>32</sup> The SAR study of newly designed TGR5 agonists were conducted *in vitro* by authors as follows (Fig. 21).

Compound 24a ( $EC_{50} > 10$  nm) with triazole ring completely lost activity, compound 24b with Oxadiazole scaffold ( $EC_{50}$   $79 \pm 0.009$  nm) was more potent than imidazoline ( $EC_{50}$   $1.461 \pm 0.341$   $\mu$ M). Researcher found compound 26b most potent and selected for further exploration. Authors turned their focus on phenyl ring attached to oxadiazole ring. Substitution of electron-withdrawing (chloro) and donating groups at various positions on phenyl ring were tried. Results revealed 24c ( $EC_{50}$   $0.015 \pm 0.001$   $\mu$ M) as most potent with 2 furanyl group attached to phenyl ring. Further focus turned to 4-phenylpyridine moiety. Removal of fluorine from phenyl ring (24c) resulted in loss of activity. This revealed that weak electron group like fluorine is important for optimum activity. Introduction of di or trifluoro substitution leads to enhanced activity. At last, 2, 6 difluoro (compound 24d) on phenyl ring substitution retained most potency ( $EC_{50}$   $15 \pm 0.001$  nm). At last, modification of pyridine became important point of the study.

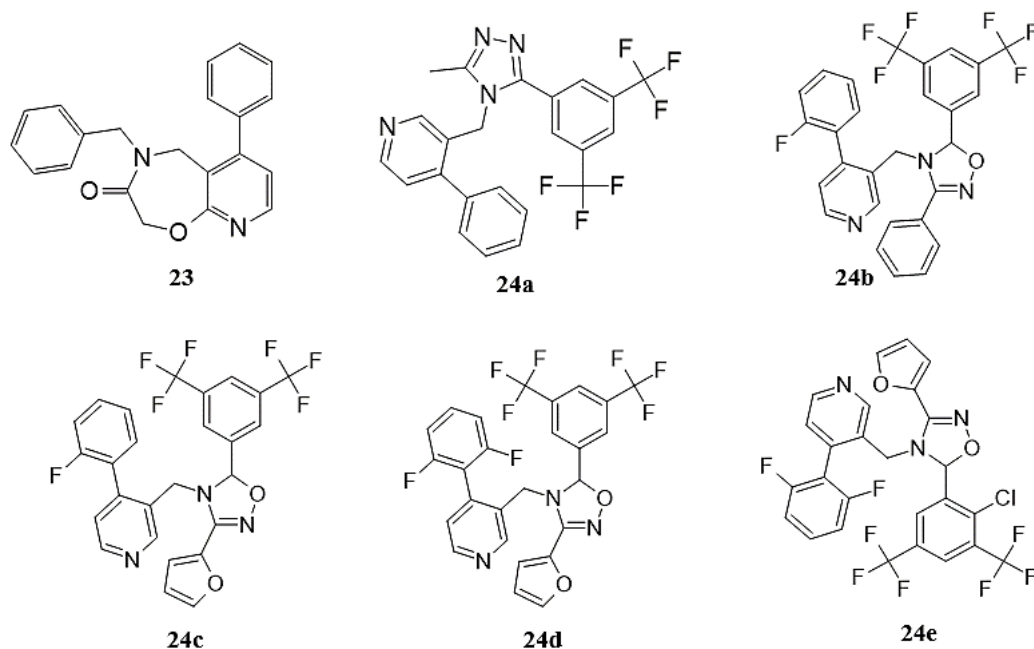


**Figure 21: Oxadiazole derivatives**

### 2.3.3. 4-Phenoxy nicotinamide derivatives

Inspired by structural similarities between Tekeda Corp (23) and Roche Corp (21), Duan, H., *et al.*<sup>70</sup> investigated a novel scaffold i.e. (pyrimidine) to introduce variations. Author explored the potential role of central aromatic ring, for which different analogues were conceptualized and synthesized by incorporating either one (25a) or two nitrogen (25b) at different positions in the core ring as follows (Fig. 22).

Replacement of core aromatic ring as morpholine (25a') or thiomorpholine (25b') decreased the TGR5 activity as compared to parent compounds. A cyclopropyl group was introduced at 4<sup>th</sup> position of central part of compound 25b" and 25a", which yielded potent compounds with  $2.9 \pm 0.43$  nM and  $1.5 \pm 0.21$  nM EC<sub>50</sub> values on hTGR5, respectively. Larger alkyl substituent's resulted in compounds with poor agonistic activity. The authors concluded from the above studies that the 4-phoxynicotinamide derivatives were superior to the 4-phoxypyrimidine 5-carboxamides in terms of TGR5 activation. Further author turned their attention toward upper phenoxy moiety modification. Mono and di substitutions were tried on phenoxy moiety with chloro (25c), methyl (25d) and 2, 5 dimethyl groups (25e).

The most potent among them, was compound 25e with hTGR5 EC<sub>50</sub>  $0.72 \pm 0.08$  nM (Fig. 22). *In vivo* studies conducted by authors demonstrated that this compound induced dose-dependent GLP-1 secretion and reduced levels of blood sugar in oral glucose tolerance test. In comparison to control, oral administration of compound 25 at three doses (25, 50, and 100 mg/kg) resulted in increases of 31%, 96%, and 282% in plasma GLP-1 levels.

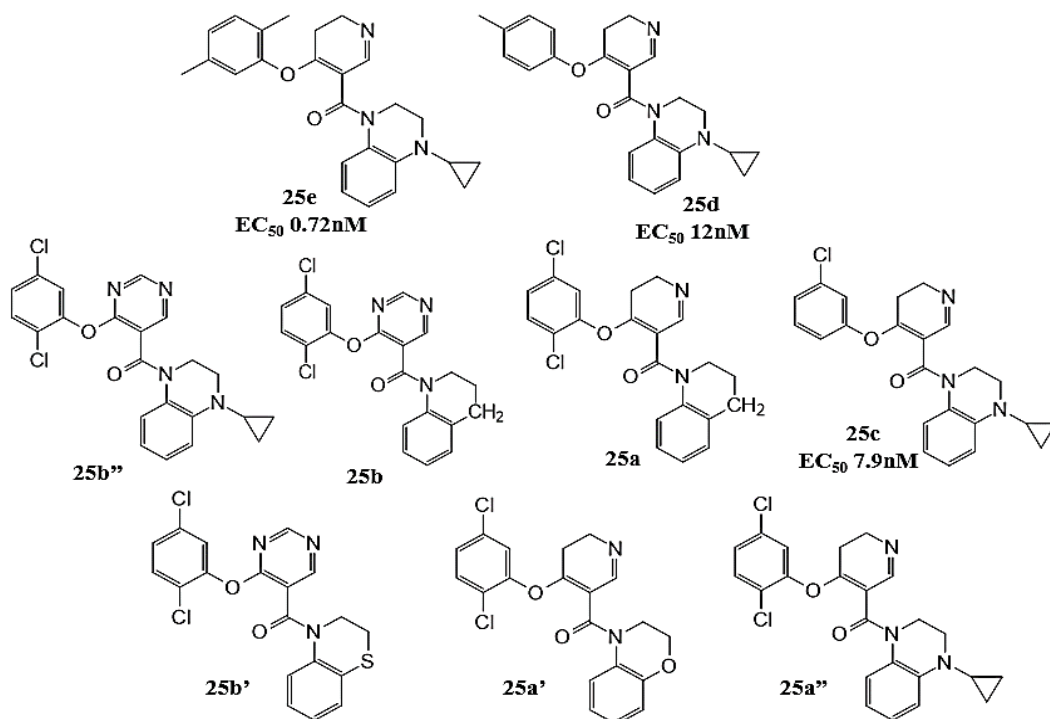


**Figure 22: 4-phenoxy nicotinamide-5-carboxamide derivatives**

#### 2.3.4. Pyridine derivatives

Continuing with their previous work<sup>69</sup>, Zhu and colleagues directed their attention to the 4-phenyl pyridine scaffold found in compounds 21 and 23.<sup>71</sup> consequently, the initial approach by researchers involved opening oxazepine ring of compound 23 and introducing an additional substituent on amide chain to alter the overall structure. A (CRE)-driven luciferase assay in HEK293 cells were carried out by the authors to study SAR by varying the nature of substitution as follows.

Introduction of alkyl groups such as methyl resulted into moderate potency with  $EC_{50}$   $0.91 \pm 0.21$   $\mu$ M (compound 26a). Alteration of substitution to ethyl group showed decreased activity with  $EC_{50}$   $1.27 \pm 0.58$   $\mu$ M (compound 26b). Authors also electron withdrawing and electron donating substitutions on amide group but it resulted in diminished activity of all the resulted compounds. Substitution with phenyl ring improved the  $EC_{50}$  value to  $0.35 \pm 0.19$   $\mu$ M (compound 26c) and activity further increased with substitution of heterocyclic ring. 3-thienyl substituted compound 26d ( $EC_{50}$   $0.12 \pm 0.02$   $\mu$ M) was most potent in the series (Fig. 23).

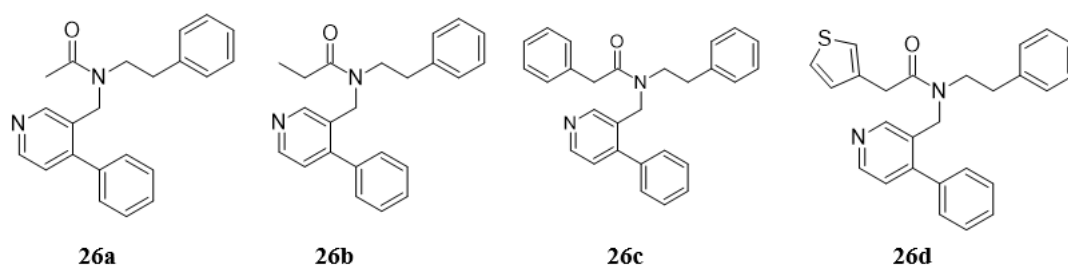


**Figure 23: 4-Phenyl pyridine derivatives**

In another study, Zou *et al.*<sup>72</sup> identified potential TGR5 agonist (27), which demonstrated an  $EC_{50}$  of 2.3 nM against hTGR5 (Fig. 24). This discovery led to the creation of a double-ring structure attached to the phenoxy moiety and this structural alteration was suggested to be linked to an increased affinity for TGR5 by the authors.

Benzo fused naphthyl, quinolyl 5-benzofuranyl analogues were synthesized and examined for ability to activate TGR5 by authors. Benzo1-naphthyl derivatives 28a ( $EC_{50}$   $17 \pm 3.6$  nM) were found to have better potency as compared to Benzoquinoyl 28b ( $EC_{50}$   $40 \pm 9.6$  nM). A slight increase in potency was observed by addition of 5-benzofuranyl to the phenoxy moiety  $EC_{50}$   $10.7 \pm 2.4$  nM (compound 28c). According to the results, benzofuran may enhance the binding affinities of compounds with its oxygen atom. Furthermore, the Author explored the effects of substitutions on the benzofuran ring of compound 28c at positions 2 and 3.

The study resulted in the discovery of derivative with 6-benzofuranyl and chloro atom at 2<sup>nd</sup> position of phenoxy ring (compound 28d) showed improved in the activity with  $0.28 \pm 0.05$  nM and  $0.92 \pm 0.05$  nM  $EC_{50}$  values for hTGR5 and mTGR5 respectively. Authors also conducted an OGTT study and found 33% reduction in blood glucose area under curve after administration of 28 (50 mg/kg) orally which was tested at 120 minutes.

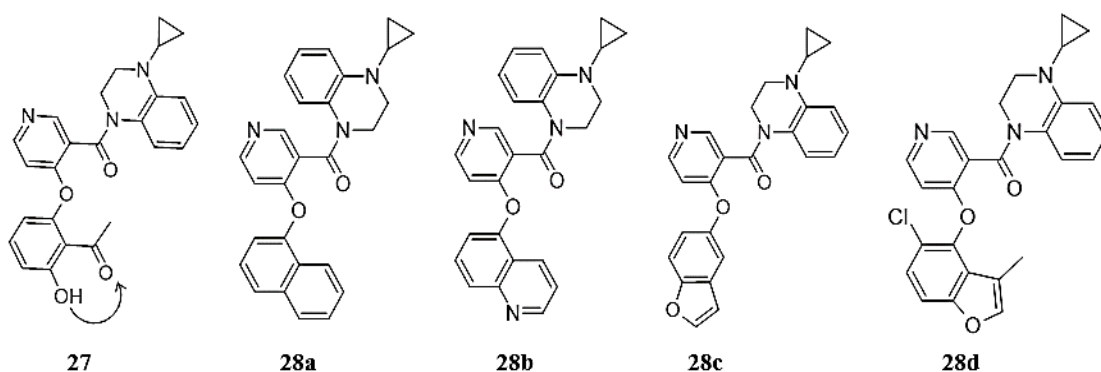


**Figure 24: 4-Benzofuranyloxynicotinamide derivatives as TGR5 agonists**

### 2.3.5. Thiazole derivatives

Chen and colleagues conducted another study in which they designed and evaluated a series of 2-Phenoxy-nicotinamides (21) as TGR5 agonists, demonstrating good potency, selectivity, and favourable pharmacokinetic profiles. Various derivatives with scaffolds, including pyrazoles (29a), triazoles (29b), and thiazoles (29c), were designed and evaluated by luciferase assay in HEK293 cells to identify potency. *In vitro* activity and variation in structures for all three scaffolds were studied by authors as follows.

Various electron donating and electron withdrawing substitution at phenyl ring attached to pyrazole scaffold showed no activity in luciferase assay. Compound 29a' (3-methoxy group on phenyl) showed moderate activity, with a hEC<sub>50</sub> 129 nM. 1, 2, 3 triazole derivatives with dichloro and methoxy (29b') substitution on phenyl ring was explored and found to be inactive in the assay for TGR5 agonistic activity. Further, 2-methyl-thiazole series with substitution of chloro, bromo, methyl at 2, 5 position of phenyl ring attached to thiazole was evaluated for activity. Out of all compounds evaluated 29c' and 29c'' were found to be active with hTGR5 EC<sub>50</sub> 1.1 ± 0.07 nM and 0.97 ± 0.15 nM respectively (Fig. 25).<sup>73</sup>

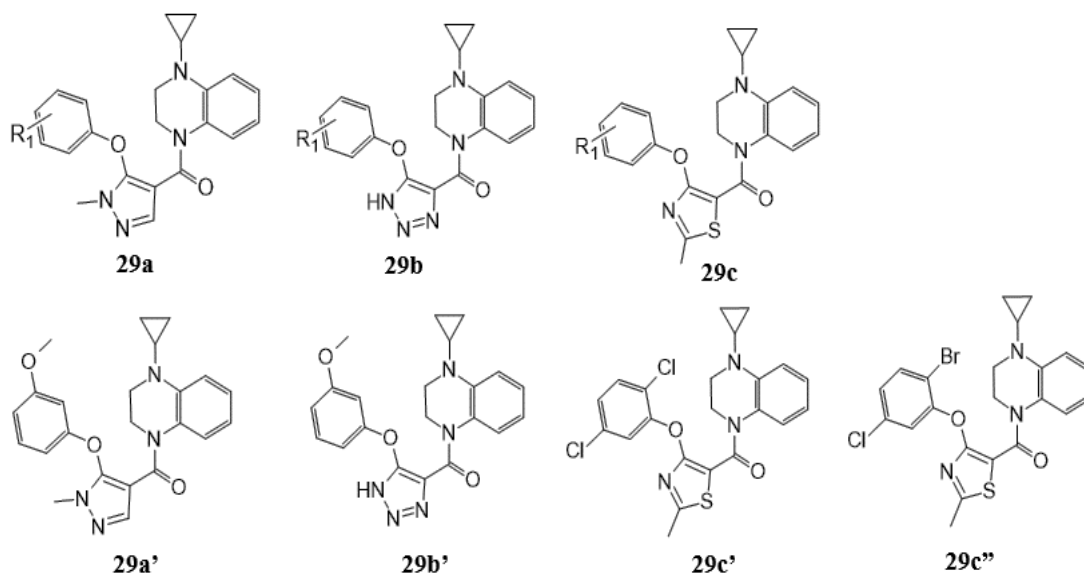


**Figure 25: Thiazole derivative as TGR5 agonist**

### 2.3.6. Benzimidazole derivatives

Zhang *et al.*<sup>74</sup> uncovered Tetrahydrobenzimidazoles scaffold (30) as a fresh and potent series of TGR5 agonists. In the process of optimizing lead compound, author studied SAR by studying substitution pattern on ring A and B (30). Substitution of 3, 4-dimethoxy (R<sup>1</sup>) on Ring A provides optimal TGR5 agonistic activity. Even lipophilic linker S adjacent to Ring A (R) delivered potent TGR5 agonist (30a) with EC<sub>50</sub> of 0.16  $\mu$ M in STC-1 cells. Replacing S with polar substituent's like O and NH resulted in loss in demolished activity (compound 30b) with EC<sub>50</sub> of 5.68  $\mu$ M. Polar group substitution on ring B (R<sup>2</sup>) was explored. CN substitution on phenyl group gave analogue 30b with EC<sub>50</sub> of 290 nM in STC-1 cells. Further, incorporating more polar carboxylic acid (30c) or tetrazole group (30d) produces analogue with EC<sub>50</sub> 6.08  $\mu$ M and 2.06  $\mu$ M in STC-1 respectively (Fig. 26).

An optimized lead compound 30d with TGR5 activity was identified by researchers and further evaluated *in vivo* for OGTT and gall bladder filling capability.

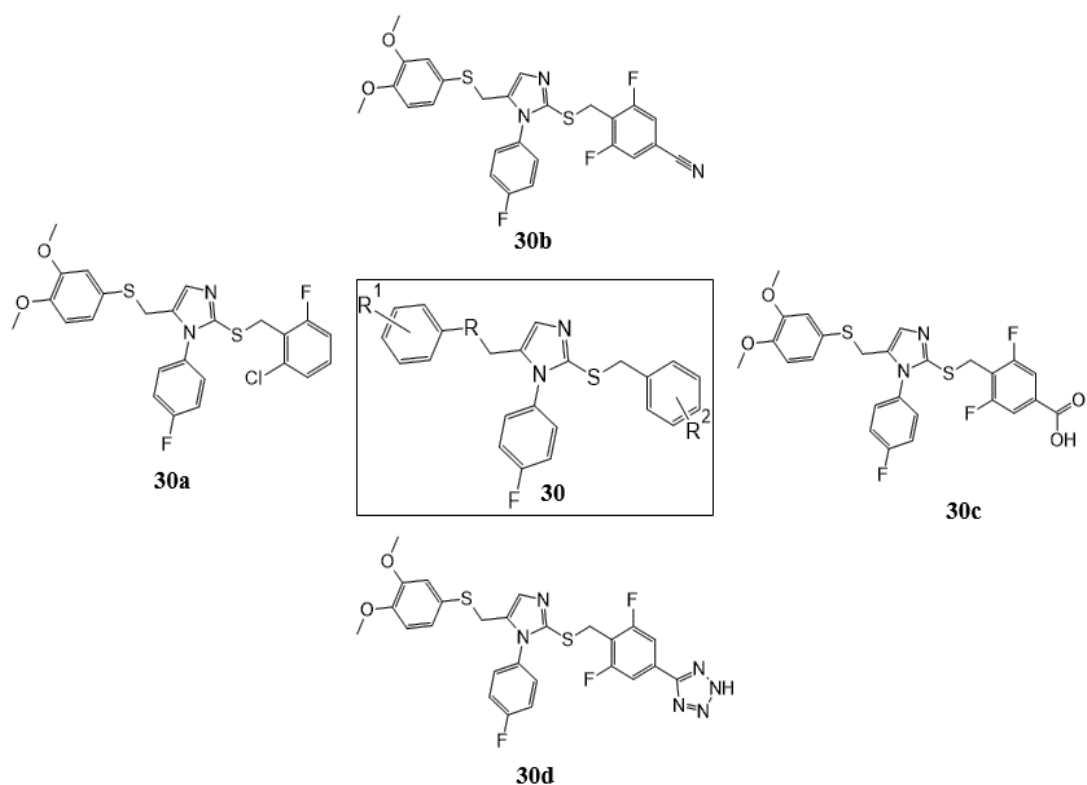


**Figure 26: Tetrahydrobenzimidazoles derivative**

### 2.3.7. Imidazole derivatives

In their pursuit of discovering novel and selective TGR5 agonists, Agrawal and colleagues identified imidazole derivatives.<sup>75</sup> To design new agonists, authors designed homology model of TGR5 receptor and modelling studies concluded that aryl group at the end 31 important from attachment point of view in the receptor pocket. Thus, exploration of SAR for designed compounds revealed that adding linker oxygen between the terminal phenyl ring and heterocyclic group leads to identification of numerous potent compounds. Addition of polar heterocyclic substitution on terminal phenyl ring were tried such as pyrrole (31a), pyrazole (31b), triazole (31c) that produce compounds with EC<sub>50</sub> 7.8 nM, 19.6 nM and 16.8 nM respectively indicating that nitrogen containing heterocycle induce a positive activity.

Notably, among these compounds, compound 31d (EC<sub>50</sub> 0.057 nM) incorporating an imidazole substituent, emerged as most potent TGR5 agonist (Fig. 27). The effectiveness of imidazole derivative in reducing glucose levels was demonstrated through orally administered OGTT. *In vitro* studies included luciferase



assays conducted in TGR5 over-expressing CHO K1 and NCI-H716 cells in a human GPBAR1 assay. The findings revealed that compound 31d, with an EC<sub>50</sub> of 57 pM, corresponds to hTGR5, while the mTGR5 EC<sub>50</sub> is 62 pM.

In another study, Zhou and colleagues<sup>76</sup>, designed and synthesized series of imidazole 5-carboxamide derivatives. Attached amide at 2<sup>nd</sup> position of imidazole ring and phenylethyl at 1<sup>st</sup> position generate numbers of derivatives. The effectiveness of imidazole derivative in reducing glucose levels was demonstrated through GLP1 assay and OGTT test. The finding revealed that compound 31e with hTGR5 EC<sub>50</sub> 6.8 ± 0.43 nM and compound 31f with EC<sub>50</sub> 9.5 ± 0.61 nM in *in vitro* biological evaluation (Fig. 27).

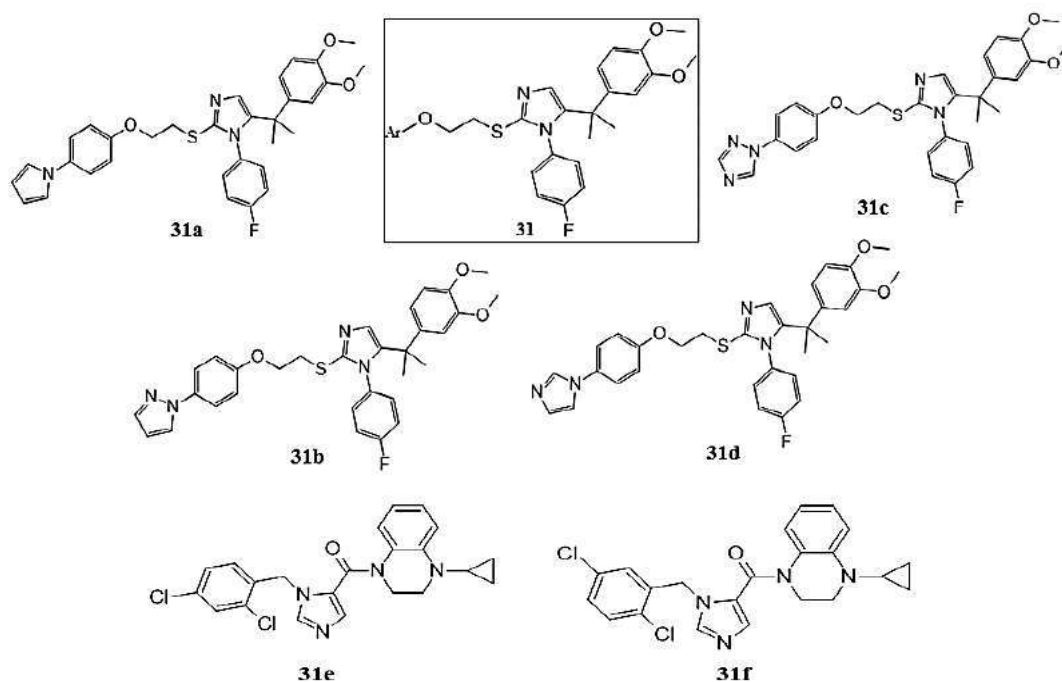


**Figure 27: Imidazole derivatives**

### 2.3.8. Triazole derivatives

Continuing docking studies in homology model of TGR5<sup>75</sup>, Agrawal *et al.*, hypothesized that introducing an amide linker in 32 could improve binding affinity and facilitate development of novel, potent TGR5 agonists. To assess the impact of amide linker and substituent's several compounds were synthesized, and evaluated for TGR5 agonistic activity (Fig. 28). Substitution of amide linker in imidazole gave compound 32a with hTGR5 EC<sub>50</sub> 16 nM. Different derivatives of imidazole ring were

synthesized and evaluated. Compound 32b, heteroaryl fused system attached to amide linker to the terminal end, found to be less potent with EC<sub>50</sub> 88 nM.

Further, the substitution of imidazole ring with a triazole (32c) led to creation of innovative 2-mercapto-triazole derivatives with EC<sub>50</sub> 25 nM and clogP value (2.92) of its make it ideal drug for oral administration. Additionally, Schrodinger's Glide program to access the binding ability of 32c in the putative pocket of TGR5 homology model.

The piperazine ring, fluorenyl group from 32c fitted best in the binding pocket with pi-pi interaction and hydrogen bonding.<sup>77</sup>

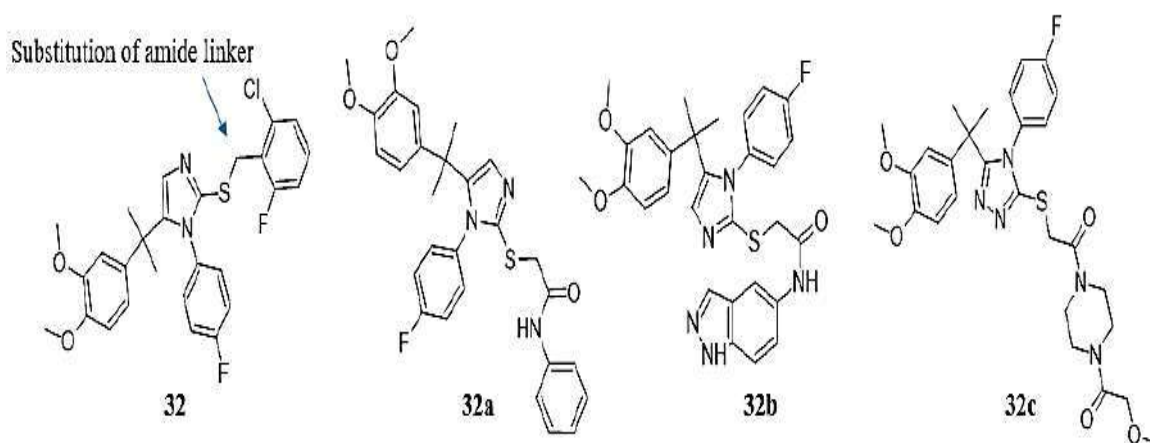


**Figure 28: 2-mercapto triazole derivatives**

### 2.3.9. Pyrimidine amide derivative

Tetrahydropyrido[4,3-d]pyrimidine analogues were derived through high-throughput screening (HTS) of new class of collection compounds from Pfizer as a hit by Piotrowski and group.<sup>78</sup> SAR was explored for compounds into three fragments i.e. A part –2-substitution of pyrimidine, B part- acyl linker and C part- aryl group (Fig. 29). Part A: Substitution of ether, alkyl, or alkylamino, groups was tried at C-2 of pyrimidine core. Alkylamino substitution was found to be favourable for the activity (compound 33a).

Part B: A change to the linking ethylene decreased the potency of compounds.

Part C: Author explored aryl group for substitution in larger extends. Various substitutions like methyl (33b), ethyl (33c), methoxy (33d), trifluoromethoxy (33e) at para position of aryl group.

All designed compounds were demonstrated *in vitro* using cAMP assays and compound 32e was found to be most potent with hTGR5 EC<sub>50</sub> 2.3 ± 1.5 nM (Fig. 29).

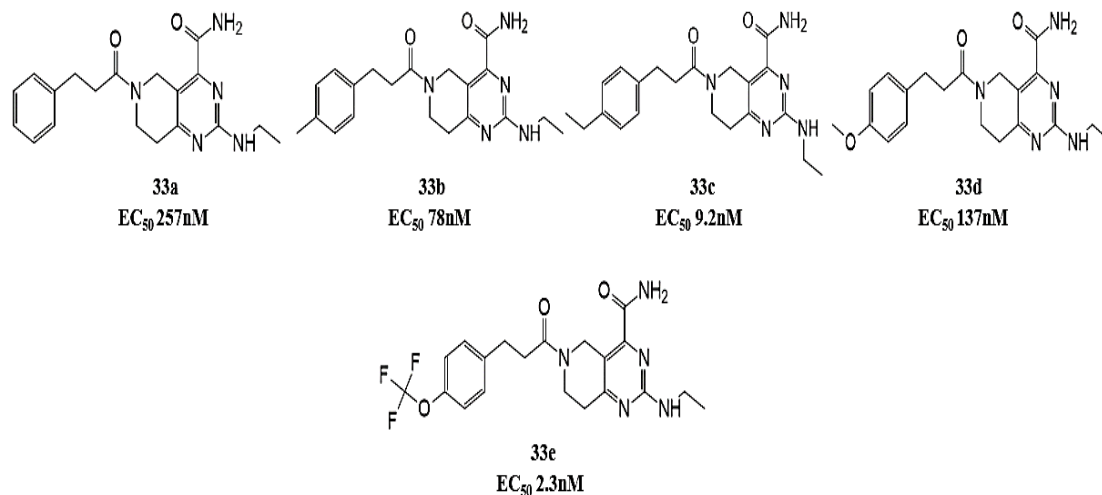


**Figure 29: Tetrahydropyrido[4,3-d]pyrimidine amide derivative**

### 2.3.10. Isooxazole derivative

Budzik, B. W. and colleagues<sup>79</sup> conducted HTS on GSK proprietary compound collection, leading to identification of isooxazole scaffold (34) as starting point for designing and optimizing a new series with improved potency. Author explored SAR that revealed various substitutions on amide phenyl ring at *ortho*, *meta*, and *para* positions, were tried. The result revealed that substitution at *para* position (compound 34a) is most preferred over *ortho* and *meta*. *Para* Substitution with chloro, methyl group is preferred over methoxy group. Compound 34a with *para* chloro substitution on amide phenyl ring demonstrated pEC<sub>50</sub> 7.5.

Further, Variations of substitution on the isoxazole phenyl ring was explored. *Ortho*, *meta* and *para* substituted set of compounds were designed and tested for potency. The results revealed that *meta* and *ortho* substitution is preferred over *para* substitution on isoxazole phenyl ring. Through various optimizations in this series, researchers discovered most potent compound, compound 34b and 34a, with a pEC<sub>50</sub> of 9.0 and 7.5 respectively.

Thus, they identified novelty in 3-aryl-4-isoxazolecarboxamides series of agonists of G-protein-coupled TGR5 receptor (Fig. 30).

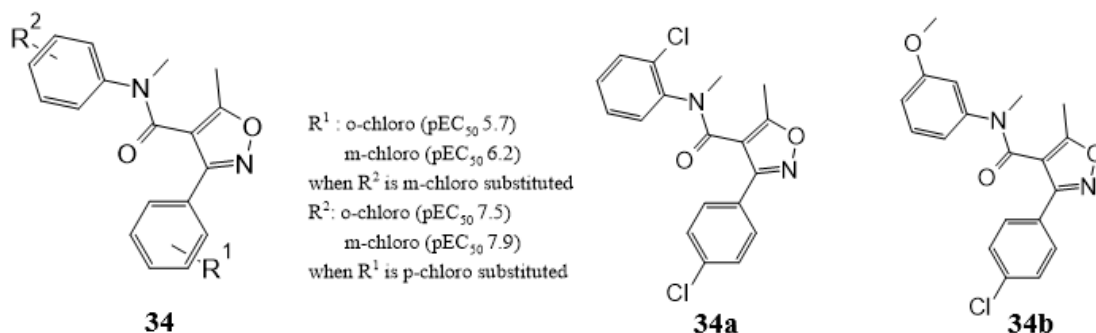


**Figure 30: 3-aryl-4-isoxazolecarboxamides derivatives**

Throughout all reviewed synthetic compounds, the carboxamide derivatives played a key role in achieving the lowest  $EC_{50}$  values. Furthermore, various natural and semi synthetic derivatives of bile acid were reviewed along with the synthetic TGR5 agonists. Betulinic acid (3) potent natural TGR5 agonist exhibited an efficacy of 83% and an  $EC_{50}$  of 1.04  $\mu$ M. In combination with all modifications in semi synthetic compounds, 7-methylated oxadiazole analogues of chenodeoxycholic acid (15) exhibited high receptor agonist activity.

#### 2.4. Coumarin as Antidiabetic

Over the years, the versatility of coumarin and its derivatives gained considerable attention. These properties include antimicrobial, antiviral, anticancer, anti-hyperlipidemia, antioxidant, anti-inflammatory, anti-Alzheimer etc. Coumarin affects different targets associated with diabetes by inhibiting  $\alpha$ -glucosidase and activating PPAR- $\gamma$ , etc. potentially improving symptoms linked to diabetes.<sup>80</sup>

*As  $\alpha$ -Glucosidase inhibitor:*  $\alpha$ -glucosidase inhibitors such as acarbose frequently trigger gastrointestinal adverse effects like nausea and vomiting. Consequently, researchers have investigated alternative compounds for their potential as antidiabetic agents. Among these alternatives are derivatives such as coumarin-hydrazone hybrids, 3-aryl coumarins, coumarin-triazole hybrids, and coumarin-1, 2, 3-triazole-acetamide hybrids, which have shown effectiveness in inhibiting the  $\alpha$ -glucosidase enzyme.

Tariq *et al.*<sup>81</sup> synthesized various coumarin-hydrazone hybrids and tested for its  $\alpha$ -Glucosidase inhibitor activity. Out of all compounds, compound 35 showed significant IC<sub>50</sub> values ranging between 2.39 -57.52  $\mu$ M (Fig. 31).

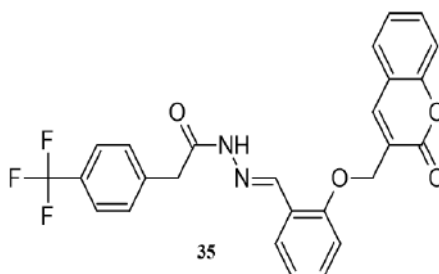


**Figure 31: Coumarine-hydrazone derivative**

Khouzani and collaborators developed and produced derivatives of coumarin-1, 2, 3-triazole-acetamide with the aim of assessing their antidiabetic potential. The *in vitro*  $\alpha$ -glucosidase testing of these compounds revealed inhibitory activity for all of them.

Furthermore, Xu *et al.*<sup>82</sup> synthesized various coumarin derivatives by combining substituted cinnamic acid with 4-hydroxycoumarin and 7-hydroxycoumarin, and then assessed their ability to inhibit  $\alpha$ -glucosidase. The findings indicated that a majority of synthesized derivatives presented noteworthy inhibitory effects on  $\alpha$ -glucosidase. Of particular interest were compound 36, which displayed most potent inhibition, with IC<sub>50</sub> values 12.98  $\mu$ M (Fig. 32).

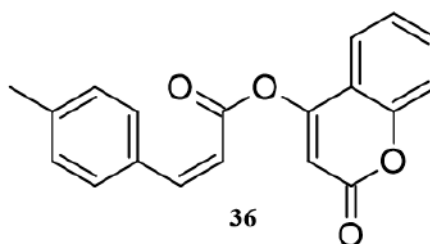


**Figure 32: Cinnamic acid-coumarin hybrid derivative**

Zhang and co-authors<sup>83</sup> developed potent coumarin derivatives that integrate oxime ester functionality, aiming to serve as inhibitors of  $\alpha$ -glucosidase. Of particular note, compound 37, which contains a bromine substituent at 7<sup>th</sup> position of coumarin,

displayed remarkable inhibition against  $\alpha$ -glucosidase. This compound, created oxime linkage between coumarin and cinnamic/benzoic acid, was engineered to generate novel  $\alpha$ -glucosidase inhibitors. Compound 37 demonstrated an  $IC_{50}$  value of  $2.54 \pm 0.04 \mu M$ , significantly lower than the  $IC_{50}$  value of  $640.57 \pm 1.13 \mu M$  observed for Acarbose (Fig. 33).

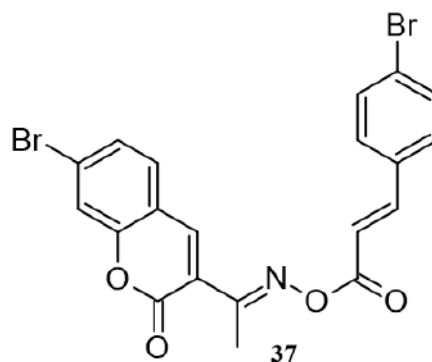


**Figure 33: Coumarin derivative with oxime ester**

*AGEs (advanced glycation end products) inhibitory activity:* Formation of AGEs played a pivotal role in development of diabetes. Consequently, targeting inhibition of AGE formation has become a therapeutic strategy for managing diabetes and its complications. Compounds like 3-(4'-benzoyl amino-phenyl) coumarin derivative (38)<sup>84</sup> and 3-aryl coumarin are being investigated for their potential in this aspect.

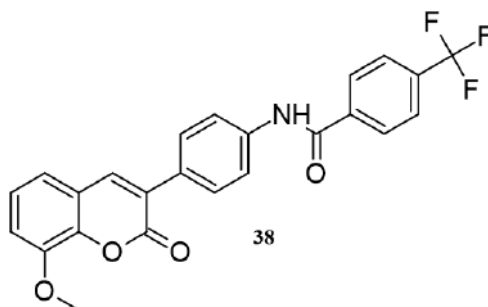


**Figure 34: 3-(4'-benzoyl amino-phenyl) coumarin derivative**

In summary, coumarins and its derivatives exhibit potential as candidates for anti-diabetic agents. However, further investigation is necessary to develop a promising anti-diabetic drug based on coumarin structures as TGR5 agonist.

# RATIONAL, AIM AND OBJECTIVE



## **CHAPTER 3**

### **3. RATIONALE, AIM AND OBJECTIVE**

#### **3.1. Rationale**

Type II Diabetes, a chronic condition characterized by inadequate insulin use and resistance. Many current treatments strategies are available for the diabetes treatment and are associated with various side effects. In search of novel therapy action, we found TGR5 (Takeda G-protein-coupled) as an unexplored target for Type II diabetes. Considering these factors and investigating TGR5 as a therapeutic target for diabetes may offer a new angle for developing innovative TGR5 agonists.

As the TGR5 protein structure was not available in (RCSB PDB) Research Collaboratory for Structural Bioinformatics Protein Data Bank a homology model of TGR5 receptor was constructed and validated. During the course of our research work, later in 2020, Yang et al. deposited crystal structure of TGR5 (PDB ID: 7CFN), including the native ligand 6a-ethyl-23(S)-methylcholic acid (INT777). INT777 interacted with hydrogen bonding with Ser247, Tyr240 of TGR5. Additionally, an active site residue contains Tyr89, Leu244, Leu263, Leu266, Leu166, Leu74, Trp75, Phe96, and Phe161 (Fig. 35). Acknowledging this development, we conducted docking of our designed test compounds.

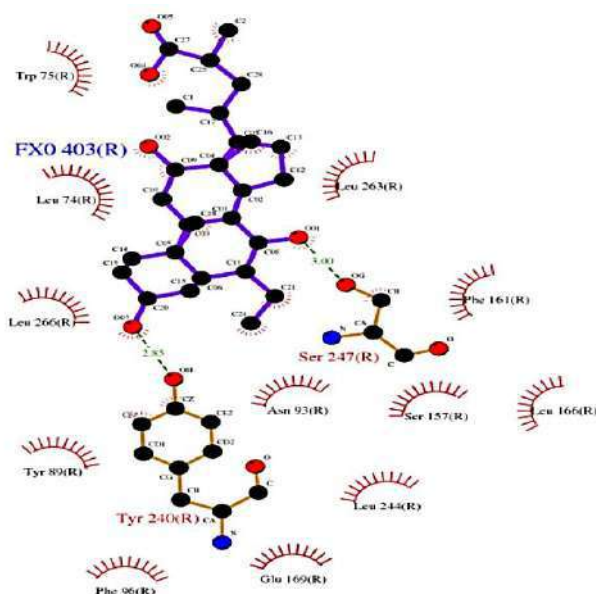


**Figure 35: LigPlot of interaction of TGR5 with INT777**



*Design model:* During the literature review of synthetic TGR5 agonists, we came across pyridine derivatives developed by Roche (1) and Takeda group (2) and noticed that both showed structural similarities. The structural analysis of both TGR5 agonists i.e. compounds 1 and 2 unveiled distinctive features with pyridine ring as monocyclic hydrophobic central core moiety connected to a heteroaromatic ring through an amide linkage and a subsequent directly linked phenyl ring or via an oxygen atom to the opposite end of central core moiety. Thus, this comprehension of the structure of 1 and 2, laid the groundwork for our conceptualization to include central core aromatic ring linked to phenyl ring via amide linkage (Ring A) and phenoxy substitution to other end (Ring B) led to design of compounds (Fig. 36a).

For the purpose of further exploration, the created pharmacophore was divided into three fragments: the aryl amide moiety (Ring A), the central core and the phenoxy moiety (Ring B)

*Design approach for Central core:* To initiate the identification of the central core, the observation was made that compounds 1 and 2 possess the central monocyclic ring containing one or two heteroatoms. In the past, structural investigations primarily concentrated on Ring A and Ring B, with limited exploration of the central core. In this study, we explored the modifications in the central core to produce more potent TGR5 agonists, paving the way for further research. We therefore hypothesized that replacement of pyridine scaffold from compound 1 and 2 with bi-cyclic rings may yield new TGR5 agonists with better or equivalent potency.

OpenEye Scientific Software's ROCS v3.2.2 tool was used to explore a central core with shape-based virtual screening. INT777 was employed as the query molecule for screening compounds from ZINC database. It determined that best hit compound 3 exhibited a 65.5% shape similarity and a 10% electrostatic similarity to the query molecule, with a coumarin ring and benzyloxy group (Fig. 36b).

Further to confirm our hypothesis, the binding mode analysis of compound 3 with TGR5 receptor was also studied and compared with INT777. It was found that the central heterocycle (coumarin) of compound 3 aligns with the steroid core moiety of INT777. Thus, for new derivatives discovery, coumarin ring has been selected as central core. Considering the hydrophobic nature of binding site of TGR5 receptor

and binding analysis of INT777 with TGR5, it was hypothesized that more bulky group in the structure of designed compounds could increase its binding affinity (Fig. 36b).

*Design approach for Ring B:* In the literature it was reported that the binding pocket in TGR5 is predominantly hydrophobic. Therefore, it was hypothesized that an interrering carbon chain linker (2-carbon atoms chain length) between Ring B and the central core might be able to fit satisfactorily in narrow channel and provide conformational and positional flexibility (Fig. 36c).

*Design approach for Ring A:* Modifications on the phenyl ring (Ring A) linked by an amide group was undertaken to enhance comprehension of the impact of substitutions on this ring. In this context, it was hypothesized that substitution on Ring A with various electron donating and withdrawing groups may help us to give better designed compounds (Fig. 36c).

### 3.2. Aim

Design, Synthesis, and Evaluation of some new coumarin derivatives for antidiabetic activity

### 3.3. Objectives:

- ✓ To prepare homology model and validation of prepared model of TGR5.
- ✓ Molecular docking studies of the designed compounds (coumarin derivatives) in the active site of TGR5 target.
- ✓ Synthesis and characterization of compounds using IR, <sup>1</sup>H NMR, Mass spectrometric analysis
- ✓ *In vitro* and *In vivo* studies.

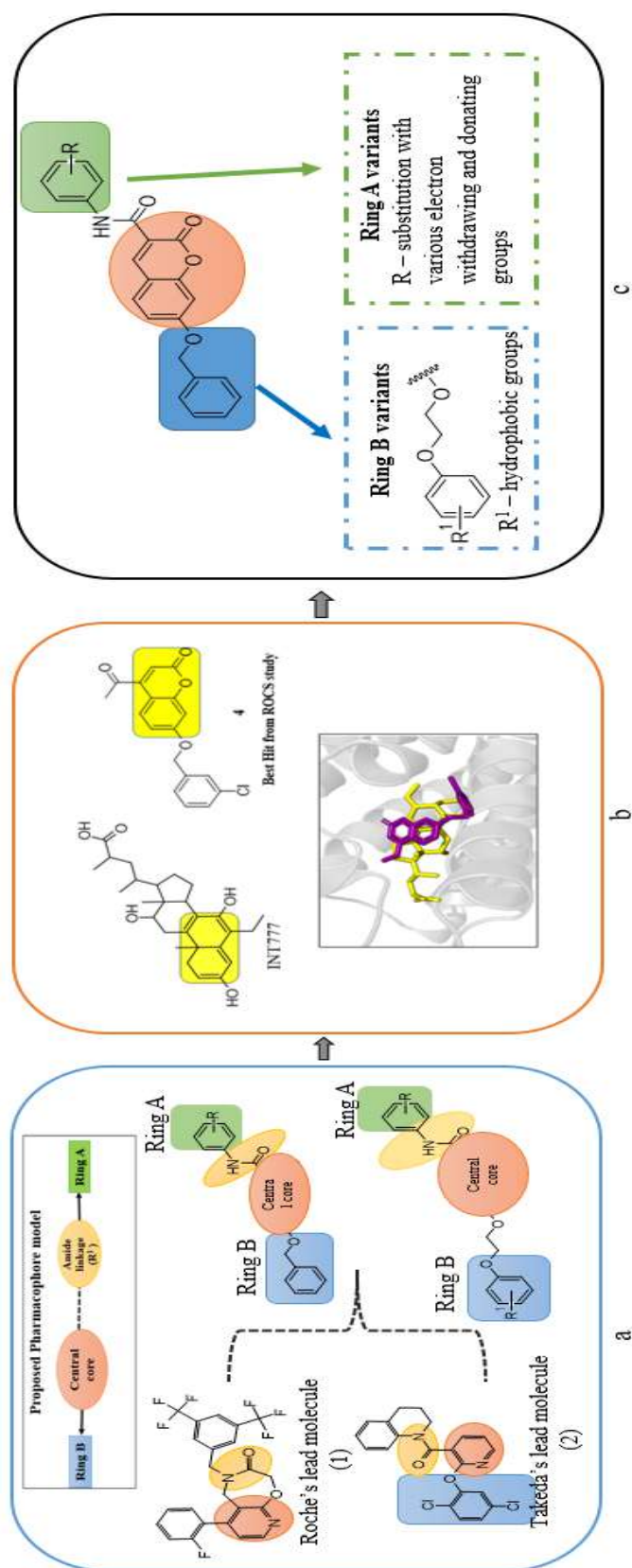


Figure 36: Design strategy of a) Pharmacophore model b) Central core c) Ring A and Ring B

# WORK PLAN



## **CHAPTER 4**

### **4. WORK PLAN**

#### **4.1. Preparation and Validation of Homology model of TGR5**

Significance: During initial stages of our studies, as the TGR5 protein structure was not available in RCSB PDB Data Bank, a homology model of TGR5 receptor was constructed and validated.

Homology modelling also known as comparative modelling is an *in silico* method in structural biology where a three-dimensional structure of a protein is predicted by using amino acid sequence of similar protein structure template.<sup>85</sup> In present study, Homology modelling reveals the folding and functional structure of TGR5 coding protein, which would aid in understanding and combating the disease. As part of homology modelling, many known protein structures are identified that have similar structure to that of query sequence. The sequence alignment of target protein and selected templates produced a model of target protein. Homology models are dependent upon the alignment of sequences and the structure of templates. A homology modelling workflow includes the entire process of identifying templates, align them, and building models for protein structure. The complete homology modelling sequence includes

- Prediction of protein structure
- To identify template
- Sequence alignment with template
- Building of Model

1. ***Sequence retrieval and analysis:*** The TGR5 sequence was extracted from Universe Protein Resource (UniProtKB) (<http://www.uniprot.org/>) with accession number Q8TDU6.
2. ***The modelling workflow of Swiss Model:*** By using the protein sequence retrieved, search was carried out for related protein structures within Swiss Model template library. A comparison was made between top-ranked templates and alignments presented in order to determine if these represent different conformational states based on their ranking. Every template was

automatically converted into a 3D protein model based on its alignment with the target template and ProMod3.

3. ***The modelling workflow of I-Tasser:*** As a result of I-Tasser simulations, large assemblies of structural conformations were generated for each target. I-Tasser uses pair-wise structure similarity to cluster all decoys and report up to five different models.
4. ***Validation of Model:*** The best receptor model out of both servers was selected using the SAVES (Structure Analysis and Verification Server), RAMPAGE (Ramchandran plot Assessment) , ProSA (Protein Structure Analysis)

## 4.2. Molecular Docking Studies

Significance: Molecular docking integrates biological research with computational algorithms in a systematic approach designed to assess interactions between ligands and target biomolecules for drug design and development.<sup>86</sup> We performed docking studies to study *in silico* interactions of designed compounds with amino acids present in the active site of TGR5 that can predict the biological actions of designed compounds in *in vitro* and *in vivo* studies..

Steps involves in Molecular docking studies are,

1. Preparation of Ligands: The database of 3D structures of all ligands was prepared using Chem Draw and minimization of ligands energy was carried out using Chem3D. All the optimised ligands were saved in PDB format.
2. Preparation of Protein: The protein structure modelled from homology modelling was optimised by adding hydrogens, deleting water molecules, adding charges, energy minimised and saved in PDBQT format. TheTGR5high-resolution crystal structure (PDB ID: 7CFN) was introduced in 2020, providing an excellent opportunity to determine potential agonists using computational methods. Docking studies of the designed compounds was done in PDB ID: 7CFN. With the use of Autodock Tools, optimization of ligands and proteins were done and grid box was generated.

3. Docking studies: Proteins and ligands were selected from a database, docking parameters were set, and docking calculations were performed after analysing the interactions between the proteins and ligands.
4. Analysis of docking result: Results were analysed by comparing docking results of designed ligands with standard native ligands

#### **4.3. Synthesis and characterization of compounds**

On basis of docking studies and protein-ligand interaction, top compounds were selected for synthesis. The compound's synthesis was carried out as shown in Fig. 41, Chapter 5. Characterization of the synthesized compounds will be carried out using FTIR, <sup>1</sup>H NMR, <sup>13</sup>C NMR, and HR-MS.

#### **4.4. *In Vitro* evaluation of synthesized compound**

Significance: Performing the *in vitro* GLP-1 secretion assay and TGR5 gene expression assay on synthesized compounds using the Human NCI-H716 enteroendocrine cell line is crucial for evaluating their potential in managing metabolic disorders such as type 2 diabetes and obesity.

GLP-1 (glucagon-like peptide-1) is a key incretin hormone that enhances insulin secretion, improves glucose tolerance, and promotes satiety.<sup>87</sup> By measuring GLP-1 secretion, compounds can be evaluated for stimulating the release of GLP-1, an important function for glucose homeostasis and diabetes management.<sup>29</sup> Testing TGR5 gene expression helps determine whether the synthesized compounds influence this receptor's activity, thereby potentially modulating metabolic pathways related to energy balance and glucose regulation.<sup>36</sup> Together, these assays help identify the therapeutic potential of the compounds in modulating key metabolic pathways.<sup>88</sup> In the present study, the results of synthesized compounds were compared with the selected standard.

#### **4.5. *In Vivo* evaluation of synthesized compound**

Significance: *In vivo* evaluation of a synthesized compound is essential for assessing its therapeutic potential, safety, and pharmacokinetic profile within a living organism.

While *in vitro* studies offer initial cellular insights, *in vivo* testing reveals how the compound functions within complex biological systems.<sup>89</sup> *In vivo* testing allows to confirm if the compound achieves its intended therapeutic effects, assess its performance over time, and determine its targeting accuracy.<sup>90</sup>

In the present study, *In vivo* evaluation was carried out on the compounds that showed potency in In-vitro assays. The acute toxicity of the test compounds was investigated in Wister rats. Several acute toxicity signs were evaluated in test mice, including lacrimation, blinking, hair erection, muscle weakness, urinations and convulsions, reduction in motor activity, diarrhoea, coma, and death. A further study of anti-hyperglycaemic activity was conducted on those compounds that were found to be non-toxic. Following the administration of the drugs, the glucose level in blood of the animals was determined.



# MATERIAL AND METHODS



## **CHAPTER 5**

### **5. MATERIAL AND METHODS**

The present work consists of several aspects, such as the homology modeling of the targeted receptor, the design of novel test compounds, as well as molecular docking studies. A further step was to synthesize selected test compounds in the lab through wet lab experiments and determine biological activity of resultant test compounds by *in vitro* and *in vivo* studies.

#### **5.1. MATERIALS**

Homology Modelling was performed using Swiss Model (<https://swissmodel.expasy.org/>) I-Tasser (<https://zhanggroup.org/I-TASSER/>) UniProt (<http://www.uniprot.org/>), SAVES v6.0 (<https://saves.mbi.ucla.edu/>), ProQ (<https://proq.bioinfo.se/>), Castp (<http://sts.bioe.uic.edu/castp/index.html?2was>). In a study, AutodockVina 1.5.7 (The Scripps Research Institute USA) was employed for performing docking studies. The process involved the utilization of drawing tools like ChemDraw, facilitating the creation and representation of molecular structures. For molecular docking, crystal structure of TGR5 complexed with INT777 obtained using electron microscopy with a 3.0Å resolution was downloaded from Protein Databank (PDB). TGR5 crystal structure consists of five heteromer chains make up TGR5 - chains A, B, C, D, and E - whose sequence length ranges from 394, 358, 58, 128, and 330 amino acids. From all, Chain E was selected. For docking results visualization purposes, Biovia Discovery Studio visualizer was employed. In addition to docking and visualization, the study incorporated *in silico* ADME prediction tool. Molinspiration and Swiss ADME were applied to predict various pharmacokinetic properties of the ligands. Desmond (version: desmond/2020.4) simulation package of Schrodinger LLC was used to perform molecular dynamics study.

All chemicals and reagents used in synthesis process were acquired from Merck (India) Ltd., S.D. Fine Ltd. (India). Analytical grade pure solvents were used. The synthesis of compounds was carried out using Parallel synthesizer (Radley's Carousel 6 Plus reaction station). The compounds synthesized were characterised using FT-IR, melting point, <sup>1</sup>H NMR, Mass spectroscopy, <sup>13</sup>C NMR. FTIR spectra's

were recorded using (Fourier Transform InfraRed Spectrometer Shimadzu (8400S). Bruker Avance III HD NMR 500 MHz was used to record  $^1\text{H}$  NMR i.e. proton nuclear magnetic spectra and  $^{13}\text{C}$  NMR i.e. carbon nuclear magnetic spectra using DMSO and  $\text{CDCl}_3$  as solvents. Bruker Impact II UHR-TOF Mass Spectrometer System was used to get HR-MS. Melting point in degree Celsius of test derivatives was done using Electronics Digital melting point apparatus.

The entire work methodology was divided into three parts for ease of understanding and presentation:

- I. *In Silico* studies (Homology modelling and molecular docking)
- II. Synthesis and characterization of the identified test compounds
- III. Biological evaluation through *In vitro* and *In vivo* studies

## 5.2. METHODS

### 5.2.1. *In-Silico* studies (Homology modelling and molecular docking studies)

#### 5.2.1.1. HOMOLOGY MODELLING

In this study, preparation and validation of Homology model of TGR5 receptor was performed due to the unavailability of TGR5 protein structure in RCSB PDB database in the year 2019. During the course of our research work, later in 2020, Yang et al. deposited the crystal structure of TGR5 (PDB ID: 7CFN), including the native ligand 6 $\alpha$ -ethyl-23(S)-methylcholic acid (INT777). Acknowledging this development, we conducted docking studies of our designed compounds.

Steps involved in Homology Modelling<sup>85</sup>

Developing a homology model comprises a series of consecutive steps, summarized as follows (Fig. 37):

- Retrieval of sequence
- Template identification
- Sequence alignment
- Building a model for target using 3D structure of chosen template

Validation of model

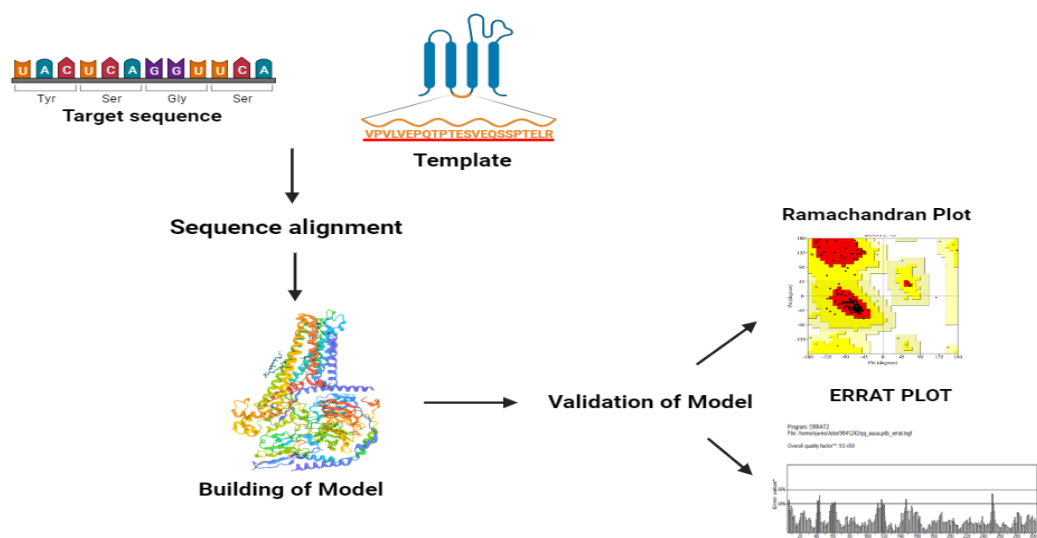


**Figure 37: Flow diagram of Homology Modelling**

### Sequence retrieval and analysis

From UniProt, the TGR5 protein sequence was obtained (<http://www.uniprot.org/>) with accession number Q8TDU6.<sup>91, 92</sup> UniProtKB serves as the primary repository for gathering functional information about proteins. The sequence of the *Homosapiens* protein was selected and downloaded with a length of 330 amino acids.

### The modelling workflow of Swiss Model

By using the protein sequence retrieved, search was carried out for related protein structures within Swiss Model template library.<sup>93</sup> For this purpose, Swiss Model utilizes two approaches to search databases: BLAST<sup>94, 95</sup> for close homology of templates, and HHBLITS<sup>96</sup> for remote homology. A template search was completed by selecting multiple templates, building and ranking different models according to global model quality estimates (GMQE)<sup>97</sup> and quaternary structure quality estimates (QSQE).<sup>98</sup> Swiss Model provided various templates, the highest-ranked six templates were elected based on its similarity and identity of the sequence of the TGR5 protein (Table 2).

A comparison was carried out between the highest-ranked templates and alignments to determine if that represent different conformational states<sup>111</sup> according to their ranking. Every template is automatically converted into a 3D protein model based on

its alignment with the target template. Full-atom protein models were generated by using ProMod3 and non-conserved amino acid side chains.<sup>99, 100</sup>

### **The modelling workflow of I-Tasser (Iterative Threading ASSEmbly Refinement)**

During simulations, variety of structural conformations, referred to as decoys, were generated for each target. These decoys were then grouped based on pair-wise structural similarity, leading to the identification of five significant models (Table 3). A C-score, which ranges from -5 to 2, is determined from analysis of significant alignments between threading templates and convergence parameters. The TM-Score (Template Modelling Score) is another important parameter to consider. If TM-score falls from 0 to 1, where 1 indicates a model with a correct topology, but if the TM-score falls below 0.17 it indicates a model with lower similarity.<sup>101-103</sup> Best Homology model (Model 1) was selected based on its identity, coverage and C score.

**Table 2: List of Templates from Swiss model**

<b>Template code</b>	<b>5mzj</b>	<b>5iu7</b>	<b>2r43</b>	<b>3emL</b>	<b>4ww3</b>	<b>3qak</b>
<b>Identity</b>	19.44%	19.93%	21.48%	19.49%	15.49	19.49
<b>Similarity</b>	29%	30%	30%	29%	20%	25%
<b>Coverage</b>	87%	85%	82%	84%	86%	84%

**Table 3: List of Models from I-Tasser**

<b>Template code (Model)</b>	<b>1</b>	<b>2</b>	<b>3</b>	<b>4</b>	<b>5</b>
<b>Identity 1</b>	21%	20%	18%	16%	15%
<b>Identity 2</b>	22%	27%	23%	25%	25%
<b>Coverage</b>	85%	88%	84%	88%	88%
<b>C score</b>	-0.67	-1.17	-2.95	-1.00	-3.44

### **Validation of Model**

The best receptor model out of both servers was selected using the SAVES (Structure Analysis and Verification Server). In order to determine the overall quality score of a receptor structure, RAMPAGE (Ramachandran plot Assessment) <sup>104, 105</sup> was used along with ProSA (Protein Structure Analysis) <sup>106</sup> and ProQ (Protein Quality predictor).

### ***Prediction of active sites***

Based on Computed Atlas of Surface Topography of Proteins (CASTp) 3.0, active sites within protein structure were predicted. CASTp is specialized in recognizing and quantifying voids in 3D protein structures, was utilized for this purpose. The 3D protein structure underwent submission to the server, leading to the subsequent prediction of crucial amino acids for binding interactions. The residues are obtained from the active site prediction server includes Tyr 240, Tyr 89, Ser 270, Trp237, Trp 75 (Fig. 38).

### **5.2.1.2. MOLECULAR DOCKING STUDIES**

Yang *et al.* <sup>107</sup> presented cryo-electron microscopy structure of TGR5 complexed with bile acid derivative INT-777 (PDB ID: 7CFN) in 2020. In this current investigation, molecular docking were conducted utilizing the PDB ID: 7CFN for the designed test compounds. Fig. 39 illustrate structural view of the TGR5 protein.

### **Preparation and optimization of Protein**

In order to prepare proteins, structure of protein was pre-processed, loops and residues were corrected, hydrogens and charges were added, and water molecules were extracted with Autodock Tools. Discovery Studio Biovia 2017 was used for protein optimization. Additionally, UCSF Chimera ([www.cgl.ucsf.edu/chimera](http://www.cgl.ucsf.edu/chimera)) was used to minimize energy.<sup>108</sup>

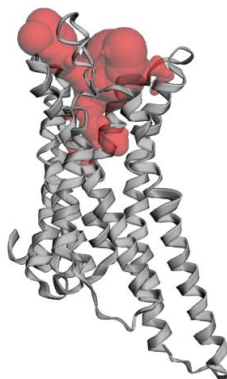
### **Preparation and optimization of ligands**

Based on designing of test compounds, almost 42 compounds were designed and docked in TGR5 protein (PDB ID: 7CFN) (Table 4). Structures of compounds were

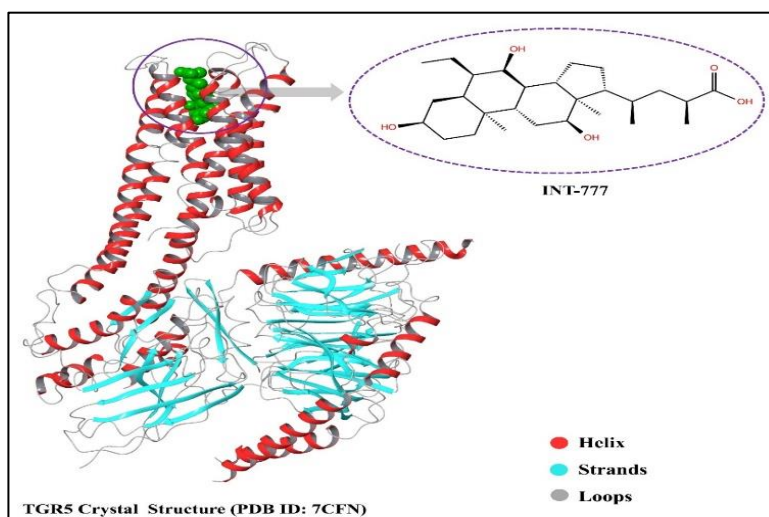
drawn using ChemBioDraw Ultra 14.0. After incorporating 3D coordinates, a .mol file was generated. Avogadro software was then employed to minimize energy of designed compounds using "force field" and a steepest descent algorithm. The results were converted into a PDB file.<sup>109</sup>

#### Dataset preparation (Preparation of compound library)

Series A, B, C, and D containing coumarin rings were designed (Table 4). These were designed by varying the substituents. This was done to determine the most probable active compound.

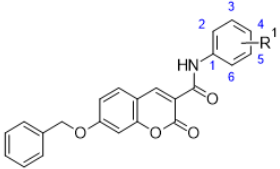
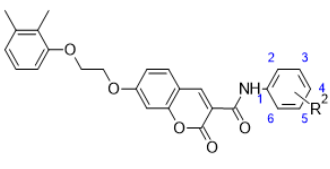
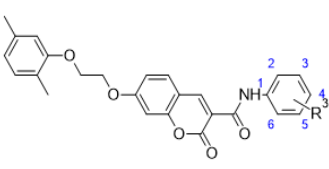
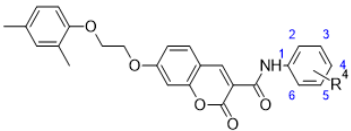


**Figure 38: Active sites in the modelled protein (indicated by red colour)**



**Figure 39: Structural view of TGR5 complex with INT-777 (co-crystal ligand)**

**Table 4: Designed compounds library**

Sr. No.	Designed series	Compound Code	R <sup>1</sup>
<div style="display: flex; justify-content: space-around; align-items: center;"> <div style="text-align: center;">  <p>Series A</p> </div> <div style="text-align: center;">  <p>Series B</p> </div> <div style="text-align: center;">  <p>Series C</p> </div> <div style="text-align: center;">  <p>Series D</p> </div> </div>			
1.	A	3	H
2.	A	4	OH
3.	A	5a	4-OCH <sub>3</sub>
4.	A	5b	3-OCH <sub>3</sub>
5.	A	5c	2-OCH <sub>3</sub>
6.	A	5d	3,4-di OCH <sub>3</sub>
7.	A	6a	4-CH <sub>3</sub>
8.	A	6b	3-CH <sub>3</sub>
9.	A	6c	2-CH <sub>3</sub>
10.	A	7a	2,3-diCH <sub>3</sub>
11.	A	7b	2,4-diCH <sub>3</sub>
12.	A	7c	2,6-diCH <sub>3</sub>
13.	A	8a	4-Cl
14.	A	8b	3-Cl
15.	A	8c	2-Cl
16.	A	9a	4-Br
17.	A	9b	3-Br
18.	A	9c	2-Br
19.	A	10a	4-NO <sub>2</sub>
20.	A	10b	3-NO <sub>2</sub>



21.	A	10c	2-NO <sub>2</sub>
22.	B	13a	H
23.	B	14a	4-OH
24.	B	15a	3,4-diOCH <sub>3</sub>
25.	B	16a	4-CH <sub>3</sub>
26.	B	17a	4-Cl
27.	B	18a	4-NO <sub>2</sub>
28.	B	19a	4-Br
29.	C	13b	H
30.	C	14b	4-OH
31.	C	15b	3,4-diOCH <sub>3</sub>
32.	C	16b	4-CH <sub>3</sub>
33.	C	17b	4-Cl
34.	C	18b	4-NO <sub>2</sub>
35.	C	19b	4-Br
36.	D	13c	H
37.	D	14c	4-OH
38.	D	15c	3,4-diOCH <sub>3</sub>
39.	D	16b	4-CH <sub>3</sub>
40.	D	17c	4-Cl
41.	D	18c	4-NO <sub>2</sub>
42.	D	19c	4-Br

*In silico* docking studies were conducted using Autodock Vina that uses the PDBQT molecular structure file format for input and output. A Lamarckian genetic algorithm (LGA) was implemented during the docking process, which combines a global search algorithm with a local search algorithm as well as a simulated annealing algorithm. Using the graphical user interface program Autodock Tools, the ligands and receptors were optimized and grid boxes were created. By arranging the grid coordinates (X, Y, and Z) around the active site of the receptor using the co-crystal ligand, a grid box

was generated. A grid size of 40 x 40 x 40 xyz points was specified for the target area, with the grid centre located at dimensions (x, y, z): (96.30,121.46,109.69) (Fig. 40).

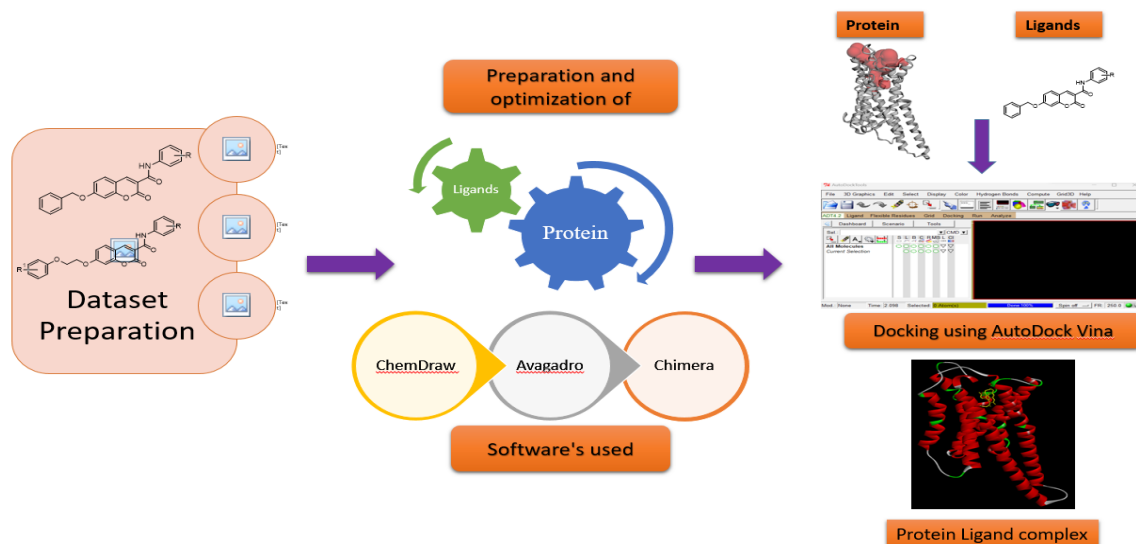


**Figure 40: Flow diagram of Molecular docking study**

### Validation of docking protocol

Validation of docking protocol was conducted to understand the accuracy and reproducibility of the docking process and the target selections. The native ligand INT777 present in target protein (PDB ID: 7CFN) was removed from the receptor. The chemical structure of co-crystal ligand was re-drawn using ChemDraw, followed by energy minimization and docking at the active site of the receptor. Best pose Docked complex was superimposed on its co-crystallized reference complex, and the root mean square deviation (RMSD) was calculated.

#### 5.2.1.3. MOLECULAR DYNAMICS (MD) STUDY

Desmond software is a powerful and flexible system for calculating forces, atomic motion, and binding energy.<sup>110, 111</sup> Desmond, on the other hand, features a more comprehensive temperature, pressure, and volume system and offers more functionality to estimate protein-ligand interactions. The MD study illustrate the complex behaviours of proteins as they bind to ligands or macromolecules by following steps.

### **Set-up the process**

The MD simulation was run to 100 ns to obtain the binding strength of the TGR5-compound complexes between the best docked designed compounds and the TGR5 binding pocket.<sup>112, 113</sup>

### **Energy minimization**

The steepest descent method is utilized in MD to minimize the overall energy of both the receptor and the ligand.

### **Solvation and equilibration of system**

The cumulative charge of the solvent system was neutralized by the random addition of a counter ion sufficient to balance the cumulative charge. In this study, the OPLS-2005 force field was selected, since it is an improved force field suitable for simulations of molecular dynamics calculations of proteins. For the same, the ligand and protein complexes are immersed in a water-filled cubic using a three-point water model (TIP3P) with periodic boundary conditions using Desmond's system builder (Schrodinger Release 2020-4). All the complex systems were solvated and neutralized by these parameters: TGR5-6a (TIP3P = 9564, Cl<sup>-</sup> = 10 (19.011 mM) ); TGR5-16a (TIP3P = 9571, Cl<sup>-</sup> = 9 (10.097 mM)); TGR5-14b (TIP3P = 9568, Cl<sup>-</sup> = 10 (19.003 mM)); TGR5-16b (TIP3P = 9566, Cl<sup>-</sup> = 10 (19.007 mM)); TGR5-14a (TIP3P = 9565, Cl<sup>-</sup> = 10 (19.009 mM)); TGR5-INT777 (TIP3P = 9530, Cl<sup>-</sup> = 8 (13.813 mM)); and TGR5-Bile Acid (TIP3P = 9580, Cl<sup>-</sup> = 8 (15.183 mM)).

### **Examination of trajectories**

Once the system is equilibrated, the conformation trajectories are captured and examined. The conformational modifications induced by compounds binding were compared to the original conformations of the crystal structure (PDB ID: 7CFN) in terms of Root Mean Square Deviation (RMSD). Also, the Radius of Gyration (Rg), Solvent Accessible Surface Area (SASA) and the protein-ligand contact map during the simulation was performed.

### Binding Free Energy Calculations

The MM/GBSA method<sup>111</sup> was used to calculate binding energies for TGR5-test compounds complex during the simulation. The changes in the binding free energy were calculating by capturing the trajectories generated during the simulation. For MM/GBSA calculations, trajectories at 10ns interval were considered along with the initial frame of docked complex. The free energy upon binding of lead compounds and the standards to the receptor was examined using the equation below:

$$\Delta G_{bind} = G_{complex} - (G_{protein} + G_{ligand})$$

Where,  $G_{protein}$  stands for the energy of the unbound (free) protein,  $G_{ligand}$  for the energy of the free ligand, and  $G_{complex}$  for the energy of the protein-ligand complex.

#### 5.2.1.4. *IN SILICO* DRUG-LIKENESS ANALYSIS

Using a web-based application i.e., SwissADME, physiochemical properties, pharmacokinetic properties, ADME parameters (absorption, distribution, metabolism, and excretion) of all the designed compounds were predicted.<sup>114</sup> herein, all designed compounds were uploaded in SMILES format to SwissADME website to predict drug-likeness and ADMET properties.

#### 5.2.2. Synthesis of the identified test compounds

The designing of test compounds was done based on structure based drug design. Review of literature revealed that coumarin derivatives have not been explored TGR5 agonist as anti-diabetic. After analysing the *in silico* studies, several hits were identified among all designed test compounds as potential TGR5 agonist. All potential hits were subjected to *in silico* drug-likeness analysis and 27 potential hits were identified for synthesis and characterization.

The synthetic scheme was presented in Figure 41.

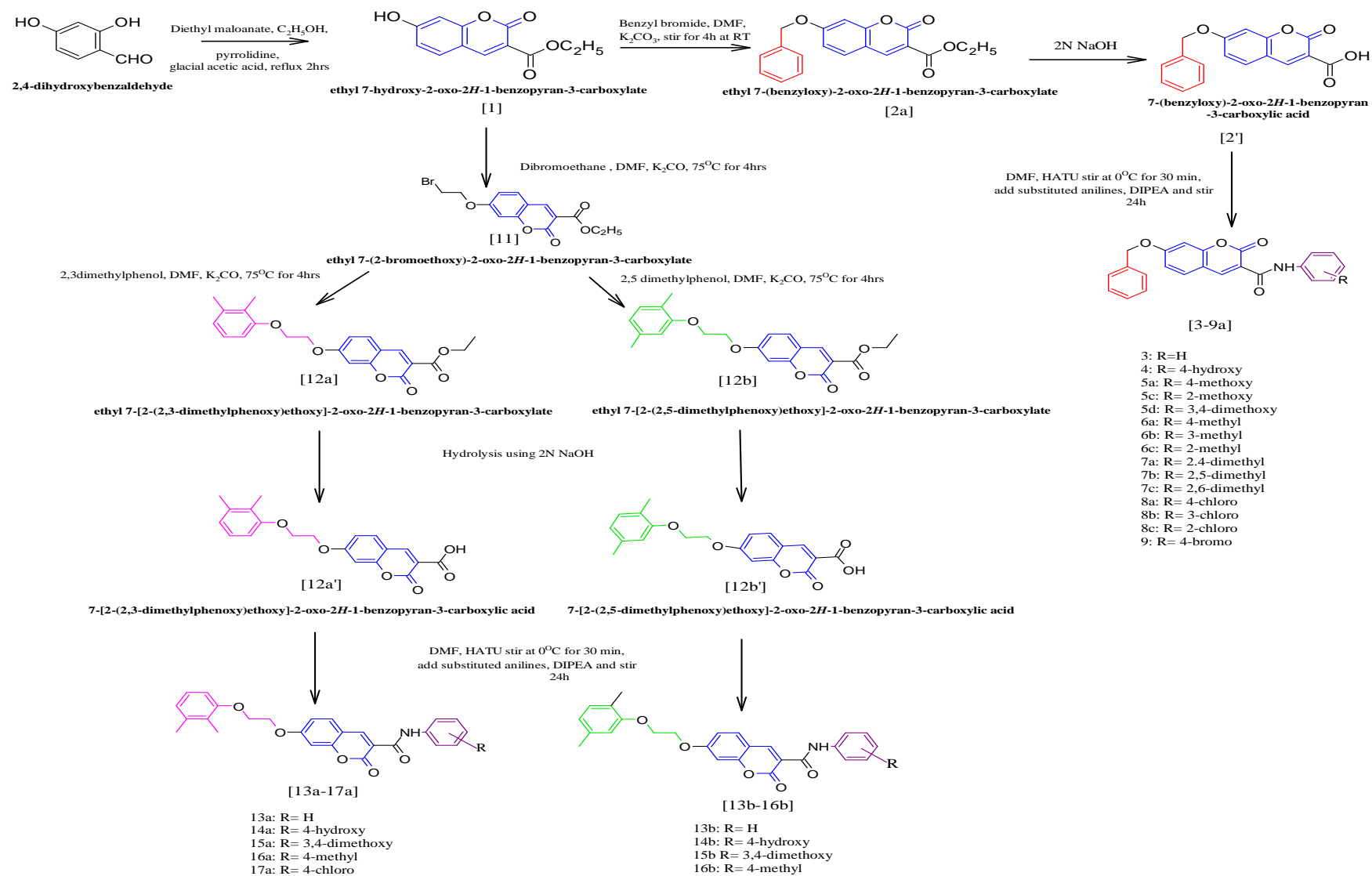


**Figure 41: Synthetic Scheme**

Synthesis of chemicals was performed using a Parallel Synthesizer. Purification of synthesized compounds was performed using column chromatography.

#### **5.2.2.1. Synthesis of Ethyl 7-hydroxy-2-oxo-2H-1-benzopyran-3-carboxylate (1)**

2, 4 dihydroxy benzaldehyde (2.0 mmol, 1 equiv) and Diethylmalonate (2.4 mmol, 1.2 equiv) were mixed in 2mL of ethanol at room temperature. Subsequently, pyrrolidine 2-3 drops and glacial acetic acid were added in order and mixture was refluxed for two hours. Once reaction completed, resulting product was poured into chilled water to obtain product. The product was filtered, then washed and further dried. The purified solid was obtained using column chromatography (hexane: ethyl acetate).<sup>115</sup>  
<sup>117</sup> Yellow solid; % Yield 85%; mp. 140-141°C; *R*<sub>f</sub>: 0.33 (7:13 EtOAc: hexane).

#### **5.2.2.2. Synthesis of ethyl 7-(benzyloxy)-2-oxo-2H-1-benzopyran-3-carboxylate (2a)**

Appropriate quantity ethyl 7-hydroxy-2-oxo-2H-chromene-3-carboxylate (0.236g, 1.0mmol), dissolve in 2mL of dimethyl formamide (DMF) at room temperature. Subsequently, Benzyl bromide (0.171 mL, 1.2 mmol) was added. The potassium carbonate (0.151 g, 1.1 mmol) as catalyst was added in reaction mixture and stirred for 4 hrs at RT. Afterwards, product precipitate out using ice water and filtered, washed, and dried. Using hexane: ethyl acetate as a solvent, a column chromatography was performed to purify the crude solid.<sup>118</sup> Yellow solid; % Yield: 91%; mp. 180-182°C; *R*<sub>f</sub>: 0.54 (7:13 EtOAc: hexane).

#### **5.2.2.3. Synthesis of 7-(benzyloxy)-2-oxo-2H-1-benzopyran-3-carboxylic acid (2a')**

Appropriate quantity ethyl 7-(benzyloxy)-2-oxo-2H-chromene-3-carboxylate (2.0 mmol) was dissolved in ethanol as a solvent. A solution of 40 mL 2N NaOH was added and stirring of solution was carried out overnight. In following step, 2N HCl was added to neutralize the solution, which resulted in precipitate that was filtrated, washed twice with water. The resulted product was used as it is for further reaction.  
<sup>118</sup> Pale Yellow solid; % Yield: 85%; mp. 184-185°C; *R*<sub>f</sub>: 0.45 (7:13 EtOAc: hexane).

#### 5.2.2.4. Synthesis of Compounds (3-9a)

An 7-(benzyloxy)-2-oxo-2*H*-1-benzopyran-3-carboxylic acid (1.0 mmol, 1 equiv) was dissolved in 4-5 mL of DMF previously kept in ice. Further Hexa fluorophosphates Azabenzotriazole Tetramethyl Uronium (HATU) (0.72 mmol) was added in above solution and it was stirred for 30 minutes. Next, corresponding substituted anilines (0.75 mmol) and N, N-Diisopropylethylamine (DIPEA) (1.4 mmol) were added and stirred overnight. This mixture was poured into chilled water, then extracted with ethyl acetate as solvent, and final product was obtained. After drying with magnesium sulphate, rotary evaporation was used to remove the ethyl layer. Through column, solvent system ethyl acetate: n-hexane was used for purification of crude product (3-9a).<sup>119-121</sup>

#### 5.2.2.5. Synthesis of 7-(2-bromoethoxy)-3-propanoyl-2*H*-1-benzopyran-2-one (11)

A suitable quantity ethyl 7-hydroxy-2-oxo-2*H*-1-benzopyran-3-carboxylate (0.236 g, 1.0 mmol) and potassium carbonate (0.828 g, 6 mmol) were mixed in 10 mL of DMF and heated for 15 min at 75°C. In reaction mixture, 1, 2 dibromoethane (0.561 mL, 1.5 mmol) dissolved in 5mL of DMF and then heated at 75°C for 2-3 hrs. As soon as reaction was complete, using water product was washed and dried. For purification of product, column chromatography (hexane: ethyl acetate) was used. White powder; % Yield 80%, *R*<sub>f</sub>: 0.69 (7:13 EtOAc: hexane); mp. 120-121°C

#### 5.2.2.6. Synthesis of ethyl 7-[2-(2,3-dimethylphenoxy)ethoxy]-2-oxo-2*H*-1-benzopyran-3-carboxylate (12a)

2,3dimethylphenol (0.13 mL, 1.0 mmol) and potassium carbonate (0.414 g, 3 mmol) were mixed in DMF (10 mL) and was heated (75°C) for 15 min. Then 7-(2-bromoethoxy)-3-propanoyl-2*H*-1-benzopyran-2-one (0.34 g, 1 mmol) dissolved in DMF (5 mL), added in above mixture and further heated upto 4 hrs. Once reaction had been completed, mixture was poured into cold water. The precipitated product was filtered, washed and dried. Product is purified using column chromatography. Brown powder; % Yield: 55%; mp. 112-113°C; *R*<sub>f</sub>: 0.75 (7:13 EtOAc: hexane).

#### **5.2.2.7. Synthesis of ethyl 7-[2-(2,5-dimethylphenoxy)ethoxy]-2-oxo-2H-benzopyran-3-carboxylate (12b)**

2,5dimethylphenol (0.122 g, 1.0 mmol) and potassium carbonate (0.414 g, 3 mmol) in 10 mL of DMF was heated at 75°C for 15 minutes. Then 7-(2-bromoethoxy)-3-propanoyl-2H-1-benzopyran-2-one (0.34 g, 1 mmol) dissolved in DMF (5 mL) was added in reaction mixture that further was heated (75°C) for next 4 hrs. After reaction, mixture was poured in chilled water. Using a vacuum, product was filtered, washed and dried. A column chromatography technique (hexane: ethyl acetate) is used for the purification of the product. Brown powder; % Yield: 60%; mp. 110-111°C; *Rf*: 0.80 (7:13 EtOAc: hexane)

#### **5.2.2.8. Synthesis of 7-[2-(2,3-dimethylphenoxy)ethoxy]-2-oxo-2H-1-benzopyran-3-carboxylic acid (12a')**

A suitable quantity of ethyl 7-[2-(2,3-dimethylphenoxy)ethoxy]-2-oxo-2H-1-benzopyran-3-carboxylate (0.237 g) was added in dimethyl sulfoxide (DMSO) as a solvent. 4 mL 2N NaOH was added and was refluxed at 100°C for 2 hrs. In the following step, 2N HCl was added to neutralize the solution, which resulted in precipitation. The resulted precipitate was filtrated. The resulted product was used as it is for further reaction. Pale brown powder; % Yield: 75%; mp. 130-133°C; *Rf*: 0.48 (7:13 EtOAc: hexane).

#### **5.2.2.9. Synthesis of 7-[2-(2,5-dimethylphenoxy)ethoxy]-2-oxo-2H-1-benzopyran-3-carboxylic acid (12b')**

A suitable quantity of ethyl 7-[2-(2,5-dimethylphenoxy)ethoxy]-2-oxo-2H-1-benzopyran-3-carboxylate (0.237 g) was dissolved in dimethyl sulfoxide (DMSO) as a solvent. A solution of 4 mL 2N NaOH was added into it and was refluxed at 100°C for two hrs. In the following step, 2N HCl was added to neutralize the solution, which resulted in precipitation. It was filtrated, washed twice with water. Resulted product was used as it is for further reaction. Pale brown powder; % Yield: 80%; mp. 132-134°C; *Rf*: 0.45 (7:13 EtOAc: hexane).



#### 5.2.2.10. Synthesis of Compounds (13a, 14a, 15a, 16a, 17a) <sup>121, 122</sup>

An 7-[2-(2,3-dimethylphenoxy)ethoxy]-2-oxo-2*H*-1-benzopyran-3-carboxylic acid (0.354 g, 1.0 mmol) was dissolved in 4-5 mL of DMF previously kept in ice. Further Hexafluorophosphate Azabenzotriazole Tetramethyl Uronium (HATU) (0.274 g, 0.72 mmol) was added in above solution and it was stirred for 30 minutes. Then corresponding substituted anilines (0.75 mmol) and DIPEA (0.127 g, 1 mmol) were added and stirred at RT overnight. On reaction completion, mixture is dumped in ice and extracted with ethyl acetate. Ethyl layer was dried with magnesium sulphate and evaporated. The crude product was purified using column chromatography to afford final compounds (13a, 14a, 15a, 16a, 17a).

#### 5.2.2.11. Synthesis of Compounds (13b, 14b, 15b, 16b) <sup>122</sup>

An 7-[2-(2,5-dimethylphenoxy)ethoxy]-2-oxo-2*H*-1-benzopyran-3-carboxylic acid (0.354 g, 1.0 mmol) was dissolved in 4-5 mL of DMF previously kept in ice. Further Hexa fluorophosphates Azabenzotriazole Tetramethyl Uronium (HATU) (0.274 g, 0.72 mmol) was added in above solution and it was stirred for 30 minutes. Then corresponding substituted anilines (0.75 mmol) and DIPEA (0.127 g, 1 mmol) were added and stirred at RT overnight. Mixture is then added to ice and extracted with ethyl acetate. Using magnesium sulphate, the ethyl layer was dried and rotary evaporated. Final pure compounds were obtained using column chromatography (Mobile Phase: ethyl acetate and n-hexane) (13b, 14b, 15b, 16b).

### 5.2.3. Biological evaluation through *In Vitro* and *In Vivo* studies

#### 5.2.3.1. *In Vitro* studies <sup>123</sup>

*In vitro* assays are frequently used to assess potential drugs or therapies, understand basic biological mechanisms, identify drug targets, determine effective dosages, and evaluate toxicity, offering crucial insights for further *in vivo* studies. The current investigation involves conducting *in vitro* experiments, starting with a cell toxicity test to assess how test compounds affect a particular cell line. Subsequently, a GLP-1 assay is carried out to measure the release of GLP-1 levels following treatment with

the test compounds. Finally, the chosen compounds undergo a TGR5 gene expression analysis.

#### **5.2.3.1.1. Nature of cell**

Human NCI-H716 enteroendocrine cells were obtained and maintained in RPMI 1640 with added L-glutamine (GenClone). The cell culture media comprised 100  $\mu\text{g mL}^{-1}$  of streptomycin (GenClone), 100 unit's  $\text{mL}^{-1}$  of penicillin (FBS), and 10% fetal bovine serum. Cells were grown in 'complete' culture medium, containing both FBS and antibiotics, maintained in atmosphere of 5%  $\text{CO}_2$  at 37°C.

#### **5.2.3.1.2. Cell viability assay**

Human NCI-H716 cells were subjected to compounds in a full culture medium, maintaining a constant concentration of DMSO as the negative control. The cells underwent overnight treatment with the compounds in complete media, while being kept at a temperature of 37°C in a 5% carbon dioxide environment. Assessment of viability of cells was done using the Cell Titer-Glo Luminescent Cell Viability Assay (Fig. 39). Luminescence measurements were performed using a Flex Station III plate reader. The luminescence readings were compared to control and presented as relative cell viability.

#### **5.2.3.1.3. GLP-1 secretion assay**

NCI-H716 cells were seeded onto Matrigel-coated cell culture plates (Corning Life Sciences, catalog no. 356234) by adhering to the recommended Matrigel dilution guidelines in Hanks' balanced salt solution. For two days, cells were grown in RPMI media. Cells were washed on day of treatment with RPMI 1640 low-serum without antibiotics. DMSO-dissolved test samples were added to cells in low-serum medium. As a negative control, DMSO concentrations were kept constant across treatments. After 2-hour incubation, the medium was harvested into 96-well plates and for subsequent analysis was stored at -20 °C (Fig. 40). The secreted total GLP-1 levels were quantified using In-vitrogen Human GLP-1 (1-37a) ELISA Kit from ThermoFisher Scientific (catalog #EH221RB), following the manufacturer's instructions.

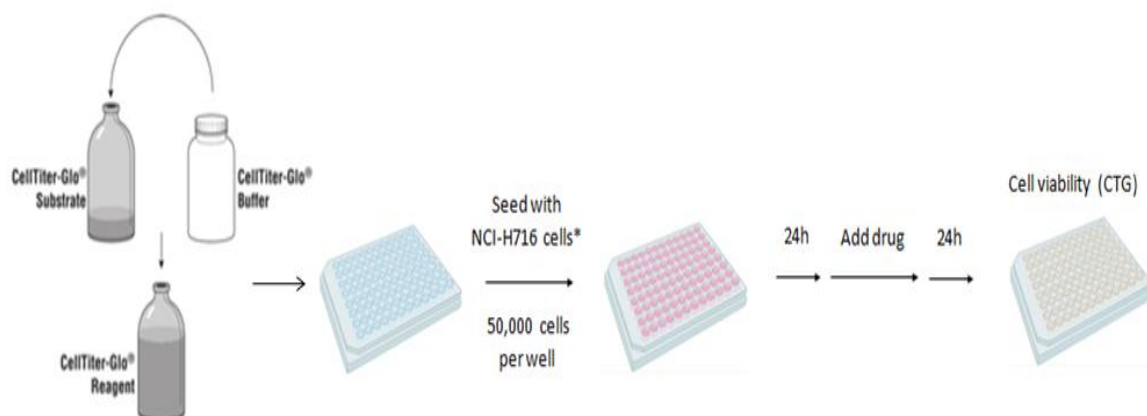


**Figure 42: Flow diagram for Cell Titer-Glo assay**

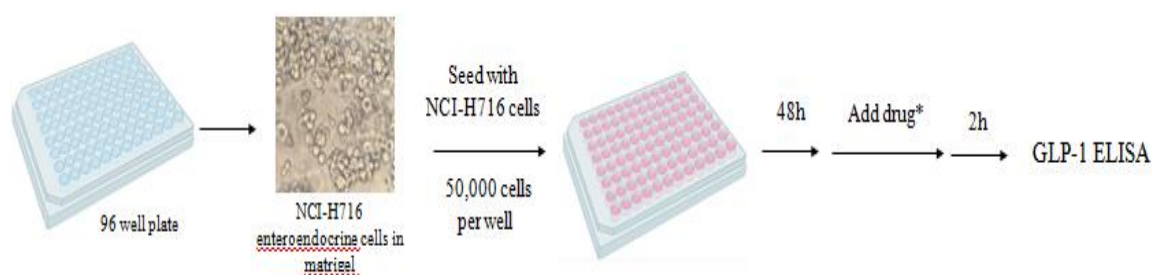


**Figure 43: Flow diagram for GLP-1 secretion Assay**

#### 5.2.3.1.4. Real-time qPCR assay

Human NCI-H716 enteroendocrine cells in complete media, with a consistent DMSO concentration serving as the negative control. The cells underwent overnight incubation with the compounds in complete media in 5% carbon dioxide environment at 37°C. Subsequently, cells were taken in RNase-free Eppendorf tubes, followed by washing with 1X PBS through centrifugation at 4°C at 500 g. TRIzol (Thermo Fisher Scientific) was added to cell pellets, and the tubes were promptly frozen in liquid nitrogen until further analysis.

For RNA extraction, cells were thawed on ice and maintained on ice whenever possible. The tubes were vortexed for 30 seconds to release RNA and disrupt membranes. 200 µL Chloroform in TRIzol (1 mL) was introduced and stirred for 30 seconds. At 4°C, tubes were centrifuged for 15 min at 12,000 rpm. After transfer to

Eppendorf tubes free from RNase containing 2-propanol (500 mL 2-propanol/1 mL TRIzol), the tubes were inverted to mix. Cells were centrifuged for 10 minutes at 4°C. The pellets were centrifuged at 4°C for 5 minutes at 14,000 rpm after washing with 70% ethanol. As a final step, air-drying of the RNA pellet was followed by resuspension in RNase-free H<sub>2</sub>O. For cDNA synthesis, High Capacity cDNA Reverse Transcription Kit was employed. Quantitative PCR (qPCR) was performed using Light Cycler 480 SYBR Green I Master in 384-well format on Quant Studio Pro (ThermoFisher). For determining relative change in gene expression in the groups, the 2- $\Delta\Delta C_t$  method was used, and the data were compared to controls or estimates for comparison between the groups.

qPCR primers used were human *Tgr5*: Forward: 5'-CCTAGGAAGTGCCAGTGCAG-3', Reverse: 5'-CTTGGGTGGTAGGCAATGCT-3'; human *Gapdh*: Forward: 5'-GAAGGTGAAGGTCGGAGT-3', Reverse: 5'-CATGGGTGGAATCATATTGGAA-3'.

#### 5.2.3.1.5. Quantification and Statistical analysis

GraphPad Prism was used to plot data and quantify the data using software linked to the instrument indicators. Microsoft Excel and GraphPad Prism were used for statistical analyses. Whenever possible, one-way ANOVA and Dunnett's multiple comparisons tests were used for assessing statistical significance.

Further, based on results of *In Vitro* studies, test compounds 2a, 14a and 15a were selected for *In Vivo* studies.

#### 5.2.3.2. *In vivo* Studies

The current research includes *in vivo* studies commencing with the Brine shrimp lethality assay. The bioassay operates on principle of assessing mortality induced in the basic aquatic organism, brine shrimp (*Artemia salina*), by the test compounds. It functions as an initial screening measure for toxicity prior to advancing to experiments involving mammalian animal models.<sup>119</sup> Afterward, acute toxicity experiments were carried out for compound 15a to assess its toxicity characteristics as per OECD guidelines. Subsequently, an OGTT was conducted to evaluate the antidiabetic properties of the compound.

#### **5.2.3.2.1. Brine shrimp lethality assay** <sup>124, 125</sup>

Sample preparation: Samples preparation was carried out by dissolving 10 mg in 2 mL of DMSO and adjusting the volume to 10 mL with distilled water, resulting in a stock solution of 1000 µg/mL. From stock, 10 µL, 100 µL, and 1000 µL were withdrawn, make up volume upto 5 mL with water to achieve final concentrations of 10, 100, and 1000 µg/mL, respectively. Three replicates for each dose level were prepared. In the control vials, equivalent volumes of distilled water were added.

Preparation of Sea water: The solution of Crude sea salt was prepared in distilled water to get concentration of 25 g/L, and dried Brewer's yeast at a concentration of 6 mg/L was added to create a solution for feeding brine shrimp. Subsequently, the solution was filtered before being put to use.

Hatching of Brine shrimp eggs: The designated chamber was supplied with 2 litres of seawater, and 40 mg of eggs. Subsequently, these eggs were washed and dispersed into the shaded compartment. After 48-hour duration, phototropic nauplii were retrieved from illuminated side using a capillary and utilized for the bioassay.

Bioassay: The bioassay was carried out as per protocol outlined by Meyer *et al.* The nauplii were extracted with water using a glass capillary, and after being counted in capillary against an illuminated background, 10 shrimps were transferred into each sample vial containing 4 mL of brine solution (in combination with a specific volume of brine and yeast suspension). At each concentration, 0.5 mL of test compound solution was added to brine solution (4.5 mL). For the control vial, 4.5 mL of artificial seawater with 0.2% DMSO was added, and 0.5 mL of artificial seawater without DMSO. The percentage of survivors was calculated using Ramachandran et al.'s 2011 formula based on the number of survivors counted after 24 hours with 3x magnifying glasses.

#### **5.2.3.2.2. Acute Toxicity Studies** <sup>127</sup>

Selection of animal: In the study, Albino Wister rats was used to carry out acute toxicity study (Fig. 44). The rats were acquired from the National Institute of

Biosciences, Pune 412205. **It's noteworthy that Institutional Animal Ethical Committee approved experimental protocol under protocol number 'BiRo/Sangli/IAEC/03'.** All the procedures were followed as per the guidelines for guiding the care and use of animals in experimentations.



**Figure 44: Albino Wister rats**

**Condition of housing:** The animals were kept in cages made up with polycarbonate, and the animal rooms adhered to standard conditions of animal husbandry. Animal room's temperature was maintained at  $22\pm 3^{\circ}\text{C}$ , with a humidity ranging from 30 to 70%. It was decided to maintain a period of 12 hours of light and 12 hours of darkness.

**Procedure:** The procedure utilized the OECD 423 (Acute Toxic Class Method). Seven-week-old Wistar rats were selected, ensuring weight variation within  $\pm 20\%$  of the mean body weight for each gender. The experimental group made up of 6 animals (3 males and 3 females). The objective of the sighting study was to establish the appropriate initial dose for the main study. A single animal received the test substance (15a) sequentially, starting from fixed dose levels of 5, 50, 300, and 2000 mg/kg. The dose intervals were determined by monitoring mortality and any of toxic signs over a 24-hour period. This was done with a particular focus on the initial 4 hours.

**Observations:** Food and water were provided four hours post-administration, and observations were made daily for 14 days, assessing factors such as duration, onset,

and severity of toxic signs, food, and water intake. Animal weights were recorded weekly. Subsequent experiments involved six animals per dose level based on mortality results from the sighting study. The animals were observed once during first half of an hour then for the first four hours after giving test compound. For clinical signs, if any, a 14-day period was monitored.

#### **5.2.3.2.3. Oral Glucose Tolerance Test (OGTT) <sup>69</sup>**

This investigation aimed to assess the Oral Glucose Tolerance Test using a synthetic compound 15a, in experimental rats. The rats were accommodated in animal house facility with appropriate environmental conditions, maintaining a  $20 \pm 3^{\circ}\text{C}$  temperature and 30-70% RH. 12-hour light and dark cycle was manually upheld throughout the study.

Grouping of animals: Animals were categorized into three groups, comprise of six rats in one, and the specific details of the treatment administered to each group are outlined in Table 5. Group I - the control, where Carboxy Methyl Cellulose (CMC) was administered at a concentration of 0.5% w/v. Group II - the positive control, receiving Sitagliptin at a dose of 10 mg/kg. Group III - the test group, receiving the test compound at a dosage of 400 mg/ kg.

Procedure: The OGTT was performed on rats that had been fasting overnight. Three groups of rats received different treatments: Distilled water, Test compound (15a) at a dosage of 400 mg/kg, and Sitagliptin at a dosage of 10mg/kg. After pre-treatment, glucose (2 g/kg) was administered 30 minutes before measuring glucose levels in blood at 0, 30, 60, 90, 120, and 240 minutes following glucose load. The assessment involved using blood glucose test strips and a glucometer to determine the influence of the test compound on glucose levels in the glucose-loaded animals.

**Table 5: Allocation of groups of animals**

Groups	Treatment	Dose & Route	No. of animals
G1	Control	-	6
G2	Standard (Sitagliptin)	10mg/kg,p.o.	6
G3	Test compound (high dose)	400mg/kg,p.o.	6



**Figure 45: Use of glucometer to determine blood glucose level**

Statistical Analysis: It was performed utilizing software GRAPHPAD PRISM 5.0. For evaluating statistical significance, ANOVA was employed, with subsequent comparison conducted through Dunnett's t test. The test results were expressed as Mean  $\pm$  Standard deviation (SD). The level of significance were defined as follows: *P* values if less than 0.05 were categorized as Significant, *P* values less than 0.01 very significant, *P* values less than 0.001 highly significant, while "ns" denoted non-significance.



# RESULT AND DISCUSSION



## **CHAPTER 6**

### **6. RESULT AND DISCUSSION**

#### **6.1. *IN-SILICO* STUDIES**

##### **6.1.1. Homology Modelling**

The purpose of current study was to perform homology modelling for revealing the folding and functional structure of TGR5 coding protein. In present study, best TGR5 homology model was selected from models generated by two software tools: Swiss Model and I-Tasser., I-Tasser generated top five models and Swiss Model generated six homology models for TGR5.

Table 2 and 3 showed the identity and similarity of the generated models from both the server.

##### **6.1.1.1. Protein modelling using Swiss Model**

In the process, among all generated templates, the highest-ranked six templates were elected based on its similarity and identity of the sequence of the TGR5 protein as shown in Table 2. The highest value of sequence similarity was found with the template 5mzj and 5iu7. The 5iu7 template, when compared to the 5mzj, showed greater structural similarity (Table 2). The sequence identity, sequence similarity, and range of protein sequences of 5iu7 were the highest. Therefore, by using template 5iu7, a three-dimensional (3D) structure homology model was developed for TGR5. In Fig. 46a, a sequence alignment of modelled protein and template 5iu7 was shown. Secondary structure of both 5iu7 and model were generated and shown in Fig. 46b and Fig. 46c respectively.

Validation result for model (PDB ID: 5iu7) generated by Swiss Model

The model generated was validated using PROCHECK, PROSA, SAVES. Ramachandran plot was generated by PROSA shown in Fig. 47. For further analysis, the

model with most residues in allowed region (red) and fewest in disallowed (yellow) was chosen. According to the Ramachandran plot generated for the selected model, 225 residues are present in the preferred region (94.5%), and 12 residues are present in the allowed region (5.0%). In the selected model, PROSA revealed a Z-score of -5.73, which indicates structures similar to native structures. The ERRAT server (Fig. 48) indicated an overall quality factor of 92.806. Identity and similarity index is 19.93% and 30% respectively. LG score calculated by ProQ was 3.030 (Table 2).

#### **6.1.1.2. Protein modelling using I-Tasser**

In the process of protein modelling, 3D model was generated from large assembly of structural conformations; TGR5 was modelled using the 3emL structure as a template for generating the 3D model structure. I-Tasser evaluates the model using two parameters: the C-score and the TM-Score. It has been found that the C-score for the homology model 1 generated from template 3emL is adequate, and is found to be -0.67, making it the most confident model. The TM-score ( $0.63 \pm 0.14$ ) and values ( $7.9 \pm 4.4 \text{ \AA}$ ) of the modelled protein are acceptable for a proper design. The alignment between the homology model and 3emL illustrated in Fig. 49a exhibits heightened levels of identity, similarity, and coverage. Secondary structure of both template 3emL and model were predicted using I-Tasser and shown in Fig. 49b and Fig. 49c.

Validation result for model 1 by I-Tasser

The model was validated using PROCHECK, PROSA Web server and SAVES. Ramachandran plot was generated by PROSA shown in Fig. 50. A model with the maximum residues in allowed region (red) and lowest number in disallowed region (yellow) was selected for further analysis. Using Ramachandran plot generated for selected model, number of residues present in favoured regions is 221 (81.0%), number of residues present in allowed region is 39 (14.3%), residues in generously allowed region is 9 (3%) and residues in disallowed regions is 4. Residues in disallowed regions are Leu 246, Phe 161, Ser and Arg 254 (A). An assessment of the selected model with

PROSA revealed that it had structures similar to native structures with a Z –score of -5.51. ERRAT server (Fig. 51) indicated an overall quality factor 93.458. Identity and similarity index is 21 and 22 percent respectively. LG score calculated by ProQ was 4.173 (Table 3).

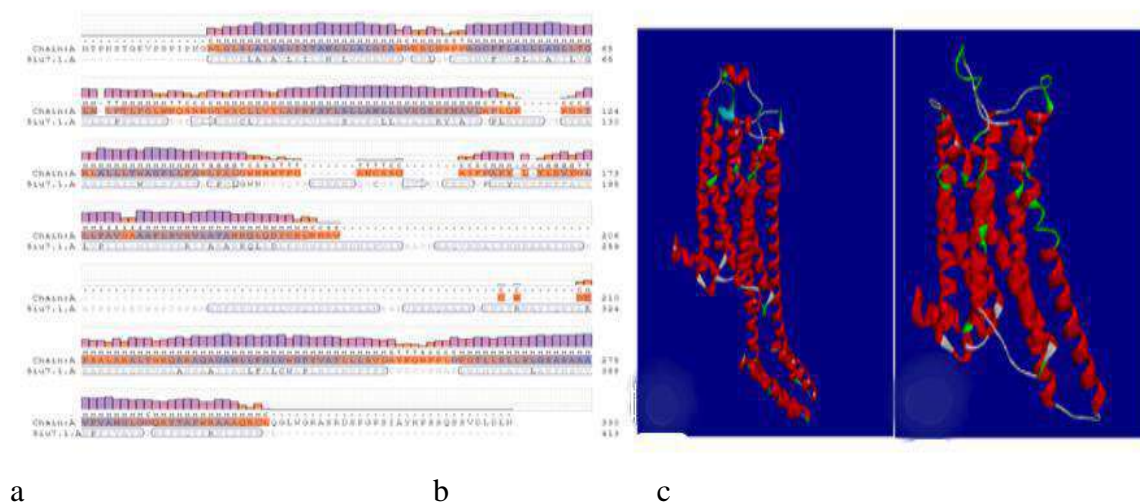


**Figure 46: a) Sequence alignment of Chain A of model and Secondary structure of (b) 5iu7 and model using (c) Swiss model 5iu7**

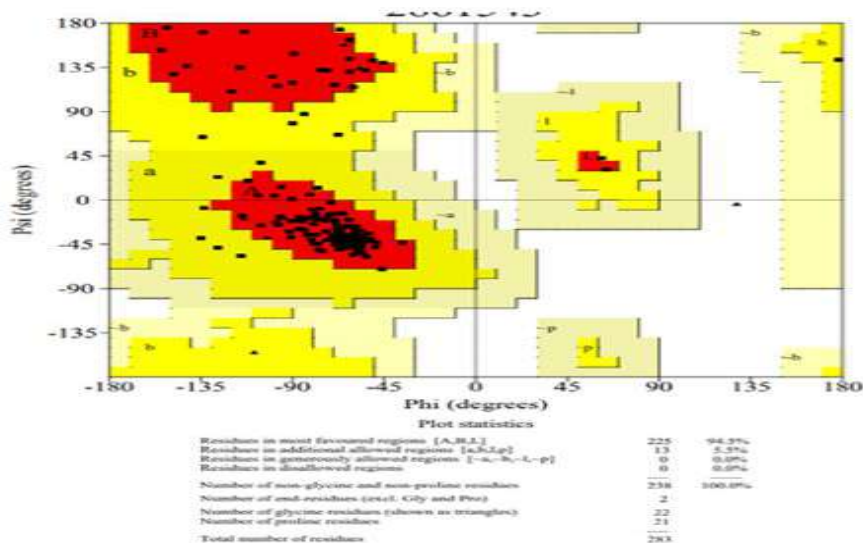
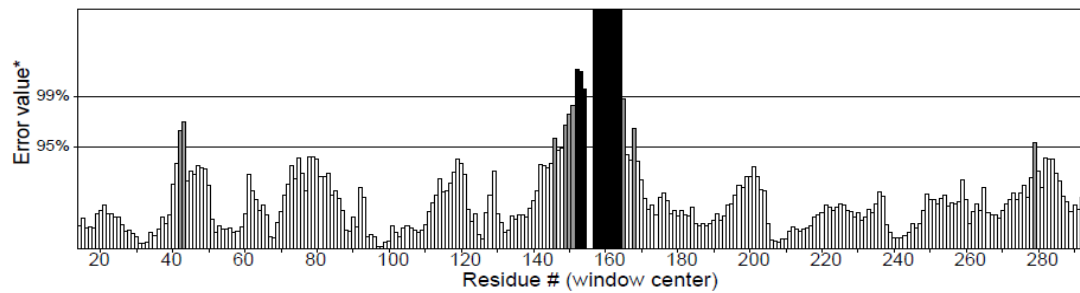


**Figure 47: Ramachandran Plot of Model (PDB ID: 5iu7) generated by Swiss Model server**

Program: ERRAT2  
File: /home/saves/Jobs/2941974/qq\_aaaa.pdb\_errat.logf

Overall quality factor\*: 92.806



\*On the error axis, two lines are drawn to indicate the confidence with which it is possible to reject regions that exceed that error value.  
\*\*Expressed as the percentage of the protein for which the calculated error value falls below the 95% rejection limit. Good high resolution structures generally produce values around 95% or higher. For lower resolutions (2.5 to 3Å) the average overall quality factor is around 91%.

**Figure 48: ERRAT Results of Model generated by Swiss Model**

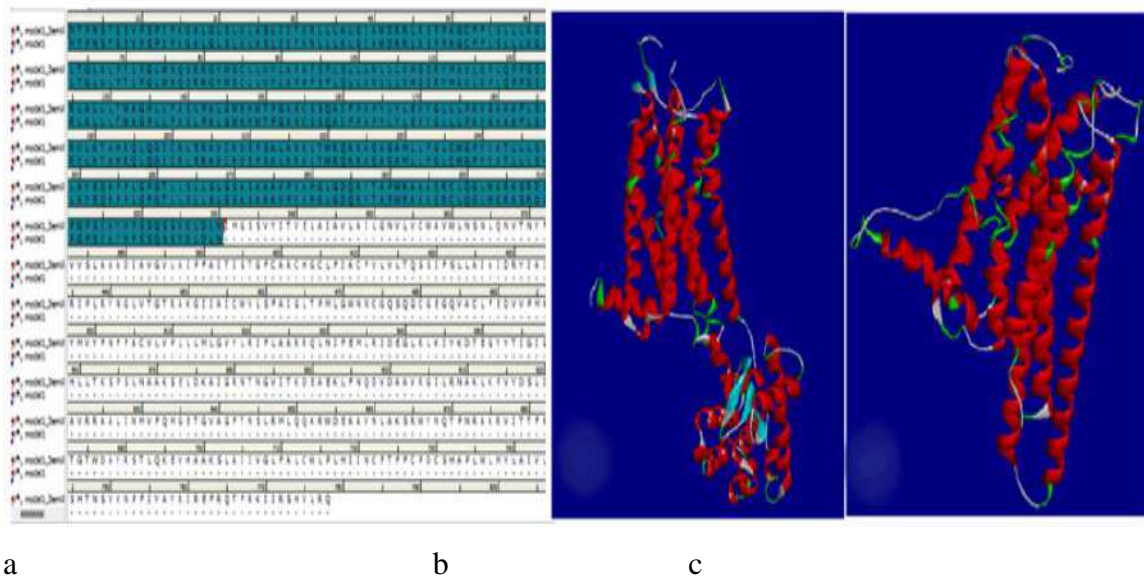


**Figure 49: a) Sequence alignment of model and template b) Secondary structure of template and (c) model generated using I- Tasser**

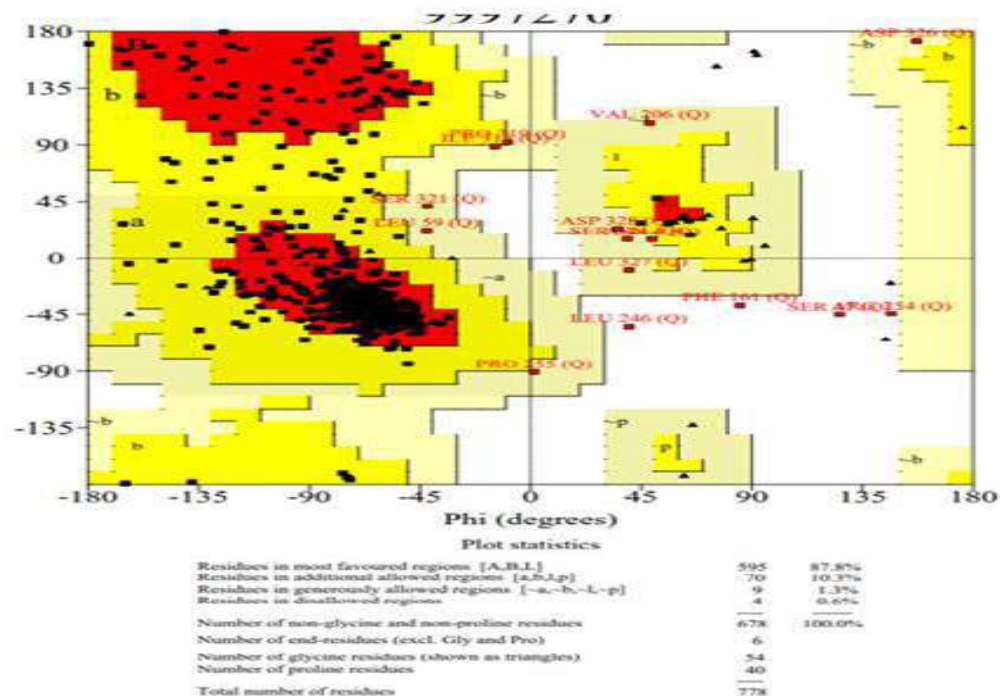
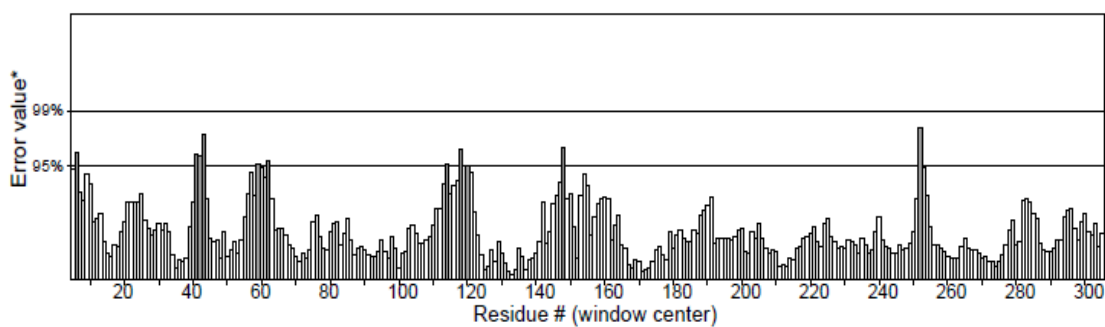


**Figure 50: Ramchandran Plot of Model generated by I-Tasser**

Program: ERRAT2  
File: /home/saves/Jobs/9841242/qq\_aaaa.pdb\_errat.logf

Overall quality factor\*\*: 93.458



\*On the error axis, two lines are drawn to indicate the confidence with which it is possible to reject regions that exceed that error value.

\*\*Expressed as the percentage of the protein for which the calculated error value falls below the 95% rejection limit. Good high resolution structures generally produce values around 95% or higher. For lower resolutions (2.5 to 3Å) the average overall quality factor is around 91%.

**Figure 51: ERRAT Results of Model generated by I-Tasser**

For selection of best model out of those generated by both Swiss Model and I-Tasser, a comparative study was carried out between the models generated by these two servers. A comparison of results from Swiss Model and I-Tasser is presented in Table 6 that helps confirm which model is appropriate for further investigation. Comparative study of the model generated by both software's was done for selection of best model among the model generated by two different servers. The model generated by Swiss Model does not have any residue in the disallowed region when compared with model generated by I-Tasser which has 1.46 % outliers also had 93.458 overall quality factor. Therefore, model generated by Swiss model was selected for further studies.

**Table 6: Comparison results for TGR5 Model using Swiss Model and I- Tasser**

Homology modelling tools		Swiss Model	I-Tasser
<b>PROCHECK</b>	<b>Allowed region</b>	100%	98.53%
	<b>disallowed region</b>	0%	1.46%
<b>Z score</b>		-5.73	-5.51
<b>ERRAT</b>		92.806	93.458

### 6.1.2. MOLECULAR DOCKING STUDIES<sup>128</sup>

The high-resolution TGR5 crystal (PDB ID: 7CFN) has been downloaded from RCB PDB database. Following this, docking studies were done out using Autodock Vina and docking results are presented in Table 7.

#### 6.1.2.1. Validation of docking studies

The target validation performed using the selected target (PDB ID: 7CFN) and native co-crystallized ligand (INT777) indicated low RMSD values (1.2Å) between runs, indicating the docking procedure is accurate and repeatable (Fig. 52a). The re-docking analysis of INT777 with TGR5 showed the docking score of -8.2 kcal/mol. INT777 showed H bond



interactions with active site residues of TGR5 such as Tyr240, Ser270 (bond distance of 2.89Å and 2.69Å respectively). In addition, active site residues Leu263, Leu266, Leu166, Leu74, and Ala250 were involved in  $\pi$ - $\pi$  stacking and  $\pi$ -alkyl interactions with INT777 (Fig. 52b).

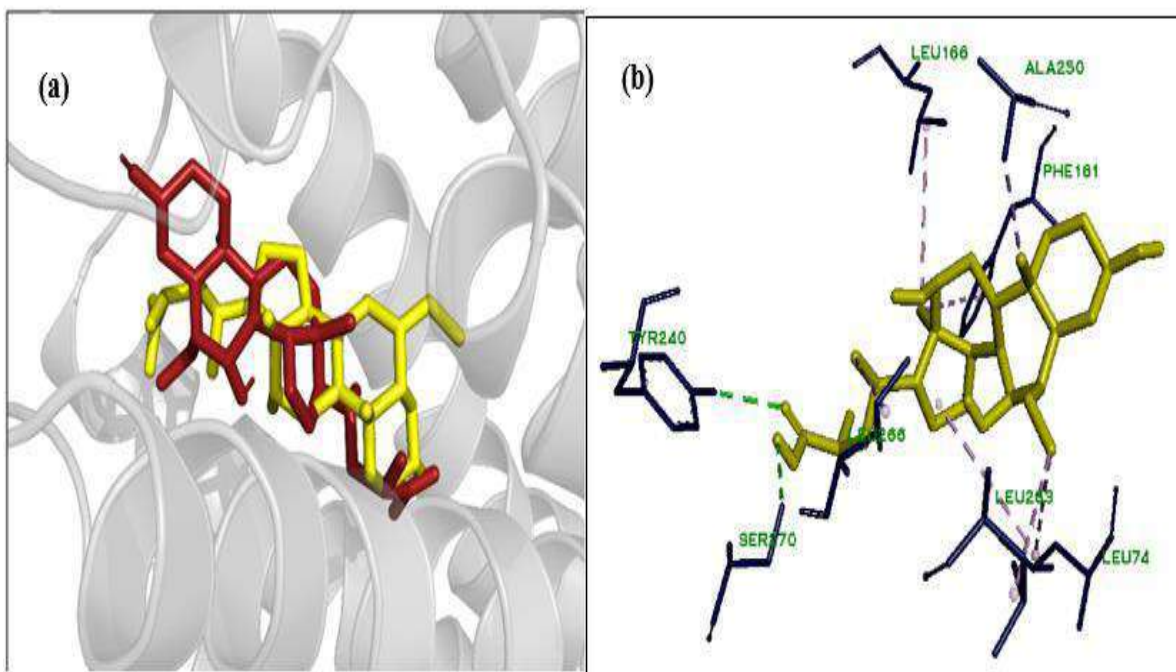


**Figure 52: (a) Superimposition of re-docked INT777 (red) onto co-crystallized form (yellow) in the active site (b) Molecular Interaction of INT777 with TGR5.**

From total docked compounds, all compounds showed binding energies ranging from -10.2 to -9.0 kcal/mol toward the TGR5 receptor in comparison with standard INT777 (Docking scores -8.2 kcal/mol). The binding scores and RMSD values of captured poses were used to select poses, especially those that were found to have very close binding modes when compared to INT777. Table 7 summarizes the detailed intermolecular interactions and binding affinity of the compounds for TGR5. The binding interaction of ten best molecules for TGR5 is given in Fig. 53.



**Table 7: The intermolecular interactions and binding affinity of compounds for  
TGR5**

<b>Sr. No.</b>	<b>Compound Name</b>	<b>Binding energy (kcal/mol)*</b>	<b>Interacting Amino Acids</b>	<b>Bond Type</b>	<b>No. of H bonds</b>
1.	INT777	-8.2	Tyr240 Ser270 Leu266 Leu263,166 Leu74 Ala250	H bond H bond	2
2.	6a	-9.9	Phe 96 Leu 266 Leu 262 Leu 74 Ala 250 Pro 255	$\pi$ - $\pi$ stacking	0
3.	16b	-9.8	Trp75 Ala250 Leu244 Leu166 Leu74 Leu174	H bond $\pi$ - $\pi$ stacking	1
4.	14b	-9.8	Ser 247 Trp 75 Ala 250 Leu 244 Leu 166 Val170	H bond H bond $\pi$ - $\pi$ stacking	2
5.	14a	-9.8	Ser 157 Tyr 240 Trp 75 Ala 250 Leu 244 Leu 74, 97 Phe 96	H bond H bond H bond $\pi$ - $\pi$ stacking	3
6.	16a	-9.8	Trp 75 Ala 250 Leu 166 Leu 244 Leu 74 Val 170	H bond $\pi$ - $\pi$ stacking	1

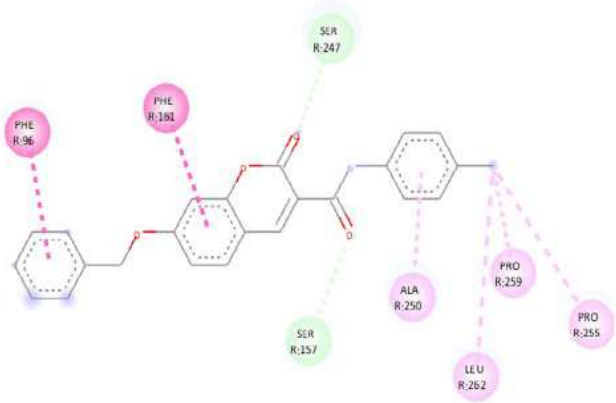
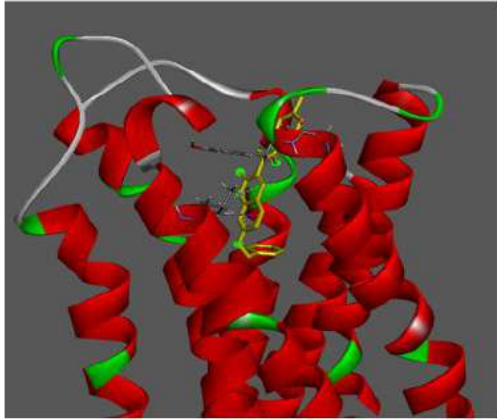
7.	15a	-9.8	Ser 157 Tyr 240 Ala 250 Leu 74 Leu 266 Leu174 Leu97 Phe 96	H bond H bond $\pi$ - $\pi$ stacking	2
8.	6b	-9.7	Ser 247 Ala 250 Leu 262 Pro 255 Phe 96	H bond $\pi$ - $\pi$ stacking	6b
9.	6c	-9.7	Leu 244 Leu166 Leu 74 Leu263 Val170	$\pi$ - $\pi$ stacking	6c
10.	8a	-9.7	Ser 157 Leu 166 Ala250	H bond $\pi$ - $\pi$ stacking	1
11.	8b	-9.6	Ala 250 Leu 262 Leu166	$\pi$ - $\pi$ stacking	0
12.	8c	-9.6	Trp 75 Leu 266 Leu 74 Leu 262 Ala 250 Phe 96 Pro 255	H bond $\pi$ - $\pi$ stacking	1
13.	9a	-9.6	Trp 75 Leu 266 Leu 74 Phe 96	H bond $\pi$ - $\pi$ stacking	1
14.	7a	-9.6	Ser 27 Ser 157 Ala 250 Leu 262 Pro 255 Pro 259 Phe 96, 161	H bond H bond $\pi$ - $\pi$ stacking	2

15.	7b	-9.6	Leu 74 Leu 266 Ala 250 Leu 262 Phe 96 Pro 255	$\pi$ - $\pi$ stacking	0
16.	7c	-9.5	Leu 74 Leu 266 Ala 250 Leu 262 Phe 96	$\pi$ - $\pi$ stacking	0
17.	5a	-9.5	Ser 247 Ala 250 Pro 259,255 Ser 157 Phe 96 Phe 161	H bond $\pi$ - $\pi$ stacking $\pi$ - alkyl interaction H Bond $\pi$ - $\pi$ stacking	
18.	5c	-9.4	Ser 247 Ala 250 Leu 266, Leu 262, 263 Ser 157 Phe 96 Phe 161	H bond $\pi$ - $\pi$ stacking $\pi$ - alkyl interaction  H bond $\pi$ - $\pi$ stacking	2
19.	5d	-9.4	Ser 247 Ser 157 Phe 161 Phe 96 Leu 263 Ala 250 Pro 259	H bond H bond $\pi$ - $\pi$ stacking	2
20.	13a	-9.4	Ser 157 Tyr 240 Ala 250 Leu 244 Phe 96	H bond H bond $\pi$ - $\pi$ stacking	2
21.	13b	-9.4	Ser 157 Tyr 240 Trp 75 Ala 250 Leu 244	H bond H bond H bond $\pi$ - $\pi$ stacking	3
22.	17a	-9.4	Trp75 Ala250 Leu244	H bond $\pi$ - $\pi$ stacking	1

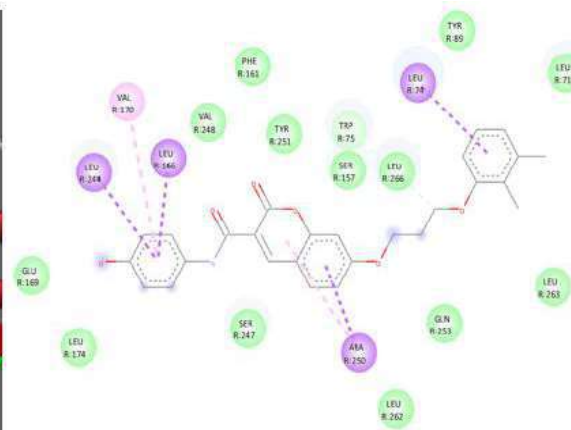
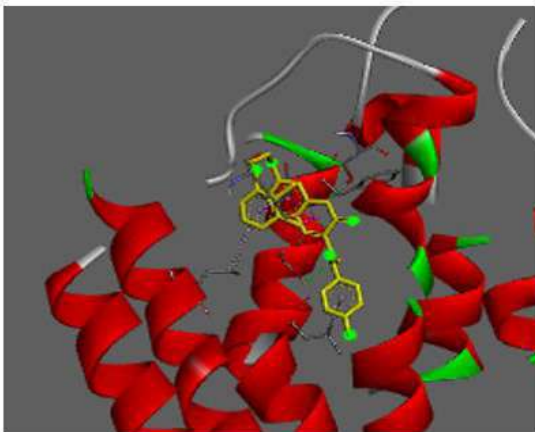
			Leu166 Leu74 Leu174 Val 170		
23.	3	-9.4	Trp 75 Leu 266, Leu 262 Leu 74 Ala 250	H bond $\pi$ - $\pi$ stacking	1
24.	5b	-9.4	Ser 247 Ala 250 Leu 263 Ser 157 Phe 96 Phe 161	H bond $\pi$ - $\pi$ stacking $\pi$ - alkyl interaction H Bond $\pi$ - $\pi$ stacking	2
25.	4	-9.2	Ser 157 Ala 250 Leu 166 Leu 244,262 Val 170	H bond $\pi$ - $\pi$ stacking	1
26.	9b	-9.2	Trp 75 Leu166 Leu 74 Phe 96	H bond $\pi$ - $\pi$ stacking	1
27.	9c	-9.2	Trp 75 Leu 266 Leu 74	H bond $\pi$ - $\pi$ stacking	1
28.	10a	-9.2	Ser 247 Ser 157 Pro 259 Ala 250 Phe 96 Phe 161	H bond H bond H bond $\pi$ - $\pi$ stacking	3
29.	10b	-9.2	Ser 247 Ala 250 Leu 266 Leu 262 Phe 96	H bond $\pi$ - $\pi$ stacking	1
30.	10c	-9.2	Leu 263 Leu 266, 262 Leu 74 Ala 250 Pro 255, 259	H bond $\pi$ - $\pi$ stacking	1

31.	15b	-9.1	Ser157 Tyr240 Ala250 Leu74 Leu244 Leu174 Phe96	H bond H bond $\pi$ - $\pi$ stacking	2
32.	18a	-9.1	Ser157 Tyr240 Leu74 Ala250	H bond H bond $\pi$ - $\pi$ stacking	2
33.	18b	-9.1	Ser157 Tyr240 Leu74 Ala250	H bond H bond $\pi$ - $\pi$ stacking	2
34.	18c	-9.1	Ser247 Ser157 Tyr240 Leu74 Ala250	H bond H bond H bond $\pi$ - $\pi$ stacking	3
35.	16c	-9.1	Ser157 Trp75 Leu174 Leu74	H bond H bond $\pi$ - $\pi$ stacking	2
36.	19a	-9.1	Ser247 Trp75 Leu244 Leu74	H bond H bond $\pi$ - $\pi$ stacking	2
37.	14c	-9.0	Ser247 Ser1578 Leu244 Leu74 Ala250	H bond H bond $\pi$ - $\pi$ stacking	2
38.	15c	-9.0	Ser 157 Ala 250 Leu74 Leu174 Tyr240	H bond $\pi$ - $\pi$ stacking	1
39.	17c	-8.8	Ser 157 Ala 250 Leu74	H bond $\pi$ - $\pi$ stacking	1
40.	17b	-8.8	Trp75 Ala250	H bond $\pi$ - $\pi$ stacking	1

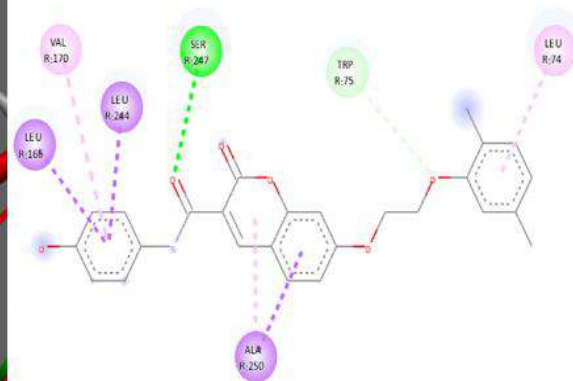
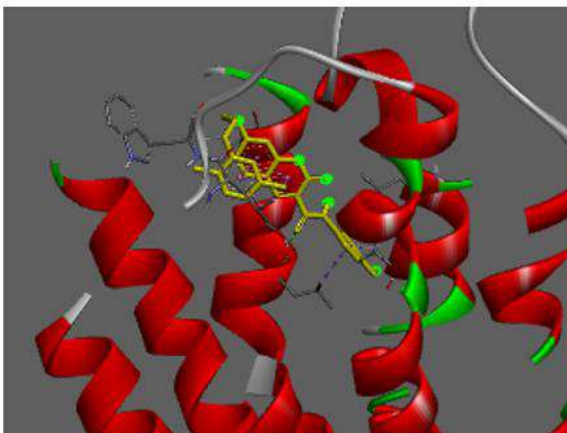
			Leu166 Leu244 Leu74 Leu174	$\pi$ - $\pi$ stacking	
41.	19c	-8.7	Ser247 Leu244 Leu74	H bond $\pi$ - $\pi$ stacking	1
42.	19b	-8.6	Ser157 Trp75 Leu244 Leu74	H bond H bond $\pi$ - $\pi$ stacking	2
43.	13c	-8.6	Ser 157 Ala 250 Leu74 Leu174 Tyr240	H bond H bond $\pi$ - $\pi$ stacking	2



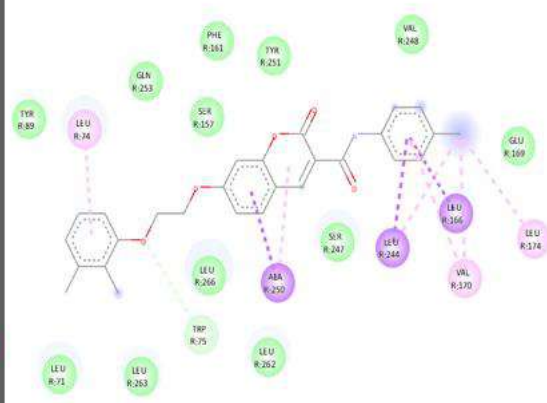
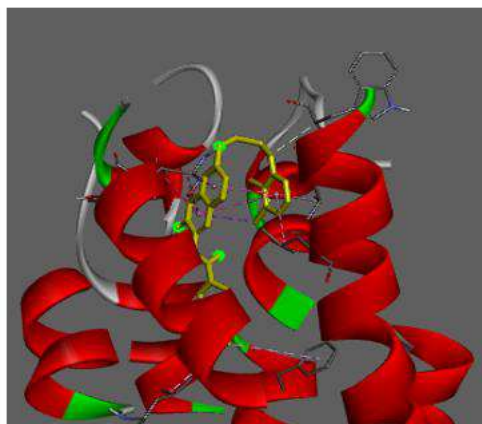
A



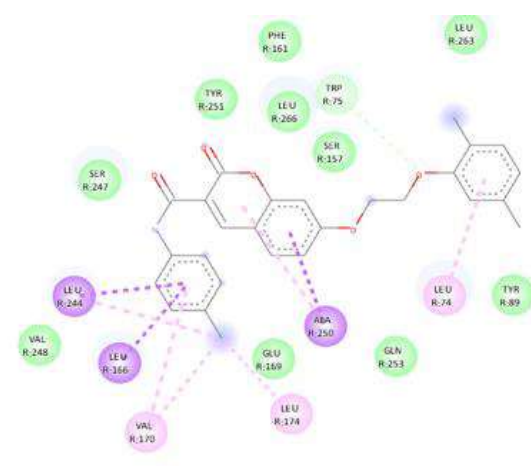
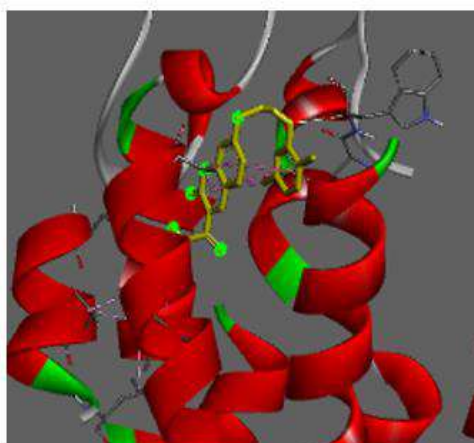
B



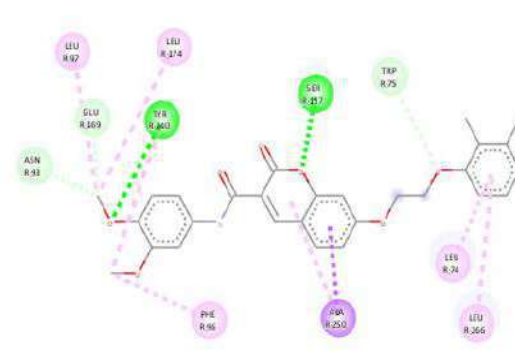
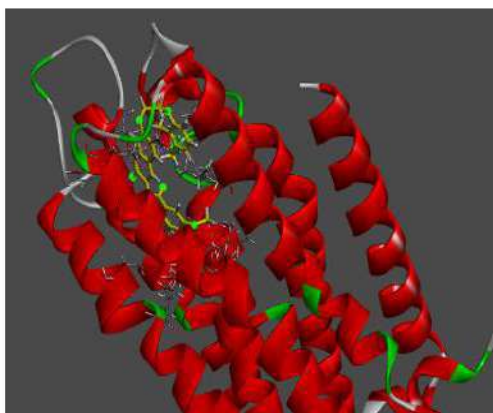
C



D

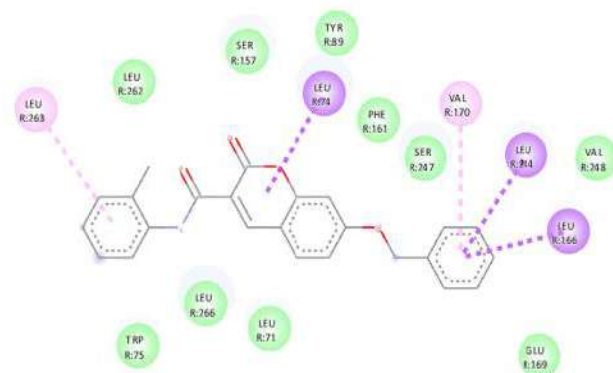
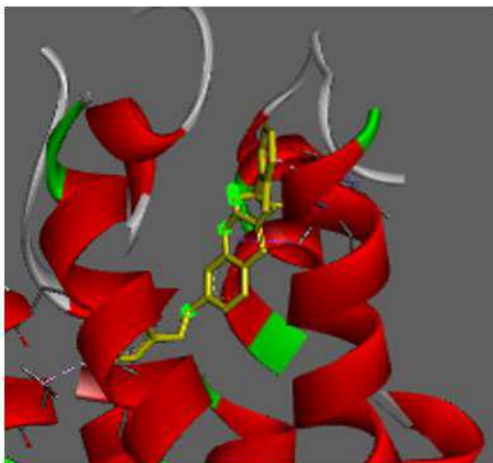


E

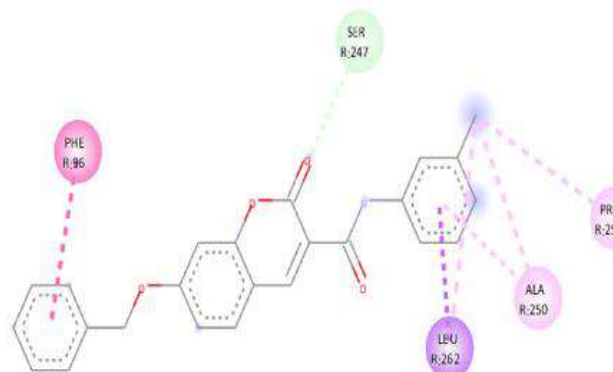
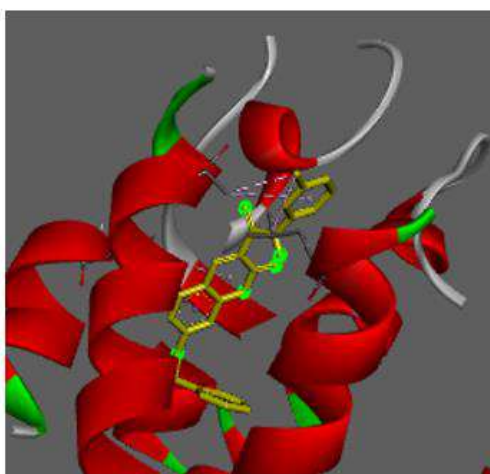


F

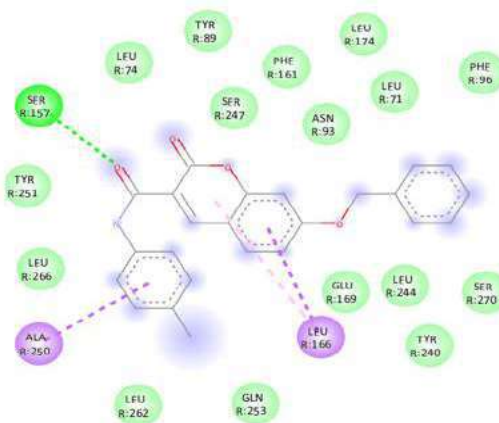
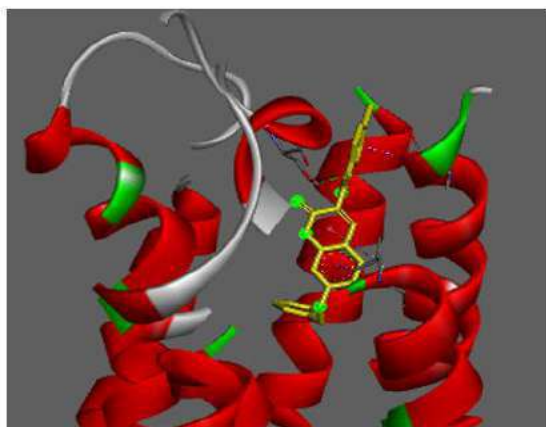




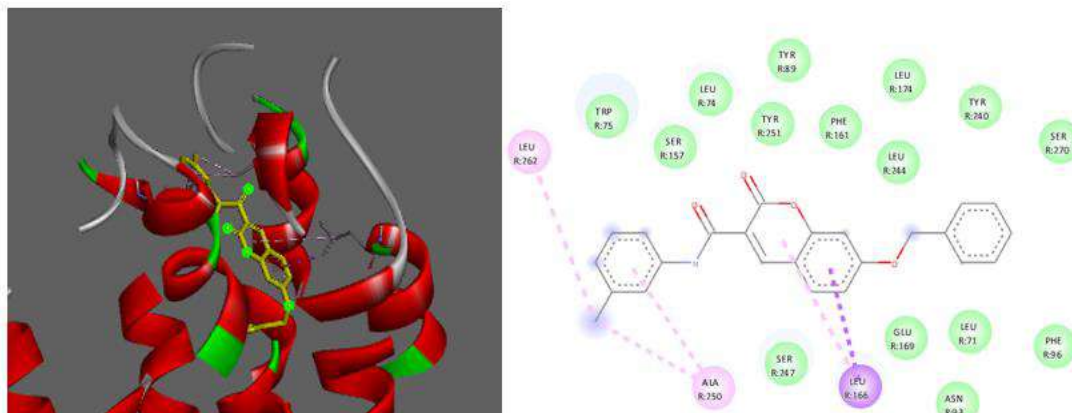
G



H



I



J

**Figure 53: 3D and 2D Intermolecular interactions between top 10 lead compounds with TGR5 (A) 6a, (B) 14a, (C) 14b, (D) 16a, (E) 16b, (F) 15a, (G) 6c, (H) 6b, (I) 8a and (J) 8b**

The molecular docking study reveal that compound 6a, compound 14a and 14b have the highest binding affinity towards TGR5 with docking scores of -9.9,-9.8 and -9.8kcal/mol respectively.

In compound 6a, the oxo group, a part of the coumarin ring, forms hydrogen bonds with Ser 247 at a distance of 2.83Å. Another hydrogen bond was found between Ser157 and oxygen atom in amide linkage. Also, the coumarin and aniline rings present in 6a were found to form  $\pi$ - $\pi$  stacking interactions with Phe96 and Ala250. Furthermore, amino acids such as Pro259, Leu262, and Pro255 interact with methyl groups on toluidine rings by means of  $\pi$ -alkyl interaction (Fig. 53A). A second lead hit compound 14a, interacts with TGR5 through four stacked  $\pi$ - $\pi$  interactions. In compound 14a coumarin ring, phenyl ring, and phenolic ring interact with Ala250, Leu74, Leu244, and Leu166 amino acids through a  $\pi$ - $\pi$  stacking mechanism (Fig. 53B). Similarly, compound 14b has been shown to interact with TGR5 via one hydrogen bond and five  $\pi$ -  $\pi$  stacking interaction (-9.8kcal/mol) (Fig. 53C). The polar residue Ser 247 forms hydrogen bond with the oxo group of the amide linkage of compound 14b. The coumarin ring form

interaction with Ala250 whereas Leu244, Leu166 and Leu74 were found to interact with the aromatic groups of compound 14b.

Both the rings of coumarin present in 16a also established the hydrophobic contact with residue of Ala 250 and was found to have binding affinity of -9.8 kcal/mol towards TGR5 (Fig. 53D). It was also observed that methyl group attached to the aniline ring interacted with three amino acids namely Leu244, Leu174 and Val170 of TGR5. Leu 74, Leu 244 and Leu166 was found to form  $\pi$ - $\pi$  stacking interaction with phenyl and aniline ring at the extreme end of compound 16a.

Furthermore, docking studies revealed binding energies of -9.8 kcal/mol for 16b in the active site of TGR5 (Fig. 53E). The four amino acids residue namely Ala250, Leu166, Leu244 and Leu74 was observed to have hydrophobic interaction with aromatic rings present in compound 16b, which provided additional stability to the complex. The compound 15a was found to interact through two types of molecular interactions with TGR5: hydrogen bond and  $\pi$ - $\pi$  interactions (Fig. 53F). The two hydrogen bonds are formed between Ser157- oxo group and Tyr240-methoxy group present in 15a with a bond length of 2.91 Å and 2.92Å. The coumarin and phenyl ring present in 15a was crucially important to form  $\pi$ - $\pi$  interactions with residues Ala250, Leu74, Leu 266. Furthermore, Leu 174, Leu97, Phe96 form alkyl interaction with methoxy group present in 15a.

Moreover, the docking studies of 6c, 6b, 8a and 8b revealed the binding energy of -9.6 to -9.7 kcal/mol each in the active site of TGR5. The coumarin ring present in compound 6c are involved in formation of  $\pi$ -  $\pi$  stacking interaction of 6c with Leu74 (Fig. 53G). The docking results of compound 6b revealed the hydrogen bond interaction with Ser247 owing to the presence coumarin ring present in 6b. The aniline and phenyl ring present in 6b was crucially revealed as important for hydrophobicity and established the hydrophobic contacts with amino acids like Ala 250, Leu262 and Phe96 present in the active site of TGR5. Additionally the methyl groups attached to the phenyl ring of 6b accounted for the interaction with Ala250 and Pro255 (Fig. 53H). The ten-membered ring of coumarin and six-membered ring of phenyl present in 8a was found to be important for

$\pi$ - $\pi$  stacking interaction with Ala250 and Leu 166. Moreover the oxygen atom present in amide group was found to be involved in hydrogen bonding with Ser157 at bond distance of 3.39 Å (Fig. 53I).

Further, compound 8b has been found to docked with TGR5 via  $\pi$ - $\pi$  and  $\pi$ -alkyl interaction (-9.6 kcal/mol) (Fig. 53J). Le166 and Ala250 from the active site of TGR5 were involved in the  $\pi$ - $\pi$  stacking interaction with the aromatic group present in 8b. Moreover the alkyl group on phenyl ring was also found to be crucial for forming the  $\pi$ -alkyl interaction with Leu262 and Ala250.

Thus, the molecular docking studies of designed compounds showed that the selected lead substances bind to TGR5 in a similar pattern as that of native ligand INT777. Active site residues includes Tyr240, Ser270, Leu263, Leu266, Leu166, Leu74, and Ala250 that were involved in  $\pi$ - $\pi$  stacking and  $\pi$ -alkyl interactions with INT777. Many of the designed compounds with coumarin ring showed hydrophobic  $\pi$ - $\pi$  stacking interactions with Leu166, Ala250. Thus, overall proposed compounds would be potent TGR5 agonist in comparison with the native ligand in the active site of the protein.

### **6.1.3. Molecular dynamic studies:<sup>127</sup>**

The docked complexes structure of TGR5 had been simulated unconstrained for 100ns using the best-docked poses of compounds 6a, 16a, 14b, 16b, 14a, INT-777, and Bile Acid. The thermodynamic stability of all the complex systems had been examined by using the parameters RMSD (Root Mean Square Deviation) and RMSFs (Root Mean Square Fluctuations), which were captured during a molecular dynamics simulation. The RMSD and RMSF are important parameters that provide data about structural stability and adaptability during the duration of the MD simulation.

#### **6.1.3.1. RMSD Plot evaluation:**

The RMSD plot of TGR5 C- $\alpha$  atoms illustrated in Fig. 54(a) suggested that, all the complexes equilibrated within 7 Å of RMSD and the selected lead compounds introducing higher stability to the TGR5 conformation upon binding. The co-crystal

ligand i.e., TGR5-INT777 complex equilibrated from 20ns to 60ns within 5 Å of RMSD, afterwards minimal deviation (within 6 Å) found in the structure in the production phase. In the case of Bile Acid, two equilibrations were found during the simulation. In the early stage, after 5ns the TGR5-complex started equilibrating within 4 Å - 6 Å till 60ns, after that the complex deviate little higher and started another equilibration in the production phase. In the other hand lead compounds 6a and 14a shows higher stability in comparison with others. The complexes, TGR5-6a, and TGR5-14a started equilibration from 20ns to production phase in the range of 3 Å -4 Å of RMSD.

Likewise, the complexes TGR5-16a, TGR5-16b and TGR5-14a, shows similar patterns when compared with the standard one. The complex TGR5-16a started equilibrating from 10ns to 100ns within the range of 4 Å to 5.5 Å RMSD. In the case of complex TGR5-14b, the complex was not stable in the initial phase of simulation, but after 42ns, the complex reaches the equilibration state with 6 Å of RMSD till 100ns. The TGR5 showing unstable during the simulation after complexing with lead compound D9, but the deviation within the structure is not beyond the 7 Å of RMSD. The average RMSD for TGR5-6a, TGR5-16a, TGR5-14b, TGR5-16b, TGR5-14a, TGR5-INT-777, and TGR5-Bile Acid complexes were  $3.71 \pm 2.92\text{\AA}$ ,  $4.82 \pm 3.99\text{\AA}$ ,  $5.09 \pm 4.22\text{\AA}$ ,  $4.45 \pm 4.68\text{\AA}$ ,  $3.36 \pm 2.14\text{\AA}$ ,  $4.40 \pm 2.68\text{\AA}$ , and  $5.14 \pm 4.42\text{\AA}$ , respectively. In this result, it can be concluded that lead compounds 6a, 16a, and 14a undergo minimal structural conformational changes throughout the simulation event.

#### 6.1.3.2. RMSF Plot evaluation:

The quality of local protein was assessed by comparing the time-averaged RMSF value of the selected lead compounds, co-crystal ligand and the standard Bile Acid (Fig. 54b), following its interaction with TGR5 against the number of residues found in the 100ns trajectory data. The average RMSFs values measured for TGR5-6a, TGR5-16a, TGR5-14b, TGR5-16b, TGR5-14a, TGR5-INT-777, and TGR5-Bile Acid complexes were  $1.86 \pm 0.96\text{\AA}$ ,  $1.60 \pm 0.82\text{\AA}$ ,  $2.04 \pm 1.39\text{\AA}$ ,  $2.28 \pm 1.34\text{\AA}$ ,  $1.66 \pm 1.08\text{\AA}$ ,  $1.88 \pm 1.09\text{\AA}$ , and  $2.19 \pm 1.36\text{\AA}$ , respectively, suggesting that the minimal fluctuation in the TGR5 structure

upon binding of the selected lead compounds, INT777 and Bile Acid (Fig. 54b). Based on RMSF values, all lead compounds exhibit relative stability in the binding site region of TGR5, as the interacting residues not fluctuating more than 3 Å of RMSF. It is also noted that, after binding of Bile Acid to TGR5, fluctuation in the binding site residues viz. Tyr240, Ser247, Ala250, Tyr251, and Pro255 RMSF values were more as compared to other compounds.

#### **6.1.3.3. Radius of gyration evaluation:**

The curve of the radius of gyration ( $R_g$ ) as a function of time for all protein-ligand complexes was depicted in Fig. 55a. The average  $R_g$  value of the complexes TGR5-6a, TGR5-16a, TGR5-14b, TGR5-16b, TGR5-14a, TGR5-INT-777, and TGR5-Bile Acid were  $21.50 \pm 0.29$  Å,  $21.60 \pm 0.17$ ,  $21.05 \pm 0.52$ ,  $21.47 \pm 0.77$ ,  $21.81 \pm 0.32$ ,  $21.93 \pm 0.29$ , and  $21.63 \pm 0.33$ , respectively. When compared to the standard and co-crystal ligand, it was discovered that all lead complexes showed generally similar and consistent values of  $R_g$  (except TGR5-D9 complex), indicating that are perfectly overlapped and have good stability. Similarly, the SASA value was calculated to determine the percentage of the protein surface that was accessible by the water solvent during MD simulation. The plot of SASA value vs. time for all of the protein-ligand complexes during the simulation is shown in Fig. 55b. Comparing all of the complexes to the TGR5-INT777 and TGR5-Bile Acid complexes, SASA values were quite close. We infer that TGR5-Lead complexes are relatively constant from the SASA analysis.

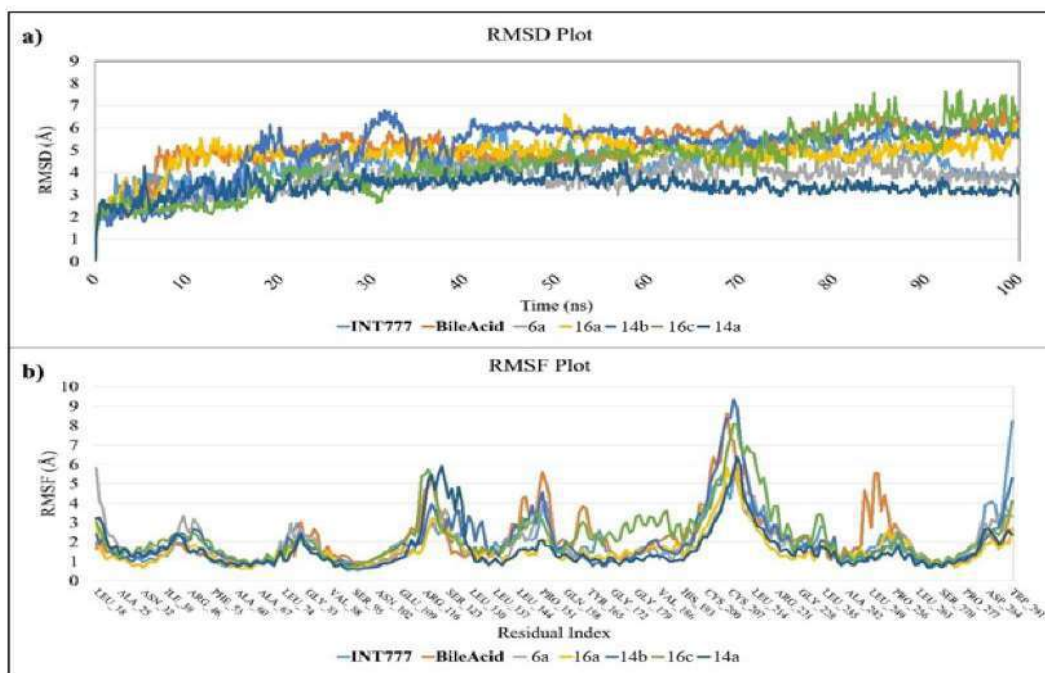


**Figure 54: (a) RMSD plot (b) RMSF plot for TGR5 – complex atoms upon binding of lead compounds, INT-777 and Bile Acid, during 100ns MD simulation.**

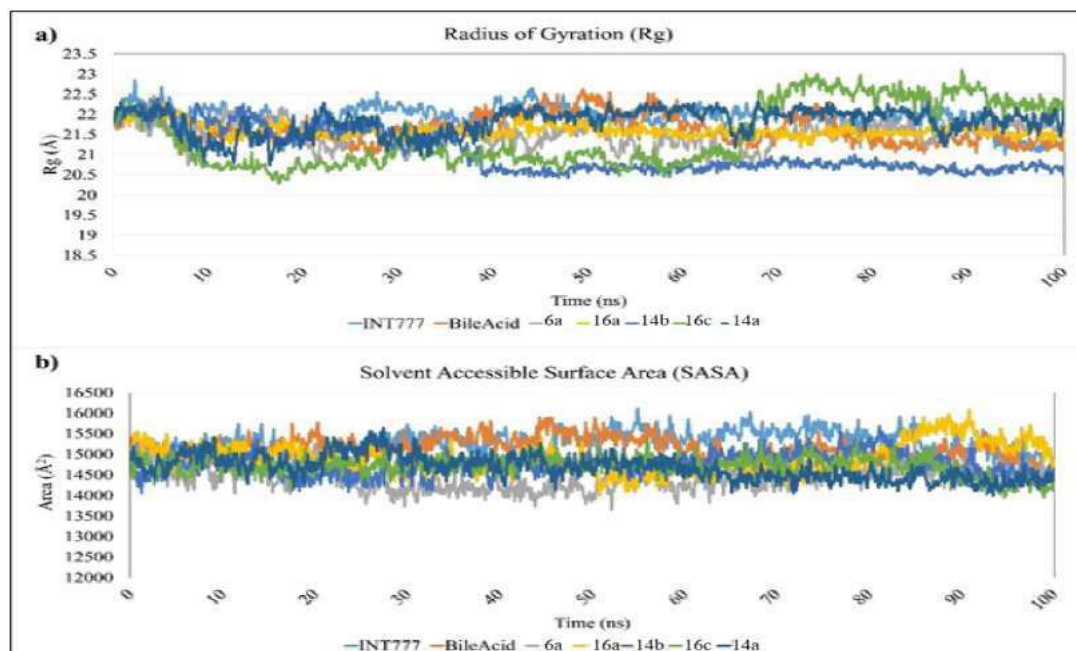


**Figure 55: (a) Radius of gyration plot reflecting the changes observed in the conformational behaviour of the protein and all protein–ligand complexes (b) The SASA curve depicts the change in the protein-ligand complexes' solvent accessibility**

#### 6.1.3.4. Interaction profiling and per residue energy contribution

Furthermore, the Protein interactions with the lead compounds were tracked throughout the simulation. Unlike molecular docking, where you obtain the optimal orientation for the binding of a ligand, MD simulation assesses all binding modes by averaging the interactions between proteins and ligands and determining the best interactions. The per-residue contribution was computed in terms of binding to examine the specific binding stability of a few lead molecules with the receptor. The protein-ligand contact plot, shown in Fig. 56, is a timeline representation of the contacts and interactions (H-bonds, Hydrophobic, Ionic, Water bridges).

From the docking analysis, the binding site residues were provided for all the compounds. Fig. 56 supports finding and string binding of these lead compounds to the TGR5. In case of TGR5-INT-777 complex, it is noted that the amino acid residues viz. Tyr89, Asn93, Ser157, Gln158 and Pro259 contacted majorly with INT-777 during 100ns of MD simulation (Fig.56a). Similarly, the standard compound i.e., Bile Acid binds very well in the TGR5 binding pocket by forming interactions with Leu74, Tyr89, Arg93, Ser157, Glu169, and Thr243 constantly during the simulation (Fig.56b). In case of all the selected lead compounds the similar binding patterns were observed. From the intermolecular interaction profile, it is noted that the key residues Leu74, Trp75, Tyr89, Arg93, Ser157, Leu166, Glu169, Thr243, Ala250, Pro259, and Leu263 play a crucial role in the strong binding of small molecules.

Similarly, Table 8 and Fig.57 represent per residue energies contributed to the docking score.

#### 6.1.3.5. Binding Free Energies:

The cumulative binding free energy for each complex system are described in Table 9. Remarkably, the selected lead compounds are having greater binding affinity ( $-77.891 \pm 8.37$  kcal/mol to  $-96.636 \pm 9.18$  kcal/mol) and stability toward selected receptors than that of the INT-777 ( $-69.43 \pm 9.17$  kcal/mol) and Bile Acid ( $-63.432 \pm 6.14$



kcal/mol). The lead compounds are thermodynamically more stable inside the binding cavity, according to these MM/GBSA binding free energies.

**Table 8: Per residue interaction score contributed to the total docking score of the compound.**

Complex Name	Residue Number and Interaction Energy in kcal/mol												
	Trp7 5	Tyr8 9	Ser1 57	Leu1 66	Leu1 74	Tyr2 40	Ser2 47	Ala2 50	Tyr2 51	Pro2 55	Leu2 62	Leu2 66	Ser2 70
TGR5-INT 777	0.41	-1.25	-5.49	-1.93	-0.32	0.15	-2.93	-1.59	-2.71	-2.37	-2.62	-2.93	-0.60
TGR5-Bile Acid	1.24	-4.11	-4.99	-1.88	-0.23	0.23	-1.94	-1.03	-1.62	-0.54	-0.80	-2.33	-0.27
TGR5-6a	-2.60	-2.37	-1.73	-0.62	-0.80	-1.13	-0.59	-0.48	-0.38	-0.20	-1.80	-3.38	-0.50
TGR5-16a	-3.18	-0.67	-2.83	-1.73	-0.59	-2.03	-3.40	-1.44	-3.73	-0.32	-1.62	-2.81	-0.01
TGR5-14b	-3.53	-2.01	-2.71	-1.56	-0.83	-0.10	-0.98	-1.87	-1.80	-1.52	-1.32	-0.56	0.07
TGR5-16c	-4.37	-1.09	-2.08	-1.36	-0.86	-0.45	-2.30	-2.36	-3.24	-0.32	-0.96	-0.88	0.06
TGR5-14a	-2.82	-1.63	-1.41	-1.39	-0.40	-2.36	-2.56	-1.72	-1.50	-0.18	-1.79	-2.78	-0.91

**Table 9: Data for the selected lead compound, INT-777, and bile acids cumulative binding free energies within the binding pocket of TGR5.**

Name of the complex	$\Delta G_{Bind}$						
	$\Delta G_{Bind}$	Coulomb	Covalent	Hbond	Lipo	Solv_GB	vdW
TGR5-INT 777	-69.43±9.1	-58.2±16.7	1.70±1.0	-1.36±0.4	-27.44±3.2	69.48±14	-53.60±5.8
TGR5-Bile Acid	-63.43±6.1	-57.75±14.5	3.15±3.1	-3.07±1.1	-24.33±3.9	66.57±10	-47.96±3.4
TGR5-6a	-96.63±9.1	-10.25±4.0	2.26±1.1	-0.39±0.2	-37.18±5.4	17.15±1.3	-61.22±5.3
TGR5-16a	-93.95±9.3	-8.46±3.2	1.09±3.4	-0.23±0.2	-34.24±4.0	18.90±2.6	-63.76±6.1
TGR5-14b	-81.42±8.5	-17.71±4.9	1.877±3.7	-0.99±0.3	-26.33±5.9	19.81±2.7	-55.37±6.5
TGR5-16c	-77.89±8.3	-8.60±3.2	0.40±2.7	-0.27±0.3	-27.75±3.0	16.98±1.8	-54.43±4.1
TGR5-14a	-85.55±6.8	-8.33±3.7	4.48±2.4	-0.42±0.3	-32.39±2.1	18.06±2.6	-64.89±3.4

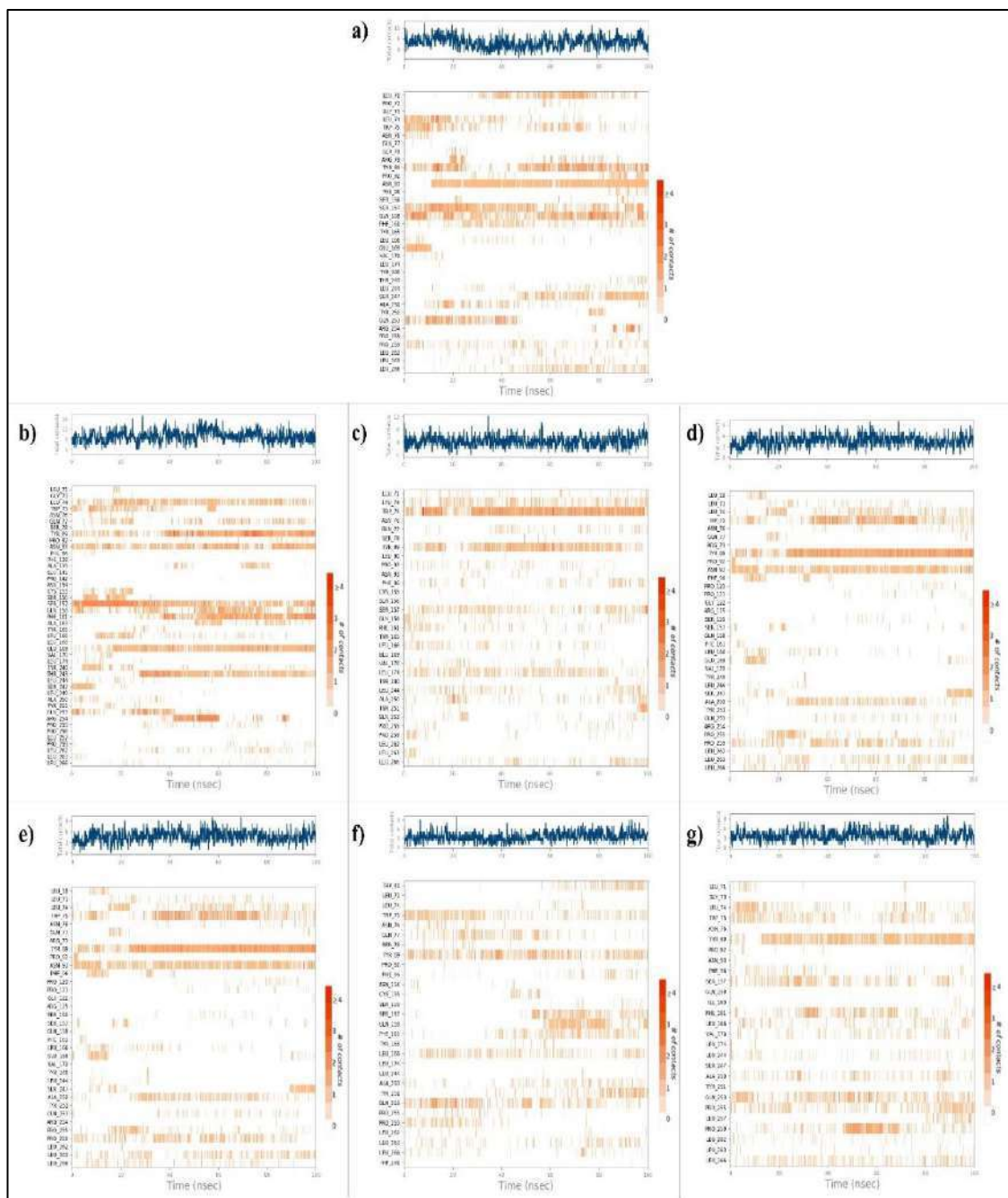


**Figure 56: Protein-ligand contact plot: showing a timeline representation of the interactions and contacts (H-bonds, Hydrophobic, Ionic, Water bridges). (a) TGR5-INT-777, (b) TGR5-Bile Acid, (c) TGR5-6a, (d) TGR5-16a, (e) TGR5-14b, (f) TGR5-16b, and (g) TGR5-14a complexes.**

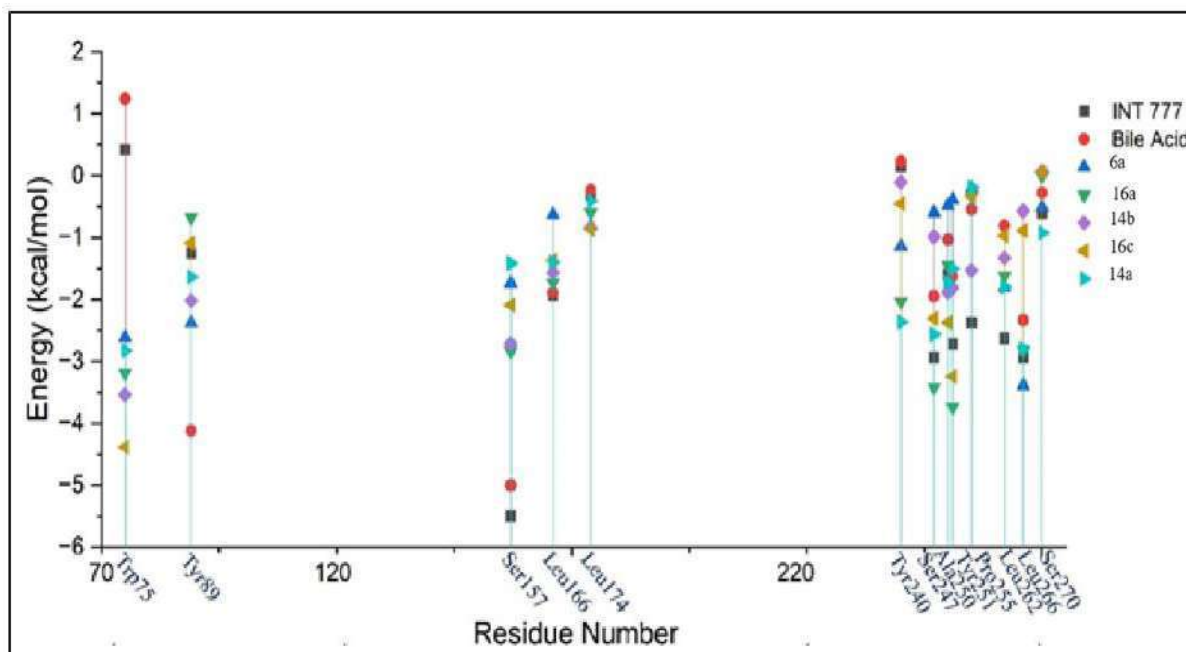


**Figure 57: Scatter Plot for the per residue interaction contribution to the total docking score.**

Thus, in the present study Molecular dynamics study offers valuable insights into the structural stability and conformational dynamics of TGR5-ligand complexes through molecular dynamics simulations. RMSD and RMSF analyses reveal that lead compounds 6a, 16a, and 14a significantly enhance the stability of the TGR5 structure, showing minimal conformational changes and residue fluctuations compared to co-crystal and standard ligands. Additionally, consistent radius of gyration (Rg) and solvent-accessible surface area (SASA) values confirm the structural compactness and integrity of TGR5 upon binding with these leads. These findings highlight the potential of the selected compounds to stabilize TGR5, making them promising candidates for therapeutic applications.

#### 6.1.4. *In silico* Drug-likeness analysis of selected Lead compounds

In the drug discovery process, understanding and modelling a compound's action is dependent on information about its physicochemical properties. The ADMET properties of an agent are determined by its physicochemical and biological characteristics. According to docking studies, the best lead compounds were selected to be studied for their drug likeliness properties using Swiss ADME online server, which has been shown to prevent the failure of drugs in clinical trials. A number of physicochemical properties, including lipophilicity (logP), gastrointestinal (GI) absorption etc., can be used to determine the compounds' drug-likeness properties.

To verify distribution profiles of the selected lead compounds, Swiss ADME calculates physicochemical properties like molecular weight, number of H bonds donor and acceptor, and logP. Additionally, pharmacokinetic parameters such as intestinal absorption, blood-brain barrier permeation, and metabolic parameter (Pgp substrate) was predicted. As displayed in Table 10, all the lead molecules showed unveiled drug-like properties as these inviolate Lipinski's rule of 5 (Molecular weight  $\leq 500$ , H bond acceptor  $< 10$ , and H bond donor  $\leq 5$ ) that support them to be a potential drug-like molecules. All the designed compounds showed high GI absorption. Compound 16a was predicted to be the Pgp substrate.

**Table 10: ADME properties predicted of top lead compounds**

Compound code	Mol wt (g/mol)	LogP	Lipinski	H bond acceptor	H bond donor
<b>6a</b>	385.41	3.48	Yes	4	1
<b>14a</b>	445.46	3.45	Yes	6	2
<b>14b</b>	445.46	3.41	Yes	6	2
<b>16a</b>	425.52	4.55	Yes	3	1
<b>16b</b>	425.52	4.35	Yes	3	1
<b>6c</b>	385.41	3.26	Yes	4	1
<b>15a</b>	489.52	3.96	Yes	7	1

<b>6b</b>	385.41	3.47	Yes	4	1
<b>8a</b>	405.83	3.56	Yes	4	1
<b>8b</b>	405.83	3.46	Yes	4	1

## 6.2. Synthesis of most potent compounds

Most potentially active compounds on basis of binding affinity and feasibility in chemical synthesis were identified and these were proposed for the synthesis.

### 6.2.1. Synthesis of compounds from Series A

Based on the molecular docking results we synthesized selected compounds.

Ethyl 7-hydroxy-2-oxo-2H-1-benzopyran-3-carboxylate (1) was synthesized based on principle of Knoevenagel condensation of Diethylmalonate and 2, 4-dihydroxybenzaldehyde in presence of a basic catalyst.

When 2, 4-dihydroxybenzaldehyde underwent a reaction with diethyl malonate under reflux conditions lasting 4 hours in ethanol, utilizing pyrrolidine as base, it resulted in formation of compound 1, with good yield. Following completion of reaction, the introduction of chilled water led to precipitation of the product. In the reaction, Ethanol served as the solvent, providing a suitable medium for the reaction to take place under reflux conditions, ensuring efficient mixing and reaction kinetics. The use of pyrrolidine as a base likely assisted in catalysing the reaction by deprotonating the acidic proton of diethyl malonate, facilitating nucleophilic attack of enolate ion on carbonyl group of 2,4-dihydroxybenzaldehyde. The resulting compound exhibited solubility in the reaction solvent, ethanol, and upon the addition of ice-cold water, its solubility decreased further, leading to the precipitation of the product. Further, purification of compound 1 was carried out, enabling further characterization and analysis.

Furthermore, a reaction was attempted involving compound 1, potassium carbonate, and benzyl bromide using diverse solvents such as ethanol, acetonitrile, and acetone. The reaction progression was systematically observed through TLC; however, no observable reaction took place in ethanol as a solvent. In acetonitrile, the reaction does

not fully proceed. Notably, compound 1 was reacted in presence of potassium carbonate with benzyl bromide using DMF, as a polar solvent. A significant intermediate 2a was successfully formed under continuous stirring at room temperature for a duration of 4 hours. DMF is acknowledged for its efficacy in facilitating reactions governed by polar mechanisms, including  $\text{S}_{\text{N}}2$  (substitution nucleophilic bimolecular) reactions. The described reaction aligns with the Williamson ether synthesis mechanism, employing an  $\text{S}_{\text{N}}2$  process. In this mechanism, a nucleophile initiates an attack on an electrophile through a backside, leading to a coordinated reaction. The  $\text{S}_{\text{N}}2$  mechanism requires a highly electronegative leaving group, typically a halide. In the Williamson ether synthesis, an alkoxide ion functions as the nucleophile, initiating an attack on the electrophilic carbon containing the leaving group, commonly an alkyl halide

Followed by step II, ester derivative 2a was hydrolysed to carboxylic acid derivative 2a' by dissolving it in ethanol and then 2N NaOH added and stirred overnight. 2N HCl was added in resulting solution to neutralise NaOH till the product precipitate out. After filtering and vacuum drying, the product was ready.

Finally, coupling of 2a' with diverse anilines afforded the corresponding amide derivatives (3-9a) in moderate to excellent yields in presence of coupling reagent HATU and DIPEA. The DIPEA base removes a proton from the carboxylic acid, resulting in the formation of a carboxylate anion. This anion attacks HATU's carbon atom, resulting in a HOAt anion. It is through the reaction of HOAt anion with activated carboxylic acid intermediate that an OAt activated ester is formed, which is then reacted with an amine to form amide.

The influence of electron donating (methyl, methoxy) and electron withdrawing (chloro, bromo) groups on yield of the final products was investigated. The results showed that in all instances, desired products were obtained in satisfactory to excellent yields. Compounds with electron-donating groups (5a, 6a, 6b, and 7a) exhibited superior yields compared to those containing electron-withdrawing groups (8a, 8b, 8c, 9a). However, when para-substituted compounds were compared, those with *ortho*-

substituents yielded lower product yields, likely due to the steric hindrance caused by the *ortho* substituent.

### 6.2.2. Synthesis of compounds from Series B and C

In the first step of series B and C, the intermediate 7-(2-bromoethoxy)-3-propanoyl-2H-1-benzopyran-2-one (compound 11) was synthesized by reacting Ethyl 7-hydroxy-2-oxo-2H-1-benzopyran-3-carboxylate (compound 1) and dibromoethane in presence of potassium carbonate stirring at 75°C for 2hrs. Diverse solvents such as ethanol, acetonitrile, and DMF were tried. The progression of reaction was carefully monitored using TLC; however, there was no observable reaction when ethanol was utilized as the solvent. In acetonitrile, the reaction goes incomplete. As a result, DMF was selected as the solvent. Initially, reaction mixture was agitated at room temperature, but no reaction occurred. Subsequently, heating with stirring was attempted at different temperatures. The best yield was attained by stirring the reactants at 75°C for 2 hours.

The synthesis follows  $SN_2$  (nucleophilic substitution bimolecular) mechanism. Here, bromine acts as the electronegative leaving group, initiating the formation of a carbon electrophile. The electrophilic carbon then forms a bond with the alkoxide ion, generated in presence of a base. The alkoxide ion functions as the nucleophile, attacking the electrophilic carbon and facilitating the formation of compound 11.

Moreover, compound 11 undergoes a conversion to ethyl 7-[2-(2,5-dimethylphenoxy)ethoxy]-2-oxo-2H-1-benzopyran-3-carboxylate (12a) and ethyl 7-[2-(2,3-dimethylphenoxy)ethoxy]-2-oxo-2H-1-benzopyran-3-carboxylate (12b) (Fig. 55). This transformation occurred by reacting compound 11 with 2, 5-dimethylphenol and 2, 3-dimethylphenol, respectively, in presence of a base at 75°C in dimethyl formamide (DMF).

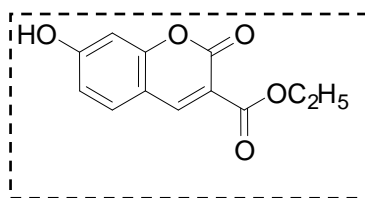
Hydrolysis of the ester derivatives 12a and 12b was performed that lead to formation of the carboxylic acid derivatives 12a' and 12b', respectively. This conversion was carried out by dissolving them in DMSO as solvent and subsequently adding 2N NaOH. The resulting solution was heated followed by stirring for 2hrs. 2N HCl was

incorporated into the solution until product precipitated. Resultant product was then filtered and dried.

Ultimately, combining 12a' and 12b' with different anilines yielded the formation of corresponding amide derivatives: specifically, 13a-17a and 13b-16b, respectively.

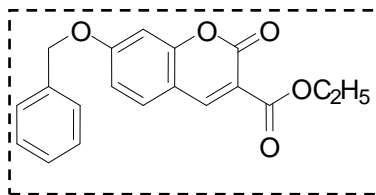
### 6.2.3. Spectral characterization of compounds (1-9a)

#### Ethyl 7-hydroxy-2-oxo-2H-1-benzopyran-3-carboxylate (1):



Yellow solid; %Yield 85%; mp. 140-141<sup>0</sup>C; *R<sub>f</sub>* : 0.33 (7:13 EtOAc: hexane); IR (cm<sup>-1</sup>): 3500.92(OH), 1724.42 (C=O Ester), 1600.97 (C=O lactone), 1496.30 (C=C), 1242.20 (C-C), 1026.16 1141.50 (C-O-C), <sup>1</sup>H NMR (500MHz, CDCl<sub>3</sub>) δ: 1.39-1.42 (t, 3H, CH<sub>3</sub>), 4.39-4.43 (q, 2H, CH<sub>2</sub>), 6.87-6.89 (d, *J*=10Hz, 1H, -C<sub>5</sub>H-chrom), 6.92 (s, 1H, C<sub>8</sub>H-chrom.), 7.50-7.51 (d, *J*=5Hz, 1H, -C<sub>6</sub>H-chrom), 8.53 (s, 1H, C<sub>4</sub>H-chrom.), <sup>13</sup>C NMR (500 MHz, CDCl<sub>3</sub>) δ: 165.55, 163.91, 157.78, 156.97, 149.74, 132.52, 114.91, 110.55, 102.33, 61.17, 24.11, 14.62.

#### Ethyl 7-(benzyloxy)-2-oxo-2H-1-benzopyran-3-carboxylate (2a):

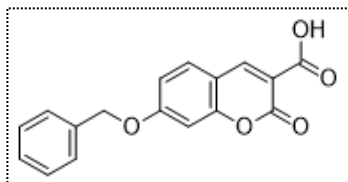


Yellow solid; %Yield: 91%; mp. 180-182<sup>0</sup>C; *R<sub>f</sub>*: 0.54 (7:13 EtOAc: hexane); IR (KBr) (cm<sup>-1</sup>): 1745.64 (C=O ester), 1610.61 (C=O lactone), 1392.65 (C=C), 1024.26 1120.68 (C-O-C); <sup>1</sup>H NMR (500MHz, DMSO) δ: 1.28-1.31 (t, 3H, CH<sub>3</sub>), 4.25-4.29 (q, 2H, CH<sub>2</sub>),



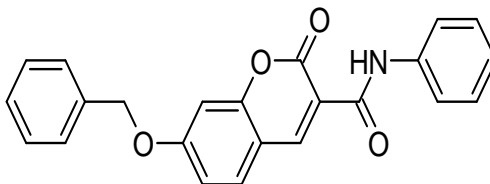
5.26 (s, 2H, OCH<sub>2</sub>Ar), 7.07-7.09 (d, *J* =10Hz, 1H, C<sub>5</sub>H-chrom.), 7.13 (s, 1H, C<sub>8</sub>H-chrom.), 7.35–7.37 (t, 1H, Ar), 7.40-7.43 (t, 2H, Ar), 7.47- 7.49 (d, *J* =10Hz, 2H, Ar), 7.85-7.86 (d, *J* =5Hz, 1H, C<sub>6</sub>H-chrom.) , 8.72 (s, 1H, C<sub>4</sub>H-chrom.); <sup>13</sup>C NMR (125 MHz, CDCl<sub>3</sub>) δ: 164.24, 163.29, 157.35, 156.71, 149.56, 136.45, 132.16, 129.03, 128.69, 128.47, 114.31, 113.99, 112.08, 101.67, 70.69, 61.41, 14.59; HR-MS (m/z):m/z calcd for [M+H]<sup>+</sup> C<sub>19</sub>H<sub>16</sub>O<sub>5</sub> 325.45; found 325.10

**7-(benzyloxy)-2-oxo-2*H*-1-benzopyran-3-carboxylic acid (2a'):**



Pale Yellow solid; %Yield: 85%; mp. 184-185<sup>o</sup>C; *R*<sub>f</sub>: 0.45 (7:13 EtOAc: hexane); IR (cm<sup>-1</sup>): 3043.77 (C-H), 1716.70 (C=O acid), 1595.18 (C=O), 1408.03 (C=C), 1246.05 (C-C), 1132.25 (C-O-C)

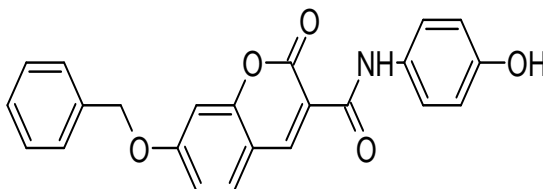
**7-(benzyloxy)-2-oxo-*N*-phenyl-2*H*-1-benzopyran-3-carboxamide (3) :**



Pale Yellow solid; Yield: 43%; mp. 220-221<sup>o</sup>C; *R*<sub>f</sub>: 0.69 (7:13 EtOAc: hexane); IR (cm<sup>-1</sup>): 3423.41 (N-H), 3047.32 (C-H), 1701.10 (C=O lactone), 1608.52 (C=O amide), 1496.66 (C=C), 1373.22 (C-N), 1222.79 (C-C), 1026.06 (C-O-C), <sup>1</sup>H NMR (500MHz, CDCl<sub>3</sub>) δ: 5.19 (s, 2H, OCH<sub>2</sub>Ar), 6.97 (s, 1H, C<sub>8</sub>H- chrom), 7.03-7.05 (d, *J*=10Hz, 1H, C<sub>5</sub>H-chrom.), 7.14-7.17 (t, 1H, Ar), 7.38-7.39 (t, 3H, Ar), 7.42-7.44 (d, *J*=10Hz, 4H, Ar), 7.62-7.64 (d, *J*=10Hz, 1H, C<sub>6</sub>H-chrom), 7.73-7.74 (d, *J*=5Hz, 2H, Ar), 8.94 (s, 1H, C<sub>4</sub>H-chrom.), 10.79 (s, 1H, amide); <sup>13</sup>C NMR (125 MHz, CDCl<sub>3</sub>) δ: 164.04, 162.21, 159.63, 156.61, 148.82, 135.29, 131.15, 129.03, 128.61, 128.87, 127.56, 124.63, 122.07,

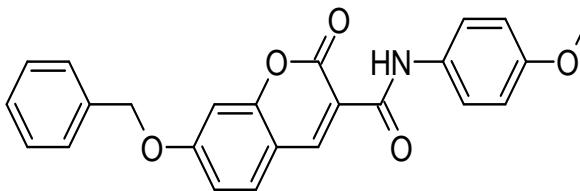
120.50, 115.11, 114.88, 112.73, 101.39, 70.85, 55.49; HR-MS (ESI):  $m/z$  calcd for  $[M+H]^+$   $C_{23}H_{18}NO_4$  372.39; found 372.1234.

**7-(benzyloxy)-*N*-(4-hydroxyphenyl)-2-oxo-2*H*-1-benzopyran-3-carboxamide (4)**



Yellow solid ; Yield: 60%; mp: 160-161 $^{\circ}$ C; *R*<sub>f</sub>: 0.64 (7:13 EtOAc: hexane); IR (cm $^{-1}$ ): 3419.56 (N-H), 3045.39 (C-H), 1693.38 (C=O lactone), 1622.02 (C=O amide), 1510.16 (C=C), 1367.44 (C-N), 1236.29 (C-C), 1020.27 (C-O-C);  $^1H$  NMR (500MHz,  $CDCl_3$ )  $\delta$ : 5.19 (s, 2H,  $OCH_2Ar$ ), 6.83-6.85 (d, 2H, Ar), 6.97 (s, 1H,  $C_8H$ -chrom.), 7.03-7.05 (d,  $J=10Hz$ , 1H,  $C_5H$ -chrom), 7.38-7.39 (d,  $J=5Hz$ , 2H, Ar), 7.41-7.44 (m, 3H, Ar), 7.59-7.61 (d,  $J=10Hz$ , 2H, Ar.), 7.62-7.63 (d,  $J=5Hz$ , 1H,  $C_6H$ -chrom.), 8.93 (s, 1H,  $C_4H$ -chrom.), 10.66 (s, 1H, amide);  $^{13}C$  NMR (125 MHz,  $CDCl_3$ )  $\delta$ : 163.05, 159.65, 148.56, 131.08, 130.40, 128.86, 128.61, 127.55, 122.30, 115.90, 115.64, 115.07, 114.84, 101.39, 89.08, 70.86, 29.70, 29.67; HR-MS (ESI):  $m/z$  calcd for  $[M+H]^+$   $C_{23}H_{18}NO_5$  388.39; found 388.1181.

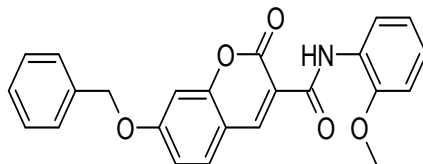
**7-(benzyloxy)-*N*-(4-methoxyphenyl)-2-oxo-2*H*-1-benzopyran-3-carboxamide (5a):**



Yellowish brown solid; Yield: 62%; mp: 170-172 $^{\circ}$ C; *R*<sub>f</sub>: 0.70 (7:13 EtOAc: hexane); IR (cm $^{-1}$ ) 3788.88 (N-H), 2873.96 (C-H), 1704.62 (C=O), 1573.23 (C=O), 1490.74 (C=C), 1374.31 (C-N), 1212.71 (C-C), 1068.59 (C-O-C);  $^1H$  NMR (500MHz,  $CDCl_3$ )  $\delta$ : 3.82 (s, 3H,  $OCH_3$ ), 5.20 (s, 2H,  $OCH_2Ar$ ), 6.90-6.92 (d,  $J=10Hz$ , 2H, Ar), 6.96 (s, 1H,  $C_8H$ -

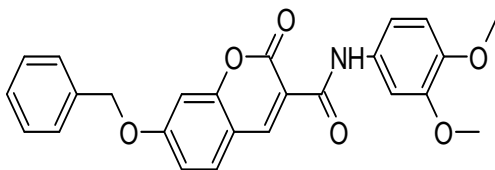
chrom), 7.03-7.05 (d,  $J=10\text{Hz}$ , 1H, C<sub>5</sub>H-chrom.), 7.42-7.44 (d,  $J=10\text{Hz}$ , 4H, Ar), 7.61-7.63 (d,  $J=10\text{Hz}$ , 2H, C<sub>6</sub>H-chrom.), 7.63-7.65 (m, 2H, Ar), 8.93 (s, 1H, C<sub>4</sub>H-chrom.), 10.67 (s, 1H, amide)

**7-(benzyloxy)-*N*-(2-methoxyphenyl)-2-oxo-2*H*-1-benzopyran-3-carboxamide (5c):**



Yellowish brown solid; Yield: 84%; mp: 164-165<sup>o</sup>C;  $R_f$ : 0.78 (7:13 EtOAc: hexane); IR (cm<sup>-1</sup>) 3781.39 (N-H), 2872.88 (C-H), 1710.65 (C=O), 1610.26 (C=O), 1442.30 (C=C), 1373.20 (C-N), 1208.71 (C-C), 1156.22 (C-O-C); <sup>1</sup>H NMR (500MHz, CDCl<sub>3</sub>)  $\delta$ : 3.97(s, 3H, OCH<sub>3</sub>), 5.18(s, 2H, OCH<sub>2</sub>Ar), 6.93-6.94(d,  $J=10\text{Hz}$ , 1H, C<sub>5</sub>H-chrom), 6.96 (s, 1H, C<sub>8</sub>H-chrom), 7.00-7.03(m, 1H, Ar), 7.08-7.11(t, 1H, Ar), 7.41-7.43(m, 5H, Ar), 7.61-7.63(d, 1H, C<sub>6</sub>H-chrom), 8.54-8.55(d, 1H, Ar), 8.92 (s, 1H, C<sub>4</sub>H-chrom.), 11.24 (s, 1H, amide)

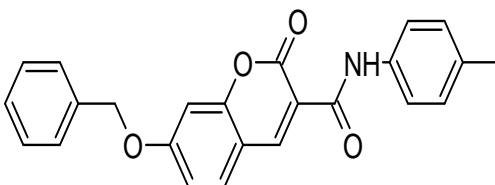
**7-(benzyloxy)-*N*-(3,4-dimethoxyphenyl)-2-oxo-2*H*-1-benzopyran-3-carboxamide (5d)**



Yellow solid; Yield: 65%; mp. 180-181<sup>o</sup>C;  $R_f$ : 0.56 (7:13 EtOAc: hexane); IR (cm<sup>-1</sup>): 3419.56 (N-H), 3045.39 (C-H), 1693.38 (C=O lactone), 1622.02 (C=O amide), 1510.16 (C=C), 1367.44 (C-N), 1236.29 (C-C), 1020.27 (C-O-C); <sup>1</sup>H NMR (500MHz, CDCl<sub>3</sub>)  $\delta$ : 3.89 (s, 3H, OCH<sub>3</sub>), 3.93(s, 3H, OCH<sub>3</sub>), 5.19(s, 2H, OCH<sub>2</sub>Ar), 6.85-6.87(s, 1H, Ar), 6.97-6.98(s, 1H, C<sub>8</sub>H-chrom.), 7.03-7.05(d,  $J=10\text{Hz}$ , 1H, C<sub>5</sub>H-chrom), 7.17-7.19(d,  $J=10\text{Hz}$ , 1H, Ar), 7.42-7.44(m, 5H, Ar), 7.50-7.51(s, 1H, Ar), 7.61-7.63(d,  $J=10\text{Hz}$ , 1H, C<sub>4</sub>H-

chrom), 8.93 (s, 1H, C<sub>4</sub>H-chrom.), 10.70(s, 1H, amide); <sup>13</sup>C NMR (125 MHz, CDCl<sub>3</sub>) δ: 164.11, 162.23, 159.60, 156.61, 149.28, 148.53, 146.08, 135.24, 131.50, 131.10, 128.88, 128.63, 127.55, 115.05, 114.89, 112.72, 111.33, 105.05, 101.4, 70.86, 56.11, 29.70 ; HR-MS (ESI): m/z calcd for [M+H]<sup>+</sup> C<sub>25</sub>H<sub>22</sub>NO<sub>6</sub> 432.44; found 432.1441.

**7-(benzyloxy)-N-(4-methylphenyl)-2-oxo-2H-chromene-3-carboxamide (6a):**



Brown solid, Yield: 75%; mp: 220-222°C; R<sub>f</sub>: 0.80 (7:13 EtOAc: hexane); IR (cm<sup>-1</sup>): 3419.56 (N-H), 3033.82 (C-H), 1703.03 (C=O lactone), 1610.45 (C=O amide), 1508.23 (C=C), 1373.22 (C-N), 1253.64 (C-C), 1074.28 (C-O-C); <sup>1</sup>H NMR (500MHz, CDCl<sub>3</sub>) δ: 2.34 (s, 3H, CH), 5.19 (s, 2H, OCH<sub>2</sub>Ar), 6.96-6.97 (s, 1H, C<sub>8</sub>H- ch<sub>3</sub>rom), 7.03-7.05 (d, J=10Hz, 2H, C<sub>5</sub>H-chrom.), 7.17-7.18 (d, J=5Hz, 2H, Ar), 7.42-7.44 (m, 4H, Ar), 7.61-7.62 (d, 2H, C<sub>6</sub>H-chrom), 7.2-7.64 (d, 2H, Ar), 8.94 (s, 1H, C<sub>4</sub>H-chrom.), 10.71 (s, 1H, amide); <sup>13</sup>C NMR (125 MHz, CDCl<sub>3</sub>) δ: 164.07, 162.20, 159.73, 156.62, 148.65, 135.29, 134.29, 131.11, 129.54, 128.61, 128.87, 127.56, 120.50, 115.11, 114.84, 112.72, 101.9, 70.86, 20.95; HR-MS (ESI): m/z calcd for [M+H]<sup>+</sup> C<sub>24</sub>H<sub>20</sub>NO<sub>4</sub> 386.42; found 386.1399.

The fragmentation pattern of compound 6a (C<sub>24</sub>H<sub>18</sub>NO<sub>4</sub>) exhibited molecular ion peak at m/z 386.1399 Da as [M + H]<sup>+</sup> (calculated for , exact mass 386.42, Figure 58). It was further fragmented in collision cell (Q2) into major fragments at m/z 91.0544, 161.1072, 206.1655, 318.1496, 386.1399. The elemental composition, exact mass, assigned structures of these major fragments was illustrated in Figure 58. The molecular ion peak (m/z 386.1399 Da) was fragmented in ion with m/z 318.1496 (calculated formula C<sub>19</sub>H<sub>13</sub>NO<sub>4</sub><sup>+</sup>) by the loss of C<sub>5</sub>H<sub>6</sub>, that further fragment into m/z 206.1655 (calculated formula C<sub>10</sub>H<sub>7</sub>NO<sub>4</sub><sup>+</sup>) formed by loss of C<sub>14</sub>H<sub>12</sub> and fragment ion m/z 91.0544 (calculated formula C<sub>7</sub>H<sub>7</sub><sup>+</sup>). Further, fragment ion m/z 206.1655 resulted in formation of fragment ion m/z 161.1072 (calculated formula C<sub>9</sub>H<sub>6</sub>O<sub>3</sub><sup>+</sup>) with loss of CHON ion.

Fragmentation pathway described above and presented in figure is a probable pathway; formation of fragments can be simultaneous because of multiple transitions can occur simultaneously.

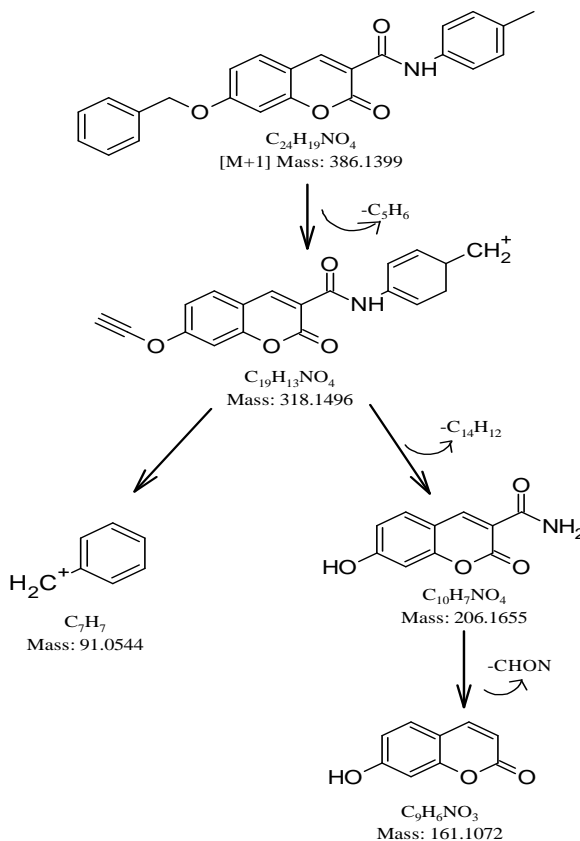
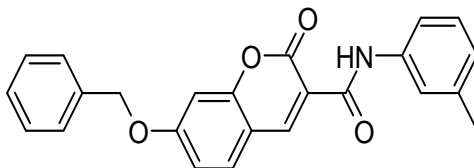


**Figure 58: Proposed fragments and probable fragmentation pathway for compound 6a**

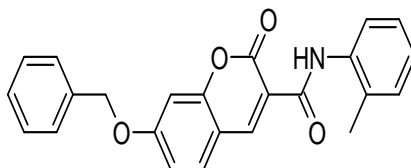
**7-(benzyloxy)-*N*-(3-methylphenyl)-2-oxo-2*H*-1-benzopyran-3-carboxamide (6b):**



Brown solid; Yield: 77%; mp: 210-211°C; *R*<sub>f</sub>: 0.77 (7:13 EtOAc: hexane); IR (cm<sup>-1</sup>): 3687.98 (N-H), 2935.20 (C-H), 1742.98, 1705.69 (C=O lactone), 1609.73 (C=O amide),

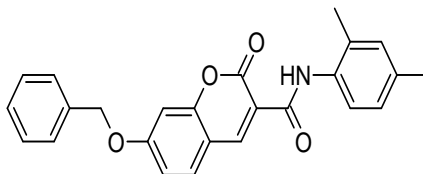
1447.24 (C=C), 1369.64 (C-N), 1281.15 (C-C), 1160.78 (C-O-C);  $^1\text{H}$  NMR (500MHz,  $\text{CDCl}_3$ )  $\delta$ : 2.37 (s, 3H,  $\text{CH}_3$ ), 5.18 (s, 2H,  $\text{OCH}_2\text{Ar}$ ), 6.96-6.97 (s, 2H, Ar,  $\text{C}_5\text{H}$ -chrom), 7.02-7.04 (d, 1H,  $\text{C}_8\text{H}$ -chrom.), 7.41-7.43 (m, 5H, Ar), 7.53-7.55 (d,  $J=10\text{Hz}$ , 2H, Ar), 7.61-7.63 (d,  $J=10\text{Hz}$ , 1H,  $\text{C}_6\text{H}$ -chrom), 8.93 (s, 1H,  $\text{C}_4\text{H}$ -chrom.), 10.71 (s, 1H, amide)

**7-(benzyloxy)-*N*-(2-methylphenyl)-2-oxo-2*H*-1-benzopyran-3-carboxamide (6c):**



Brown solid; Yield: 50%; mp: 180-182 $^{\circ}\text{C}$ ; *R*<sub>f</sub>: 0.75 (7:13 EtOAc: hexane); IR ( $\text{cm}^{-1}$ ): 3475.49 (N-H), 3045.39 (C-H), 1704.96 (C=O lactone), 1693.38 (C=O amide), 1622.02 (C=O), 1510.16 (C=C), 1367.44 (C-N), 1236.29 (C-C), 1020.27 (C-O-C);  $^1\text{H}$  NMR (500MHz,  $\text{CDCl}_3$ )  $\delta$ : 2.42 (s, 3H,  $\text{CH}_3$ ), 5.19 (s, 2H,  $\text{OCH}_2\text{Ar}$ ), 6.98 (s, 1H,  $\text{C}_5\text{H}$ -chrom), 7.03-7.06 (d, 1H,  $\text{C}_8\text{H}$ -chrom), 7.07-7.10 (d, 2H, Ar), 7.42-7.44 (m, 6H, Ar), 7.63-7.65 (d,  $J=10\text{Hz}$ , 1H,  $\text{C}_6\text{H}$ -chrom), 8.24-8.25 (d,  $J=5\text{Hz}$ , 1H, Ar), 8.96 (s, 1H,  $\text{C}_4\text{H}$ -chrom.), 10.73 (s, 1H, amide).

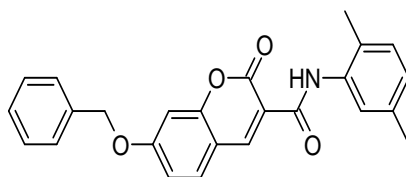
**7-(benzyloxy)-*N*-(2,4-dimethylphenyl)-2-oxo-2*H*-1-benzopyran-3-carboxamide (7a):**



Brown solid; Yield: 85%; mp. 200-201 $^{\circ}\text{C}$ ; *R*<sub>f</sub>: 0.71 (7:13 EtOAc: hexane); IR ( $\text{cm}^{-1}$ ): 3789.33 (N-H), 2873.27 (C-H), 1704.44 (C=O lactone), 1610, 1573.50 (C=O amide), 1438.51 (C=C), 1373.28 (C-N), 1211.81 (C-C), 1068.78 (C-O-C);  $^1\text{H}$  NMR (500MHz,  $\text{CDCl}_3$ )  $\delta$ : 2.31 (s, 1H,  $\text{CH}_3$ ), 2.37 (s, 1H,  $\text{CH}_3$ ), 5.19 (s, 2H,  $\text{OCH}_2\text{Ar}$ ), 6.96 (s, 1H,  $\text{C}_5\text{H}$ -chrom), 7.03-7.05 (d,  $J=10\text{Hz}$ , 1H,  $\text{C}_8\text{H}$ -chrom.), 7.05-7.07 (d, 3H, Ar), 7.43-7.44 (m,  $J=5\text{Hz}$ , 5H, Ar), 7.62-7.63 (d,  $J=10\text{Hz}$ , 1H,  $\text{C}_6\text{H}$ -chrom), 8.07-8.08 (d,  $J=5\text{Hz}$ , Ar), 8.95

(s, 1H, C<sub>4</sub>H-chrom.), 10.64 (s, 1H, amide); <sup>13</sup>C NMR (125 MHz, CDCl<sub>3</sub>) δ: 164.02, 162.31, 159.73, 156.57, 148.63, 135.26, 134.58, 134.43, 133.65, 131.11, 130.88, 128.84, 128.73, 128.66, 128.16, 129.03, 128.61, 128.87, 127.56, 121.99, 115.26, 114.77, 112.71, 101.36, 70.65, 20.89, 18.00; HR-MS (ESI): m/z calcd for [M+H]<sup>+</sup> C<sub>25</sub>H<sub>22</sub>NO<sub>4</sub> 400.45; found 400.1555.

**7-(benzyloxy)-N-(2,5-dimethylphenyl)-2-oxo-2H-1-benzopyran-3-carboxamide (7b):**

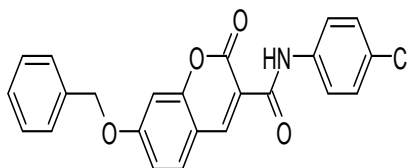


Brown solid; Yield: 62%; mp. 171-172°C; *R*<sub>f</sub>: 0.75 (7:13 EtOAc: hexane); IR (cm<sup>-1</sup>): 3782.26 (N-H), 2876.28 (C-H), 1663.63 (C=O lactone), 1609 (C=O amide), 1490.00 (C=C), 1380.72 (C-N), 1214.66 (C-C), 1074.60 (C-O-C); <sup>1</sup>H NMR (500MHz, CDCl<sub>3</sub>): 2.36 (s, 1H, CH<sub>3</sub>), 2.37 (s, 1H, CH<sub>3</sub>), 5.19 (s, 2H, OCH<sub>2</sub>Ar), 6.89-6.91 (d, *J*=10Hz, 1H, Ar), 6.98 (s, 1H, C<sub>8</sub>H- chrom), 7.03-7.05 (d, *J*=10Hz, 1H, C<sub>5</sub>H-chrom.), 7.10-7.11 (d, *J*=5Hz, 1H, Ar), 7.43-7.44 (d, *J*=5Hz, 5H, Ar), 7.63-7.65 (d, *J*=10Hz, 1H, C<sub>6</sub>H-chrom), 8.07 (s, 1H, Ar), 8.95 (s, 1H, C<sub>4</sub>H-chrom.), 10.68 (s, 1H, amide).

**7-(benzyloxy)-N-(2,6-dimethylphenyl)-2-oxo-2H-1-benzopyran-3-carboxamide (7c):**

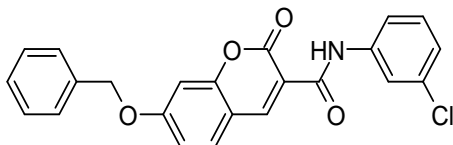
Brown solid; Yield: 62%, mp. 172-173°C; *R*<sub>f</sub>: 0.71 (7:13 EtOAc: hexane); IR (cm<sup>-1</sup>): 3782.26 (N-H), 2876.28 (C-H), 1710.34 (C=O lactone), 1611.02 (C=O amide), 1490.00 (C=C), 1380.72 (C-N), 1214.66 (C-C), 1074.60 (C-O-C); <sup>1</sup>H NMR (500MHz, CDCl<sub>3</sub>): 2.30 (s, 2H, 2CH<sub>3</sub>), 5.21 (s, 2H, OCH<sub>2</sub>Ar), 6.99-7.00 (s, 1H, C<sub>8</sub>H- chrom), 7.05-7.07 (d, *J*=10Hz, 1H, C<sub>5</sub>H-chrom.), 7.14-7.15 (t, *J*=5Hz, 1H, Ar), 7.43-7.46 (m, *J*=5Hz, 5H, Ar), 7.63-7.65 (d, *J*=10Hz, 1H, C<sub>6</sub>H-chrom), 8.97 (s, 1H, C<sub>4</sub>H-chrom.), 10.14 (s, 1H, amide).

**7-(benzyloxy)-N-(4-chlorophenyl)-2-oxo-2H-chromene-3-carboxamide (8a):**



Pale brown solid, Yield: 67%; mp. 220-221°C; *R*<sub>f</sub>: 0.83 (7:13 EtOAc: hexane); IR (cm<sup>-1</sup>): 3267.19 (N-H), 1706.88 (C=O amide), 1610.45 (C=O), 1236.29 (C-C), 1010.63, 1091.63 (C-O-C); <sup>1</sup>H NMR (500MHz, CDCl<sub>3</sub>) δ: 5.19 (s, 2H, OCH<sub>2</sub>Ar), 6.97 (s, 1H, C<sub>8</sub>H- chrom), 7.04-7.06 (d, *J*=10Hz, 1H, C<sub>5</sub>H-chrom.), 7.32-7.34 (d, *J*=10Hz, 3H, Ar), 7.43-7.44 (d, *J*=5Hz, 4H, Ar), 7.63-7.65 (d, *J*=10Hz, 1H, C<sub>6</sub>H-chrom), 7.68-7.70 (d, *J*=10Hz, 2H, Ar), 8.93(s, 1H, C<sub>4</sub>H-chrom.), 10.83 (s, 1H, amide); HR-MS (ESI): *m/z* calcd for [M+H]<sup>+</sup> C<sub>23</sub>H<sub>17</sub>NO<sub>4</sub>Cl 406.84; found 406.0841.

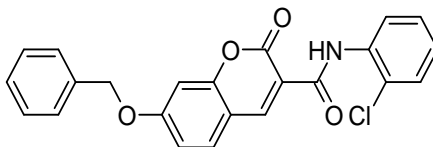
**7-(benzyloxy)-N-(3-chlorophenyl)-2-oxo-2H-1-benzopyran-3-carboxamide (8b):**



Pale brown solid; Yield: 83%; mp. 160-161°C; *R*<sub>f</sub>: 0.78 (7:13 EtOAc: hexane); IR (cm<sup>-1</sup>): 3291.32 (N-H), 2874.09, (C-H), 1701.97 (C=O lactone), 1683 (C=O amide), 1571.46 1489.39 (C=C), 1373.67 (C-N), 1210.84(C-C), 1072.41, (C-O-C); <sup>1</sup>H NMR (500MHz, CDCl<sub>3</sub>) δ: 5.19 (s, 2H, OCH<sub>2</sub>Ar), 6.97 (s, 1H, C<sub>8</sub>H- chrom), 7.04-7.06 (d, *J*=10Hz, 1H, C<sub>5</sub>H-chrom.), 7.12-7.13 (d, *J*=5Hz, 1H, Ar), 7.43-7.44 (d, *J*=5Hz, 5H, Ar), 7.35-7.55 (d, *J*=10Hz, 1H, Ar), 7.63-7.65 (d, *J*=10Hz, 1H, C<sub>6</sub>H-chrom), 7.89 (s, 1H, Ar), 8.93 (s, 1H, C<sub>4</sub>H-chrom.), 10.84 (s, 1H, amide)

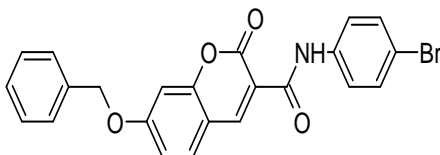


**7-(benzyloxy)-N-(2-chlorophenyl)-2-oxo-2H-1-benzopyran-3-carboxamide (8c):**



Pale brown solid, Yield: 52%, mp. 120-122°C; *R*<sub>f</sub>: 0.75 (7:13 EtOAc: hexane); IR (cm<sup>-1</sup>): 2882.60, (C-H), 1708.89 (C=O lactone), 1611.68 (C=O amide), 1439.75 (C=C), 1374.85 (C-N), 1207.47(C-C), 979.89 (C-O-C) ; <sup>1</sup>H NMR (500MHz, CDCl<sub>3</sub>) δ: 5.21 (s, 2H, OCH<sub>2</sub>Ar), 6.99 (s,1H, C<sub>8</sub>H- chrom), 7.07-7.09 (d, *J*=10Hz, 1H, C<sub>5</sub>H-chrom.), 7.10-7.12 (t, 1H, Ar), 7.32-7.35 (t, 1H, Ar), 7.44-7.46 (m, 5H, Ar), 7.65-7.66(d, *J*=5Hz, 1H, C<sub>6</sub>H-chrom), 7.57-7.59 (d, *J*=10Hz, 1H, Ar), 8.96(s, 1H, C<sub>4</sub>H-chrom.), 11.30 (s, 1H, amide)

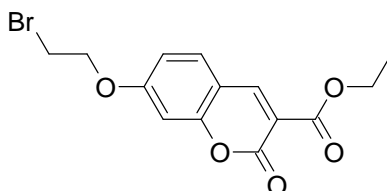
**7-(benzyloxy)-N-(4-bromophenyl)-2-oxo-2H-chromene-3-carboxamide (9a):**



Brown solid; Yield: 45%; mp. 180-182°C; *R*<sub>f</sub>: 0.80 (7:13 EtOAc: hexane); IR (cm<sup>-1</sup>): 3496.13 (N-H), 3026.41(C-H), 1703.20 (C=O lactone), 1599.04 (C=O amide),1491.02 (C=C), 1375.29 (C-N), 1257.63 (C-C), 1124.54, 1018.45 (C-O-C); <sup>1</sup>H NMR (500MHz, CDCl<sub>3</sub>) δ: 5.19 (s, 2H, OCH<sub>2</sub>Ar), 6.97 (s,1H, C<sub>8</sub>H- chrom), 7.04-7.06 (d, *J*=10Hz, 1H, C<sub>5</sub>H-chrom.), 7.42-7.44 (m, 5H, Ar), 7.47-7.49 (d, *J*=10Hz, 2H, Ar), 7.63-7.65 (d, *J*=10Hz, 3H, Ar, C<sub>6</sub>H-chrom.), 8.93 (s, 1H, C<sub>4</sub>H-chrom.), 10.83 (s, 1H, amide); HR-MS (ESI): *m/z* calcd for [M+H]<sup>+</sup> C<sub>23</sub>H<sub>16</sub>NO<sub>4</sub>Br 450.28; found 450.0329.

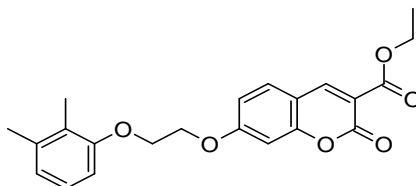
#### 6.2.4. Spectral characterization of compounds (11-17a)

##### 7-(2-bromoethoxy)-3-propanoyl-2H-1-benzopyran-2-one (11):



White powder; % Yield 80%, *R*<sub>f</sub>: 0.69 (7:13 EtOAc: hexane); mp. 120-121°C, IR (cm<sup>-1</sup>): 1758.96(C=O), 1620.09(C=O), 1496.66(C=C), 1282.57(C-C), 1022.20(C-O-C), 669.25 (C-Br); <sup>1</sup>H NMR (500MHz, CDCl<sub>3</sub>) δ: 1.39-1.42(t, 3H, CH<sub>3</sub>), 3.67-3.69(t, 2H, CH<sub>2</sub>), 4.37-4.40 (q, 2H, CH<sub>2</sub>), 4.40-4.42 (t, 2H, CH<sub>2</sub>), 6.81-6.82 (s, 1H, C<sub>5</sub>H-chrom), 6.91-6.93 (d, *J*=10Hz, 1H, C<sub>8</sub>H-chrom.), 7.52-7.53 (d, *J*=5Hz, 1H, C<sub>6</sub>H-chrom.), 8.50 (s, 1H, C<sub>4</sub>H-chrom.)

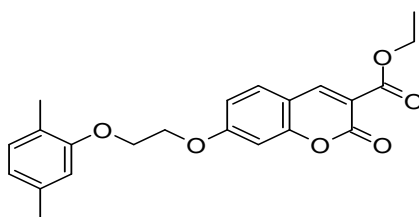
##### Ethyl 7-[2-(2,3-dimethylphenoxy)ethoxy]-2-oxo-2H-1-benzopyran-3-carboxylate (12a):



Brown powder; % Yield: 55%; mp. 112-113°C; *R*<sub>f</sub>: 0.75 (7:13 EtOAc: hexane); IR (cm<sup>-1</sup>): 2941.24 (C-H), 1768.60 (C=O ester), 1616.24 (C=O), 1488.94 (C=C), 1201.57 (C-C), 1037.63 (C-O-C); <sup>1</sup>H NMR (500MHz, CDCl<sub>3</sub>) δ: 1.39-1.42 (t, 3H, CH<sub>3</sub>), 2.13 (s, 3H, CH<sub>3</sub>), 2.27 (s, 3H, CH<sub>3</sub>), 4.34-4.36 (q, 2H, CH<sub>2</sub>), 4.39-4.41 (m, 1H, CH<sub>2</sub>), 4.42-4.44 (q, 3H, CH<sub>2</sub>), 6.74-6.76 (d, *J*=10Hz, 1H, Ar), 6.82-6.83 (d, *J*=5Hz, 1H, Ar), 6.89-6.90 (s, 1H, C<sub>8</sub>H-chrom.), 6.94-6.96 (d, *J*=10Hz, 1H, C<sub>5</sub>H-chrom.), 7.05- 7.08 (t, 1H, Ar), 7.51-7.52 (d, *J*=5Hz, 1H, C<sub>6</sub>H-chrom), 8.51 (s, 1H, C<sub>4</sub>H-chrom.); <sup>13</sup>C NMR (125MHz, CDCl<sub>3</sub>) δ:

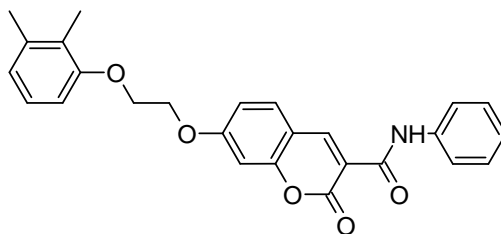
164.27,163.46,157.49,157.10, 156.33, 148.89, 138.29, 130.76, 125.86, 123.09, 114.38, 114.02, 111.87, 109.55, 103.44, 101.16, 99.54, 67.53, 66.75, 61.75, 20.09, 14.29, 11.70;  
HR-MS (ESI): m/z calcd for  $[M+H]^+$  C<sub>22</sub>H<sub>23</sub>O<sub>6</sub>383.41; found 383.1982.

**Ethyl 7-[2-(2,5-dimethylphenoxy)ethoxy]-2-oxo-2H-1-benzopyran-3-carboxylate (12b):**



Brown powder; % Yield: 60%; mp. 110-111°C; *R*<sub>f</sub>: 0.80 (7:13 EtOAc: hexane); IR (cm<sup>-1</sup>): 2941.24 (C-H), 1757.03 (C=O ester), 1610.45 (C=O), 1492.80 (C=C), 1218.9 (C-C), 1041.49 (C-O-C); <sup>1</sup>H NMR (500MHz, CDCl<sub>3</sub>) δ: 1.39-1.42 (t, 3H, CH<sub>3</sub>), 2.16 (s, 3H, CH<sub>3</sub>), 2.33 (s, 3H, CH<sub>3</sub>), 4.34-4.36 (q, 2H, OCH<sub>2</sub>), 4.38-4.41 (m, 2H, CH<sub>2</sub>), 4.42-4.44 (m, 2H, CH<sub>2</sub>), 6.69 (s, 1H, Ar), 6.71-6.72 (d, *J*=5Hz, 1H, Ar), 6.89-8.90 (s, 1H, C<sub>5</sub>H-chrom), 6.94-6.96 (d, *J*=10Hz, 1H, C<sub>8</sub>H-chrom), 7.01- 7.03 (d, *J*=10Hz, 1H, Ar), 7.51-7.52 (d, *J*=5Hz, 1H, C<sub>6</sub>H-chrom), 8.51 (s, 1H, C<sub>4</sub>H-chrom)

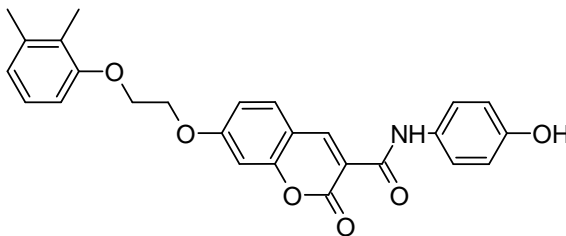
**7-[2-(2,3-dimethylphenoxy)ethoxy]-N-phenyl-2-oxochromene-3-carboxamide (13a):**



Brown solid, Yield: 55%, mp. 180-181°C; *R*<sub>f</sub>: 0.85 (7:13 EtOAc: hexane); IR (cm<sup>-1</sup>): 3378.54 (N-H), 2872.87 (C-H), 1662.49 (C=O lactone), 1570.35 (C=O amide), 1486.37 (C=C), 1136.60 (C-C), 1394.37 (C-N), 1081.78 (C-O-C); <sup>1</sup>H NMR (500MHz, CDCl<sub>3</sub>) δ: 2.14 (s, 3H, CH<sub>3</sub>), 2.27 (s, 3H, CH<sub>3</sub>), 4.36-4.38 (t, 2H, CH<sub>2</sub>), 4.45-4.47 (t, 2H, CH<sub>2</sub>),

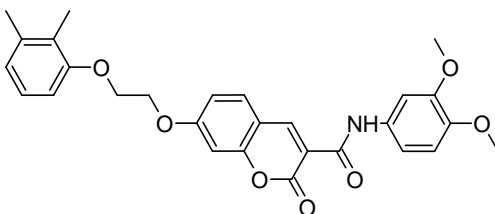
6.75- 6.77(d,  $J=10\text{Hz}$ , 1H, Ar), 6.82-6.84 (d,  $J=10\text{Hz}$ , 1H, Ar), 6.99 (s, 1H, C<sub>8</sub>H-chrom.), 7.02-7.04 (d,  $J=10\text{Hz}$ , 1H, C<sub>5</sub>H-chrom), 7.05-7.09 (t, 1H, Ar), 7.15-7.17 (t, 1H, Ar), 7.37-7.40 (t, 2H, Ar), 7.64-7.65 (d, 1H, C<sub>6</sub>H-chrom ), 7.73-7.75 (d,  $J=10\text{Hz}$ , 2H, Ar), 8.96 (s, 1H, C<sub>4</sub>H-chrom.), 10.80 (s, 1H, amide); <sup>13</sup>C NMR (125MHz, CDCl<sub>3</sub>)  $\delta$ : 164.27, 162.19, 159.87, 156.67, 156.30, 148.81, 138.31, 131.29, 11.17, 129.04, 125.73, 124.63, 123.12, 120.53, 115.08, 114.63, 112.74, 109.54, 101.18, 67.62, 66.74, 20.09, 11.70; HR-MS (ESI):  $m/z$  calcd for  $[\text{M}+\text{H}]^+$  C<sub>26</sub>H<sub>24</sub>NO<sub>5</sub> 430.47; found 430.1653.

**7-[2-(2,3-dimethylphenoxy)ethoxy]-N-(4-hydroxyphenyl)-2-oxochromene-3-carboxamide (14a):**



Brown solid; Yield 45%; mp. 210-211<sup>o</sup>C;  $R_f$ : 0.60 (7:13 EtOAc: hexane); IR (cm<sup>-1</sup>): 2918.40 (C-H), 1703.99 (C=O amide), 1599.04 (C=O), 1445.66 (C=C), 1232.56 (C-C), 1373.52 (C-N), 1037.74 (C-O-C); <sup>1</sup>H NMR (500MHz, CDCl<sub>3</sub>)  $\delta$ : 2.14 (s, 3H, CH<sub>3</sub>), 2.27 (s, 3H, CH<sub>3</sub>), 4.36-4.38 (t, 2H, CH<sub>2</sub>), 4.45-4.47 (t, 2H, CH<sub>2</sub>), 6.75- 6.77 (d,  $J=10\text{Hz}$ , 1H, Ar), 6.82-6.86 (t, 3H, Ar), 6.98 (s, 1H, C<sub>8</sub>H-chrom), 7.02-7.04 (d, 2H,  $J= 10\text{Hz}$ , C<sub>5</sub>H-chrom) 7.05-7.07 (d,  $J= 10\text{Hz}$ , 1H, Ar), 7.60-7.61 (d,  $J= 10\text{Hz}$ , 1H, C<sub>6</sub>H-chrom), 7.63-7.65 (d,  $J= 10\text{Hz}$ , 2H, Ar), 8.94 (s, 1H, C<sub>4</sub>H-chrom.), 10.68 (s, 1H, amide); <sup>13</sup>C NMR (125MHz, CDCl<sub>3</sub>)  $\delta$ : 164.16, 161.65, 159.84, 156.57, 154.56, 148.14, 137.87, 132.12, 130.13, 126.42, 124.95, 122.95, 122.03, 115.82, 114.69, 112.87, 110.26, 101.51, 68.13, 67.18, 20.17, 11.90.

**N-(3,4-dimethoxyphenyl)-7-[2-(2,3-dimethylphenoxy)ethoxy]-2-oxochromene-3-carboxamide (15a):**



Brown solid; Yield: 60%; mp. 140-141<sup>o</sup>C; *R*<sub>f</sub>: 0.58 (7:13 EtOAc: hexane); IR (cm<sup>-1</sup>): 2914.40(C-H), 1703.99 (C=O lactone), 1583.51 (C=O amide), 1450.52 (C=C), 1238.34 (C-C), 1039.57 (C-O-C); <sup>1</sup>H NMR (500MHz, CDCl<sub>3</sub>) δ: 2.14 (s, 3H, CH<sub>3</sub>), 2.27 (s, 3H, CH<sub>3</sub>), 3.89 (s, 3H, CH<sub>3</sub>), 3.94 (s, 3H, CH<sub>3</sub>), 4.36-4.38(t, 2H, CH<sub>2</sub>), 4.45-4.47 (t, 2H, CH<sub>2</sub>), 6.75-6.77 (d, *J*= 10Hz, 1H, C<sub>8</sub>H-chrom.), 6.82-6.84 (d, *J*=10Hz, 1H, Ar), 6.86-6.88 (d, *J*=10Hz, 1H, Ar), 6.99 (s, 1H, Ar), 7.02-7.07 (m, 2H, Ar), 7.17-7.19 (d, *J*=10Hz, 1H, Ar), 7.51 (s, 1H, Ar), 7.63-7.64 (d, *J*=5Hz, 1H, C<sub>5</sub>H-chrom), 8.94 (s, 1H, C<sub>4</sub>H-chrom.), 10.72 (s, 1H, amide); <sup>13</sup>C NMR (125MHz, CDCl<sub>3</sub>) δ: 164.23, 161.58, 160.09, 156.56, 149.17, 148.31, 147.02, 146.01, 137.87, 132.15, 131.98, 126.42, 124.95, 122.95, 115.98, 114.67, 112.94, 110.26, 105.40, 103.24, 101.53, 98.74, 68.15, 67.18, 56.16, 20.17, 11.89; HR-MS (ESI): *m/z* calcd for [M+H]<sup>+</sup> C<sub>28</sub>H<sub>27</sub>O<sub>7</sub>N 490.52; found 490.1875

The fragmentation pattern of compound 15a (C<sub>28</sub>H<sub>27</sub>NO<sub>7</sub>) exhibited molecular ion peak at *m/z* 490.1875 Da as [M + H]<sup>+</sup> (calculated for , exact mass 490.52, Figure 59). It was further fragmented in collision cell (Q2) into major fragments at *m/z* 91.0544, 130.1590, 207.1128, 252.1711, 283.1235, 408.1816 and 432.1455. The elemental composition, exact mass, assigned structures of these major fragments was illustrated in Figure 59. Predicted fragmentation pathway also presented in Figure 59; the molecular ion peak (*m/z* 490.1875 Da) was fragmented in ion with *m/z* 432.1455 (calculated formula C<sub>26</sub>H<sub>25</sub>NO<sub>5</sub><sup>+</sup>) by the loss of C<sub>2</sub>H<sub>2</sub>O<sub>2</sub>, that further fragment into *m/z* 406.1815 (calculated formula C<sub>24</sub>H<sub>24</sub>NO<sub>5</sub><sup>+</sup>) formed by loss of C<sub>2</sub>H<sup>+</sup>. Further, it fragments into two ions with *m/z* 283.1235 (calculated formula C<sub>16</sub>H<sub>13</sub>O<sub>4</sub>N<sup>+</sup>) with loss of C<sub>8</sub>H<sub>11</sub>O<sup>+</sup> ion and ion with *m/z* 252.1711 (calculated formula C<sub>12</sub>H<sub>14</sub>O<sub>5</sub>N<sup>+</sup>) with loss of C<sub>12</sub>H<sub>10</sub><sup>+</sup> ion.

Additionally, the fragment ion  $m/z$  283.1235 with loss of  $C_6H_5^+$  ion resulted into fragment ion  $m/z$  207.1128 (calculated formula  $C_{10}H_9O_4N^+$ ). There is also simultaneous formation of fragment ion  $m/z$  91.0544 (calculated formula  $C_6H_5N^+$ ). Fragmentation pathway described above and presented in figure is a probable pathway; formation of fragments can be simultaneous because of multiple transitions can occur simultaneously.

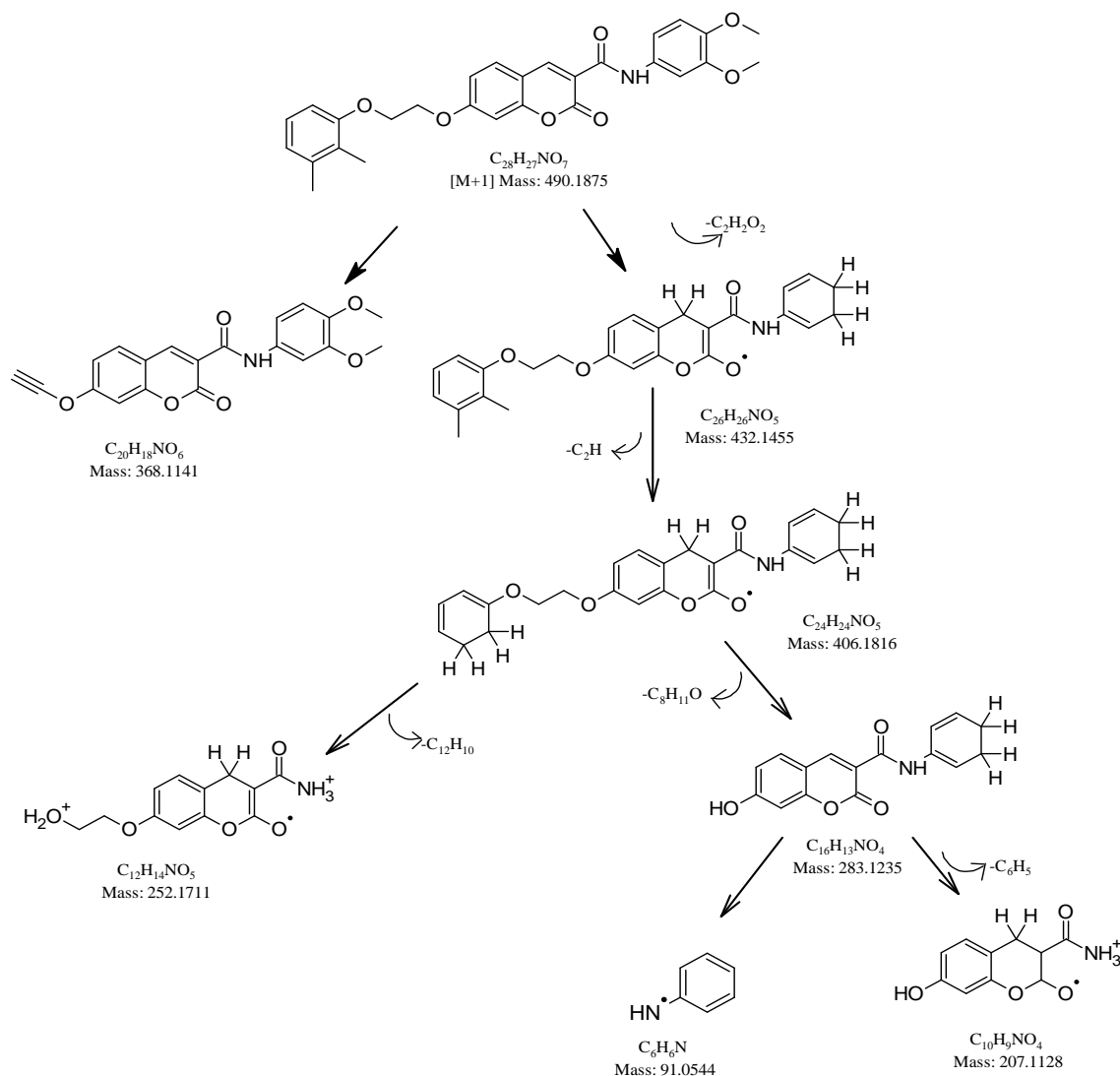
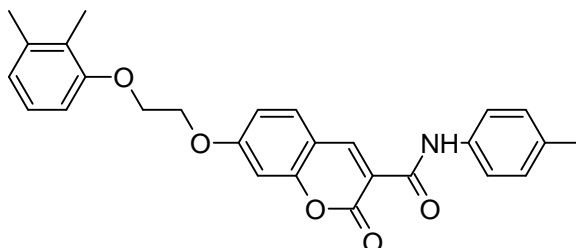


**Figure 59: Proposed fragments and probable fragmentation pathway for compound**

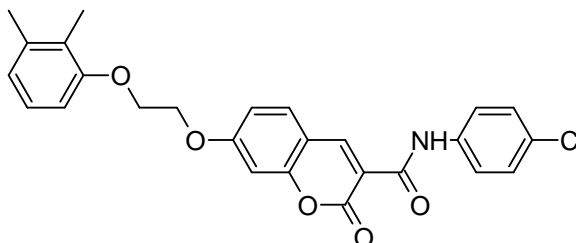
**15a**

**7-[2-(2,3-dimethylphenoxy)ethoxy]-N-(4-methylphenyl)-2-oxochromene-3-carboxamide (16a):**



Brown solid; Yield 52%; mp. 230-231°C; *R*<sub>f</sub>: 0.66 (7:13 EtOAc: hexane); IR (cm<sup>-1</sup>): 3417.14 (N-H), 2869.58 (C-H), 1702.95 (C=O lactone), 1572.63 (C=O amide), 1488.26 (C=C), 1154.90 (C-C), 1373.74 (C-N), 961.90 (C-O-C); <sup>1</sup>H NMR (500MHz, CDCl<sub>3</sub>) δ: 2.14 (s, 3H, CH<sub>3</sub>), 2.27 (s, 3H, CH<sub>3</sub>), 2.35 (s, 3H, CH<sub>3</sub>), 4.35-4.37 (t, 2H, CH<sub>2</sub>), 4.45-4.47 (t, 2H, CH<sub>2</sub>), 6.75- 6.77 (d, *J*=10Hz, 1H, Ar), 6.82-6.84 (d, 1H, Ar), 6.99 (s, 1H, C<sub>8</sub>H-chrom.), 7.02-7.04 (d, 1H, C<sub>5</sub>H-chrom), 7.05-7.09 (t, 1H, Ar), 7.17-7.19 (t, 1H, Ar), 7.61-7.65 (d, 3H, Ar, C<sub>6</sub>H-chrom ), 8.95 (s, 1H, C<sub>4</sub>H-chrom.), 10.73 (s, 1H, amide); <sup>13</sup>C NMR (125MHz, CDCl<sub>3</sub>) δ: 164.20, 162.20, 159.72, 156.63, 156.32, 148.64, 138.31, 135.30, 134.29, 131.13, 129.54, 128.87, 127.56, 125.87, 125.12, 123.12, 120.50, 115.18, 114.84, 112.77, 109.55, 101.39, 70.86, 67.61, 66.75, 22.95, 20.09, 11.70; HR-MS (ESI): *m/z* calcd for [M+H]<sup>+</sup> C<sub>27</sub>H<sub>26</sub>NO<sub>5</sub> 444.50; found 444.15.

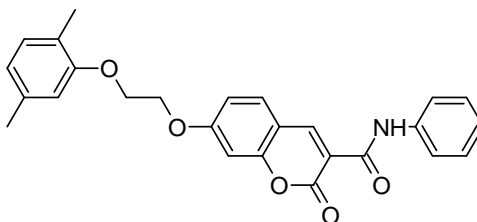
**7-[2-(2,3-dimethylphenoxy)ethoxy]-N-(4-chlorophenyl)-2-oxochromene-3-carboxamide (17a):**



Brown solid; Yield 82%; mp. 210-212°C; *R*<sub>f</sub>: 0.81 (7:13 EtOAc: hexane); IR (cm<sup>-1</sup>): 3783.71 (N-H), 2875.22 (C-H), 1710.24 (C=O lactone), 1605.84 (C=O amide), 1441.53

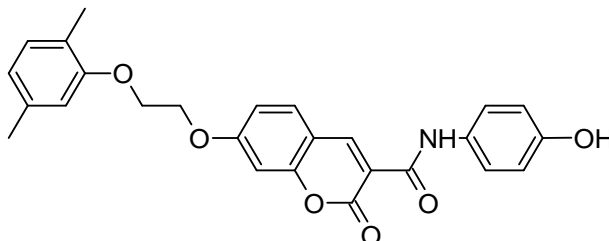
(C=C), 1143.52 (C-C), 1372.79 (C-N), 989.17 (C-O-C);  $^1\text{H}$  NMR (500MHz,  $\text{CDCl}_3$ )  $\delta$ : 2.14 (s, 3H,  $\text{CH}_3$ ), 2.27 (s, 3H,  $\text{CH}_3$ ), 4.36-4.38 (t, 2H,  $\text{CH}_2$ ), 4.46-4.48 (t, 2H,  $\text{CH}_2$ ), 6.75-6.77 (d,  $J=10\text{Hz}$ , 1H, Ar), 6.82-6.84 (d,  $J=10\text{Hz}$ , 1H, Ar), 6.99 (s, 1H,  $\text{C}_8\text{H}$ -chrom.), 7.02-7.04 (d, 1H,  $\text{C}_5\text{H}$ -chrom), 7.07-7.09 (t, 1H, Ar), 7.33-7.35 (d, 2H,  $J=10\text{Hz}$ , Ar), 7.64-7.66 (d,  $J=10\text{Hz}$ , 1H,  $\text{C}_6\text{H}$ -chrom), 7.69-7.71 (d,  $J=10\text{Hz}$ , 2H, Ar), 8.96 (s, 1H,  $\text{C}_4\text{H}$ -chrom.), 10.87 (s, 1H, amide); HR-MS (ESI):  $m/z$  calcd for  $[\text{M}+\text{H}]^+$   $\text{C}_{26}\text{H}_{23}\text{NO}_5\text{Cl}$  464.92; found 464.11.

**7-[2-(2,5-dimethylphenoxy)ethoxy]-N-phenyl-2-oxochromene-3-carboxamide (13b):**



Brown solid; Yield 65%; mp. 170-172 $^{\circ}\text{C}$ ;  $R_f$ : 0.75 (7:13 EtOAc: hexane); IR ( $\text{cm}^{-1}$ ) 3278.04 (N-H), 2873.92 (C-H), 1705.14 (C=O lactone), 1573.13 (C=O amide), 1491.61 (C=C), 1142.52 (C-C), 1374.34 (C-N), 1072.42 (C-O-C);  $^1\text{H}$  NMR (500MHz,  $\text{CDCl}_3$ )  $\delta$ : 2.17 (s, 3H,  $\text{CH}_3$ ), 2.33 (s, 3H,  $\text{CH}_3$ ), 4.36-4.38 (t, 2H,  $\text{CH}_2$ ), 4.46-4.48 (t, 2H,  $\text{CH}_2$ ), 6.69 (s, 1H, Ar), 6.72- 6.73 (d,  $J=5\text{Hz}$ , 1H, Ar), 6.99 (s, 1H,  $\text{C}_5\text{H}$ -chrom.), 7.02-7.04 (d,  $J=10\text{Hz}$ , 1H, Ar), 7.14-7.16 (d,  $J=10\text{Hz}$ , 1H,  $\text{C}_8\text{H}$ -chrom), 7.36-7.40 (t, 3H, Ar), 7.64-7.65 (d,  $J=5\text{Hz}$ , 1H,  $\text{C}_6\text{H}$ -chrom ), 7.73-7.75 (d,  $J=10\text{Hz}$ , 2H Ar), 8.96 (s, 1H,  $\text{C}_4\text{H}$ -chrom.), 10.80 (s, 1H, amide).

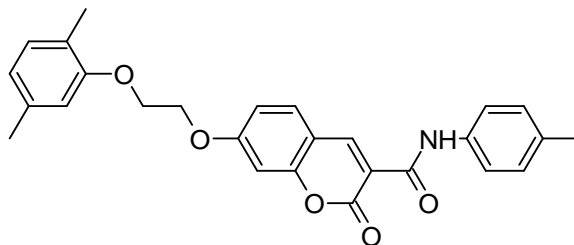
**7-[2-(2,5-dimethylphenoxy)ethoxy]-N-(4-hydroxyphenyl)-2-oxochromene-3-carboxamide (14b):**





Brown solid, Yield: 45%, mp. 180-182°C; *R*<sub>f</sub>: 0.63 (7:13 EtOAc: hexane); IR (cm<sup>-1</sup>): 3790.14 (N-H), 2880.17 (C-H), 1712.90 (C=O lactone), 1611.77 (C=O amide), 1496.42 (C=C), 1207.96 (C-C), 1373.31 (C-N), 976.34 (C-O-C); <sup>1</sup>H NMR (500MHz, CDCl<sub>3</sub>) δ: 2.18 (s, 3H, CH<sub>3</sub>), 2.31 (s, 3H, CH<sub>3</sub>), 4.36-4.38 (t, 2H, CH<sub>2</sub>), 4.45-4.47 (t, 2H, CH<sub>2</sub>), 6.69 (s, 1H, Ar), 6.72- 6.73 (d, *J*=5Hz, 1H, Ar), 6.82-6.88 (d, 3H, Ar), 6.98 (s, 1H, C<sub>5</sub>H-chrom), 7.02-7.09 (m, 2H, C<sub>8</sub>H-chrom), 7.58-7.64 (d, 3H, Ar), 8.94 (s, 1H, C<sub>4</sub>H-chrom.), 10.68 (s, 1H, amide); HR-MS (ESI): *m/z* calcd for [M+H]<sup>+</sup> C<sub>26</sub>H<sub>24</sub>O<sub>6</sub> N 446.47; found 446.1609

**7-[2-(2,5-dimethylphenoxy)ethoxy]-N-(4-methylphenyl)-2-oxochromene-3-carboxamide (16b):**



Brown solid; Yield 55%; mp. 190-192°C; *R*<sub>f</sub>: 0.65 (7:13 EtOAc: hexane); IR (cm<sup>-1</sup>): 3758.39 (N-H), 2881.75 (C-H), 1703.20 (C=O lactone), 1600.97 (C=O amide), 1483.1 (C=C), 1253.71 (C-C), 1383.01 (C-N), 1018.45 (C-O-C); <sup>1</sup>H NMR (500MHz, CDCl<sub>3</sub>) δ: 2.16 (s, 3H, CH<sub>3</sub>), 2.33 (s, 3H, CH<sub>3</sub>), 2.35 (s, 3H, CH<sub>3</sub>), 4.36-4.38 (t, 2H, CH<sub>2</sub>), 4.45-4.47 (t, 2H, CH<sub>2</sub>), 6.69 (s, 1H, Ar), 6.71- 6.73 (d, *J*=10Hz, 1H, Ar), 6.98 (s, 1H, C<sub>5</sub>H-chrom), 7.02-7.03 (d, *J*=5Hz, 2H, C<sub>8</sub>H-chrom), 7.17-7.19 (d, 2H, Ar), 7.61-7.64 (dd, 3H, C<sub>6</sub>H-chrom, Ar), 8.94 (s, 1H, C<sub>4</sub>H-chrom.), 10.72 (s, 1H, amide).

### 6.3. Biological evaluation through *In Vitro* and *In Vivo* studies

#### 6.3.1. *IN VITRO* STUDIES

##### 6.3.1.1. Cell viability assay

A cell-based assay is often used to analyse collections of compounds to determine if they exhibit direct cytotoxic effects or if they show effects on cell proliferation. The cell viability assay of the synthesized compound (1 to 17a) in Human NCI-H716 enteroendocrine cells has been evaluated in-vitro. The relative cell viability percentage of the synthesized compounds with control vehicle was calculated at three different concentrations (0.1, 1 and 10  $\mu$ M). The concentration vs. relative cell viability percentage was plotted and cell viability was determined graphically (Fig. 60). The estimation of the cell viability at three concentrations for all synthesized compounds supported a noticeable analysis that none of the synthesized compounds are toxic towards Human NCI-H716 enteroendocrine cells lines (Table 11)

**Table 11: Results of cell viability assay**

Concentrations	0.1 $\mu$ M	1 $\mu$ M	10 $\mu$ M
Compound Code	Mean* $\pm$ S.D.		
Control	100.00 $\pm$ 2.13	100.00 $\pm$ 2.13	100.00 $\pm$ 2.13
1	95.59 $\pm$ 7.38	89.78 $\pm$ 4.58	96.1 $\pm$ 5
2a	101.52 $\pm$ 3.44	93.6 $\pm$ 0.22	84.84 $\pm$ 4.12
3	87.04 $\pm$ 8.6	92.69 $\pm$ 4.03	100.1 $\pm$ 2.68
4	95.01 $\pm$ 4.58	83.1 $\pm$ 7.42	88.56 $\pm$ 4.74
5a	113.39 $\pm$ 6.75	121.76 $\pm$ 3.42	120.99 $\pm$ 2.57
5d	90.59 $\pm$ 0.74	84.38 $\pm$ 8.42	92.72 $\pm$ 7.85
5c	114.22 $\pm$ 6.56	119.23 $\pm$ 0.98	118.19 $\pm$ 2.05
6a	93.98 $\pm$ 2.64	88.51 $\pm$ 3.57	94.65 $\pm$ 0.08
6b	107.97 $\pm$ 6.79	101.75 $\pm$ 3.17	100.28 $\pm$ 5.4

6c	114.74±2.34	104.93±4.76	100.09±2.66
7a	112.59±5.09	118.57±1.69	116.32±4.6
7b	114.31±6.88	120.84±2.05	118.67±2.67
7c	115.85±6.31	125.58±0.93	123.1±4.04
8a	87.13±3.95	84.1±7.13	81.56±2.49
8b	115.36±9.03	123.14±0.76	123.14±0.76
8c	108.5±8.48	114.37±0.79	117.12±0.98
9a	94.87±1.32	86.14±0.42	92.03±7.25
12a	100.66±0.62	99.17±2	96.05±8.44
12b	97.19±1.73	93.9±9.37	93.9±9.37
13a	97.09±1.66	97.3±3.44	91.16±1.75
13b	101.86±1.63	111.32±3.75	102.52±4.36
14a	112.23±2.03	110.76±5.35	114.59±5.16
14b	104±6.99	102.99±3.49	106.53±6.57
15a	110.17±3.9	106.25±1.64	113.59±6.66
16a	104.57±2.61	98.43±1.26	92.87±2
16b	95.86±5.24	100.65±1.22	101.87±1.11
17a	99.53±6.87	98.99±0.68	104.21±1.68

\*Mean of Five readings

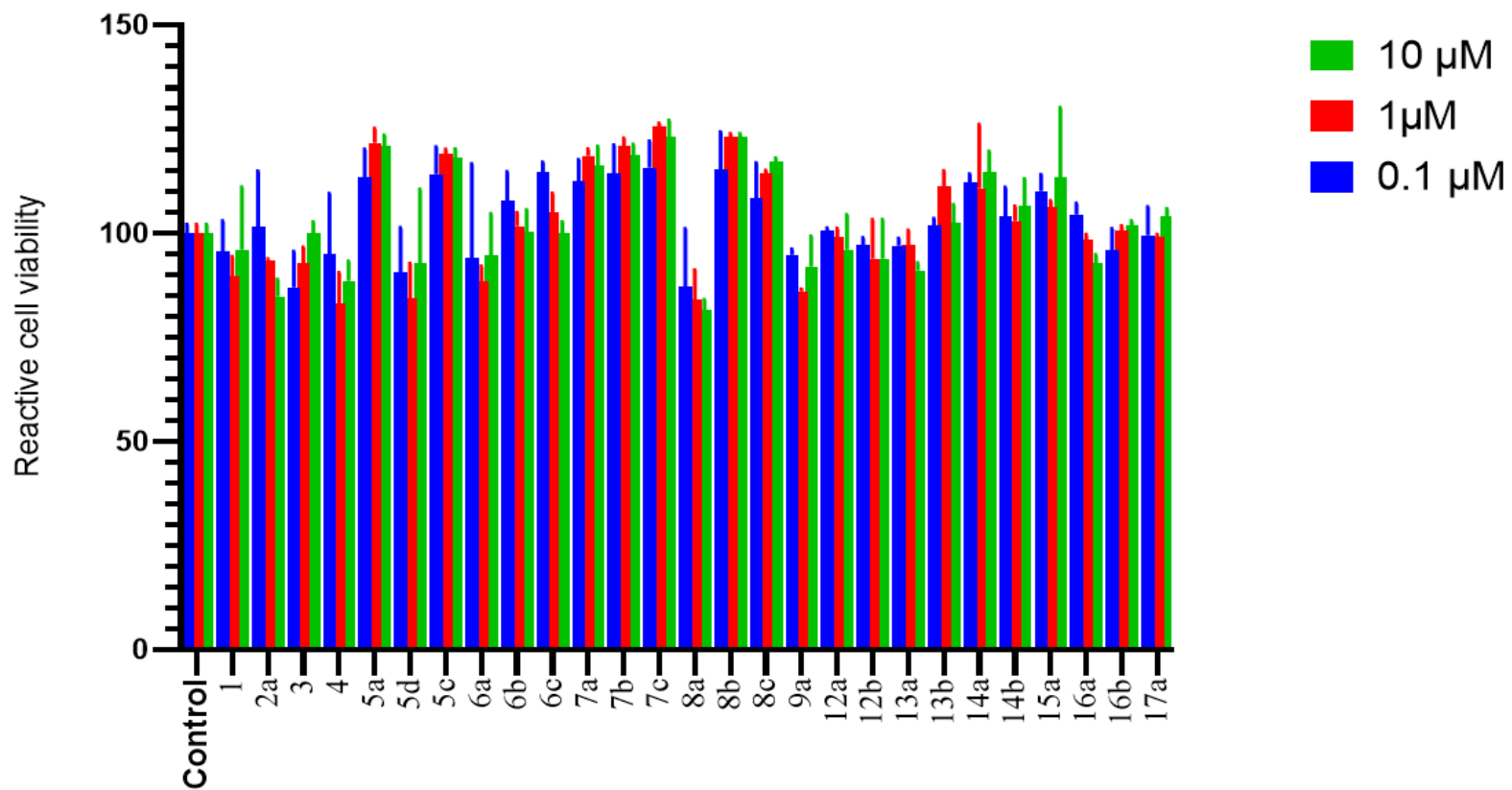


**Figure 60: Relative cell viability percentage vs synthesized compounds at three concentrations levels**

### 6.3.1.2. GLP-1 Assay

After conducting a relative cell viability assay, all compounds (1-17a) were selected for GLP-1 assays in human NCI-H716 enteroendocrine cells, ensuring constant DMSO concentrations as a negative control. The benchmark for comparison with the test compounds was established using INT 777.

Results indicated that compounds 2a and 15a demonstrated a progressive increase in GLP-1 levels across all three concentrations (0.1, 1, 10  $\mu$ M) when compared to the standard INT777 (Table 12). Particularly noteworthy was the significant elevation in GLP-1 levels exhibited by compounds 2a and 15a at concentration of 10  $\mu$ M, surpassing the levels noted with the standard compound. Compounds 6a and 9a displayed a nearly indistinguishable increase in GLP-1 levels in human NCI-H716 enteroendocrine cells as compared to standard. Conversely, compounds 14a and 15a demonstrated a proportional rise in GLP-1 levels as the concentrations varied from 0.1  $\mu$ M to 10  $\mu$ M (Fig. 61).

In conclusion, the cumulative findings strongly indicate that compounds 2a, 6a, 9a, 14a, and 15a exhibit promising potential as anti-diabetic agents, owing to their ability to enhance human NCI-H716 enteroendocrine cells GLP-1 levels.

**Table 12: Results of GLP 1 Assay**

Concentration	0.1 $\mu$ M	1 $\mu$ M	10 $\mu$ M
Compound code	Mean* $\pm$ S.D (pg/mL)		
Control	16.14 $\pm$ 1.07	16.14 $\pm$ 1.07	16.14 $\pm$ 1.07
INT777	17.15 $\pm$ 0.93	19.49 $\pm$ 1.20	23.17 $\pm$ 1.65
1	20.15 $\pm$ 4.35	20.08 $\pm$ 1.78	21.88 $\pm$ 1.63
2a	19.43 $\pm$ 2.09	19.61 $\pm$ 1.06	22.05 $\pm$ 1.71
3	18.05 $\pm$ 1.43	16.30 $\pm$ 1.69	20.56 $\pm$ 1.83
4	20.68 $\pm$ 1.69	18.88 $\pm$ 1.65	21.00 $\pm$ 0.86
5a	18.87 $\pm$ 0.78	17.02 $\pm$ 0.10	19.26 $\pm$ 0.49
5c	18.80 $\pm$ 0.07	17.85 $\pm$ 0.26	18.95 $\pm$ 0.08

5d	19.55±1.97	18.00±1.06	19.24±1.03
6a	17.58±1.65	18.21±1.06	19.60±1.08
6b	19.52±0.20	17.93±0.08	19.47±0.29
6c	18.58±0.67	17.64±0.80	19.99±0.27
7a	18.32±0.44	16.44±0.35	18.87±0.64
7b	19.46±0.80	17.43±0.28	18.08±0.26
7c	19.50±0.34	21.80±0.36	19.58±0.09
8a	16.97±1.54	17.38±1.08	19.29±1.35
8b	18.61±0.52	18.20±0.71	18.01±0.81
8c	18.18±0.95	18.82±0.55	21.77±0.83
9a	16.52±0.74	17.58±1.11	19.65±1.95
12a	19.89±1.56	20.39±1.93	22.77±1.52
12b	18.89±1.49	19.05±1.79	21.83±1.41
13a	18.33±0.31	16.05±0.52	19.20±0.36
13b	16.44±0.47	16.28±0.47	18.27±0.84
14a	16.49±1.16	16.30±1.99	21.38±1.47
14b	17.59±1.09	15.08±0.59	17.26±0.62
15a	18.32±1.15	18.89±1.43	23.90±1.04
16a	17.41±0.43	17.53±0.48	18.92±0.42
16b	16.95±0.51	17.36±0.23	19.51±0.84
17a	17.93±0.79	17.58±0.24	20.39±0.86

\*Mean of Five readings

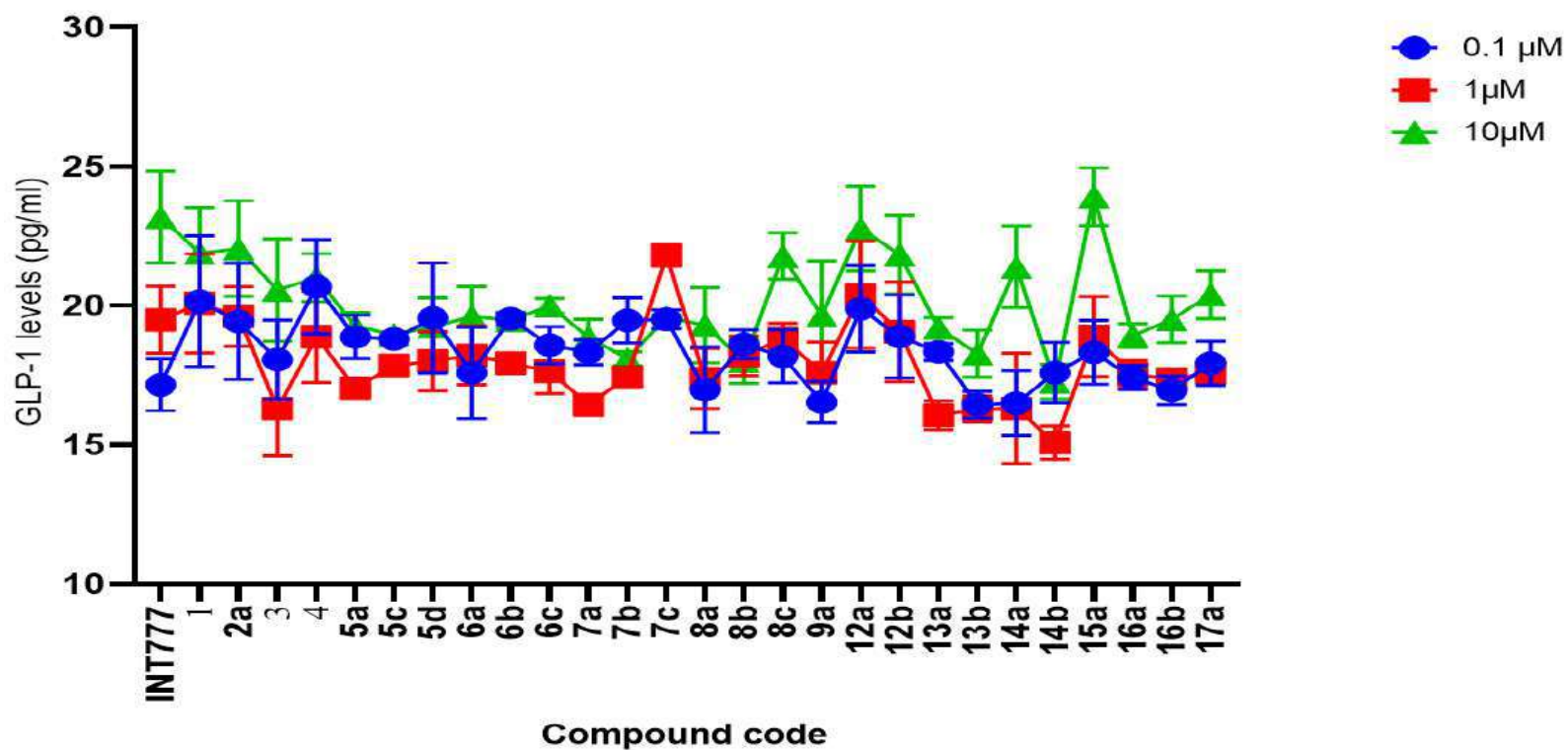


Figure 61: GLP 1 levels (pg/mL) vs synthesized compounds (1-17a) at three concentration levels 0.1 μm, 1 μm and 10 μm. Each reading is taken in multiple of five.

### 6.3.1.3. TGR5 gene expression Assay

Furthermore, the study sought to evaluate how compounds 2a, 6a, 9a, 14a, and 15a impact TGR5 expression.

To determine if these compounds not only function as agonists but also stimulate the expression of TGR5, a quantified TGR5 expression assay was carried out.

The results indicate that both compound 2a and 15a demonstrate a higher level of TGR5 expression compared to the standard INT777 (Table 13). This finding supports the hypothesis that the observed elevation in GLP-1 levels is likely facilitated through the activation of TGR5, contributing to the expected anti-diabetic effects (Fig. 62)

**Table 13: Results of Relative gene expression of TGR5**

Compound code	Control	INT777	2a	6a	9a	14a	15a
Concentration: 10 $\mu$ M							
*Mean	1	0.97	4.04	0.10	0.21	1.25	3.97
$\pm$ S.D.	0.44	0.88	1.49	0.08	0.15	0.36	1.43



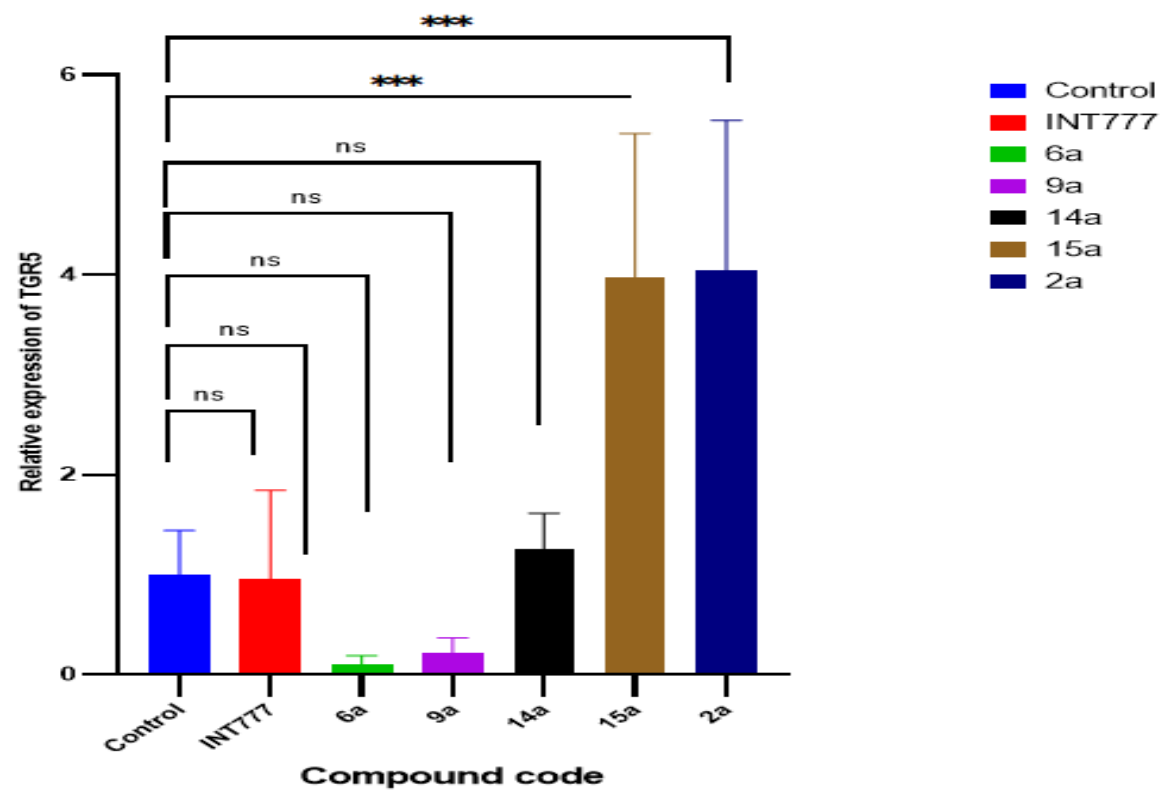


Figure 62: Relative gene expression of TGR5 for compounds. Each reading is the mean of four replicates. The significance level for the data was \*\*\*  $P < 0.001$ , ns  $P > 0.0$

### 6.3.2. *IN VIVO* STUDIES

Based on *In vitro* results, top three compounds 2a, 15a and 14a were selected for *in vivo* studies.

#### 6.3.2.1. Brine shrimp lethality Assay

Compound 2a, 15a and 14a was tested for Brine shrimp lethality Assay at three different concentrations (10, 100 and 1000 µg/mL). All sample showed less mortality, so the samples are nontoxic to the brine shrimp as percentage mortality is only 3.33% at 1000 µg/mL. Out of three compounds tested, compound 15a was found to be less toxic to brine /mL of concentration. Hence, compound 15a was selected for acute toxicity study in Albino rat.

**Table 14: Details of Brine shrimp lethality Assay**

Compound	Conc. of Sample (µg/mL)	Total No. of shrimp used/ 3 Tubes	Total no. of Shrimp survived	Percentage mortality
2a	Control	10	30	00
	10		30	3.33
	100		30	00
	1000		29	3.33
15a	Control	10	30	00
	10		29	00
	100		30	00
	1000		29	3.33
14a	Control	10	30	00
	10		29	3.33
	100		30	00
	1000		28	6.66

#### 6.3.2.2. ACUTE TOXICITY STUDIES

Test compound (15a) was administered at dose range from 5-2000 mg/kg for an acute toxicity study. No adverse effects were observed in any of tested dose groups. There were no instances of mortality recorded in the treated groups across all dose levels (i.e., from 5 mg/kg to 2000 mg/kg). Hence, LD<sub>50</sub> of test compounds is likely higher than 2000 mg/kg. Consequently, acute exposure to the test compound can be considered relatively safe.

The following parameters were observed in acute toxicity studies

- I. Pre-terminal deaths
- II. Physiological activity
- III. Clinical observations

**Pre-terminal deaths:** The pre-terminal deaths were not observed during study period.

**Physiological activity:** During the study period, the animals' food intake was normal, and no significant effects were observed. Average Food intake of treated animals was found to be 114 g in time span of 14 days. The animals gained weight normally and showed no significant effects.

**Clinical observations:** A single dose (2000 mg/kg) administered of the test item once did not induce clinical symptoms of toxicity or cause mortalities in any of the treated animals. The observation includes observations of the skin, fur, eyes, mucous membranes, respiratory system, salivation, diarrhoea and behavioural patterns. The tremors, convulsions, and coma were particularly noted.

There were no significant changes observed in physical, physiological and behavioural profile of animals (Table 15).

**Table 15: Clinical observations in treated animals**

Sr. No.	General signs	Time (Hours)		
		1	2	3
1.	Posture assessment	Normal		
2.	Convulsion (Limb paralysis)	Normal		
3.	Body tone	Normal		
4.	Lacrimation	No sign		
5.	Salivation	No sign		
6.	Tremor	Normal		
7.	skin color change	No sign		
8.	Piloerection	No sign		
9.	Defecation	Normal		
10.	Locomotion, Muscle gripnessRearing	Normal		
11.	Food intake	Normal		

**6.3.2.3. ORAL GLUCOSE TOLERANCE TEST (OGTT)**

The most active compound 15a from in-vitro studies was subjected to in vivo studies in Wister rats at 400 mg/kg. The results revealed reduced the level of glucose to normal in blood at 400 mg/kg dose as compared to Sitagliptin (positive control) at 10 mg/kg dose (Fig. 63A). Compound 15a showed better suppression of blood glucose level compared to Sitagliptin at 120 min (Table 16). The AUC<sub>0–240min</sub> (area under the curve) for glucose levels (for single administration of 15A orally) was calculated, which cause 17% reduction in glucose levels from a vehicle group (Fig. 63B).

**Table 16: Results of OGTT test**

Groups	Control	Standard (Sitagliptin)	Test (compound 15a)
	Blood glucose level (mg/dL)		
Time Interval	Mean±S.D.		
0 min	76.66±1.52	76.66±1.52	76.66±1.52
30 min	135±3.6	108±4.35	107±7.0
60 min	110±6.42	90±5.56	92±5.85
90 min	102±5.03	78.66±6.35	83±4.93
120 min	75.33±3.51	75±7.02	64±6.55
240 min	70.33±4.04	62±3.6	60.33±4.93

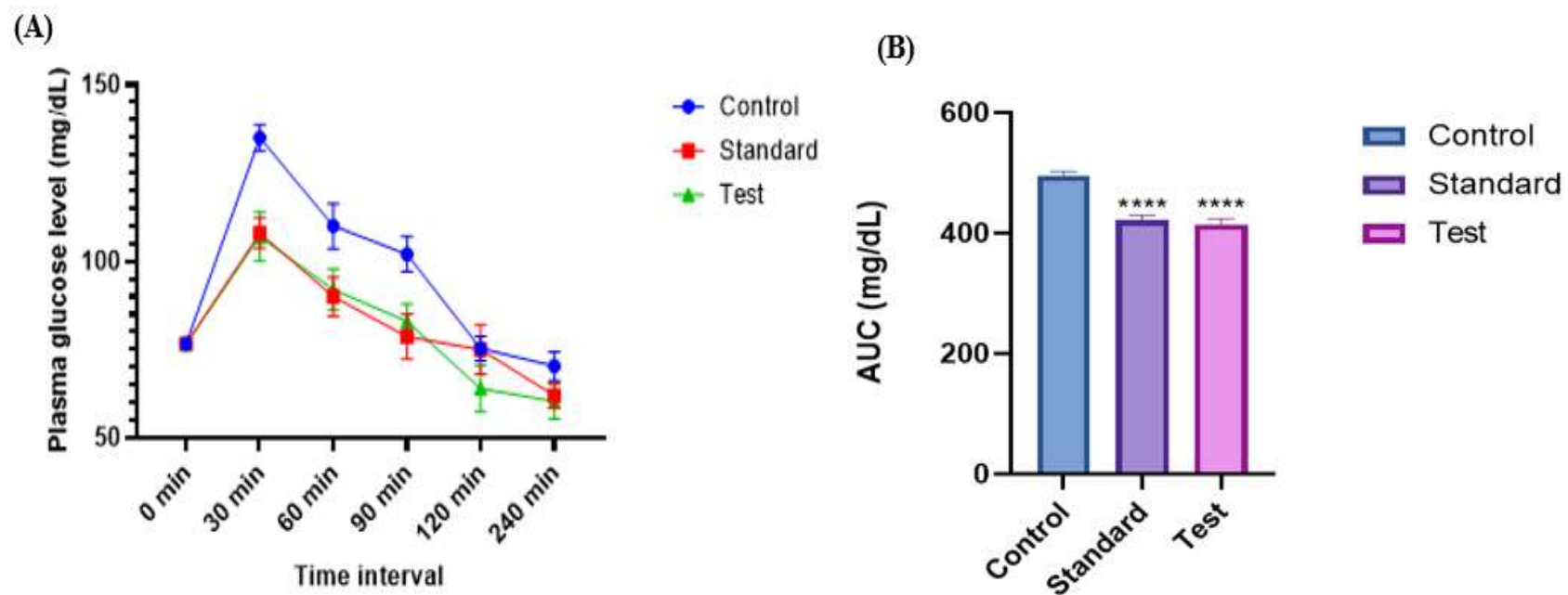


**Figure 63: Effect of 15a on OGTT: (A) Plasma blood glucose; (B) blood glucose AUC<sub>0–240 min</sub>. The significance level for the data was \*\*\*\*  $P < 0.0001$ , \*\*\*  $P < 0.001$ , \*\* $P < 0.01$ , ns  $P > 0.0$**

#### 6.4. STRUCTURE ACTIVITY RELATIONSHIP

The synthesized coumarin derivatives were evaluated for human TGR5 (hTGR5) agonistic activity using GLP-1 assay in NCI-H716 enteroendocrine cells. For same, coumarin derivatives were assayed for GLP 1 assay at three concentrations (0.1, 1, 10  $\mu$ M) compared to the standard INT 777.

##### SAR of Series A

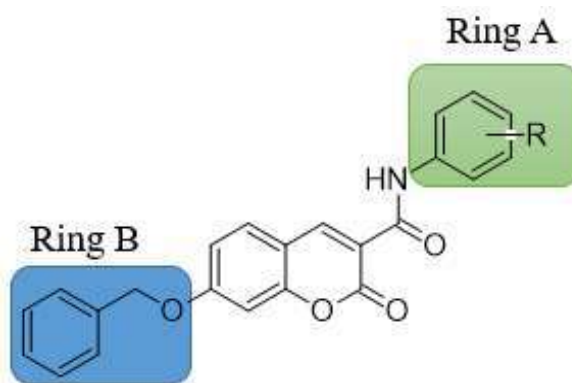


**Figure 64: General structure of Series A**

In the initial stages of our investigation into Series A structure-activity relationships, we examined impact of 7-hydroxy coumarin ring on GLP-1 assays in NCI-H716 cells. Intermediate 1 yielded a GLP-1 level of  $21.88 \pm 2.63$  pg/mL at a  $10 \mu$ M concentration.

Subsequent we began our SAR studies by substitution of the benzyloxy ring (Ring B) at the 7<sup>th</sup> position of the compound 1. benzyloxy ring at 7<sup>th</sup> position (as in compound 2a) led for increase in GLP-1 levels to  $22.05 \pm 2.71$  pg/mL at  $10 \mu$ M, indicating a gradual elevation in GLP-1 levels across 0.1 to  $10 \mu$ M concentrations of the sample. Thus, the results demonstrate the significance of the benzyloxy group for the activity. *In vitro* findings of compound 2a align with the docking results of 2a with the TGR5 receptor (PDB ID: 7CFN), revealing hydrogen bonding with the benzyloxy ring and hydrophobic interactions with the coumarin ring.

Moreover, the study examined SAR of substitutions on amide phenyl ring (Ring A). Compound 3 (no substitution on phenyl ring A) showed a slight decrease in GLP-1 levels ( $20.56 \pm 2.83$  pg/mL) as compared to 2a. Various electron-donating (methyl, methoxy) and electron-withdrawing groups (chloro, bromo) were

incorporated at different positions on the ring to investigate their impact on the activity. Some substitutions notably enhanced potency by increasing GLP-1 levels.

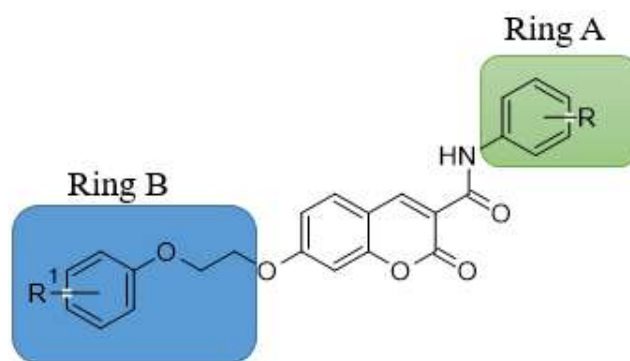
Introduction of electron donating group i.e. hydroxyl group at Ring A *para* position (Compound 4), displayed an elevation in GLP-1 levels to  $21 \pm 0.86$  pg/mL. Subsequent substitutions with more electron-donating group i.e. methoxy at *para* position of Ring A (5a: GLP-1 level  $19.26 \pm 0.49$  pg/mL) and at *ortho* position (5c: GLP-1 level  $18.95 \pm 0.08$  pg/mL) showed decrease in GLP-1 levels. Even, the di-substitution of methoxy group in compound 5d ( $19.24 \pm 3.03$  pg/mL) resulted in almost same activity as compared to mono substituted one (5a and 5c). Introduction of another electron-donating methyl group at *para* (6a), at *meta* (6b) resulted in less promising activity compared to *ortho* substituted methyl group (6c). Compound 6c found to show GLP-1 levels of  $19.99 \pm 0.27$  pg/mL at 10  $\mu$ M of sample. Further, the di-substitution of 2, 4-dimethyl (7a), 2,5-dimethyl (7b) showed remarkable decrease in GLP-1 levels but 2,6-dimethyl (7c) showed slight but uneven increase in GLP-1 levels on exposure to 0.1-10  $\mu$ M of sample.

Moreover, substitution with an electron-withdrawing group (chloro) were also examined at *ortho* (8c), *meta* (8b) and *para* position (8a) of phenyl ring A. Compound 8c identified as the most potent among the Series A compounds, with a GLP-1 level of  $21.77 \pm 0.83$  pg/mL. Notably, compound 8c, with chloro substitution at the *ortho* position, exhibited higher GLP-1 levels compared to *para* (8a:  $19.29 \pm 2.35$  pg/mL) and *meta* (8b:  $18.01 \pm 0.81$  pg/mL) substitutions in Series A.

Thus, it can be speculated that benzyloxy group at coumarin's 7<sup>th</sup> position and electron withdrawing group at *ortho* position of Ring A might be favourable for binding with the receptor and enhance TGR5 agonistic activity by increasing GLP-1 levels.



## SAR of Series B and C



**Series B: R<sup>1</sup>- 2, 3-dimethyl**

**Series C: R<sup>1</sup>- 2, 5-dimethyl**

**Figure 65: General structure of Series B and C**

Following the SAR investigation of series A, characterized by a benzyloxy ring (Ring B) positioned at coumarin ring's 7<sup>th</sup> position. Further, it was hypothesized that integrating a carbon chain (comprising 2 carbon atoms) as a linker between Ring B and the central core could provide conformational flexibility and adaptability in position, potentially offering advantages. Additionally, the introduction of methyl groups (2, 3 and 2, 5) on Ring B was explored, taking into account the hydrophobic nature of the binding pocket of the TGR5 receptor.

Introducing a (2,3-dimethylphenoxy)ethoxy group at 7<sup>th</sup> position of coumarin ring (Series B) led to compound 12a, showing higher GLP-1 levels (22.77±3.52 pg/mL) compared to compound 12b from Series C, which contains a (2,5-dimethylphenoxy)ethoxy group (GLP-1 level 21.83±2.41 pg/mL), as well as the compound 2a featuring benzyloxy substitution.

Thus, it confirmed our hypothesis of introduction of 2, 3-dimethyl and 2, 5-dimethyl on Ring A that increase the binding affinity of test compounds to TGR5 receptor.

Further, including the (2, 3-dimethylphenoxy)ethoxy group at the 7<sup>th</sup> position of the coumarin central core, 10 derivatives were synthesized with electron donating and withdrawing groups substitution on aryl amide Ring A of 12a as follows. Compound 13a, with no substitutions on Ring A, experienced decrease in GLP-1 levels

(19.20±0.36 pg/mL). Conversely, Compound 14a, featuring a hydroxyl group (an electron donating group) substituted at Ring A's *para* position, resulted in increase in GLP-1 levels to 21.38±5.47 pg/mL.

Subsequent substitutions with more electron-donating groups such as 3, 4 dimethoxy (compounds 15a) led to highest GLP-1 levels (23.90±5.04 pg/mL) compared to the standard and all compounds of series A. Moreover, substitution with an electron-withdrawing group (chloro) produced Compound 17a resulted in reduces in GLP-1 level to 20.39±0.86 pg/mL. The efficacy of 15a may also be attributed to its binding within the pocket of TGR5 receptor. Docking studies of 15a demonstrated a -9.8 kcal/mol of binding energy at active sites. The coumarin ring's oxo group within 15a forms a hydrogen bond with Ser 157 and Tyr 240. Moreover, hydrophobic interaction between 15a and Ala250, Leu266, and Leu74, facilitated by the coumarin ring and Ring B, highlights their significance in hydrophobicity and interaction with Ala 250 and Leu74 at TGR5 active site. Moreover, methoxy groups on phenyl ring A of 15a contribute to hydrogen bond interactions with Tyr 240, further enhancing its interaction with the receptor (Figure 66).

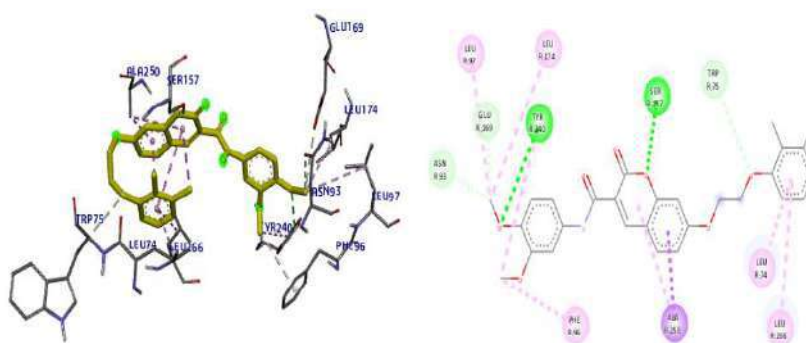


**Figure 66: 3D and 2D Intermolecular interactions between lead compound 15a with TGR5.**

Furthermore, it was found that 15a demonstrated the greatest expression of the TGR5 gene among the tested compounds. *In vivo* experiments validated the results obtained from *in vitro* studies. Compound 15a demonstrated enhanced regulation of blood glucose levels compared to Sitagliptin after 120 minutes, resulting in a 17% reduction in area under curve (AUC<sub>0–240 min</sub>) of glucose levels compared to control group.

# SUMMARY AND CONCLUSION



## **CHAPTER 7**

### **7. SUMMARY AND CONCLUSIONS**

#### **7.1. SUMMARY**

Diabetes represents a significant global health concern marked by diverse metabolic disorders, and currently available drugs often carry various side effects. A comprehensive literature review emphasized the importance of developing ligands with a strong affinity for the TGR5 receptor to enhance efficacy while reducing toxicity. To achieve this, a homology model was generated and validated, followed by docking and simulation studies using the TGR5 structure from the RCSB PDB database.

**Designing of compounds:** The present study proposed a pharmacophore consisting of a bicyclic central core (Coumarin ring) linked to a hydrophobic phenyl ring with an amide group at one end and phenoxy substitution at other. Four series of compounds (Series A, B, C and D) were designed based on this pharmacophore.

**Homology Modelling:** Due to unavailability of TGR5 protein structure in RCB Database, our study commenced with generation and validation of Homology model of TGR5 using Swiss Model and I-Tasser. Based on the validation results and Ramchandran plot, model generated from Swiss Model was finalised.

**Molecular Docking and Dynamic Studies:** In 2020, Yang et.al deposited structure of TGR5 protein in database, this discovery laid our groundwork to perform molecular docking studied in TGR5 protein (PDB ID: 7DFN). Preliminary docking studies using Autodock Vina software and molecular simulation studies were conducted to assess ligand-receptor complex stability in TGR5 receptor (PDB ID: 7DFN). Ten compounds (6a, 14a, 14b, 16a, 16b, 15a, 6c, 6b, 8a and 8b) with favourable docking scores in range of -9.9 to -9.6 kcal/mol were identified through affinity score comparison with the standard INT777. Molecular dynamics (MD) studies highlighted Leu244, Leu166, Tyr89, Ser157, Leu74 residues as crucial for conformational stability within the TGR5 receptor's binding site. *In silico* ADME evaluations

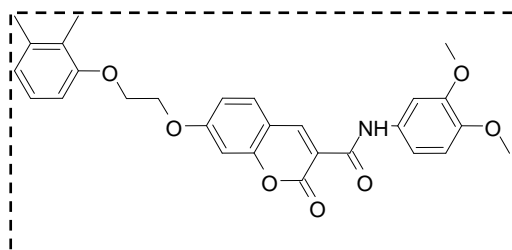
indicated that the synthesized compounds exhibited physicochemical properties, water solubility, lipophilicity, and pharmacokinetics within acceptable ranges for therapeutic use. Consequently, compounds 6a, 16a, and 14a, possessing highest docking scores, were identified as potential for TGR5 agonistic activity.

**Synthesis of test compounds:** The synthesis of the most feasible and potent compounds was undertaken based on their binding affinity, considering cost-effectiveness and the availability of starting materials. Analysis and characterization of all synthesized compounds in each series included melting point, TLC, FT-IR, NMR, and Mass.

**In vitro studies:** *In vitro* assays demonstrated the non-toxic nature of the synthesized compounds on the human NCI-H716 enteroendocrine cell line. GLP-1 assays highlighted compounds 2a, 6a, 9a, 14a, and 15a as promising anti-diabetic agents, enhancing GLP-1 levels across concentrations (0.1, 1, 10  $\mu$ M) compared to the standard INT777. Further, TGR5 gene expression assays indicated higher levels of TGR5 gene expression for compounds 2a and 15a, suggesting activation of TGR5 contributing to expected anti-diabetic effects. *In vitro* analysis identified compound 2a and 15a as the most potent on the TGR5 receptor.

**In vivo studies:** For *in vivo* evaluation, compounds 2a, 15a, and 14a underwent toxicity studies using the Brine shrimp lethality assay and acute toxicity studies. Since compound 2a and 14a showed mortality in Brine shrimp, compound 15a was chosen for acute toxicity studies, revealing its non-toxic nature in Wister rats. Based on toxicity studies, Compound 15a was selected for its antidiabetic effect against Sitagliptin in a rat model. Compound 15a demonstrated superior suppression of blood glucose levels compared to Sitagliptin at 120 min, resulting in a reduction of 17% in blood glucose AUC<sub>0–240min</sub> compared with control group.

**N-(3, 4-dimethoxyphenyl)-7-[2-(2,3-dimethylphenoxy)ethoxy]-2-oxochromene-3-carboxamide (15a)**



**Molecular weight:** 489.52

**Logp:** 3.96

**GI absorption:** High

**H bond acceptor:** 7

**H bond donor:** 1

***In vitro* cell toxicity:** non-toxic

**GLP-1 levels at 10 $\mu$ M:** 23.90 $\pm$ 1.04 pg/mL

**TGR5 gene expression:** 3.97 $\pm$ 1.43

**Brime Shrimp lethality assay:** Non-toxic

**Acute toxicity studies:** Not toxic at dose of 2000mg/Kg

**OGTT test:** 17% reduction in blood glucose compared to standard at 400 mg/kg/day

## 7.2. CONCLUSION

### 7.2.1. Introduction

The prevalence of diabetes has increased significantly in the recent decades, and the condition has also been associated with a variety of metabolic disorders, such as weight gain, digestive problems, and an increase in edema. Currently available drugs often cause various side effects such as weight gain, digestion complications, and edema. In some cases, it causes episodes of hypoglycaemic conditions that increase over time to the point that responsiveness is lost. There has been significant progress in the development of therapeutic anti-diabetic agents in recent years, but the development of these agents remains a great challenge.

In a comprehensive review of the literature, it was revealed that the development of ligands with a strong affinity for the TGR5 receptor is key to increasing the efficacy of these drugs and reducing their toxicity during their development. Upon reviewing the literature on synthetic TGR5 agonists, we were able to identify compounds with monocyclic hydrophobic cores consisting of pyridine rings, which are linked to heteroaromatic rings by an amide bond, and that are linked to phenyl rings either directly or indirectly by oxygen atoms in the opposite direction (Fig.20, 22, 24).

### 7.2.2. Design of Compounds

Considering the hydrophobic environment of the active site of the TGR5 receptor, it was hypothesized that a bicyclic ring structure would be well-suited as a central scaffold for ligand design. Among the various bicyclic scaffolds available, the coumarin ring system was selected due to its unique chemical and structural properties. Coumarins are known for their planar aromatic structure, which can facilitate  $\pi$ - $\pi$  stacking interactions, and their potential to form hydrophobic contacts with the receptor's active site residues. Despite its widespread applications in medicinal chemistry for various biological targets, the coumarin ring has not been extensively investigated as a TGR5 agonist. This lack of exploration in the existing literature presented an opportunity to evaluate its efficacy in modulating TGR5 activity.

### 7.2.3. *In Silico* Studies

Since the TGR5 protein structure is not available in the RCSB Protein Data Bank (PDB), our study began with the generation and validation of a homology model for TGR5. To achieve this, two widely used modelling tools, Swiss-Model and I-TASSER, were employed. These tools were selected for their ability to generate reliable 3D protein models based on sequence homology with available template structures. A comparative analysis was performed to evaluate the models generated by both servers to identify the most suitable model for further studies. The assessment focused on key validation parameters, including the presence of residues in disallowed regions of the Ramachandran plot and the overall quality factor of the models. The model generated by Swiss-Model demonstrated superior structural quality, with no residues located in disallowed regions of the Ramachandran plot. In contrast, the model produced by I-TASSER had 1.46% residues in disallowed regions and an overall quality factor of 93.458. Given these results, the Swiss-Model-generated structure was selected for subsequent studies due to its higher structural accuracy and reliability.

In 2020, Yang et.al deposited structure of TGR5 protein in database, this discovery laid our groundwork to perform molecular docking studied in TGR5 protein (PDB ID: 7DFN). Molecular docking studies identified compounds with favourable

docking scores in range of -9.9 to -9.6 kcal/mol were identified through affinity score comparison with the standard INT777. Molecular dynamics study offers valuable insights into the structural stability and conformational dynamics of TGR5-ligand complexes through molecular dynamics simulations. These findings highlight the potential of the selected compounds to stabilize TGR5, making them promising candidates for therapeutic applications.

#### **7.2.4. Synthesis**

All selected compounds were synthesized. Coumarin ring was synthesized using Knoevenagel condensation that further undergoes Williamson ether synthesis and coupling reactions to synthesize series of compounds. The analysis and characterization of all synthesized coumarin derivatives in each series were conducted using a comprehensive set of techniques. These included determining their melting points, performing thin-layer chromatography (TLC) to confirm purity, and utilizing Fourier-transform infrared spectroscopy (FT-IR) to identify functional groups. Additionally, nuclear magnetic resonance (NMR) spectroscopy was employed to elucidate structural details, while mass spectrometry was used to confirm molecular weights and assess the overall integrity of the compounds.

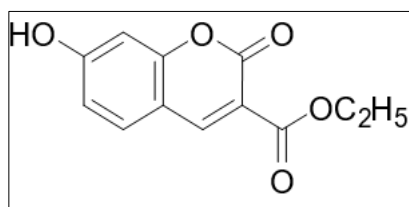
#### **7.2.5. Biological evaluation (*In-vitro* and *In-vivo* studies)**

Further in vitro experiments, including cell toxicity assays, GLP-1 secretion assays, and TGR5 gene expression assays, were conducted to evaluate the potential of the synthesized compounds to modulate pathways involved in glucose regulation. The results revealed that all synthesized compounds were non-toxic to the NCI-H716 cell line. Based on the relative cell viability assay, all compounds (1–17a) were selected for GLP-1 assays, with INT777 serving as the benchmark for comparison.

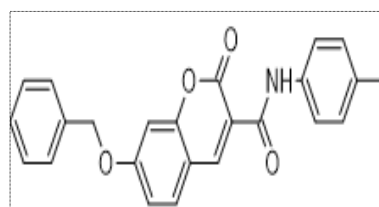
The findings strongly suggest that compounds 2a, 6a, 9a, 14a, and 15a exhibit significant potential as anti-diabetic agents, as they demonstrated an ability to enhance GLP-1 secretion levels in human NCI-H716 enteroendocrine cells. Additionally, the study investigated the impact of these compounds on TGR5 expression. Notably, compounds 2a and 15a displayed a higher level of TGR5 expression compared to the



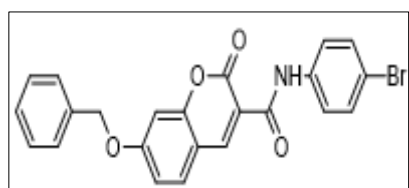
standard INT777, further highlighting their potential efficacy as therapeutic candidates for diabetes management.



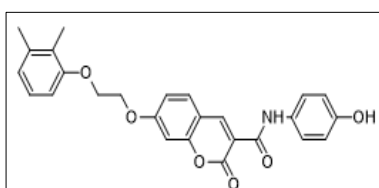
2a



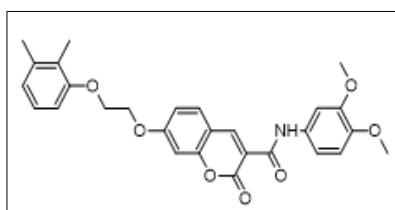
6a



9a



14a



15a

*In vivo* assessments provided critical insights into the compound's safety and effectiveness, showing that compound 15a not only had a favourable toxicity profile but also outperformed Sitagliptin—a widely used anti-diabetic drug—in reducing blood glucose levels. This improvement was evident in a more pronounced reduction of glucose levels compared to Sitagliptin, highlighting compound 15a's potent glucose-lowering properties. Overall, compound 15a stands out as a promising candidate for type 2 diabetes treatment, offering a balanced profile of efficacy and safety, and warrants further investigation in preclinical and clinical studies to confirm its therapeutic potential.

**Future scope of work:** In this study, potential active compounds were effectively designed, synthesized, characterized, and evaluated as TGR5 agonists with antidiabetic properties. However, animal studies, including GLP-1 and TGR5

luciferase assays are still required. Additionally, bulk synthesis needs to be tested for feasibility, cost-effectiveness, and reproducibility to facilitate the development of these compounds into lifesaving drugs. Further preclinical and clinical evaluations are necessary to advance these compounds as potential drug candidates for diabetes.

# REFERENCES



## **CHAPTER 8**

### **REFERENCES**

1. Mishra, A. K.; Pandey, M.; Pannu, A.; Dewangan, H. K.; Sahoo, P. K. Review on Diabetes Mellitus: An Insight into the Current Scenarios, the Challenges of Therapy, and Application of Traditional Drugs. *Curr. Tradit. Med.* **2024**, *10* (3), 1-22.
2. Kolb, H.; Martin, S. Environmental/Lifestyle Factors in the Pathogenesis and Prevention of Type 2 Diabetes. *BMC Med.* **2017**, *15*, 131-142.
3. Katsarou, A.; Gudbjörnsdottir, S.; Rawshani, A.; et al. Type 1 Diabetes Mellitus. *Nat. Rev. Dis. Primers.* **2017**, *3*, 17016.
4. Akil, A. A. S.; Yassin, E.; Al-Maraghi, A.; et al. Diagnosis and Treatment of Type 1 Diabetes at the Dawn of the Personalized Medicine Era. *J. Transl. Med.* **2021**, *19*, 137.
5. Artasensi, A.; Pedretti, A.; Vistoli, G.; Fumagalli, L. Type 2 Diabetes Mellitus: A Review of Multi-Target Drugs. *Molecules.* **2020**, *25*(8), 1987.
6. McIntyre, H. D.; Catalano, P.; Zhang, C.; Desoye, G.; Mathiesen, E.; Damm, P. Gestational Diabetes Mellitus. *Nat. Rev. Dis. Primers.* **2019**, *5*, 47.
7. IDF Diabetes Atlas Tenth Edition **2022**.
8. Tuomilehto, J.; Schwarz, P.; Lindstrom, J. Long-Term Benefits from Lifestyle Interventions for Type 2 Diabetes Prevention: Time to Expand the Efforts. *Diabetes Care.* **2011**, *34*, S210-S214.
9. Colberg, S. R.; Sigal, R. J.; Fernhall, B.; Regensteiner, J. G.; Blissmer, B. J.; Rubin, R. R.; Braun, B. Exercise and Type 2 Diabetes: The American College of Sports Medicine and the American Diabetes Association Joint Position Statement. *Diabetes Care* **2010**, *33*, 147-167.
10. Weir, G.C.; Bonner-Weir, S. Five stages of evolving beta-cell dysfunction during progression to diabetes. *Diabetes.* **2004** Dec;53 Suppl 3:S16-21
11. Bhimanwar, R. S., Mittal. A. TGR5 agonists for diabetes treatment: a patentreview and clinical advancements (2012-present). *Expert Opin on Ther Pat*, **2022**, *32*(2): 191-209.

12. Bailey, C.; Tahrani, A.; Barnett, A. Future Glucose-Lowering Drugs for Type 2 Diabetes. *Lancet Diabetes Endocrinol.* **2016**, *4*, 350-359.
13. Sarkar, A.; Tiwari, A.; Bhasin, P.; Mitra, M. Pharmacological and Pharmaceutical Profile of Gliclazide: A Review. *J. App. Pharma. Sci.* **2011**, *09*, 11-19.
14. Nanjan, M. J.; Mohammed, M.; Kumar, B. R.; Chandrasekar, N. Thiazolidinediones as Antidiabetic Agents: A Critical Review. *Bioorg. Chem.* **2018**, *77*, 548-567.
15. Hong, F.; Xu, P.; Zhai, Y. The Opportunities and Challenges of Peroxisome Proliferator-Activated Receptors Ligands in Clinical Drug Discovery and Development. *Int. J. Mol. Sci.* **2018**, *19*(8), 2189.
16. Kumar, S.; Mittal, A.; Mittal, A. A Review upon Medicinal Perspective and Designing Rationale of DPP-4 Inhibitors. *Bioorganic & Med. Chem.* **2021**, *46*, 116354.
17. Gallwitz, B. Clinical Use of DPP-4 Inhibitors. *Front. Endocrinol.* **2019**, *10*, 1-10.
18. Bailey, C. Metformin: Historical Overview. *Diabetologia.* **2017**, *60*, 1566-1576.
19. Joshi, S. R.; Standl, E.; Tong, N.; Shah, P.; Kalra, S.; Rathod, R. Therapeutic Potential of  $\alpha$ -Glucosidase Inhibitors in Type 2 Diabetes Mellitus: An Evidence-Based Review. *Expert Opin. Pharmacother.* **2015**, *16*, 1959-1981.
20. Sharma, S.; Mittal, A.; Kumar, S.; Mittal, A. Structural Perspectives and Advancement of SGLT2 Inhibitors for the Treatment of Type 2 Diabetes. *Curr Diabetes Rev.* **2022**, *18*, 12-34.
21. Hsia, D. S.; Grove, O.; Cefalu, W. T. An Update on Sodium-Glucose Co-Transporter-2 Inhibitors for the Treatment of Diabetes Mellitus. *Curr. Opin. Endocrinol. Diabetes Obes.* **2016**, *24*, 73-79.
22. Hinnen, D. Glucagon-Like Peptide 1 Receptor Agonists for Type 2 Diabetes. *Diabetes Spectrum.* **2017**, *30*, 202-210.
23. Luo, J.; Zheng, M.; Jiang, B.; Li, C.; Guo, S.; Wang, L.; Li, X.; Yu, R.; Shi, D. Antidiabetic Activity In Vitro and In Vivo of BDB, a Selective Inhibitor of

- Protein Tyrosine Phosphatase 1B, from *Rhodomela confervoides*. *Br. J. Pharmacol.* **2020**, *177*, 4464-4480.
24. Ren, Y.; Li, L.; Wan, L.; Huang, Y.; Cao, S. Glucokinase as an Emerging Anti-Diabetes Target and Recent Progress in the Development of Its Agonists. *J. Enzyme Inhib. Med. Chem.* **2022**, *37*(1), 606-615.
  25. Kaur, P.; Mittal, A.; Nayak, S.; Khatik, G.; Vyas, M.; Mishra, V. Current Strategies and Drug Targets in the Management of Type 2 Diabetes Mellitus. *Curr. Drug Targets.* **2018**, *19*, 1738-1766.
  26. Michael, N.; Jakob, W.; Juris, M. Treatment of Type 2 Diabetes: Challenges, Hopes, and Anticipated Successes. *Lancet Diabetes Endocrinol.* **2021**, *9*, 524-544.
  27. Santwana, P.; Amit, N.; Anindita, B. Type II Diabetes Mellitus: A Review on Recent Drug-Based Therapeutics. *Biomed. Pharmacother.* **2020**, *131*, 110708.
  28. Marín, J.; Timón, I.; Collantes, C.; Gómez, F. Update on the Treatment of Type 2 Diabetes Mellitus. *World J. Diabetes.* **2016**, *7*, 354-395.
  29. Katsuma, S.; Hirasawa, A.; Tsujimoto, G. Bile Acids Promote Glucagon-Like Peptide-1 Secretion through TGR5 in a Murine Enteroendocrine Cell Line STC-1. *Biochem. Biophys. Res. Commun.* **2005**, *329*, 386-390.
  30. Thomas, C.; Pellicciari, R.; Pruzanski, M. Targeting Bile-Acid Signaling for Metabolic Diseases. *Nat. Rev. Drug Discovery.* **2008**, *7*, 678-693.
  31. Forman, M.; Goode, E.; Chen, J.; Oro, E.; et al. Identification of a Nuclear Receptor That Is Activated by Farnesol Metabolites. *Cell.* **1995**, *81*, 687-693.
  32. Zhang, Y.; Woelbern, R.; Edwards, A. Natural Structural Variants of the Nuclear Receptor Farnesoid X Receptor Affect Transcriptional Activation. *J. Biol. Chem.* **2003**, *278*, 104-110.
  33. Wang, D.; Chen, D.; Moore, D.; et al. FXR: A Metabolic Regulator and Cell Protector. *Cell Research.* **2008**, *18*, 1087-1095.
  34. Maruyama, T.; Tanaka, K.; Suzuki, J.; et al. Targeted Disruption of G Protein-Coupled Bile Acid Receptor 1 (Gpbar1/M-Bar) in Mice. *J. Endocrinol.* **2006**, *191*, 197-205.
  35. Kawamata, et al. A G Protein-Coupled Receptor Responsive to Bile Acids. *J. Biol. Chem.* **2003**, *278*(11), 9435-9440.

36. Thomas, C.; Gioiello, A.; Noriega, L.; et al. TGR5-Mediated Bile Acid Sensing Controls Glucose Homeostasis. *Cell Metab.* **2009**, *10*, 167-177.
37. Tang, C.; Chan, L.; Hsiao, Y. TGR5 as a New Target in Diabetes Care. *Curr. Res. Diabetes & Obes. J.* **2018**, *9*, 555-759.
38. Stepanov, V.; Stankov, K.; Mikov, M. The Bile Acid Membrane Receptor TGR5: A Novel Pharmacological Target in Metabolic, Inflammatory, and Neoplastic Disorders. *J. Recept. Signal Transduct. Res.* **2013**, *33*, 213-223.
39. Henri, Duboc; Taché, Y.; Hofmann, A. F. The Bile Acid TGR5 Membrane Receptor: From Basic Research to Clinical Application. *Digestive and Liver Disease.* **2014**, *46*, 302-312.
40. Eggink, H.; Soeters, M.; Pols, T. TGR5 Ligands as Potential Therapeutics in Inflammatory Diseases. *Int. J. Interf. Cyto. Med. Res.* **2014**, *6*, 27-38.
41. Hodge, R.; Nunez, D. Therapeutic Potential of Takeda-G-Protein-Receptor-5 (TGR5) Agonists: Hope or Hype? *Diabetes, Obes. Metab.* **2016**, *18*, 439-443.
42. Marin, J. J.; Timón, I.; Collantes, C.; Gómez, F. Update on the Treatment of Type 2 Diabetes Mellitus. *World J. Diabetes.* **2016**, *7*, 354-395.
43. Kawamata, et al. A G Protein-Coupled Receptor Responsive to Bile Acids. *J. Biol. Chem.* **2003**, *278*(11), 9435-9440.
44. Makki, K.; Brolin, H.; Petersen, N.; Kassem, M.; et al. Sequential Ligand- and Structure-Based Virtual Screening Approach for the Identification of Potential G Protein-Coupled Estrogen Receptor-1 (GPER-1) Modulators. *RSC Adv.* **2019**, *9*, 2525-2538.
45. Martin, Y. C.; Muchmore, S. Beyond QSAR: Lead Hopping to Different Structures. *QSAR Comb. Sci.* **2009**, *28*(8), 797-801.
46. Kumar, D. P.; Rajagopal, S.; Mahavadi, S.; Murthy, K. Activation of Transmembrane Bile Acid Receptor TGR5 Stimulates Insulin Secretion in Pancreatic Cells. *Biochem. Biophys. Res. Commun.* **2012**, *427*, 600-605.
47. Yang, F.; Cao, M.; Guo, L.; Lin, J.; Ming, Q.; Xi, P.; Wu, X.; Shen, Q.; Guo, S.; Shen, D. D.; Lu, R.; Zhang, L.; Huang, S.; Ping, Y.; Zhang, C.; Ma, C.; Zhang, K.; Liang, X.; Shen, Y.; Nan, F.; Yi, F.; Luca, V. C.; Zhou, J.; Jiang, C.; Sun, J. P.; Xie, X.; Yu, X.; Zhang, Y. Structural Basis of GPBAR Activation and Bile Acid Recognition. *Nature.* **2020**, *587*(7834), 499-504.

48. Pellicciari, R.; Gioiello, A.; Macchiarulo, A.; Thomas, C.; Rosatelli, E.; Natalini, B.; Sardella, R.; Pruzanski, M.; Roda, A.; Pastorini, E.; Schoonjans, K.; Auwerx, J. Discovery of 6 $\alpha$ -Ethyl-23(S)-Methylcholic Acid (S-EMCA, INT-777) as a Potent and Selective Agonist for the TGR5 Receptor, a Novel Target for Diabetes. *J. Med. Chem.* **2009**, *52*, 7958-7961.
49. Zhou, S. F.; Zhong, W. Z. Drug Design and Discovery: Principles and Applications. *Molecules.* **2017**, *22*(2), 279.
50. Adelusi, T. I.; Oyedele, A.-Q. K.; Boyenle, I. D.; Ogunlana, A. T.; Adeyemi, R. O.; Ukachi, C. D.; Idris, M. O.; Olaoba, O. T.; Adedotun, I. O.; Kolawole, O. E.; Xiaoxing, Y.; Abdul-Hammed, M. Molecular Modeling in Drug Discovery. *J. Med. Chem.* **2022**, *29*, 100880.
51. Yu, W.; MacKerell, A. D., Jr. Computer-Aided Drug Design Methods. *Methods Mol. Biol.* **2017**, *1520*, 85-106.
52. Suchitra M. Ajjarapu; Apoorv Tiwari; Pramod Wasudeo Ramteke; Dev Bukhsh Singh; Sundip Kumar. Ligand-Based Drug Designing. In *Bioinformatics*; Academic Press, **2022**; pp 233-252. ISBN 978-0-323-89775-4.
53. Arnold, K.; Bordoli, L.; Kopp, J.; Schwede, T. The SWISS-MODEL Workspace: A Web-Based Environment for Protein Structure Homology Modelling. *Bioinformatics.* **2006**, *22*, 195-201.
54. Shafi, K.; Nafees, A.; Lay, C.; Rakesh, N.; Thet, T. Sequential Ligand- and Structure-Based Virtual Screening Approach for the Identification of Potential G Protein-Coupled Estrogen Receptor-1 (GPER-1) Modulators. *RSC Adv.* **2019**, *9*, 2525-2538.
55. Martin, Y. C.; Muchmore, S. Beyond QSAR: Lead Hopping to Different Structures. *QSAR Comb. Sci.* **2009**, *28*(8), 797-801.
56. Sharma, D.; Dhayalan, V.; Manikandan, C.; Dandela, R. Recent Methods for Synthesis of Coumarin Derivatives and Their New Applications; Intertech: **2023**; ISBN 978-1-83768-242-3.
57. Lončarić, M.; Gašo-Sokač, D.; Jokić, S.; Molnar, M. Recent Advances in the Synthesis of Coumarin Derivatives from Different Starting Materials. *Biomolecules.* **2020**, *10*(1), 151.



58. Omotuyi, O. I.; Nash, O.; Inyang, O. K.; Ogidigo, J.; Enejoh, O.; Okpalefe, O.; Hamada, T. Flavonoid-rich extract of *Chromolaena odorata* modulate circulating GLP-1 in Wistar rats: computational evaluation of TGR5 involvement. *Biotech.* **2018**, *8*, 124-132.
59. Genet, C.; Strehle, A.; Schmidt, C.; Boudjelal, G.; Lobstein, A.; Schoonjans, K.; Souchet, M.; Auwerx, J.; Saladin, R.; Wagner, A. Structure-activity relationship study of betulinic acid; a novel and selective TGR5 agonist; and its synthetic derivatives: potential impact in diabetes. *J. Med. Chem.* **2010**, *53*, 178-190.
60. Lo, S.-H.; Cheng, K.-C.; Li, Y.-X.; Chang, C.-H.; Cheng, J.-T.; Lee, K.-S. Development of betulinic acid as an agonist of TGR5 receptor using a new in vitro assay. *Drug Des. Dev. Ther.* **2016**, *10*, 2669-2676.
61. Jafri, L.; Saleem, S.; Calderwood, D.; Gillespie, A.; Mirza, B.; Green, B. D. Naturally-occurring TGR5 agonists modulating glucagon-like peptide-1 biosynthesis and secretion. *Peptides.* **2016**, *78*, 51-58.
62. Sato, H.; Macchiarulo, A.; Thomas, C.; Gioiello, A.; Une, M.; Hofmann, A. F.; Saladin, R.; Schoonjans, K.; Pellicciari, R.; Auwerx, J. Novel Potent and Selective Bile Acid Derivatives as TGR5 Agonists: Biological Screening, Structure-Activity Relationships, and Molecular Modeling Studies. *J. Med. Chem.* **2008**, *51*, 1831-1841.
63. Pellicciari, R.; Gioiello, A.; Macchiarulo, A.; Thomas, C.; Rosatelli, E.; Natalini, B.; Sardella, R.; Pruzanski, M.; Roda, A.; Pastorini, E.; Schoonjans, K.; Auwerx, J. Discovery of 6 $\alpha$ -ethyl-23(S)-methylcholic acid (S-EMCA, INT-777) as a potent and selective agonist for the TGR5 receptor, a novel target for diabetes. *J. Med. Chem.* **2009**, *52*, 7958-7961.
64. Rosatelli, E.; Carotti, A.; Cerra, B.; De Franco, F.; Passeri, D.; Pellicciari, R.; Gioiello, A. Chemical exploration of TGR5 functional hot-spots: Synthesis and structure-activity relationships of C7- and C23-Substituted cholic acid derivatives. *Eur. J. Med. Chem.* **2023**, *261*, 115851.
65. Nakhi, A.; McDermott, C. M.; Stoltz, K. L.; John, K.; Hawkinson, J. E.; Ambrose, E. A.; Khoruts, A.; Sadowsky, M. J.; Dosa, P. I. 7-Methylation of

- Chenodeoxycholic Acid Derivatives Yields a Substantial Increase in TGR5 Receptor Potency. *J. Med. Chem.* **2019**, 62(14), 6824-6830.
66. Chen, F.-F.; Wang, J.-T.; Zhang, L.-X.; Xing, S.-F.; Wang, Y.-X.; Wang, K.; Deng, S.-L.; Zhang, J.-Q.; Tang, L.; Wu, H.-S. Oleanolic acid derivative DKS26 exerts antidiabetic and hepatoprotective effects in diabetic mice and promotes glucagon-like peptide-1 secretion and expression in intestinal cells. *Br. J. Pharmacol.* **2017**, 174, 2912-2928.
  67. Makki, K.; Brolin, H.; Petersen, N.; Henricsson, M.; Christensen, D. P.; Khan, M. T.; Wahlström, A.; Bergh, P.-O.; Tremaroli, V.; Schoonjans, K.; Marschall, H.-U.; Bäckhed, F. 6 $\alpha$ -hydroxylated bile acids mediate TGR5 signalling to improve glucose metabolism upon dietary fiber supplementation in mice. *Gut.* **2023**, 72, 314-324.
  68. Martin, R. E.; Bissantz, C.; Gavelle, O.; Kuratli, C.; DehmLow, H.; Richter, H. G.; Obst Sander, U.; Erickson, S. D.; Kim, K.; Pietranico-Cole, S. L.; Alvarez-Sanchez, R.; Ullmer, C. 2-Phenoxy-nicotinamides are potent agonists at the bile acid receptor GPBAR1 (TGR5). *Chem. Med. Chem.* **2013**, 8(4), 569-576.
  69. Zhu, J.; Ye, Y.; Ning, M.; Mandi, A.; Feng, Y.; Zou, Q.; Kurtan, T.; Leng, Y.; Shen, J. Design, synthesis, and structure-activity relationships of 3,4,5-trisubstituted 4,5-dihydro-1,2,4-oxadiazoles as TGR5 agonists. *Chem. Med. Chem.* **2013**, 8(7), 1210-1223.
  70. Duan, H.; Ning, M.; Chen, X.; Zou, Q.; Zhang, L.; Feng, Y.; Zhang, L.; Leng, Y.; Shen, J. Design, synthesis, and antidiabetic activity of 4-phenoxy nicotinamide and 4-phenoxy pyrimidine-5-carboxamide derivatives as potent and orally efficacious TGR5 agonists. *J. Med. Chem.* **2012**, 55, 10475-10489.
  71. Zhu, J.; Ning, M.; Guo, C.; Zhang, L.; Pan, G.; Leng, Y.; Shen, J. Design, synthesis and biological evaluation of a novel class of potent TGR5 agonists based on a 4-phenyl pyridine scaffold. *Eur. J. Med. Chem.* **2013**, 69, 55-68.
  72. Zou, Q.; Duan, H.; Ning, M.; Liu, J.; Feng, Y.; Zhang, L.; Zhu, J.; Leng, Y.; Shen, J. 4-Benzofuranyloxynicotinamide derivatives are novel potent and

- orally available TGR5 agonists. *Eur. J. Med. Chem.* **2014**, doi:10.1016/j.ejmech.2014.05.031.
73. Chen, Z.; Ning, M.; Zou, Q.; Cao, H.; Ye, Y.; Leng, Y.; Shen, J. Discovery and Structure-Activity Relationship Study of 4-Phenoxythiazol-5-carboxamides as Highly Potent TGR5 Agonists. *Chem. Pharm. Bull.* **2016**, 64(4), 326-339.
  74. Zhang, X.; Wall, M.; Sui, Z.; Kauffman, J.; Hou, C.; Chen, C.; Du, F.; Kirchner, T.; Liang, Y.; Johnson, D. L.; Murray, W. V.; Demarest, K. Discovery of Orally Efficacious Tetrahydrobenzimidazoles as TGR5 Agonists for Type 2 Diabetes. *ACS Med. Chem. Lett.* **2017**, 8(5), 560-565.
  75. Agarwal, S.; Patil, A.; Aware, U.; Deshmukh, P.; Darji, B.; Sasane, S.; Sairam, K. V.; Priyadarsiny, P.; Giri, P.; Patel, H.; Giri, S.; Jain, M.; Desai, R. C. Discovery of a Potent and Orally Efficacious TGR5 Receptor Agonist. *ACS Med. Chem. Lett.* **2016**, 7, 51-55.
  76. Zhao, S.; Li, X.; Wang, L.; Peng, W.; Ye, W.; Li, W.; Wang, Y.-D.; Chen, W.-D. Design, Synthesis, and Evaluation of 1-Benzyl-1H-imidazole-5-carboxamide Derivatives as Potent TGR5 Agonists. *Bioorg. Med. Chem.* **2021**, 32, 115972.
  77. Agarwal, S.; Sasane, S.; Kumar, J.; et al. Novel 2-mercapto imidazole and triazole derivatives as potent TGR5 receptor agonists. *Med. Drug Discov.* **2019**, 100002, 1-5.
  78. Piotrowski, D. W.; Futatsugi, K.; Warmus, J. S.; Orr, S. T.; Freeman-Cook, K. D.; Londregan, A. T.; Wei, L.; Jennings, S. M.; Herr, M.; Coffey, S. B.; Jiao, W.; Storer, G.; Hepworth, D.; Wang, J.; Laverne, S. Y.; Chin, J. E.; Hadcock, J. R.; Brenner, M. B.; Wolford, A. C.; Janssen, A. M.; Roush, N. S.; Buxton, J.; Hinchey, T.; Kalgutkar, A. S.; Sharma, R.; Flynn, D. A. Identification of Tetrahydropyrido[4,3-d]pyrimidine Amides as a New Class of Orally Bioavailable TGR5 Agonists. *ACS Med. Chem. Lett.* **2013**, 4, 63-68.
  79. Budzik, B. W.; Evans, K. A.; Wisnoski, D. D.; Jin, J.; Rivero, R. A.; Szewczyk, G. R.; Jayawickreme, C.; Moncol, D. L.; Yu, H. Synthesis and structure-activity relationships of a series of 3-aryl-4-isoxazolecarboxamides

- as a new class of TGR5 agonists. *Bioorg. Med. Chem. Lett.* **2010**, 20(4), 1363-1367.
80. Randelovic, S.; Bipat, R. A Review of Coumarins and Coumarin-Related Compounds for Their Potential Antidiabetic Effect. *Clin Med Insights Endocrinol Diabetes.* **2021**, 14, 11795514211042023.
  81. Tariq, H. Z.; Saeed, A.; Ullah, S.; Fatima, N.; Ahsan Halim, S.; Khan, A.; El-Seedi, H. R.; Ashraf, M. Z.; Latif, M.; Al-Harrasi, A. Synthesis of novel coumarin–hydrazone hybrids as  $\alpha$ -glucosidase inhibitors and their molecular docking studies. *RSC Adv.* **2023**, 13(37), 26229–26238.
  82. Xu, X.-T.; Deng, X.-Y.; Chen, J.; Liang, Q.-M.; Zhang, K.; Li, D.-L.; Wu, P.-P.; Zheng, X.; Zhou, R.-P.; Jiang, Z.-Y.; Ma, A.-J.; Chen, W.-H.; Wang, S.-H. Synthesis and biological evaluation of coumarin derivatives as  $\alpha$ -glucosidase inhibitors. *Eur. J. Med. Chem.* **2020**, 189, 112013.
  83. Zhang, X.; Zheng, Y.-Y.; Hu, C.-M.; Wu, X.-Z.; Lin, J.; Xiong, Z.; Zhang, K.; Xu, X.-T. Synthesis and biological evaluation of coumarin derivatives containing oxime ester as  $\alpha$ -glucosidase inhibitors. *Arab. J. Chem.* **2022**, 15(9), 10407.
  84. Pan, Y.; Liu, T.; Wang, X.; Sun, J. Research progress of coumarins and their derivatives in the treatment of diabetes. *J. Enzyme Inhib. Med. Chem.* **2022**, 37(1), 616–628.
  85. Muhammed, T.; Aki-Yalcin, E. Homology modeling in drug discovery: Overview, current applications, and future perspectives. *Chem Biol Drug Des.* **2019**, 93(1), 12-20.
  86. Chaudhary, M.; and Tyagi, K. A review on molecular docking and its application. *Int. J. of Adv. Res.* **2024**, 1141-1153.
  87. Drucker DJ. The biology of incretin hormones. *Cell Metab.* **2006** Mar;3(3):153-65.
  88. Fang S, Suh JM, Reilly SM, Yu E, Osborn O, Lackey D, et al. Intestinal FXR agonism promotes GLP-1 secretion to improve metabolic outcomes in obesity. *Nat Commun.* **2015**;6:1-10.

89. Sun H, Dai M, Shen B, Peng W, Ding J, Wang W, et al. In vitro and in vivo studies on the pharmacokinetics, efficacy, and safety of novel compounds. *Drug Des Devel Ther.* **2020**;14:1-11.
90. Rang HP, Ritter JM, Flower RJ, Henderson G. *Rang & Dale's Pharmacology*. 8th ed. Elsevier; **2015**.
91. The UniProt Consortium. UniProt: the Universal Protein Knowledgebase in 2023. *Nucleic Acids Res.* **2023**, 51(D1), D523-D531.
92. Coudert, E.; et al. Annotation of biologically relevant ligands in UniProtKB using ChEBI. *Bioinformatics* **2023**, 39(1), btac793.
93. Waterhouse, A.; Bertoni, M.; Bienert, S.; Studer, G.; Tauriello, G.; Gumienny, R.; Heer, F.T.; Beer, P.; Rempfer, C.; Bordoli, L.; Lepore, R.; Schwede, T. SWISS-MODEL: homology modelling of protein structures and complexes. *Nucleic Acids Res.* **2018**, 46(W1), W296-W303.
94. Altschul, S.F.; Madden, T.L.; Schaffer, A.A.; Zhang, J.; Zhang, Z.; Miller, W.; Lipman, D.J. Gapped BLAST and PSI-BLAST: a new generation of protein database search programs. *Nucleic Acids Res.* **1997**, 25, 3389-3402.
95. Camacho, C.; Coulouris, G.; Avagyan, V.; Ma, N.; Papadopoulos, J.; Bealer, K.; Madden, T.L. BLAST+: architecture and applications. *BMC Bioinformatics.* **2009**, 10, 421.
96. Steinegger, M.; Meier, M.; Mirdita, M.; Vöhringer, H.; Haunsberger, S. J.; Söding, J. HH-suite3 for fast remote homology detection and deep protein annotation. *BMC Bioinformatics.* **2019**, 20, 1-15.
97. Bienert, S.; Waterhouse, A.; de Beer, T.A.P.; Tauriello, G.; Studer, G.; Bordoli, L.; Schwede, T. The SWISS-MODEL Repository-new features and functionality. *Nucleic Acids Res.* **2017**, 45(D), D313-D319.
98. Bertoni, M.; Kiefer, F.; Biasini, M.; Bordoli, L.; Schwede, T. Modeling protein quaternary structure of homo- and hetero-oligomers beyond binary interactions by homology. *Scientific Rep.* **2017**, 7, 10480.
99. Biasini, M.; Schmidt, T.; Bienert, S.; Mariani, V.; Studer, G.; Haas, J.; Johner, N.; Schenk, A.D.; Philippsen, A.; Schwede, T. OpenStructure: an integrated software framework for computational structural biology. *Acta Crystallogr. D, Biol. Crystallogr.* **2013**, 69, 701-709.

100. Guex, N.; Peitsch, M.C. SWISS-MODEL and the Swiss-PdbViewer: an environment for comparative protein modeling. *Electrophoresis*. **1997**, 18, 2714-2723.
101. Zhou, X.; Zheng, W.; Li, Y.; Pearce, R.; Chengxin, Z.; Eric, W.; Guijun, Z.; Yang Z. I-TASSER-MTD: a deep-learning-based platform for multi-domain protein structure and function prediction. *Nat. Protoc.* **2022**, 17, 2326-2353.
102. Zheng, W.; Zhang, C.; Li, Y.; Pearce, R.; Zhang, Y. Folding non-homologous proteins by coupling deep-learning contact maps with I-TASSER assembly simulations. *Cell Reports Methods*. **2021**, 1(100014), 1-25.
103. Yang, J.; Zhang, Y. I-TASSER server: new development for protein structure and function predictions. *Nucleic Acids Res.* **2015**, 43(W1), W174-W181.
104. Laskowski, R.A.; Rullmann, J.A.C.; MacArthur, M.W.; et al. AQUA and PROCHECK-NMR: Programs for checking the quality of protein structures solved by NMR. *J. Biomol. NMR*. **1996**, 8, 477-486.
105. Ramachandran, G.N.; Ramakrishnan, C.; Sasisekhran, V. Stereochemistry of polypeptide chain configurations. *J. Mol. Biol.* **1963**, 7, 95-99.
106. Colovos, C.; Yeates, T.O. Verification of protein structures: patterns of nonbonded atomic interactions. *Protein Sci.* **1993**, 9, 1511-1519.
107. Yang, F., Mao, C., Guo, L. *et al.* Structural basis of GPBAR activation and bile acid recognition. *Nature* **587**, 499–504 (2020).
108. Butt, S.S.; Badshah, Y.; Shabbir, M. Molecular Docking Using Chimera and Autodock Vina Software for Nonbioinformaticians. *JMIR Bioinformatics Biotechnol.* **2020**, 1(1), e14232.
109. Hanwell, M.D.; Curtis, D.E.; Lonie, D.C.; et al. Avogadro: an advanced semantic chemical editor, visualization, and analysis platform. *J. Chem inform.* **2012**, 4, 17.
110. Bowers, K.J.; Chow, E.; Xu, H.; et al. Scalable Algorithms for Molecular Dynamics Simulations on Commodity Clusters. *Proc. ACM/IEEE SC'06 2006*, 0-7695-2700-0/06.
111. Liu, X.; Shi, D.; Zhou, S.; Liu, H.; Liu, H.; YÄ, X. Molecular dynamics simulations and novel drug discovery. *Expert Opin. Drug Discov.* **2018**, 13(1), 23-37.

112. Lokhande, K.; Pawar, S.; Madkaiker, S.; et al. High throughput virtual screening and molecular dynamics simulation analysis of phytomolecules against BfmR of *Acinetobacter baumannii*: Anti-virulent drug development campaign. *J. Biomol. Struct. Dyn.* **2022**, 14, 1-15.
113. Jacobson, M.P.; Pincus, D.L.; Rapp, C.S.; et al. A hierarchical approach to all-atom protein loop prediction. *Proteins*. **2004**, 55(2), 351-367.
114. Daina, A.; Michielin, O.; Zoete, V. SwissADME: A free web tool to evaluate pharmacokinetics, drug-likeness, and medicinal chemistry friendliness of small molecules. *Sci. Rep.* **2017**, 7(1), 42717.
115. Suljic, S.; Pietruszka, J. Synthesis of 3-Arylated 3,4-Dihydrocoumarins: Combining Continuous Flow Hydrogenation with Laccase-Catalyzed Oxidation. *Adv. Synth. Catal.* **2014**, 356, 1007-1020.
116. Rahal, M.; Graff, B.; Toufaily, J.; Hamieh, T.; Noirbent, G.; Gigmes, D.; Dumur, F.; Lalevée, J. 3-Carboxylic Acid and Formyl-Derived Coumarins as Photoinitiators in Photo-Oxidation or Photo-Reduction Processes for Photopolymerization upon Visible Light: Photocomposite Synthesis and 3D Printing Applications. *Molecules*. **2021**, 26, 1753.
117. Rodrigo De Oliveira Vieira, Edson Nascimento Dos Santos, Gabriela Consolini and Mauri Sergio Alves Palma, Use of Piperidine and Pyrrolidine in Knoevenagel Condensation. *Org. Med. Chem. II*. **2018**, 5(3), OMCII.MS.ID.555668.
118. Hong Ji, Yaling Tan, Nana Gan, Jing Zhang, Shannuo Li, Xuan Zheng, Zhaohua Wang, Wei Yi, Synthesis and anticancer activity of new coumarin-3-carboxylic acid derivatives as potential lactate transport inhibitors. *Bioorg. Med. Chem.* **2020**.
119. Xiang Zhou, Xiao-Bing Wang, Tao Wang, Ling-Yi Kong. Design, synthesis, and acetylcholinesterase inhibitory activity of novel coumarin analogues. *Bioorg. Med. Chem.* **2008**, 16, 8011-8021.
120. P.S. Thacker, M. Alvala, M. Arifuddin, A. Angeli, C.T. Supuran. Design, synthesis and biological evaluation of coumarin-3-carboxamides as selective carbonic anhydrase IX and XII inhibitors. *Bioorg. Chem.* **2019**.

121. Valeur, E.; Bradley, M. Amide Bond Formation: Beyond the Myth of Coupling Reagents. *Chem. Soc. Rev.* **2009**, 38, 606-631.
122. Duengo, S.; Muhajir, M. I.; Hidayat, A. T.; Musa, W. J. A.; Maharani, R. Epimerisation in Peptide Synthesis. *Molecules.* **2023**, 28(24), 8017.
123. Chaudhari, S. N.; Luo, J. N.; Harris, D. A.; Huh, J. R.; Sheu, E. G.; Devlin, A. S. A Microbial Metabolite Remodels the Gut-Liver Axis following Bariatric Surgery. *Cell Host & Microbe.* **2021**, 29, 408-424.
124. Meyer, B. N.; Ferrigni, N. R.; Putnam, J. E.; Jacobsen, L. B.; Nichols, D. E.; McLaughlin, J. L. Brine Shrimp: A Convenient General Bioassay for Active Plant Constituents. *Planta Med.* **1982**, 45(5), 31-34.
125. Badisa, R. B.; Darling-Reed, S. F.; Joseph, P.; Cooperwood, J. S.; Latinwo, L. M.; Goodman, C. B. Selective Cytotoxic Activities of Two Novel Synthetic Drugs on Human Breast Carcinoma MCF-7 Cells. *Anticancer Res.* **2009**, 29, 2993-2996.
126. Tao, H.; Ling, Y.; Wang, X.; Chen, J.; Yu, X.; Yi, P. The Synthesis and Preliminary Cytotoxicity Evaluation of Hexahydrodispiro[indole-3,3'-indolizine-2',3''-piperidine]-2(1H),4''-dione Compounds. *J. Chem. Res.* **2019**, 43(7-8), 287-292.
127. OECD. Guidance Document on Acute Oral Toxicity. Environ. Health Saf. Monogr. Ser. Testing Assess. **2000**, 24.
128. Bhimanwar, R. S., Lokhande, K. B., Shrivastava, A., Singh, A., Chitlange, S. S., & Mittal, A. Identification of potential drug candidates as TGR5 agonist to combat type II diabetes using docking and molecular dynamics simulation studies. *J. of Biomol. Struc. and Dynamics.* **2023**, 41(22), 13314-13331.



# ANNEXURE

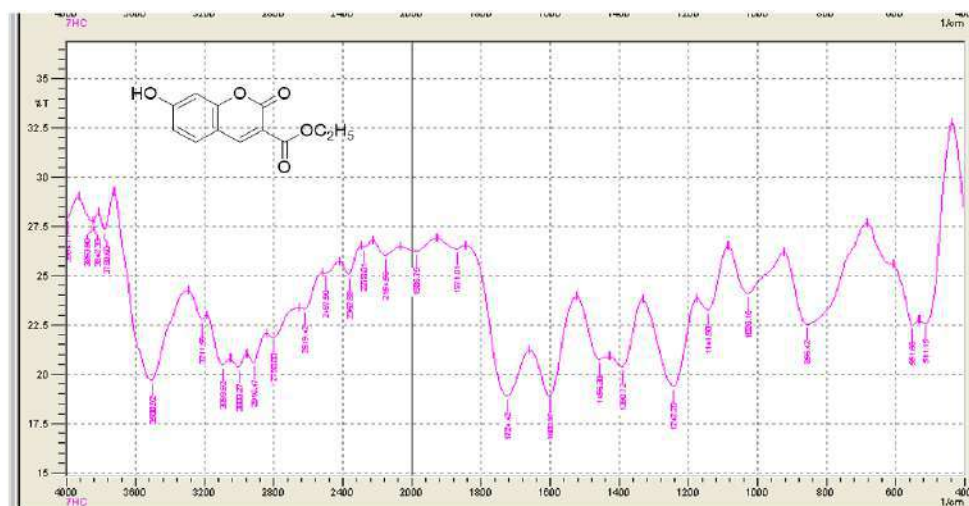


## CHAPTER 9

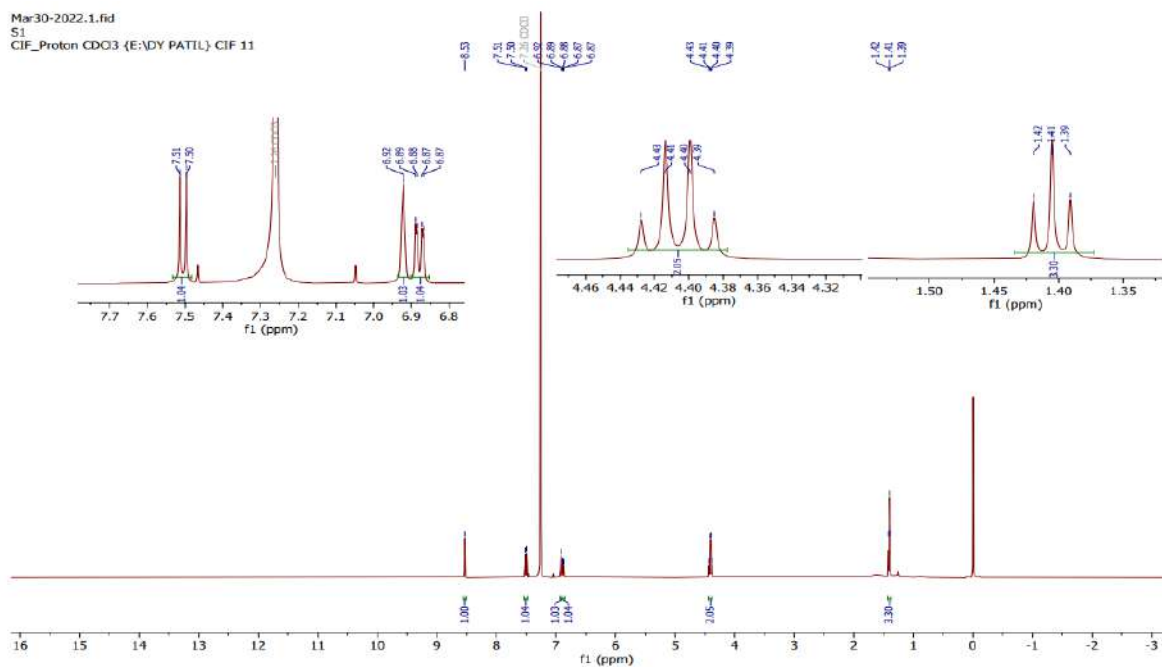
### ANNEXURE

Copies of FT-IR,  $^1\text{H}$  NMR,  $^{13}\text{C}$  NMR, and HRMS spectrum of the final compounds

#### CHARACTERIZATION OF COMPOUND 1

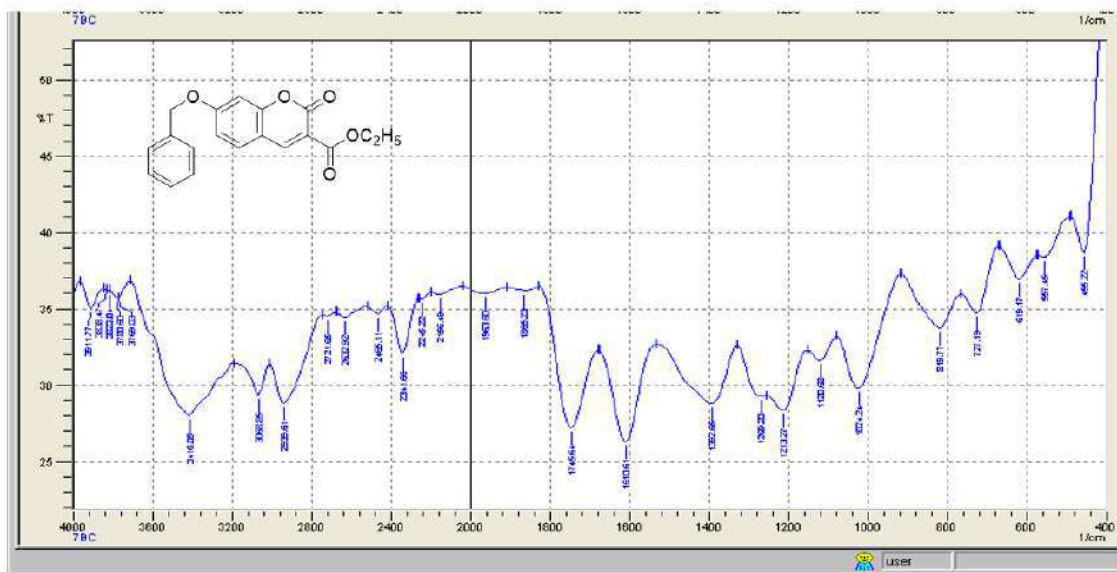


#### IR Spectra of Compound 1

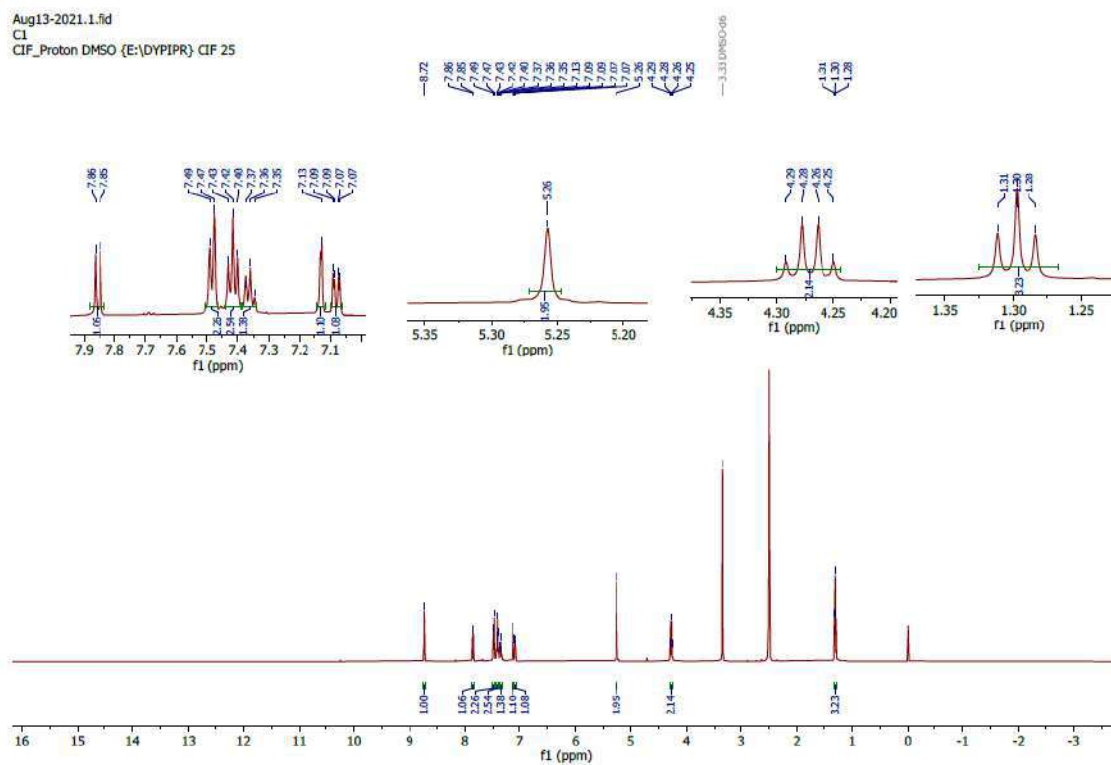


#### $^1\text{H}$ NMR spectra of Compound 1

## CHARACTERIZATION OF PRODUCT 2a:



IR Spectra of Compound 2a



<sup>1</sup>H NMR spectra of Compound 2a

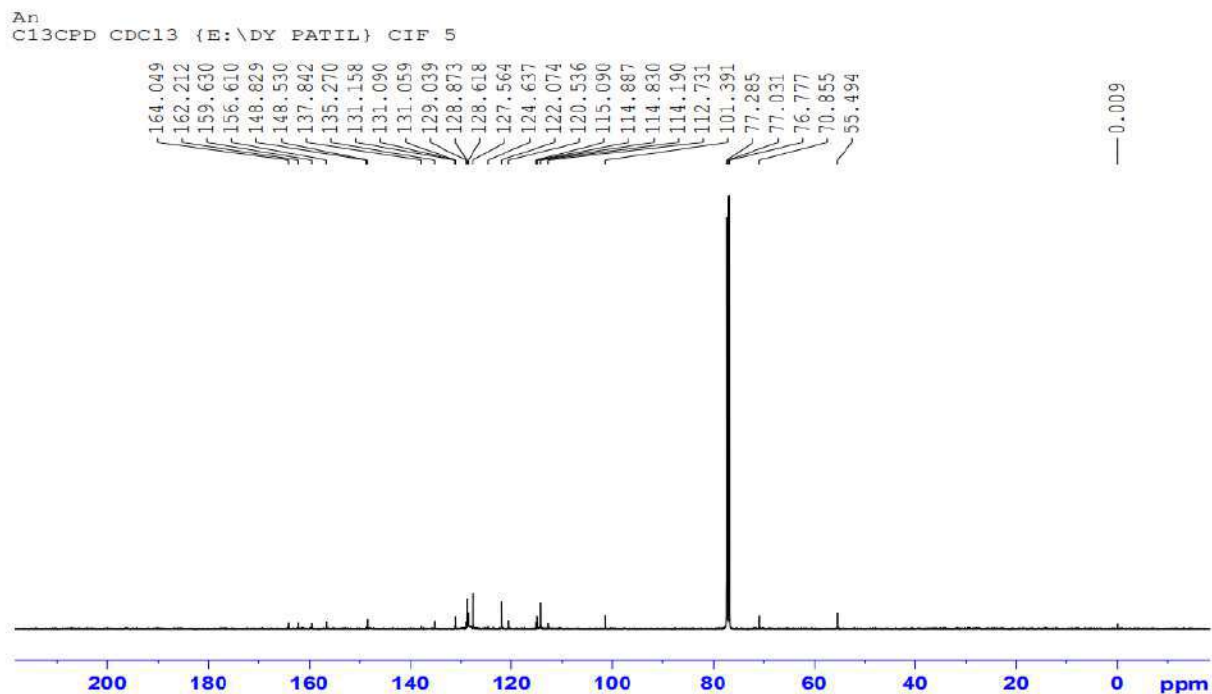
Apr27-2023.2.fid  
A-1  
CIF\_Proton CDCl3 (E:\DY PATIL) CIF 2

10.76  
8.94  
8.19  
7.74  
7.73  
7.64  
7.62  
7.44  
7.42  
7.39  
7.38  
7.17  
7.15  
7.14  
7.05  
7.03  
6.97  
5.94  
5.19

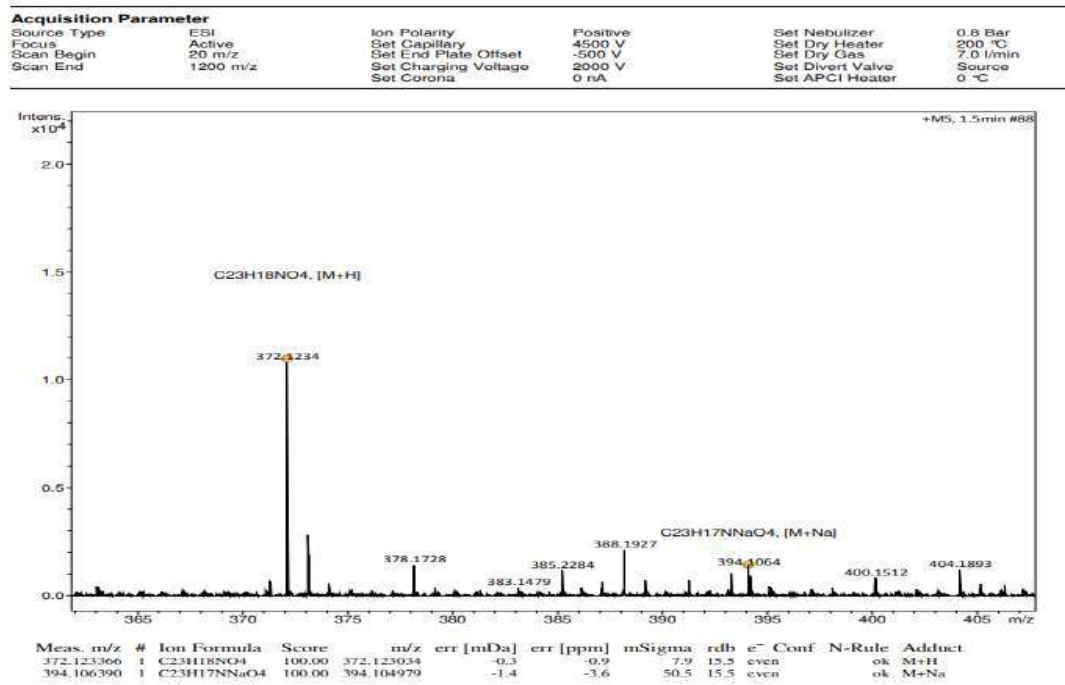
1.07  
1.00  
2.66  
1.27  
4.78  
1.30  
1.46  
1.11  
2.35  
1.00  
2.35

f1 (ppm)

154

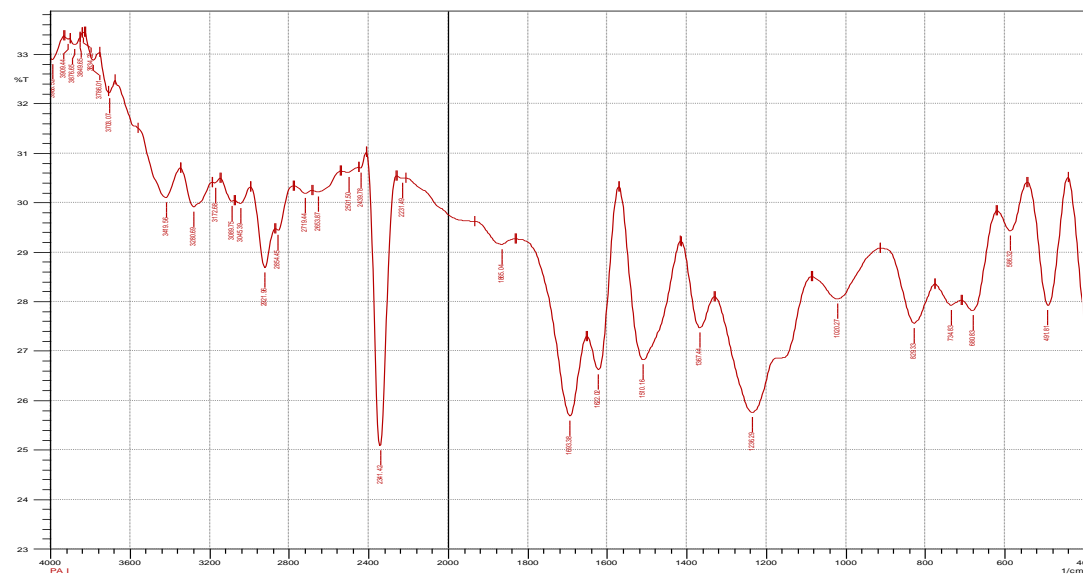


$^{13}\text{C}$  NMR spectra of compound 3

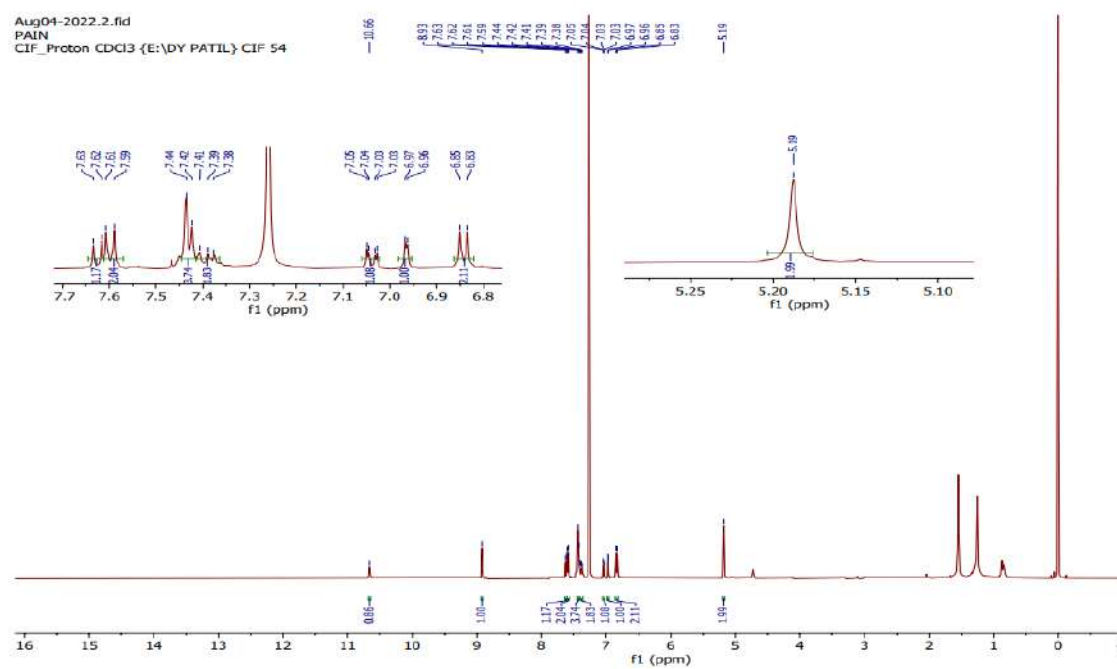


HR MS spectra of compound 3

## CHARACTERIZATION OF COMPOUND 4

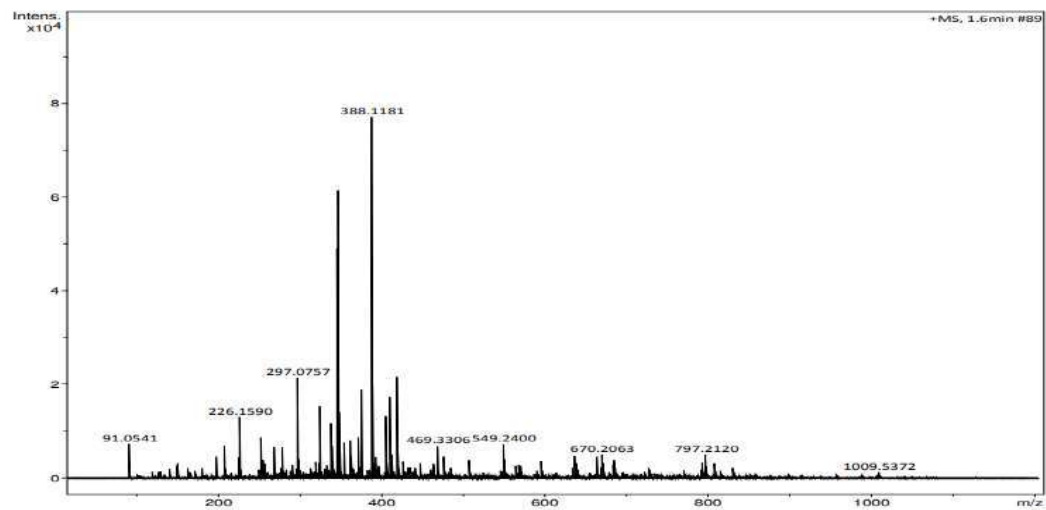


IR spectra of Compound 4



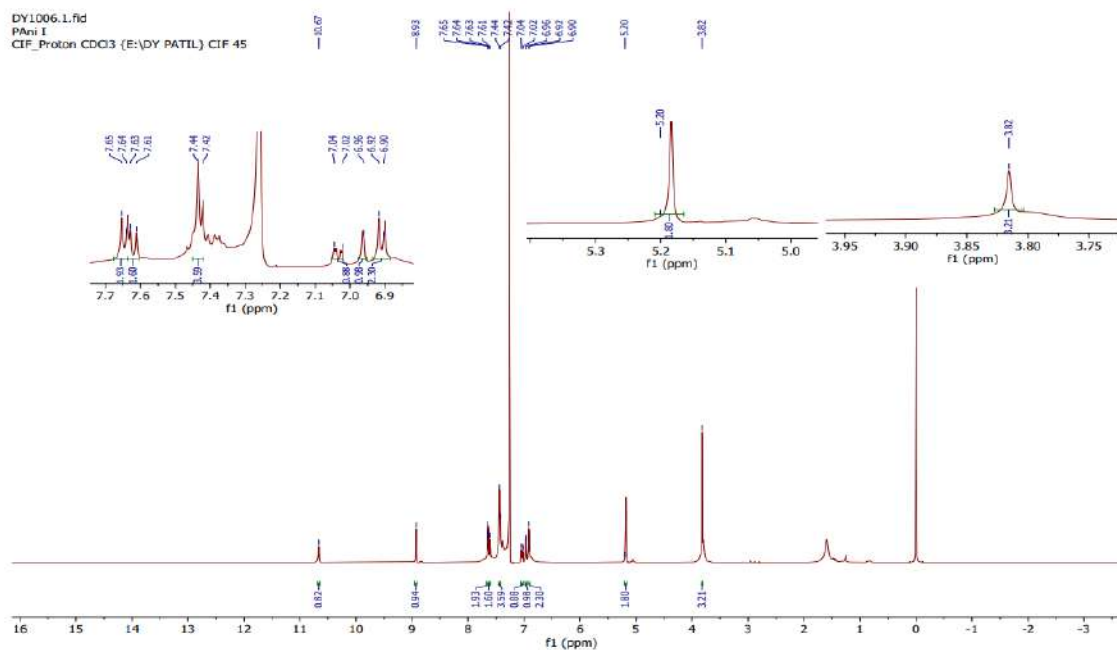
$^1\text{H}$  NMR spectra of compound 4

Acquisition Parameter					
Source Type	ESI	Ion Polarity	Positive	Set Nebulizer	1.2 Bar
Focus	Active	Set Capillary	4500 V	Set Dry Heater	200 °C
Scan Begin	20 m/z	Set End Plate Offset	-500 V	Set Dry Gas	7.0 l/min
Scan End	1200 m/z	Set Charging Voltage	2000 V	Set Divert Valve	Source
		Set Corona	0 nA	Set APCI Heater	0 °C



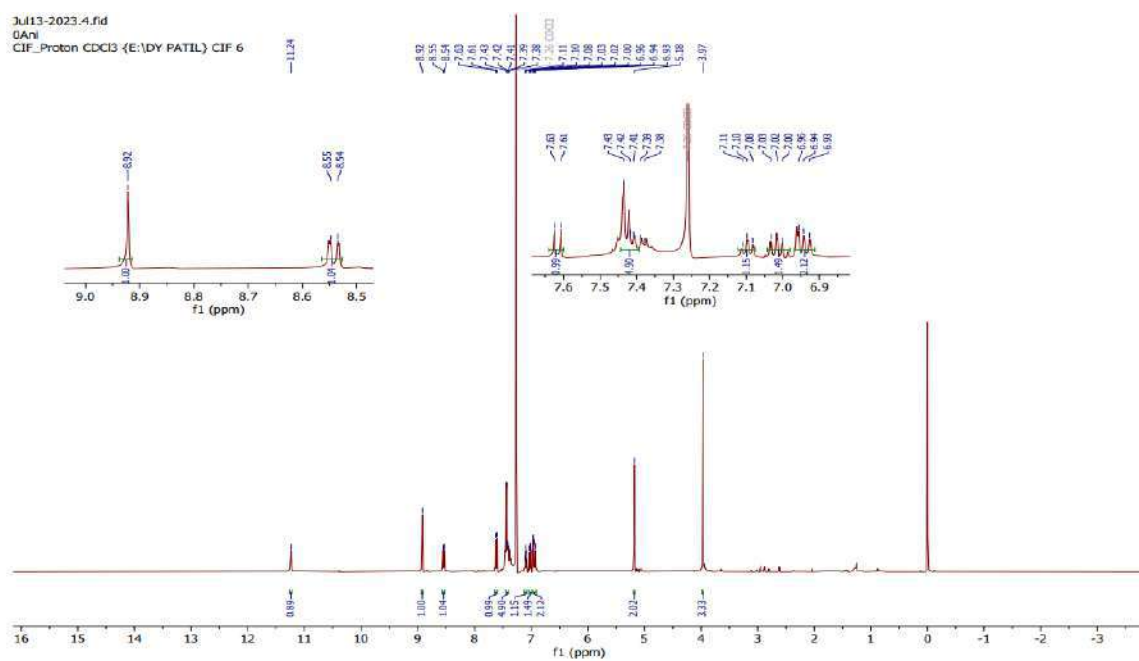
HR MS spectra of compound 4

## CHARACTERISATION OF COMPOUND 5a



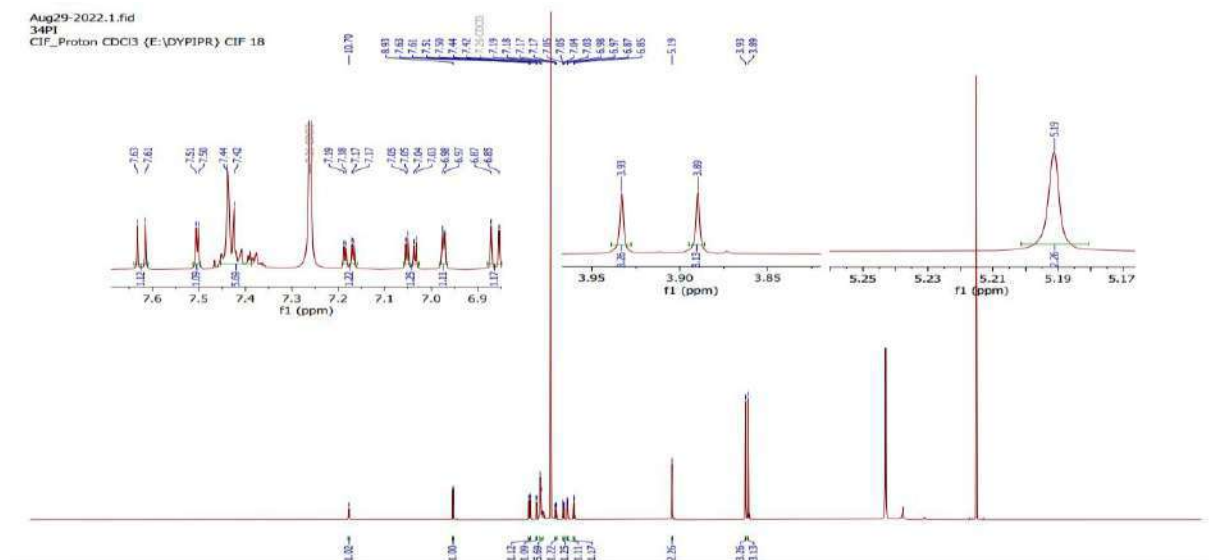
$^1\text{H}$  NMR spectra of compound 5a

## CHARACTERISATION OF COMPOUND 5c



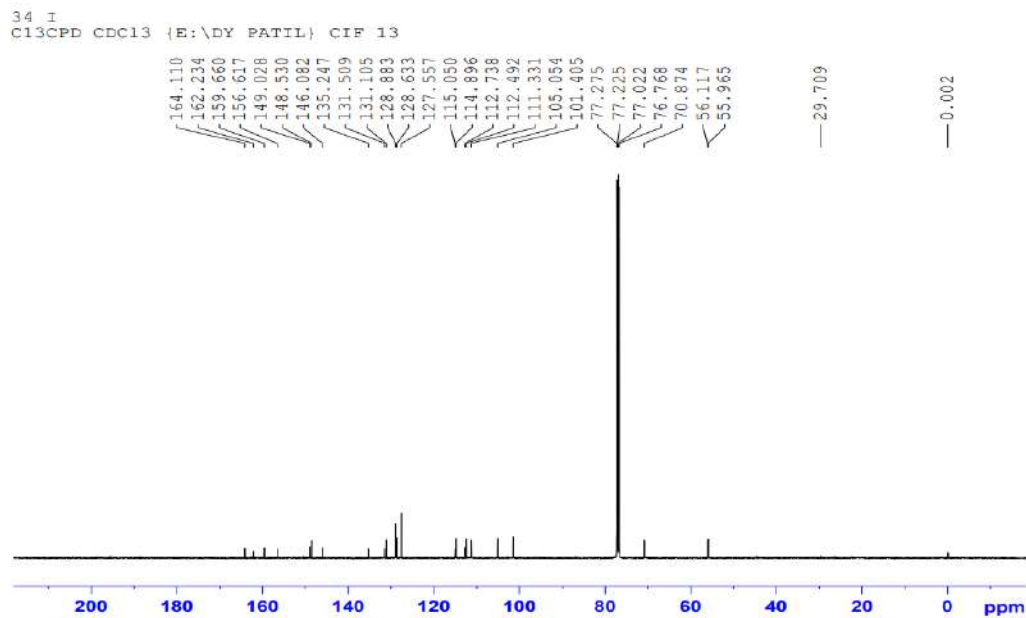
$^1\text{H}$  NMR spectra of compound 5c

## CHARACTERIZATION OF COMPOUND 5d



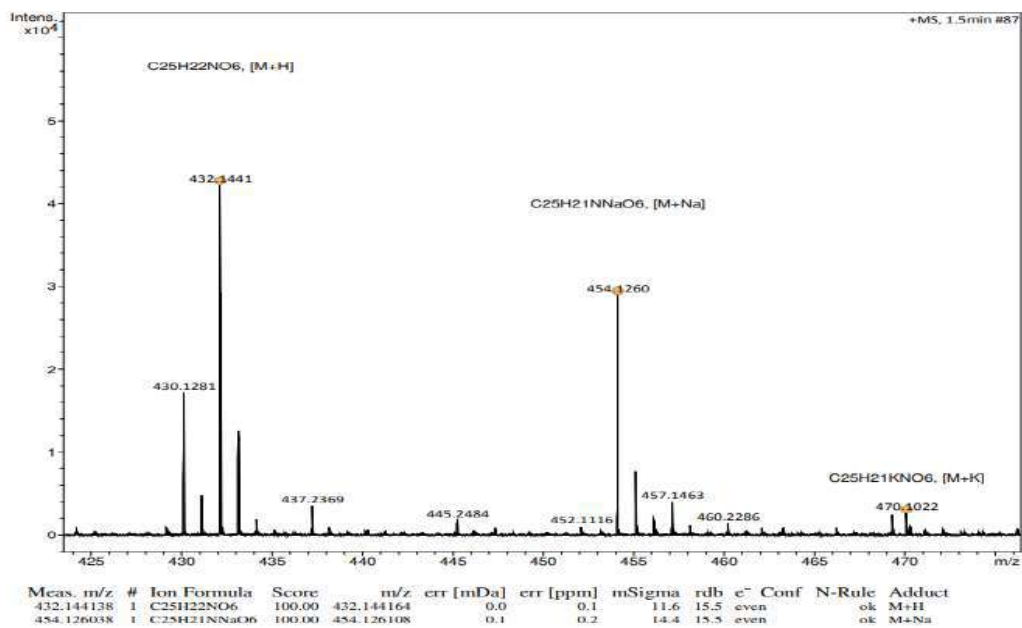
$^1\text{H}$  NMR spectra of Compound 5d





$^{13}\text{C}$  NMR spectra of compound 5d

Acquisition Parameter						
Source Type	ESI	Ion Polarity	Positive	Set Nebulizer	1.2 Bar	
Focus	Active	Set Capillary	4500 V	Set Dry Heater	200 °C	
Scan Begin	20 m/z	Set End Plate Offset	-500 V	Set Dry Gas	7.0 l/min	
Scan End	1200 m/z	Set Charging Voltage	2000 V	Set Divert Valve	Source	
		Set Corona	0 nA	Set APCI Heater	0 °C	



HR-MS spectra of Compound 5d

Nov22-2022.6.fid  
PC 1  
CIF\_Proton CDCl3 {E:\DYP\IPR} CIF 11

16 15 14 13 12 11 10 9 8 7 6 5 4 3 2 1 0 -1 -2 -3

10.71 8.94 7.63 7.62 7.44 7.42 7.37 7.27 7.25 7.24 7.03 6.97 6.96 5.19 2.34 0.00

1.00 1.00 3.46 3.60 1.47 0.99 2.11 2.91 2.34

f1 (ppm)

PT  
C13CPD CDC13 {E:\DY PATIL} CIF 11

164.079  
162.200  
159.732  
156.627  
148.655  
135.295  
135.265  
134.294  
131.113  
129.540  
128.874  
128.618  
127.564  
120.509  
115.111  
114.840  
112.729  
101.391  
77.282  
77.232  
77.028  
76.774  
70.860

— 20.959

— 0.005

200 180 160 140 120 100 80 60 40 20 0 ppm

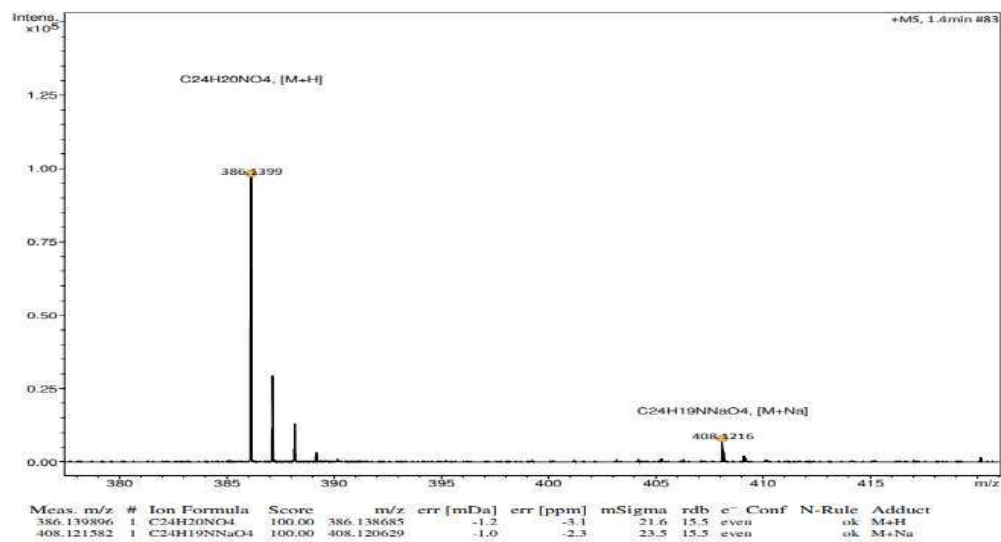
160

**Analysis Info**  
 Analysis Name: D:\Data\2023\JULY\SPPU COLLEGE\DYVPV\RACHANA BHIMANWAR\PT\_BA6\_01\_5998.d  
 Method: dlc\_ms20-1200mz\_7min\_0.120mlflow\_90b\_mar23.m  
 Sample Name: PT

Acquisition Date: 7/6/2023 12:36:14 PM  
 Operator: CIF  
 Instrument: impact HD  
 1819696.00184

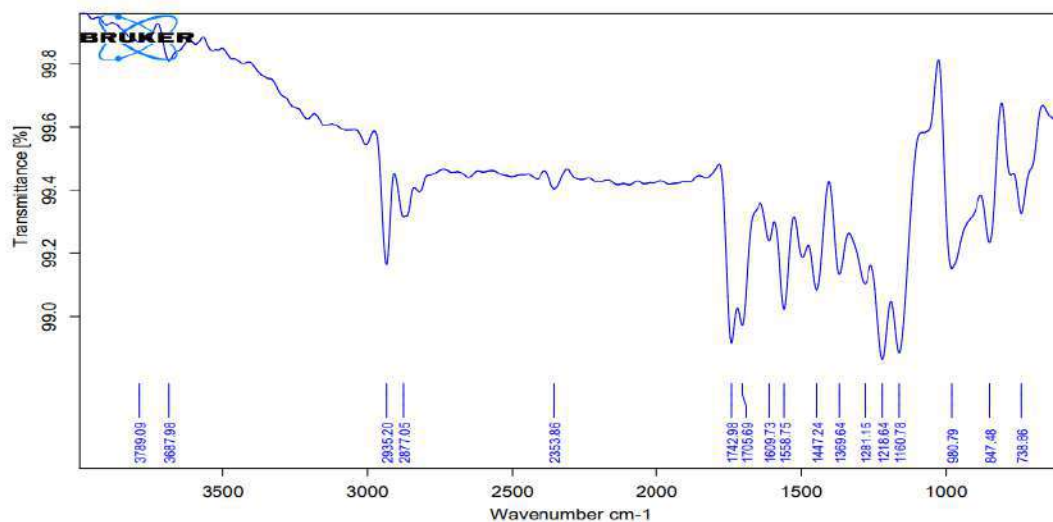
**Acquisition Parameter**

Source Type	ESI	Ion Polarity	Positive	Set Nebulizer	1.2 Bar
Focus	Active	Set Capillary	4500 V	Set Dry Heater	200 °C
Scan Begin	20 m/z	Set End Plate Offset	-500 V	Set Dry Gas	7.0 l/min
Scan End	1200 m/z	Set Charging Voltage	2000 V	Set Divert Valve	Source
		Set Corona	0 nA	Set APCI Heater	0 °C

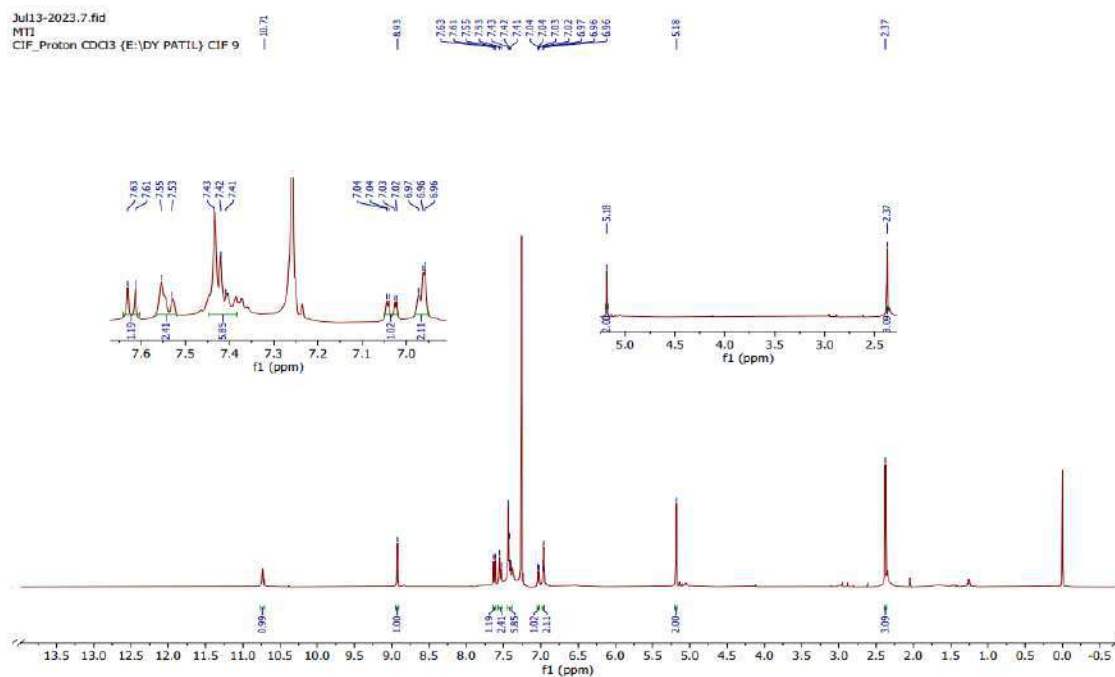


HR-MS spectra of compound 6a

## CHARACTERISATION OF COMPOUND 6b

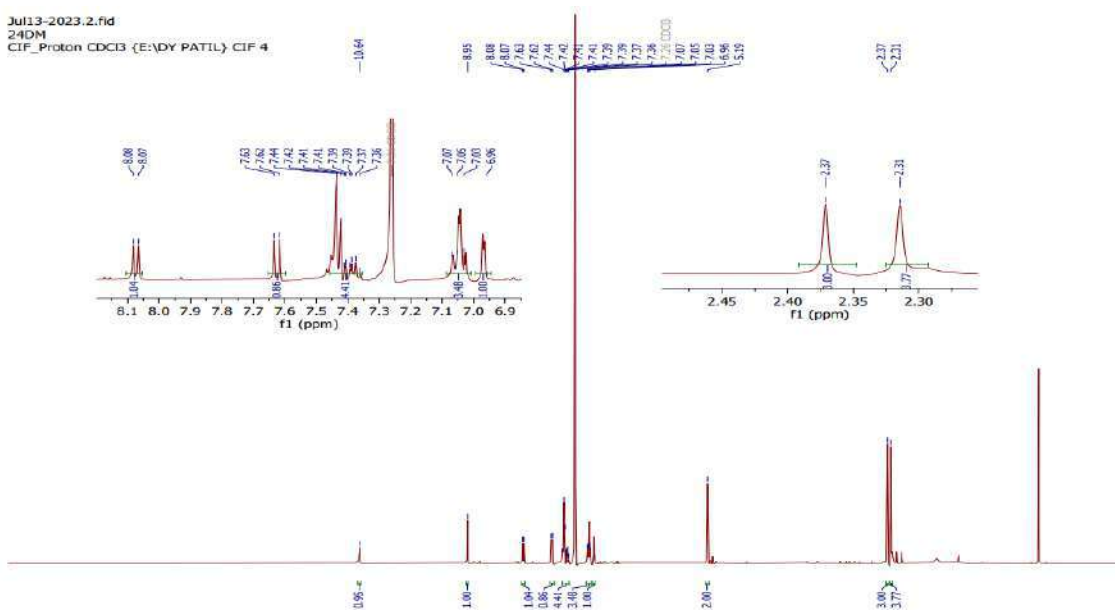


IR spectra of compound 6b

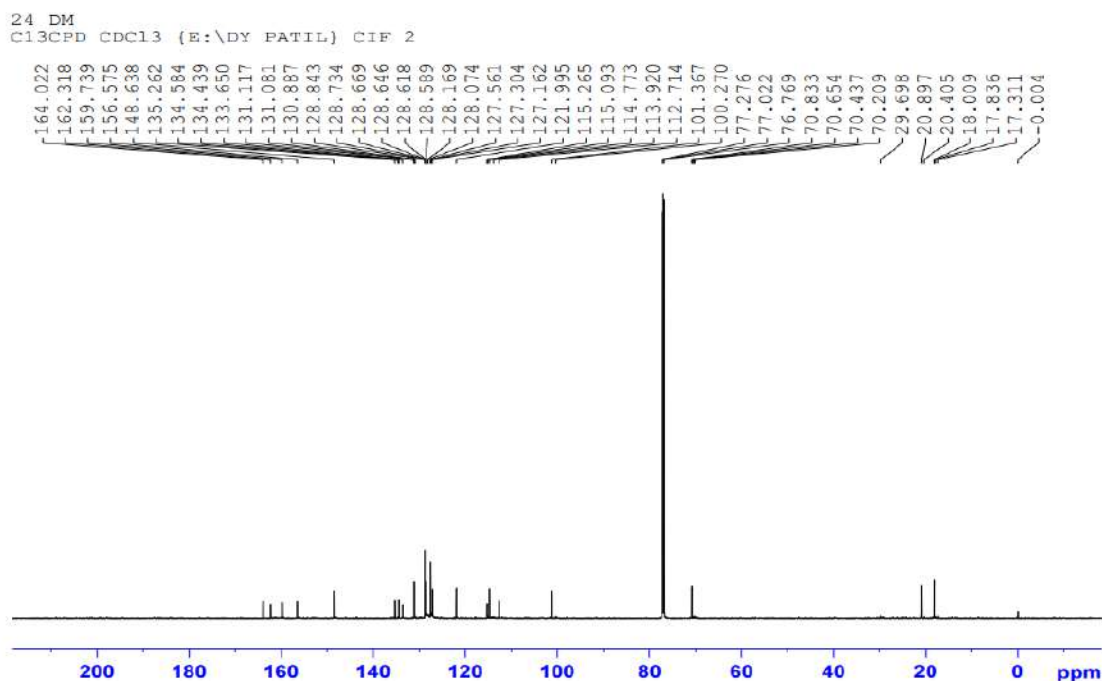


**$^1\text{H}$  NMR spectra of compound 6b**

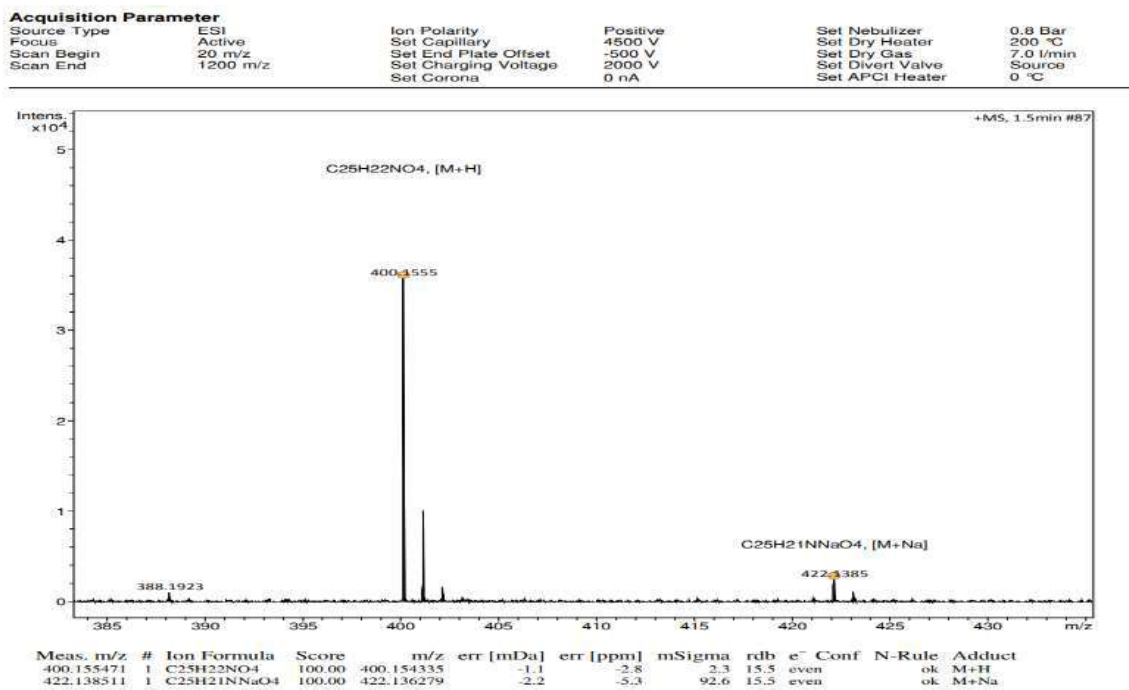
## CHARACTERISATION OF COMPOUND 7a



**$^1\text{H}$  NMR spectra of compound 7a**



$^{13}\text{C}$  NMR spectra of compound 7a



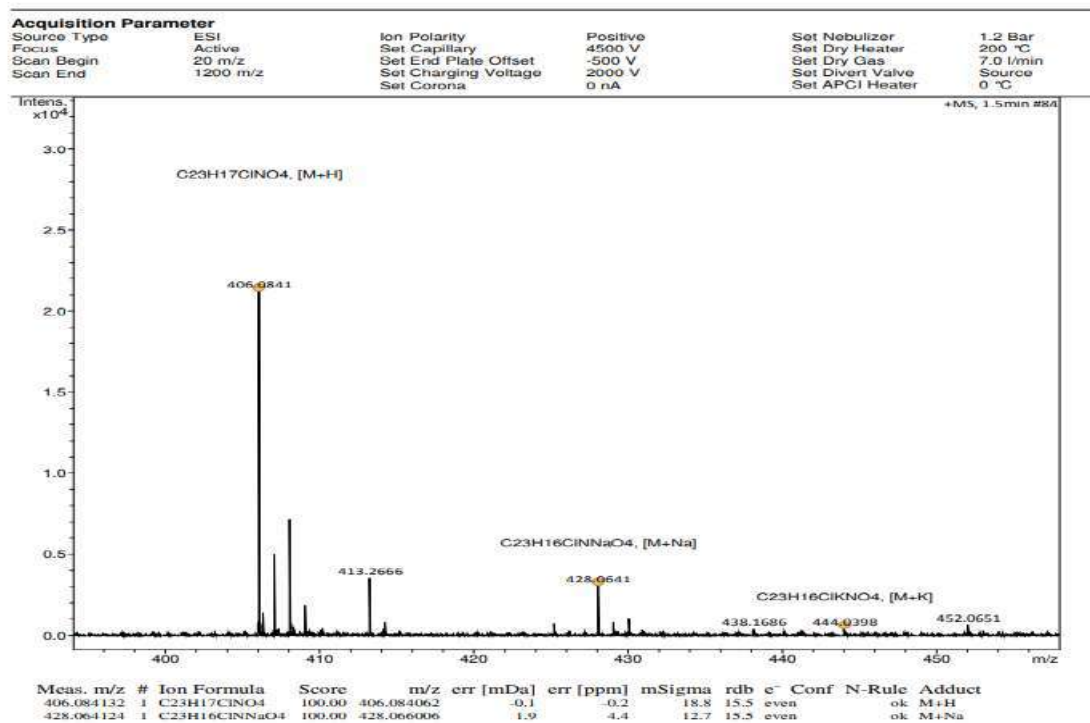
HR MS spectra of compound 7a

Jul13-2023.3.fid  
25DM  
CIF\_Proton CDC13 {E:\DY PATIL} CIF 5



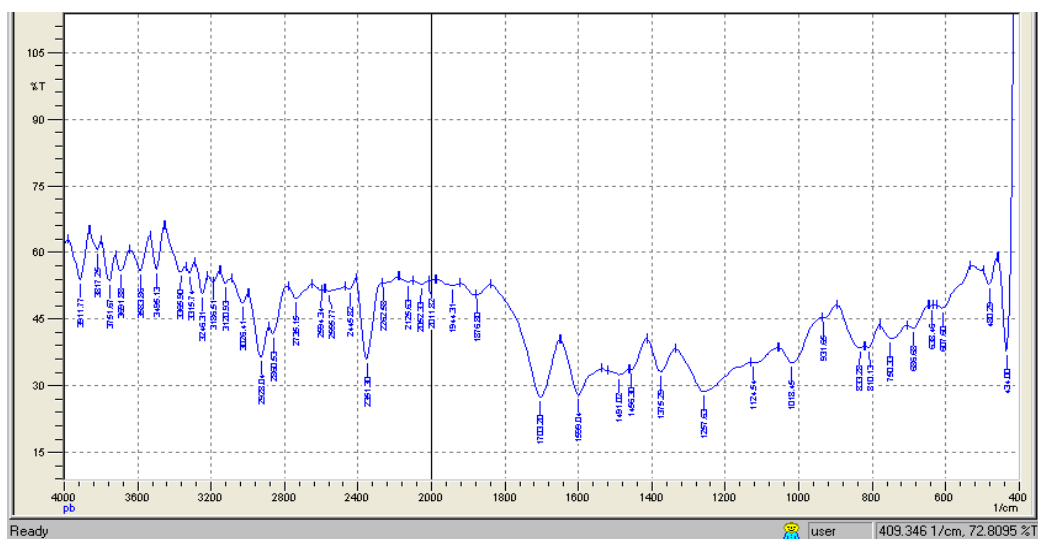
Nov22-2022.2.fid  
PT-1  
CIF\_Proton CDC13 {E:\DYPIPR} CIF 7



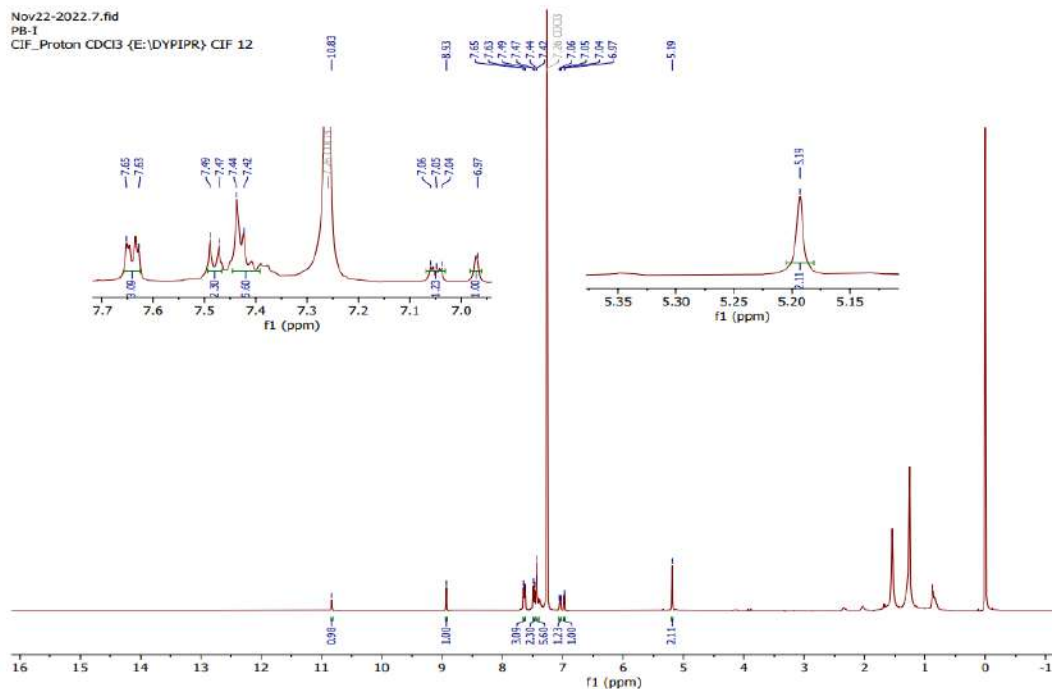


HR MS spectra of Compound 8a

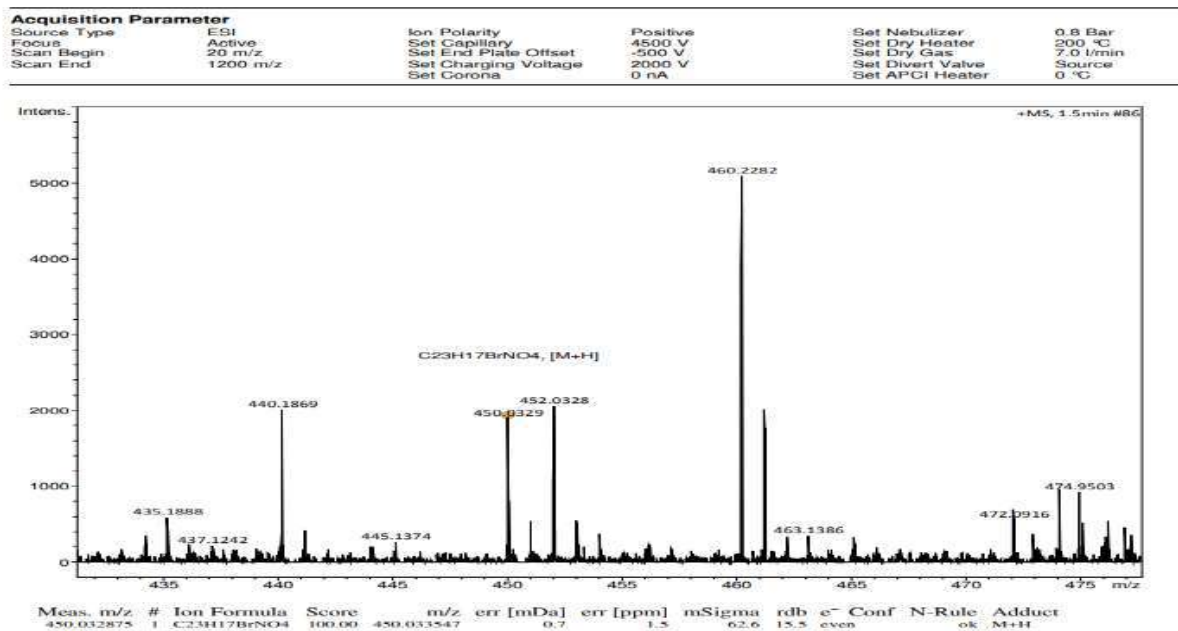
## CHARACTERIZATION OF COMPOUND 9a



IR spectra of compound 9a



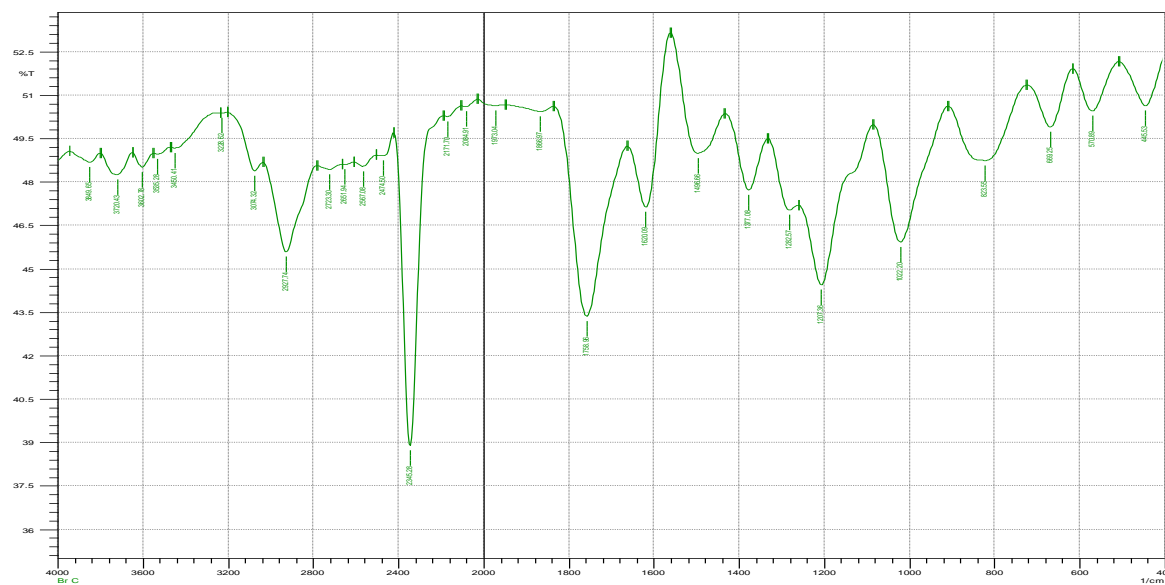
$^1\text{H}$  NMR of compound 9a



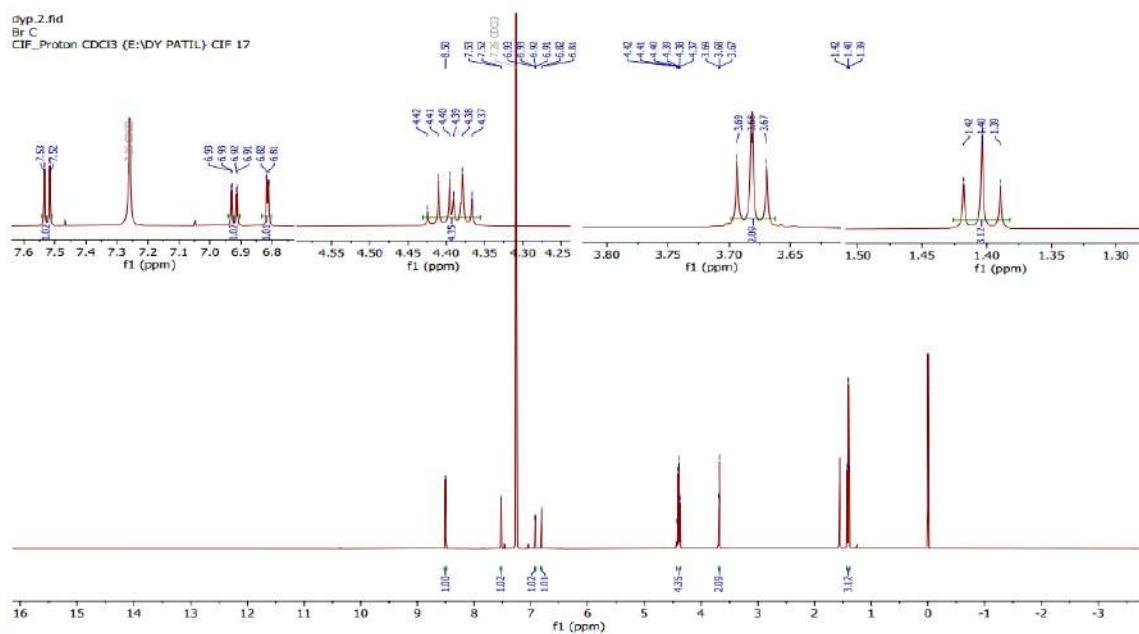
HR MS of compound 9a



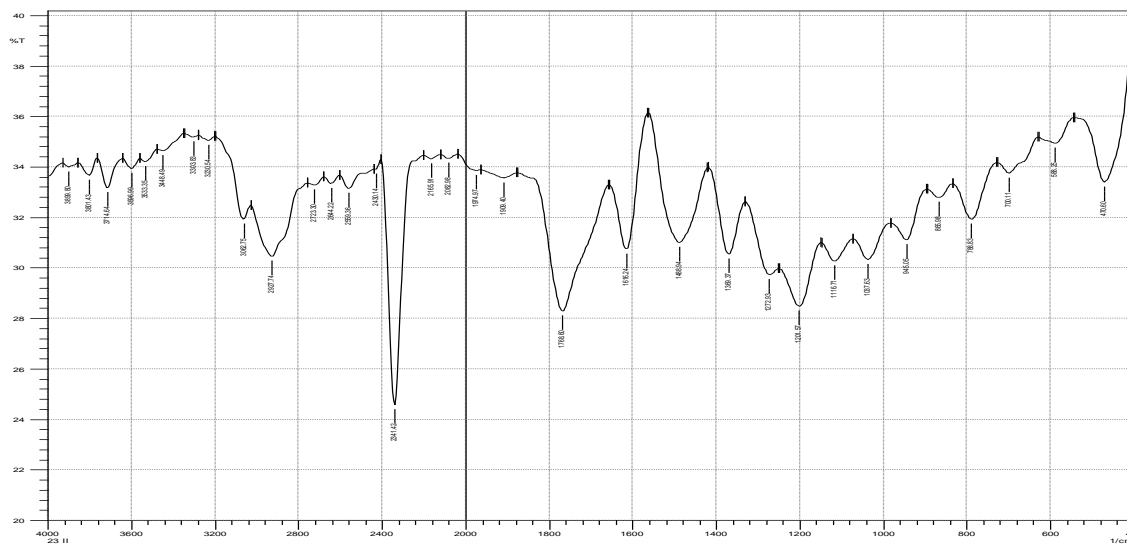
## CHARACTERIZATION OF COMPOUND 11



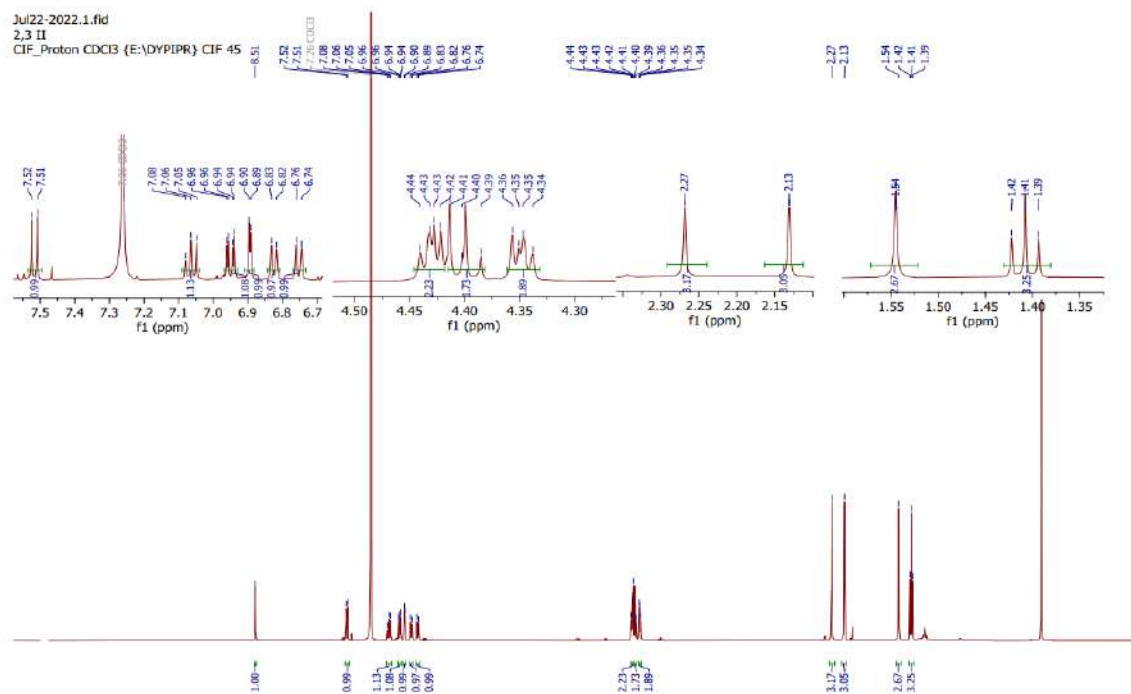
IR spectra of compound 11



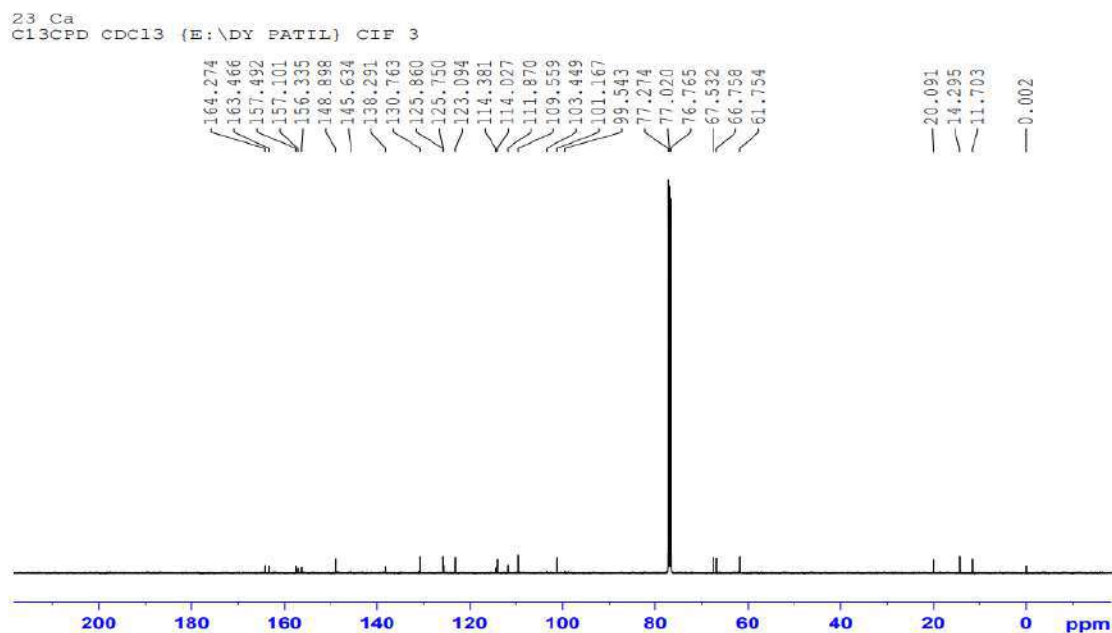
## CHARACTERISATION OF COMPOUND 12a



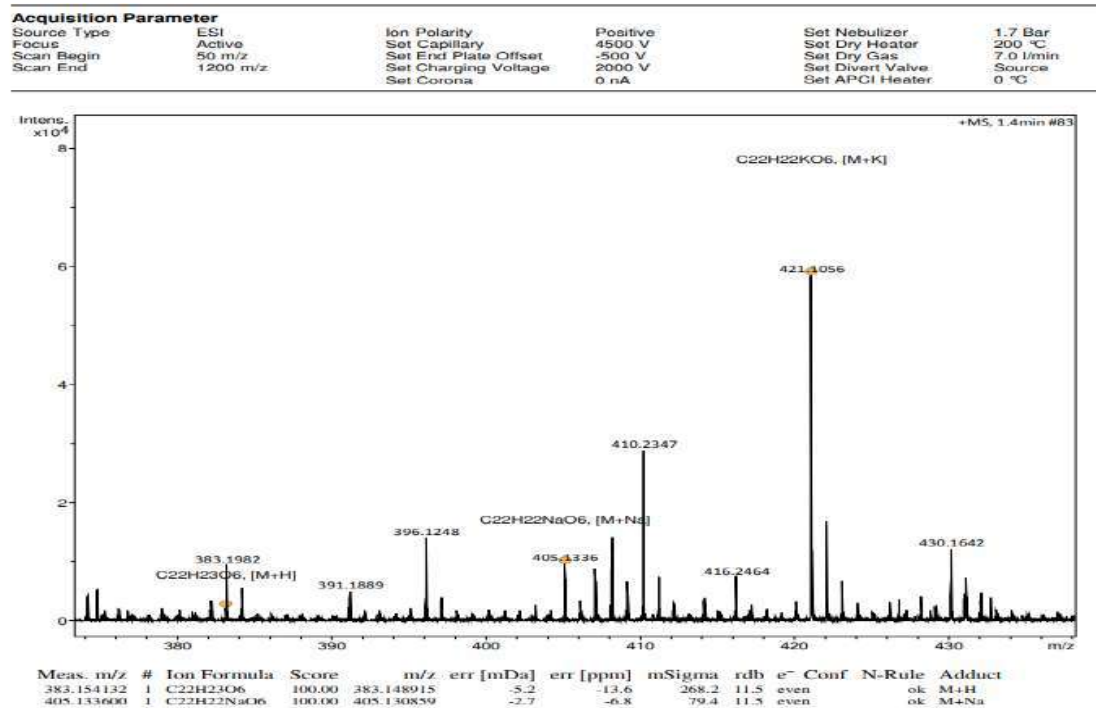
IR spectra of compound 12a



<sup>1</sup>H NMR spectra of compound 12a

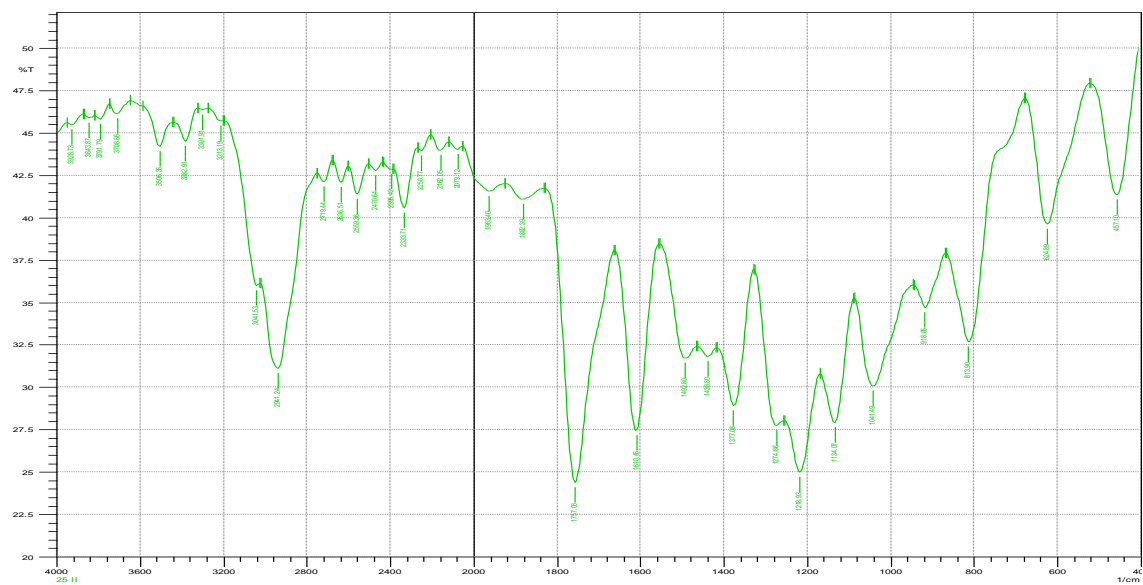


$^{13}\text{C}$  NMR spectra of compound 12a

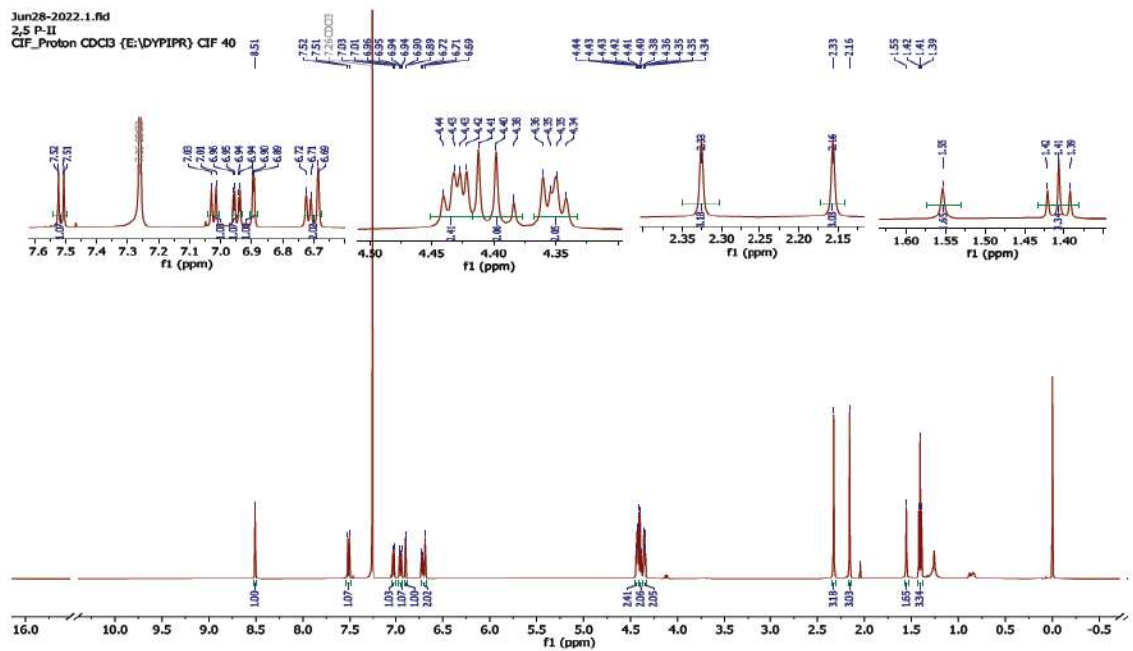


HR-MS spectra of compound 12a

## CHARACTERISATION OF COMPOUND 12b

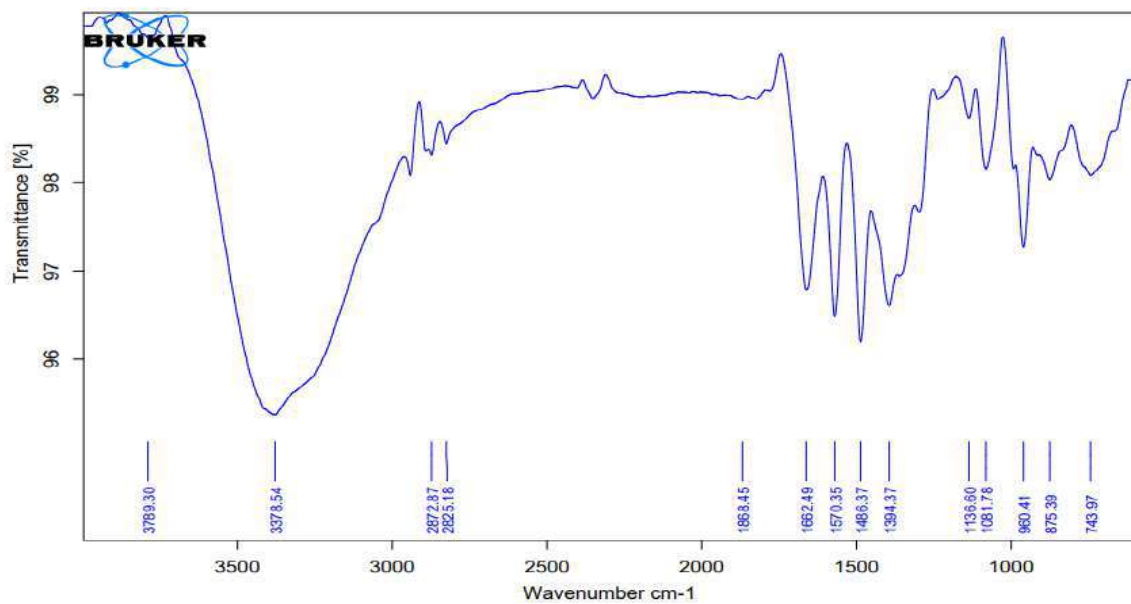


### IR spectra of compound 12b

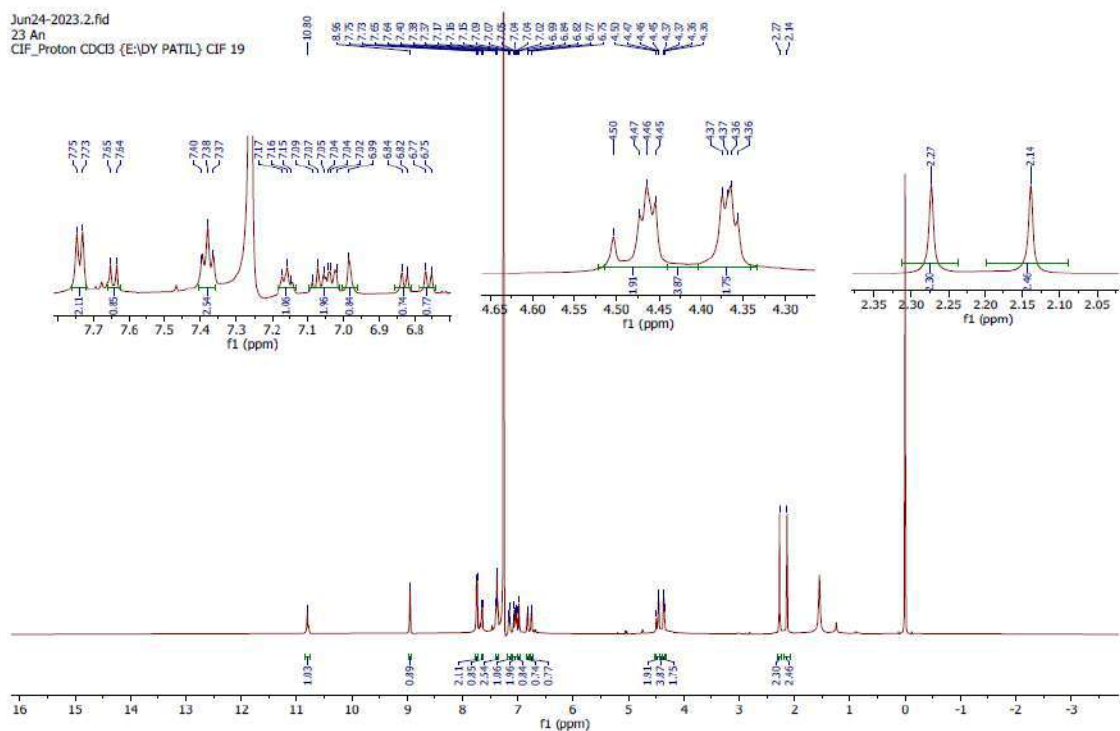


### <sup>1</sup>HNMR spectra of compound 12b

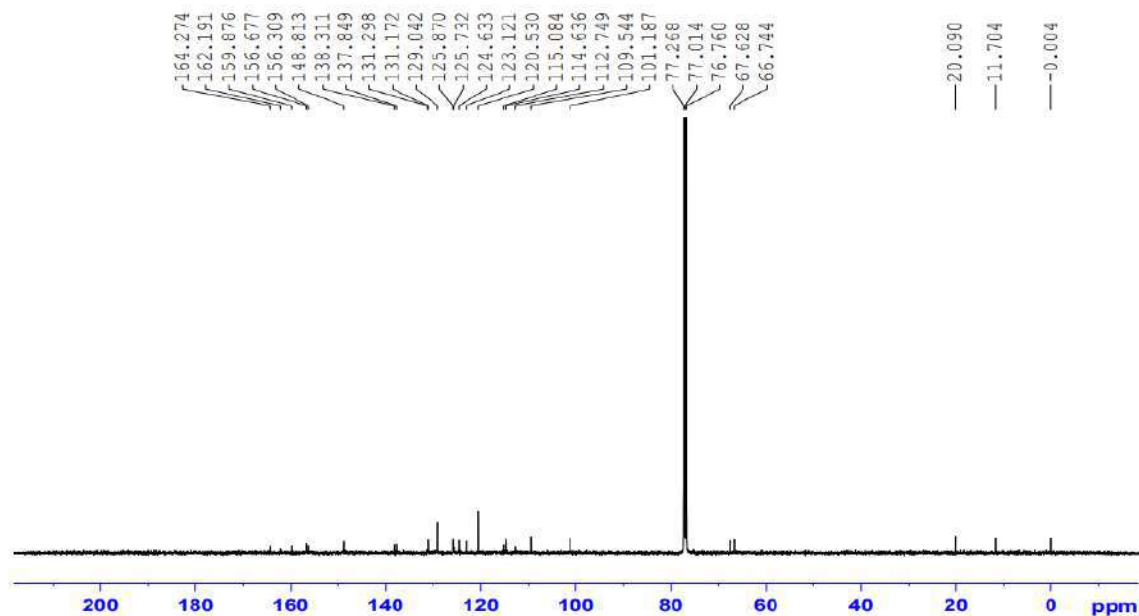
## CHARACTERISATION OF COMPOUND 13a



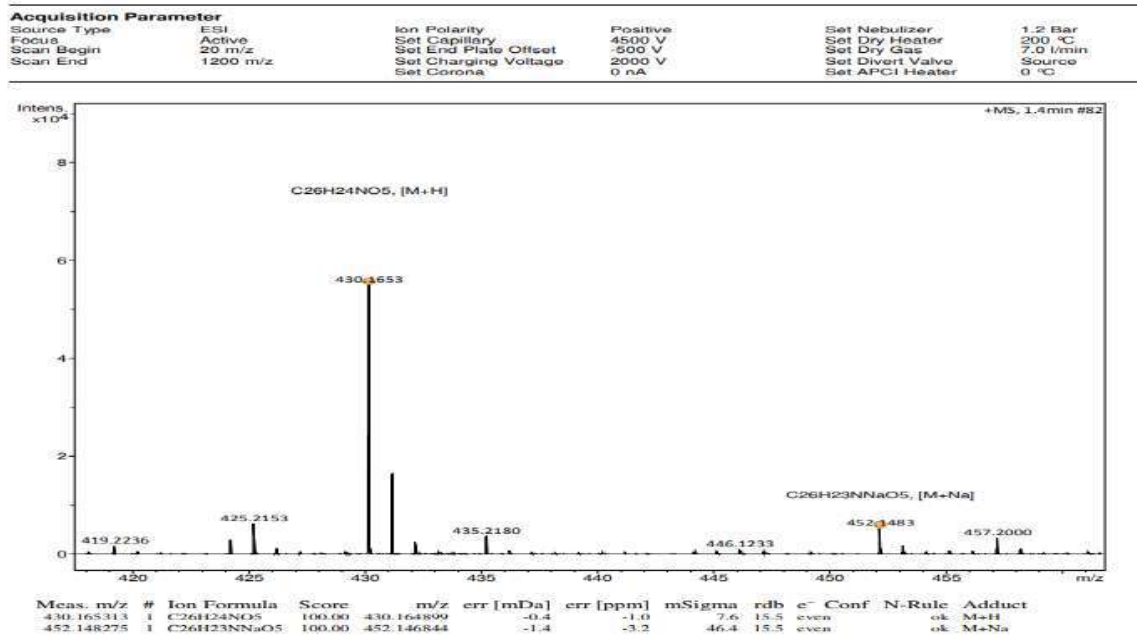
IR spectra of compound 13a



23 An  
 Cl3CPD CDC13 {E:\DY PATIL} CIF 4

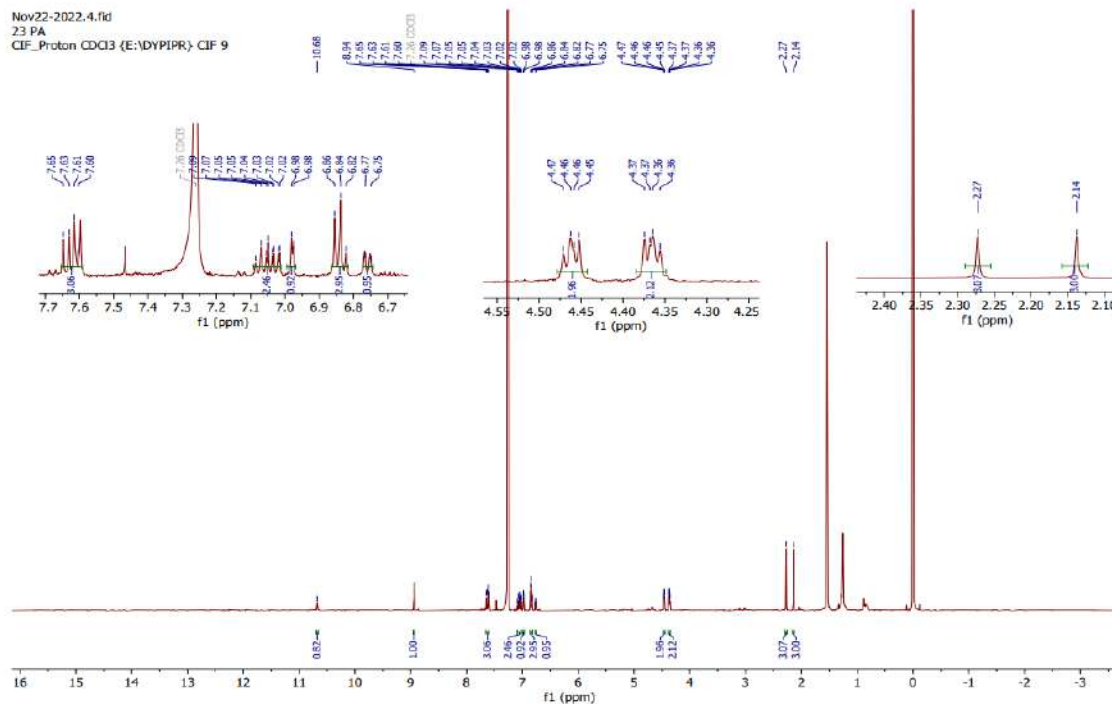


$^{13}\text{C}$  NMR spectra of compound 13a

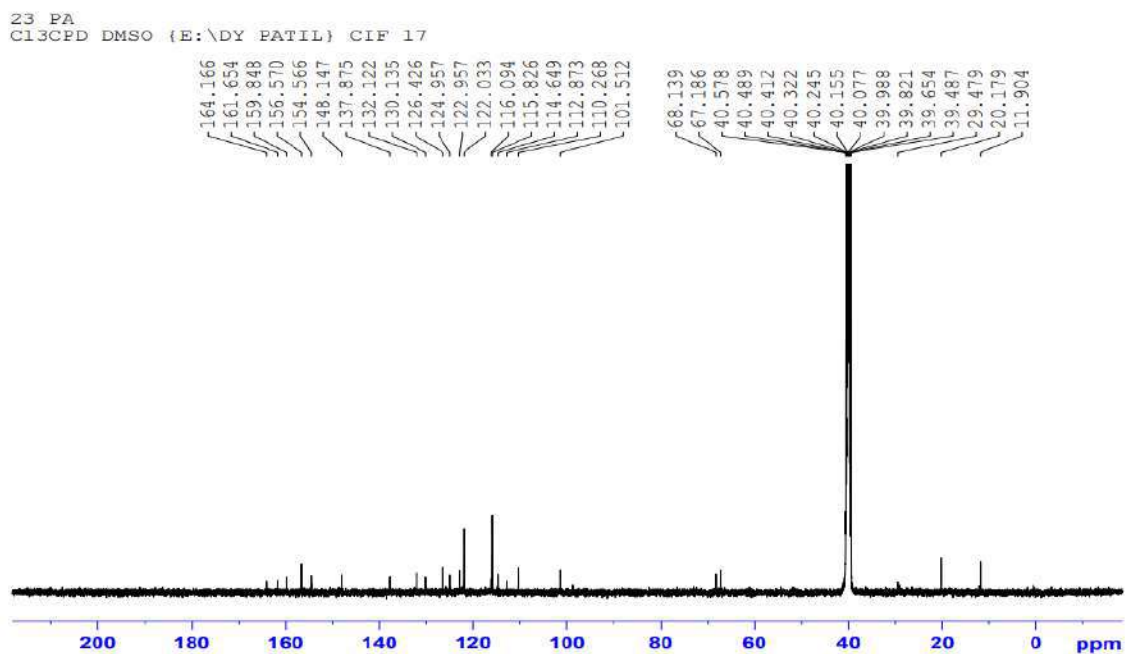


HR MS spectra of compound 13a

## CHARACTERISATION OF COMPOUND 14a



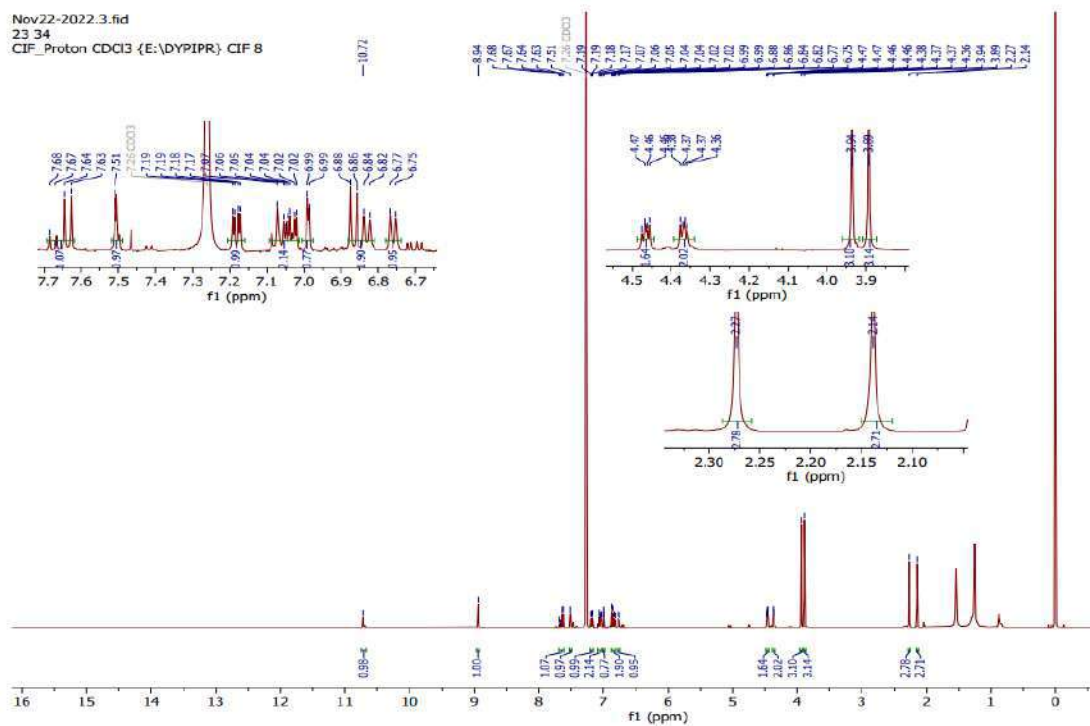
<sup>1</sup>H NMR spectra of compound 14a



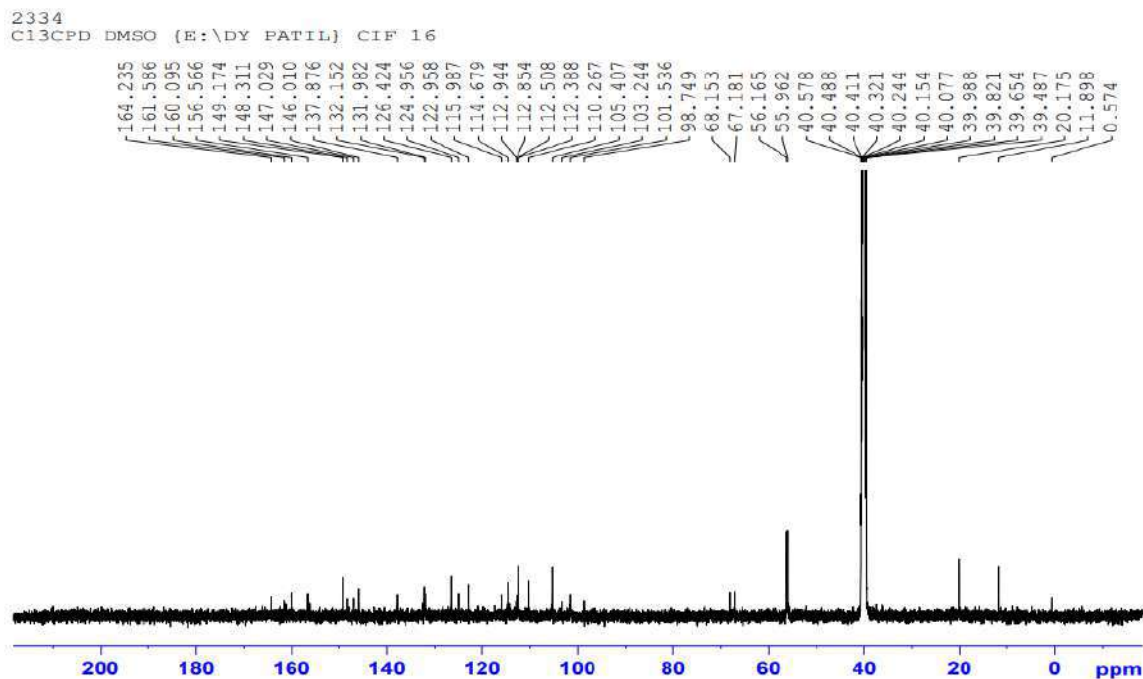
<sup>13</sup>C NMR spectra of compound 14a



## CHARACTERIZATION OF COMPOUND 15a

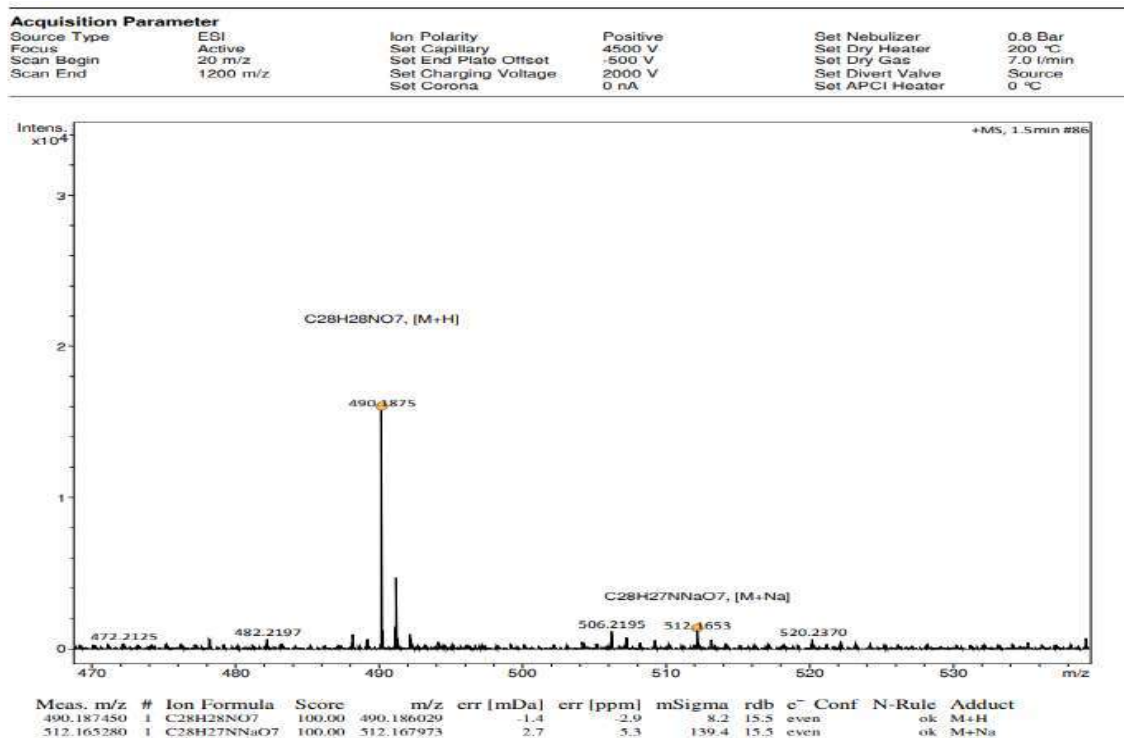


<sup>1</sup>H NMR spectra of compound 15a



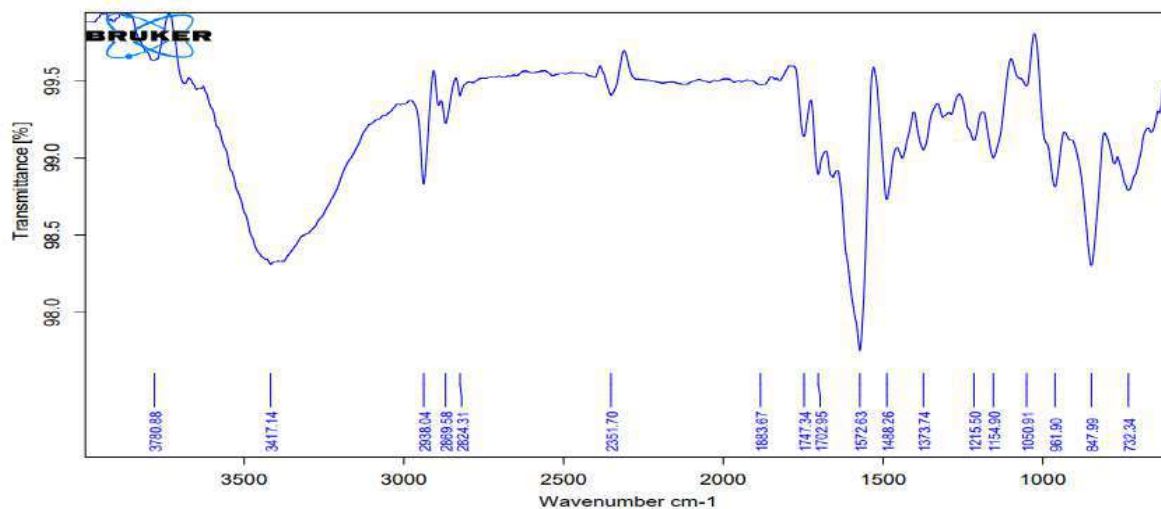
<sup>13</sup>C NMR spectra of compound 15a





HR MS spectra of compound 15a

## CHARACTERISATION OF COMPOUND 16a



IR spectra of compound 16a

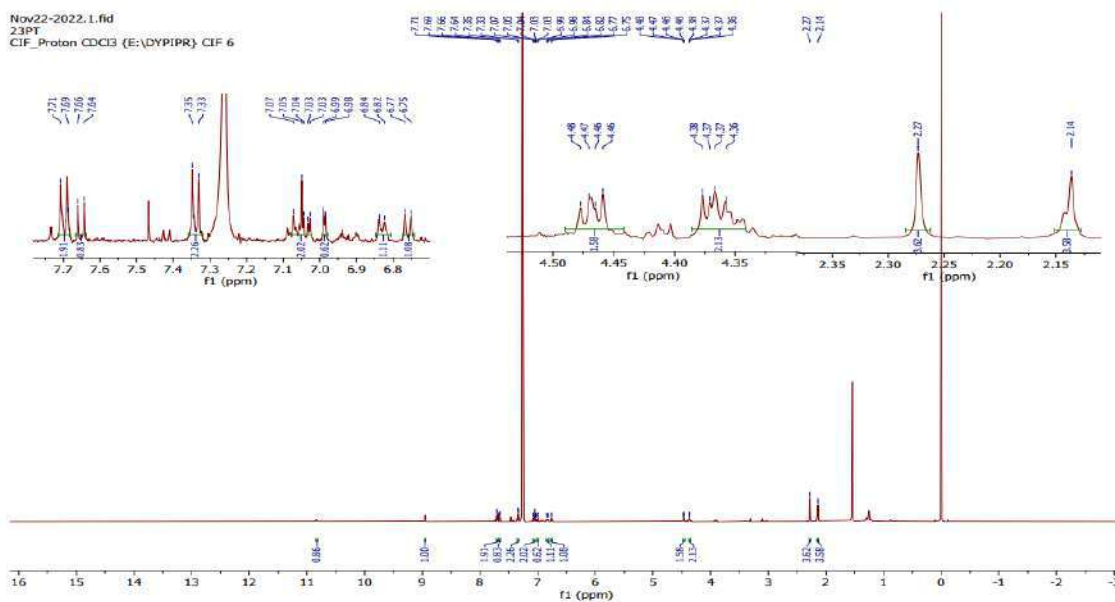


Mass spectrum plot showing intensity versus  $m/z$ . The x-axis ranges from 440 to 465  $m/z$ , and the y-axis ranges from 0 to 5000 intensity. Several peaks are labeled with their  $m/z$  values:

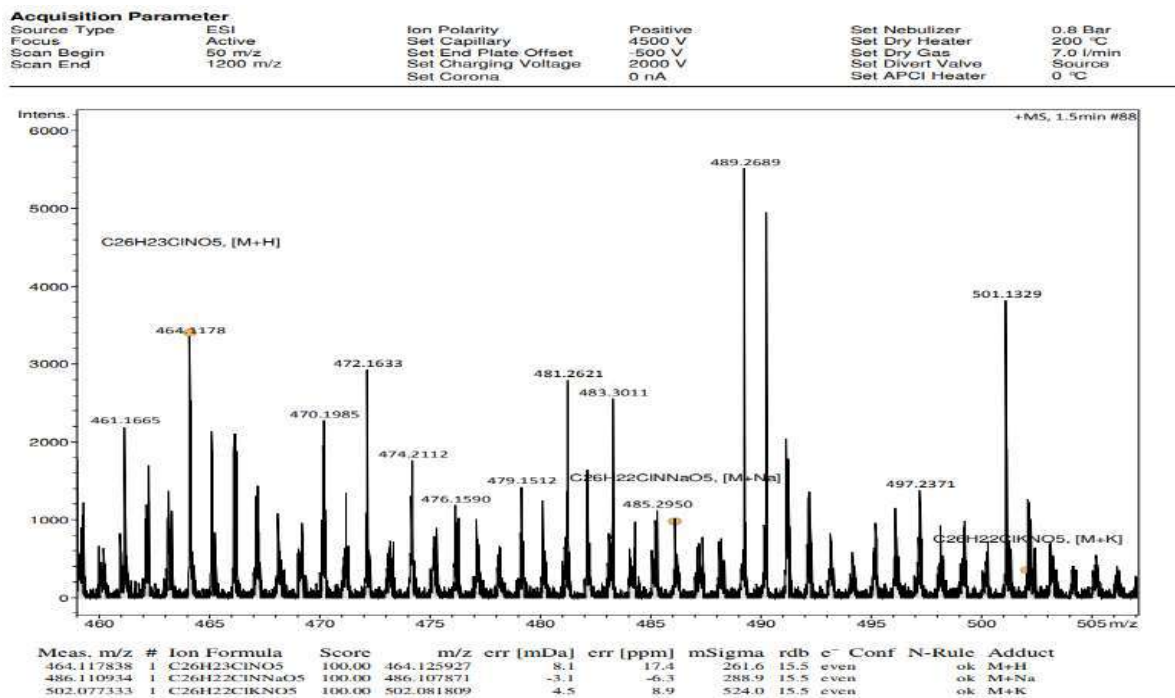
$m/z$	Approximate Intensity
441.2074	1000
444.1509	2800
446.1962	1200
450.0948	1100
453.2183	800
454.9996	3200
456.9963	4800
461.1641	1200
464.1096	2000
466.1331	1200

### HR MS spectra of compound 16a

## CHARACTERISATION OF COMPOUND 17a

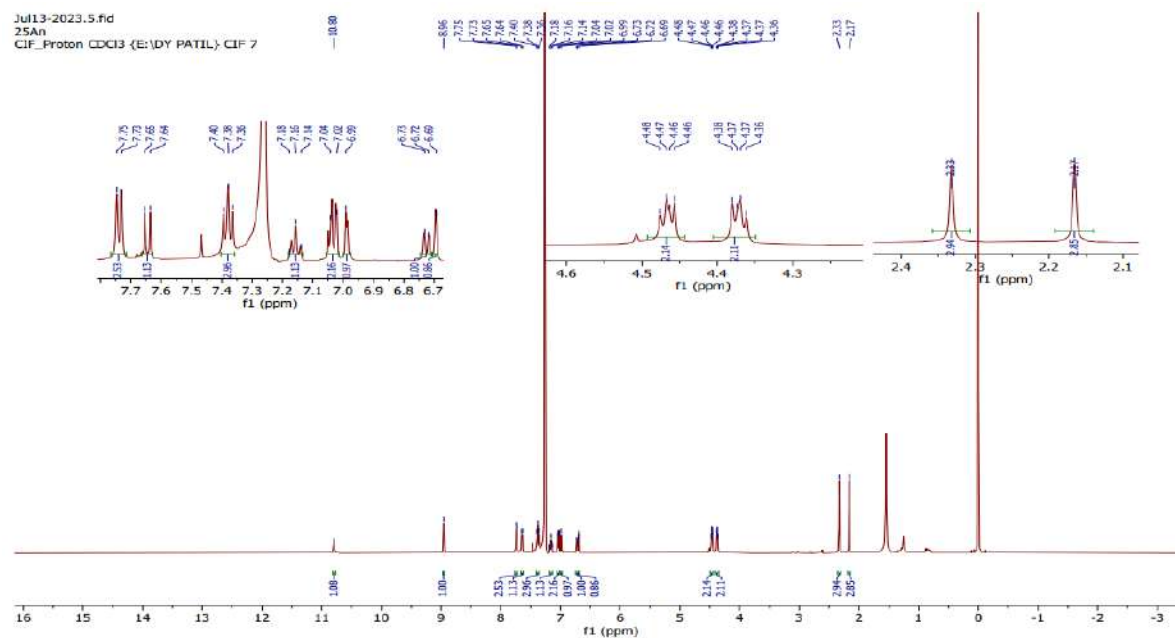


### <sup>1</sup>HNMR spectra of compound 17a



HR MS spectra of compound 17a

## CHARACTERISATION OF COMPOUND 13b



<sup>1</sup>H NMR spectra of compound 13b

Jun24-2023.3.fid  
25 PA  
CIF\_Proton CDC3 (E:\DY PATIL) CIF 20

Chemical shift (ppm): 7.64, 7.63, 7.60, 7.58, 7.03, 7.03, 6.98, 6.95, 6.94, 6.73, 6.72, 6.69, 4.48, 4.37, 2.21, 2.18, 2.11, 2.09, 1.64, 1.57, 1.56, 1.55, 1.54, 1.53, 1.52, 1.51, 1.50, 1.49, 1.48, 1.47, 1.46, 1.45, 1.44, 1.43, 1.42, 1.41, 1.40, 1.39, 1.38, 1.37, 1.36, 1.35, 1.34, 1.33, 1.32, 1.31, 1.30, 1.29, 1.28, 1.27, 1.26, 1.25, 1.24, 1.23, 1.22, 1.21, 1.20, 1.19, 1.18, 1.17, 1.16, 1.15, 1.14, 1.13, 1.12, 1.11, 1.10, 1.09, 1.08, 1.07, 1.06, 1.05, 1.04, 1.03, 1.02, 1.01, 1.00, 0.99, 0.98, 0.97, 0.96, 0.95, 0.94, 0.93, 0.92, 0.91, 0.90, 0.89, 0.88, 0.87, 0.86, 0.85, 0.84, 0.83, 0.82, 0.81, 0.80, 0.79, 0.78, 0.77, 0.76, 0.75, 0.74, 0.73, 0.72, 0.71, 0.70, 0.69, 0.68, 0.67, 0.66, 0.65, 0.64, 0.63, 0.62, 0.61, 0.60, 0.59, 0.58, 0.57, 0.56, 0.55, 0.54, 0.53, 0.52, 0.51, 0.50, 0.49, 0.48, 0.47, 0.46, 0.45, 0.44, 0.43, 0.42, 0.41, 0.40, 0.39, 0.38, 0.37, 0.36, 0.35, 0.34, 0.33, 0.32, 0.31, 0.30, 0.29, 0.28, 0.27, 0.26, 0.25, 0.24, 0.23, 0.22, 0.21, 0.20, 0.19, 0.18, 0.17, 0.16, 0.15, 0.14, 0.13, 0.12, 0.11, 0.10, 0.09, 0.08, 0.07, 0.06, 0.05, 0.04, 0.03, 0.02, 0.01, 0.00.

Integration values: 0.38, 0.39, 0.40, 0.41, 0.42, 0.43, 0.44, 0.45, 0.46, 0.47, 0.48, 0.49, 0.50, 0.51, 0.52, 0.53, 0.54, 0.55, 0.56, 0.57, 0.58, 0.59, 0.60, 0.61, 0.62, 0.63, 0.64, 0.65, 0.66, 0.67, 0.68, 0.69, 0.70, 0.71, 0.72, 0.73, 0.74, 0.75, 0.76, 0.77, 0.78, 0.79, 0.80, 0.81, 0.82, 0.83, 0.84, 0.85, 0.86, 0.87, 0.88, 0.89, 0.90, 0.91, 0.92, 0.93, 0.94, 0.95, 0.96, 0.97, 0.98, 0.99, 1.00, 1.01, 1.02, 1.03, 1.04, 1.05, 1.06, 1.07, 1.08, 1.09, 1.10, 1.11, 1.12, 1.13, 1.14, 1.15, 1.16, 1.17, 1.18, 1.19, 1.20, 1.21, 1.22, 1.23, 1.24, 1.25, 1.26, 1.27, 1.28, 1.29, 1.30, 1.31, 1.32, 1.33, 1.34, 1.35, 1.36, 1.37, 1.38, 1.39, 1.40, 1.41, 1.42, 1.43, 1.44, 1.45, 1.46, 1.47, 1.48, 1.49, 1.50, 1.51, 1.52, 1.53, 1.54, 1.55, 1.56, 1.57, 1.58, 1.59, 1.60, 1.61, 1.62, 1.63, 1.64, 1.65, 1.66, 1.67, 1.68, 1.69, 1.70, 1.71, 1.72, 1.73, 1.74, 1.75, 1.76, 1.77, 1.78, 1.79, 1.80, 1.81, 1.82, 1.83, 1.84, 1.85, 1.86, 1.87, 1.88, 1.89, 1.90, 1.91, 1.92, 1.93, 1.94, 1.95, 1.96, 1.97, 1.98, 1.99, 2.00, 2.01, 2.02, 2.03, 2.04, 2.05, 2.06, 2.07, 2.08, 2.09, 2.10, 2.11, 2.12, 2.13, 2.14, 2.15, 2.16, 2.17, 2.18, 2.19, 2.20, 2.21, 2.22, 2.23, 2.24, 2.25, 2.26, 2.27, 2.28, 2.29, 2.30, 2.31, 2.32, 2.33, 2.34, 2.35, 2.36, 2.37, 2.38, 2.39, 2.40, 2.41, 2.42, 2.43, 2.44, 2.45, 2.46, 2.47, 2.48, 2.49, 2.50, 2.51, 2.52, 2.53, 2.54, 2.55, 2.56, 2.57, 2.58, 2.59, 2.60, 2.61, 2.62, 2.63, 2.64, 2.65, 2.66, 2.67, 2.68, 2.69, 2.70, 2.71, 2.72, 2.73, 2.74, 2.75, 2.76, 2.77, 2.78, 2.79, 2.80, 2.81, 2.82, 2.83, 2.84, 2.85, 2.86, 2.87, 2.88, 2.89, 2.90, 2.91, 2.92, 2.93, 2.94, 2.95, 2.96, 2.97, 2.98, 2.99, 3.00, 3.01, 3.02, 3.03, 3.04, 3.05, 3.06, 3.07, 3.08, 3.09, 3.10, 3.11, 3.12, 3.13, 3.14, 3.15, 3.16, 3.17, 3.18, 3.19, 3.20, 3.21, 3.22, 3.23, 3.24, 3.25, 3.26, 3.27, 3.28, 3.29, 3.30, 3.31, 3.32, 3.33, 3.34, 3.35, 3.36, 3.37, 3.38, 3.39, 3.40, 3.41, 3.42, 3.43, 3.44, 3.45, 3.46, 3.47, 3.48, 3.49, 3.50, 3.51, 3.52, 3.53, 3.54, 3.55, 3.56, 3.57, 3.58, 3.59, 3.60, 3.61, 3.62, 3.63, 3.64, 3.65, 3.66, 3.67, 3.68, 3.69, 3.70, 3.71, 3.72, 3.73, 3.74, 3.75, 3.76, 3.77, 3.78, 3.79, 3.80, 3.81, 3.82, 3.83, 3.84, 3.85, 3.86, 3.87, 3.88, 3.89, 3.90, 3.91, 3.92, 3.93, 3.94, 3.95, 3.96, 3.97, 3.98, 3.99, 4.00, 4.01, 4.02, 4.03, 4.04, 4.05, 4.06, 4.07, 4.08, 4.09, 4.10, 4.11, 4.12, 4.13, 4.14, 4.15, 4.16, 4.17, 4.18, 4.19, 4.20, 4.21, 4.22, 4.23, 4.24, 4.25, 4.26, 4.27, 4.28, 4.29, 4.30, 4.31, 4.32, 4.33, 4.34, 4.35, 4.36, 4.37, 4.38, 4.39, 4.40, 4.41, 4.42, 4.43, 4.44, 4.45, 4.46, 4.47, 4.48, 4.49, 4.50, 4.51, 4.52, 4.53, 4.54, 4.55, 4.56, 4.57, 4.58, 4.59, 4.60, 4.61, 4.62, 4.63, 4.64, 4.65, 4.66, 4.67, 4.68, 4.69, 4.70, 4.71, 4.72, 4.73, 4.74, 4.75, 4.76, 4.77, 4.78, 4.79, 4.80, 4.81, 4.82, 4.83, 4.84, 4.85, 4.86, 4.87, 4.88, 4.89, 4.90, 4.91, 4.92, 4.93, 4.94, 4.95, 4.96, 4.97, 4.98, 4.99, 5.00, 5.01, 5.02, 5.03, 5.04, 5.05, 5.06, 5.07, 5.08, 5.09, 5.10, 5.11, 5.12, 5.13, 5.14, 5.15, 5.16, 5.17, 5.18, 5.19, 5.20, 5.2

Acquisition Parameter				Ion Optics				Source Parameters			
Source Type	ESI	Ion Polarity	Positive	Set Nebulizer	1.2 Bar	Set Dry Gas	200 °C				
Focus	Active	Set Capillary	4500 V	Set Dry Gas	7.0 l/min	Set Divert Valve	Source				
Scan Begin	20 m/z	Set End Plate Offset	-500 V	Set APCI Heater	0 °C						
Scan End	1200 m/z	Set Charging Voltage	2000 V								
		Set Corona	0 nA								

Mass Spectrum Data:

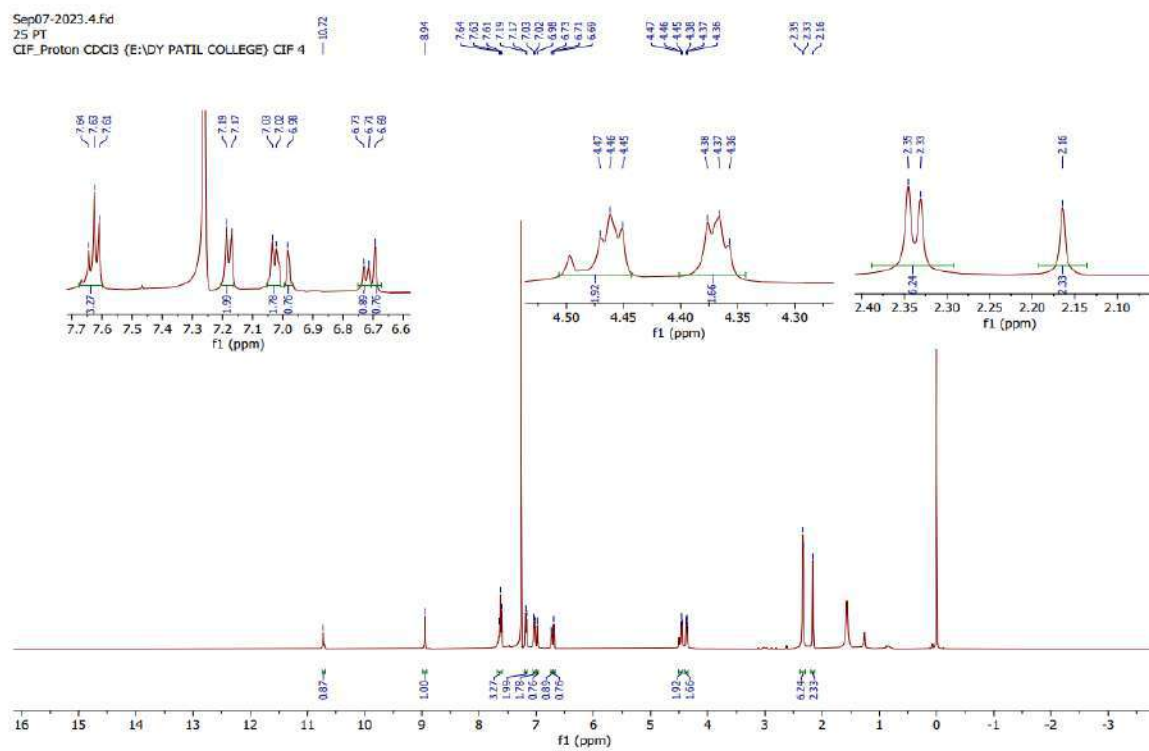
m/z	Intensity (x10 <sup>5</sup> )	Label
446.1609	~1.3	C <sub>26</sub> H <sub>24</sub> NO <sub>6</sub> , [M+H]
468.1435	~0.2	C <sub>26</sub> H <sub>23</sub> NNaO <sub>6</sub> , [M+Na]

Meas. m/z	#	Ion Formula	Score	m/z	err [mDa]	err [ppm]	mSigma	rdB	e <sup>-</sup>	Conf	N-Rule	Adduct
446.160925	1	C <sub>26</sub> H <sub>24</sub> NO <sub>6</sub>	100.00	446.159814	-1.1	-2.5	3.6	15.5	even		ok	M+H
468.143476	1	C <sub>26</sub> H <sub>23</sub> NNaO <sub>6</sub>	100.00	468.141758	-1.7	-3.7	28.9	15.5	even		ok	M+Na

179


## CHARACTERISATION OF COMPOUND 16b



$^1\text{H}$ NMR spectra of compound 16b

## IAEC APPROVAL CERIFICATE

Registered under Ministry of micro, small and medium enterprises (MSME): UAN-MH2900010740  
Registered under CPCSEA 211A/PO/Re/5/20/CPCSEA

 **BIOCYTE**  
**INSTITUTE OF RESEARCH & DEVELOPMENT**

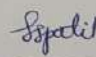
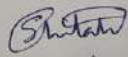

Flat No.11, Shri-Ram Residency, Near Bypass Road,  
Kalanagar, Sangli, Maharashtra – 416416

Mob.9595753875 [www.biocyte.in](http://www.biocyte.in) [E-mail-biocytelabsangli@gmail.com](mailto:E-mail-biocytelabsangli@gmail.com)

Ref No: BIRD/Sangli/IAEC/03 Date: 5<sup>th</sup> Aug. 2023

**Certificate**

This is to certify that the project proposal no IAEC/Sangli/2023-24/03 “**Design, synthesis, and evaluation of some new coumarin derivatives for antidiabetic Activity.**” entitled submitted by **Ms. Rachana Bhimanwar** has been approved/recommended by the IAEC of Biocyte Institute of Research and Development in its meeting held on 05/08/2023 (21 Wistar Albino Rat) have been sanctioned under this proposal for a duration of next Twelve months.

Authorized by	Name	Signature	Date
Chairman:	Mrs. Supriya S. Patil.		05/08/2023
Member Secretary:	Mr. Vallabh S. Chitale.		05/08/2023
Main Nominee of CPCSEA:	Dr. Shitalkumar S. Patil		05/08/23



### **LIST OF PUBLICATIONS**

<b>Sr. No.</b>	<b>Title/ Journals</b>	<b>Indexed</b>	<b>Status of Publication</b>
1	Bhimanwar RS, Mittal A. TGR5 agonists for diabetes treatment: a patent review and clinical advancements (2012-present). Expert OpinTher Pat. 2022 Feb;32(2):191-209. doi: 10.1080/13543776.2022.1994551 (IF- 6.7)	Scopus	Published
2	Bhimanwar RS,Lokhande KB, Shrivastava A, Singh A, Chitlange SS, Mittal A. Identification of potential drug candidates as TGR5 agonist to combat type II diabetes using <i>in silico</i> docking and molecular dynamics simulation studies. J BiomolStructDyn. 2023 Feb 1:1-18. doi: 10.1080/07391102.2023.2173654. (Impact Factor 5.27)	Scopus	Published
3	Rachana S. Bhimanwar <sup>a,b</sup> , Amit Mittal <sup>a,b</sup> , Kiran Bharat Lokhande <sup>c</sup> , Vikas Sharma <sup>b</sup> ·A comparative analysis of <i>In-silico</i> structural homology modelling algorithms for the prediction of TGR5 structure	Scopus	Submitted
4	Rachana S. Bhimanwar <sup>a, b</sup> , Amit Mittal <sup>b</sup> , Snehal Choudhari <sup>c</sup> , Vikas Sharma Recent advancements in the structural exploration of TGR5 agonists for Diabetes treatment RSC Med. Chem., 2024, 15, 3026-3037 <a href="https://doi.org/10.1039/D4MD00473F">https://doi.org/10.1039/D4MD00473F</a>	Scopus	Published



REVIEW



## TGR5 agonists for diabetes treatment: a patent review and clinical advancements (2012-present)

Rachana S. Bhimanwar<sup>a,b</sup> and Amit Mittal <sup>a</sup>

<sup>a</sup>Department of Pharmaceutical Chemistry, School of Pharmaceutical Sciences, Lovely Professional University, Phagwara, Punjab, India;

<sup>b</sup>Department of Pharmaceutical Chemistry, Dr. D. Y. Patil Institute of Pharmaceutical Sciences and Research, Pimpri, Pune, Maharashtra, India

### ABSTRACT

**Introduction:** A cell surface bile acid receptor TGR5 is expressed in various tissues, including the liver, kidney, intestine, and adrenal glands, causing its effect in each tissue to differ. A major role for TGR5 is to maintain blood sugar levels and increase in energy expenditure. These benefits make it a potential candidate for the treatment of type 2 diabetes, obesity, and other metabolic diseases.

**Area covered:** This paper highlights recent advances in the development of potent steroidal and non-steroidal TGR5 agonists and the peer-reviewed scientific articles that have led to understanding the structure-activity relationship for TGR5 agonists (2012–2020). The review also discusses the clinical progress made by some TGR5 agonists over the past eight years.

**Expert opinion:** In preclinical studies, TGR5 has been found to play a crucial role in GLP-1 secretion and has shown promise for weight loss, anti-diabetic outcomes etc. Semi synthetic and synthetic derivatives can be considered a potential avenue for discovering novel TGR5 agonists. Currently, few TGR5 agonists have reached the clinical trial stage, and, likely, soon novel TGR5 modulator will be discovered with fewer adverse effects. In silico studies can also be performed with various heterocyclic scaffolds to discover selective and safe TGR5 agonists.

### ARTICLE HISTORY

Received 7 June 2021

Accepted 13 October 2021

### KEYWORDS

G-protein-coupled receptor; bile acid; type 2 diabetes mellitus; glucagon-like peptide-1; structure-activity relationships; TGR5 agonists

### 1. Introduction

A diabetic syndrome is characterized by a lack of insulin in the body, causing a rise in blood glucose levels; either because cells fail to respond to the produced insulin or because the body is incapable of making insulin. Three types of diabetes have been identified, including Type I diabetes results from autoimmune reactions, Type II diabetes results from abnormal pancreatic-cell function, and Type III diabetes i.e. Gestational diabetes. Diabetes patients are also at high risk for other health complications such as obesity, cardiovascular diseases, diabetic retinopathy, etc [1].

The Ninth Edition of The IDF Diabetes Atlas 2019 predicts a rise in diabetic patients between the ages of 20–79 years from 463 million in 2019 to 700 million in 2045, with a recorded 4.2 million deaths. Globally, diabetes treatment costs increased nearly 38% from 2011 [2]. Diabetes, therefore, not only affects the health of individuals but also indirectly affects their economies. In summary, diabetes is likely to become more prevalent around the world in the years ahead as a significant health challenge. Prevention measures through physical activity, a healthy diet, and weight management can help manage diabetic complications [3,4].

The pharmacological treatment for type II diabetes is based on the use of a variety of drugs with different modes of action that target different pathways [5]. Type 2 diabetes can be controlled in a variety of ways, including:


- (1) Use of biguanides to inhibit gluconeogenesis (Metformin)
- (2) The increase in insulin secretion by pancreatic beta cells with sulphonylureas (Glipizide, Glimepiride, Gliazide, Glibenclamide), and with metaglinides (Repaglinide)
- (3) Increasing the sensitivity of insulin in the muscles, adipose tissue, and liver with thiazolidinediones (Rosiglitazone, Pioglitazone)
- (4) The inhibition of the glucosidase enzyme with the use of an alpha-glucosidase inhibitor (Acarbose) reduces carbohydrates absorption from the GIT.
- (5) Inhibition of glucose reabsorption through the kidneys and removal of excess glucose from the body through urine using SGLT2 inhibitors (Canagliflozin, Dapagliflozin, Empagliflozin) [6].

In recent years, newer antidiabetic drugs have been developed, including DPP-IV inhibitors (Sitagliptin and Linagliptin) that inhibit the DPP-4 enzyme, which in turn avoids the breakdown of GLP and influences insulin secretion. Furthermore, GLP-1 agonists, such as Exenatide [7], are also co-administered with DPP-IV inhibitors to decrease glucagon release and stimulate glucose metabolism. Glucagon antagonists, glucokinase activators, fructose 1,6 bisphosphate agonists, and fatty acid receptor agonists are also new approaches for lowering glucose in type II diabetes which may be used to develop new medications [5].

**CONTACT** Amit Mittal  amittal77@yahoo.com; amit.13145@lpu.co.in  Department of Pharmaceutical Chemistry, School of Pharmaceutical Sciences, Lovely Professional University, Jalandhar-Delhi G.T. Road NH-1, Phagwara 144411, Punjab, India

© 2021 Informa UK Limited, trading as Taylor & Francis Group

## Identification of potential drug candidates as TGR5 agonist to combat type II diabetes using *in silico* docking and molecular dynamics simulation studies

Rachana S. Bhimanwar<sup>a,b</sup> , Kiran Bharat Lokhande<sup>c</sup> , Ashish Shrivastava<sup>c</sup> , Ashutosh Singh<sup>c</sup>,  
Sohan S. Chitlange<sup>a</sup> and Amit Mittal<sup>b</sup> 

<sup>a</sup>Department of Pharmaceutical Chemistry, Dr. D. Y. Patil Institute of Pharmaceutical Sciences and Research, Pune, India; <sup>b</sup>Department of Pharmaceutical Chemistry, School of Pharmaceutical Sciences, Lovely Professional University, Phagwara, Punjab, India; <sup>c</sup>Translational Bioinformatics and Computational Genomics Research Lab, Department of Life Sciences, Shiv Nadar Institution of Eminence, Gautam Buddha Nagar, India

Communicated by Ramaswamy H. Sarma

### ABSTRACT

A cell surface bile acid receptor TGR5 being considered as a novel target for Type II diabetes found to be expressed in various tissues. A major role for TGR5 is to maintain blood sugar levels and increase in energy expenditure. These benefits make it a potential candidate for the treatment of type 2 diabetes, obesity and other metabolic disorder. To date, many novel TGR5 agonists have been synthesized and evaluated in the literature, but very few *in silico* computational studies have been reported. The discovery of a high-resolution crystal structure of TGR5 in 2020 provides an excellent opportunity for computational screening of potential agonists. In this study, we, therefore, aim to search novel, less toxic TGR5 agonists by iteratively analyzing molecular docking against TGR5 (PDB ID: 7CFN) by means of structure-based virtual screening. The docking score of the designed coumarin derivatives that have been docked successfully varies between  $-9.4$  and  $-9.0$  kcal/mol. The molecular docking and ADMET profile examinations of compounds D1, D5 and D15 revealed that these have a strong affinity for the active site residues of TGR5. In addition, molecular dynamics simulation (MDS) studies have shown the stability of compounds that bind to TGR5. It can be summarized that designed coumarin derivatives seem to have promising activity as TGR5 agonists.

### ARTICLE HISTORY

Received 22 August 2022  
Accepted 19 January 2023

### KEYWORDS

TGR5; molecular docking;  
molecular dynamic  
simulation; diabetes;  
ADMET; *in silico* analysis;  
structure based drug design

## 1. Introduction

Diabetes, ranked ninth among the leading causes of death worldwide, is the most common chronic disease. An inability of the pancreas to produce enough insulin or an inability to effectively utilize the insulin produced leads to this serious condition. In the 10<sup>th</sup> edition of the Annual IDF Report, diabetes prevalence continues to increase in the developed world, with 537 million adults (20–79 years) living with the disease. Diabetes also contributes to at least USD 966 billion in health expenditures by 2021, resulting in 6.7 million deaths. Overall, it is clear that diabetes will become a rising health concern around the globe in the coming decades (Kolb & Martin, 2017; IDF Report, 2021).

Treatment for type 2 diabetes involves various mechanisms, such as increased availability and sensitivity of insulin, decrease in carbohydrate absorption from the gastrointestinal tract, inhibition of the glucosidase enzyme (Joshi et al., 2015), inhibition of the DPP-4 enzyme (Gallwitz, 2019), GLP-1 agonists (Hinnen, 2017) etc. All of these factors result in a decrease in glucose levels in the bloodstream and a rise in the excretion of glucose through the urine. However current treatments are associated with side effects which include

gaining of weight, gastrointestinal problems and edema (Marin et al., 2016).

In search of alternative treatment of Type 2 diabetes, TGR5, G-protein coupled receptor emerged as a promising target in 2002 (Maruyama et al., 2002; Kawamata et al., 2003). TGR5 is a gene encoding 993 base pairs, 330 amino acids and seven transmembrane helices. The intestine, gall-bladder, muscle, heart and brown adipose tissue are among its various sites of expression. Upon activation of TGR5, glucagon-like peptide 1 (GLP-1) is secreted into the intestinal tract (Katsuma et al., 2005). Thomas et al. reported that GLP levels were elevated in an enteroendocrine cell line and that GLP plays an important role in glucose metabolism and energy homeostasis (Thomas et al., 2009). Furthermore, it increases the basal metabolic rate, increasing energy expenditure in brown adipose tissue and muscle (Tang et al., 2018; Watanabe et al., 2006).

Thus, TGR5 may represent a novel target that increases endogenous GLP-1 secretion and simultaneously decreases body glucose levels, body weight and associated complications. The recent surge of interest in TGR5 has led many researchers to search for new potent and selective TGR5

**CONTACT** Amit Mittal  amit.13145@lpu.co.in, amitmittal77@yahoo.com  Department of Pharmaceutical Chemistry, School of Pharmaceutical Sciences, Lovely Professional University, Phagwara, Punjab, India

© 2023 Informa UK Limited, trading as Taylor & Francis Group



## REVIEW



Cite this: *RSC Med. Chem.*, 2024, 15, 3026

## Recent advancements in the structural exploration of TGR5 agonists for diabetes treatment

Rachana S. Bhimanwar,<sup>ab</sup> Amit Mittal,<sup>b</sup> Snehal Chaudhari<sup>c</sup> and Vikas Sharma<sup>\*b</sup>

TGR5, a receptor that interacts with bile acids on cell surfaces, has become a promising therapeutic target for type II diabetes due to its ability to regulate energy expenditure and blood sugar levels. While several TGR5 agonists have been identified, only a few are currently in clinical trials. This article reviews the promising TGR5 agonists discovered in recent years, highlighting the chemical structure and pharmacological profile of the most effective compounds. With the limited number of effective drugs available for treating type II diabetes, the search for a potent TGR5 agonist with high efficacy and fewer side effects continues. The goal of this article is to provide an overview of the latest advancements in TGR5 agonists and offer insights for the future development of novel, potent TGR5 agonists for diabetes treatment. A noteworthy aspect addressed in the discussion is the common side effect associated with TGR5 agonist treatment – gallbladder filling. The review also explores potential strategies to mitigate this side effect, with the goal of improving the overall safety and tolerability of TGR5-targeted therapies.

Received 24th June 2024,  
Accepted 16th July 2024

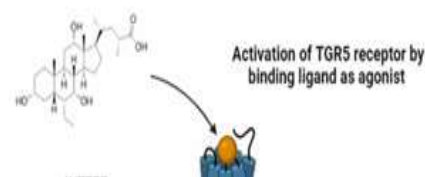
DOI: 10.1039/d4md00473f

rsc.li/medchem

## 1. Introduction

Over the past few decades, metabolic syndrome has become a pervasive and escalating global health issue, characterized by widespread prevalence and significantly raising the risk of diabetes worldwide. The 10th annual report by the International Diabetes Federation (IDF) indicates a continuous rise in diabetes cases, impacting 537 million adults in developed nations. With 6.7 million deaths and an estimated contribution of USD 966 billion to health expenditures in 2021, diabetes is projected to evolve into a growing global health issue.<sup>1</sup> The increasing incidence of type 2 diabetes emphasizes the pressing need for therapeutic strategies that not only prove effective but are also well-tolerated. Existing treatments for metabolic disorders, especially type II diabetes, are associated with various limitations in safety and tolerability; hence, developing a

A study performed by Maruyama *et al.* and Kawamata *et al.* identified the putative coding sequence of TGR5 by screening its amino acid sequences in the GenBank DNA database.<sup>7,8</sup> It consists of 993 base pairs, and has seven transmembrane domains. TGR5 is mainly activated by natural agonists *i.e.* bile acids (BAs).<sup>10</sup> The primary BAs that induce the production of cAMP are cholic acid (CA) and chenodeoxycholic acid (CDCA); the secondary BAs are deoxycholic acid (DCA) and lithocholic acid (LCA).<sup>11</sup> According to the rank order of potency in terms of EC<sub>50</sub> for



### **LIST OF PRESENTATIONS**

<b>Sr.No.</b>	<b>Details of Presentation</b>
1	Poster presentation at ICDD 2022, held on 10 <sup>th</sup> and 11 <sup>th</sup> November 2022 at Bits, Pilano Goa campus.
2.	Poster presentation at International conference on Frontiers arearsof science and technology held on 8 <sup>th</sup> and 9 <sup>th</sup> September 2023 at Shivaji University Kolhapur
3.	Oral presentation at International Symposium on medication therapy management (ISMTM 2021) on 12 <sup>th</sup> - 14 <sup>th</sup> Nov 2021 at Sultan-UI-Uloom college of pharmacy
4.	Poster presentation at UNMESH 2021 conducted at Science festival 17 <sup>th</sup> -18 <sup>th</sup> March 2021





## CERTIFICATE OF APPRECIATION

THIS CERTIFICATE IS AWARDED TO

**Rachana Bhimanwar**

has participated and presented oral abstract entitled

**To Study the Effect of co-administration of Quercetin on the Pharmacokinetic profile of Rosuvastatin in Wister rats using validated bioanalytical RP-HPLC method**

in the International Symposium on Medication Therapy Management-2021 (ISMTM) held on 12 - 14 November, 2021, jointly organized by Sultan-ul-Uloom College of Pharmacy & CliMed Research Solutions in collaboration with Indian Pharmaceutical Association, World Youth Heart Federation -India, Association of Community Pharmacists of India and International Federation for Medical Therapy Management.

**Dr. Ajit Singh**  
CEO & Co-Founder  
CliMed Research Solutions,  
Gurgaon, India

**Dr. Anupama Koneru**  
Principal  
Sultan-ul-Uloom College  
of Pharmacy, Hyderabad

**Dr. TV Narayana**  
President  
Indian Pharmaceutical  
Association (IPA)

**Dr. Anantha Nagappa Naik**  
President  
Association of Community  
Pharmacists of India (ACPI)

**Dr. Priyansh Shah**  
President  
World Youth Heart  
Federation (WYHF)